

**ISTANBUL TECHNICAL UNIVERSITY ★ EARTHQUAKE ENGINEERING AND DISASTER
MANAGEMENT INSTITUTE**

**SEISMIC BEHAVIOR OF THREE DIMENSIONAL REINFORCED
CONCRETE STRUCTURES UNDER MULTIPLE EARTHQUAKE
EXCITATIONS**

M.Sc. THESIS

Çağatay TOROS

Department of Earthquake Engineering and Disaster Management

Earthquake Engineering Programme

Thesis Advisor: Dr. Reşat Atalay OYGUÇ

JANUARY 2016

**ISTANBUL TECHNICAL UNIVERSITY ★ EARTHQUAKE ENGINEERING AND DISASTER
MANAGEMENT INSTITUTE**

**SEISMIC BEHAVIOR OF THREE DIMENSIONAL REINFORCED
CONCRETE STRUCTURES UNDER MULTIPLE EARTHQUAKE
EXCITATIONS**

M.Sc. THESIS

**Çağatay TOROS
(802121010)**

Department of Earthquake Engineering and Disaster Management

Earthquake Engineering Programme

Thesis Advisor: Dr. Reşat Atalay OYGUÇ

JANUARY 2016

**İSTANBUL TEKNİK ÜNİVERSİTESİ ★ DEPREM MÜHENDİSLİĞİ VE AFET
YÖNETİMİ ENSTİTÜSÜ**

**ÇOKLU DEPREM UYARIMLARI ALTINDA 3 BOYUTLU BETONARME
YAPILARIN SİSMİK DAVRANIŞI**

YÜKSEK LİSANS TEZİ

**Çağatay TOROS
(802121010)**

Deprem Mühendisliği ve Afet Yönetimi Anabilim Dalı

Deprem Mühendisliği Programı

Tez Danışmanı: Dr. Reşat Atalay OYGUÇ

OCAK 2016

Çağatay TOROS, a M.Sc. student of ITU **Institute of Earthquake Engineering And Disaster Management** student ID **802121010**, successfully defended the **thesis** entitled “**SEISMIC BEHAVIOR OF THREE DIMENSIONAL REINFORCED CONCRETE STRUCTURES UNDER MULTIPLE EARTHQUAKE EXCITATIONS**”, which he prepared after fulfilling the requirements specified in the associated legislations, before the jury whose signatures are below.

Thesis Advisor : **Dr. Reşat OYGUÇ**
Istanbul Technical University

Co-advisor : **Ass. Prof. Dr. Adel E. ABDELNABY**
The University of Memphis

Jury Members : **Prof. Dr. Konuralp GİRĞİN**
Istanbul Technical University

Prof. Dr. Kutlu DARILMAZ
Istanbul Technical University

Doç. Dr. Eren UÇKAN
Bogazici University

Doç. Dr. Murat Serdar KIRÇIL
Yıldız Technical University

Date of Submission : 06 November 2015

Date of Defense : 05 January 2016

To my family,

FOREWORD

I would like to express my great appreciation and gratitude to my thesis supervisor Dr. Reşat Atalay OYGUÇ and co-advisor Ass. Prof. Dr. Adel E. ABDELNABY for sharing their knowledge and experience in earthquake engineering during my MSc. education.

I owe it all TOROS family and Ms. Özge AKSAKAL for their moral contributions and supports in my whole education life.

I would like to express special thanks to Mr. Ömer ÜLKER, Mr. Mustafa Cihan PİR and Berkan Alper KAYA for helping me in all stages of my thesis.

I would like to express my sincere appreciation to Mr. Hasan Can TUNÇ for his supports during my study.

November 2015

Çağatay TOROS
(Civil Engineer)

TABLE OF CONTENTS

	<u>Page</u>
FOREWORD	ix
TABLE OF CONTENTS	xi
ABBREVIATIONS	xiii
LIST OF TABLES	xv
LIST OF FIGURES	xvii
SUMMARY	xxii
ÖZET	xxv
1. INTRODUCTION	1
1.1 Purpose of Thesis	5
2. LITERATURE REVIEW	6
2.1 Single Degree of Freedom Systems	6
2.2 Multi Degree of Freedom Systems.....	11
3. MODELING	20
3.1.1 Description of the studied buildings	20
3.1.1.1 SPEAR building.....	20
3.1.1.2 Regular case of SPEAR building.....	24
3.1.2 ICON structure.....	25
3.1.2.1 Irregular case of ICON building	30
3.1.3 School building	31
3.1.3.1 Irregular case of the School building	34
3.2 Material Models	36
3.2.1 Concrete models.....	36
3.2.1.1 Uniaxial constant confinement concrete model	36
3.2.1.2 Plastic damage concrete model	37
3.2.2 Steel models	39
3.2.2.1 Bilinear elasto-plastic steel model	39
3.2.2.2 Modified Menegotto-Pinto model.....	40
3.3 Structural Modeling.....	46
3.4 Analysis Software	46
3.4.1 Analytical modeling of members	46
4. EARTHQUAKE SEQUENCES	49
4.1 Record Selection Criteria	49
5. ANALYSIS PROCODURES	56
5.1 Nonlinear Static Procedures	56
5.1.1 N2 metod.....	56
5.1.2 Extended N2 metod.....	59
6. ANALYSIS RESULTS	62
6.1 Eigen-value Analyses and Mode Shapes	62
6.2 Nonlinear Static Procedure Results	70
6.2.1 SPEAR building.....	70

6.2.2 N2 method for original case of SPEAR building.....	70
+Y direction.....	71
-Y direction	72
6.2.3 Extended N2 Method for original case of SPEAR building	75
6.2.4 N2 method for remodeled case of SPEAR building	76
+Y direction.....	77
-Y direction	79
6.2.5 ICON building.....	83
6.2.6 N2 method for original case of ICON building	83
+X direction.....	83
-X direction	85
6.2.7 N2 method for remodeled case of ICON building	87
+X direction.....	88
-X direction	89
6.2.8 Extended N2 Method for remodeled case of ICON building.....	91
6.2.9 School building	94
6.2.10 N2 method for original case of school building.....	94
+X direction.....	95
-X direction	97
6.2.11 N2 method for remodeled case of school building	99
+X direction.....	99
-X direction	101
6.2.12 Extended N2 Method for original case of school building	104
6.3 Seismic Response of Regular and Irregular Models	109
6.3.1 Permanent Displacements	111
6.3.2 Maximum top displacements	115
6.3.3 Drifts	120
6.3.4 Inter-storey Drifts.....	122
6.3.5 Plastic Hinges.....	125
7. CONCLUSION.....	140
APPENDICES	146
APPENDIX A	147
APPENDIX B.....	153
APPENDIX C.....	156
CURRICULUM VITAE.....	179

ABBREVIATIONS

ELSA	: European Laboratory for Structural Assessment
EC	: Eurocode
FE	: Finite Element
JMA	: Japan Meteorological Agency
MDOF	: Multi Degree of Freedom
NIED	: National Research Institute for Earth Science and Disaster Prevention
NIST	: National Institute of Standards and Technology
NSA	: Nonlinear Static Analysis
PGA	: Peak Ground Acceleration
PSA	: Pseudo Spectral Acceleration
PSV	: Pseudo Spectral Velocity
RSA	: Standard Elastic Modal Response Analysis
SA	: Spectral Acceleration
SD	: Spectral Displacement
SDOF	: Single Degree of Freedom
TEC	: Turkish Earthquake Code

LIST OF TABLES

	<u>Page</u>
Table 3.1 : Material characteristics of SPEAR building	23
Table 3.2 : Torsional characteristics and the lateral stiffness of the regular and irregular case of SPEAR building in Y direction.....	25
Table 3.3 : Material characteristics of ICON building.....	29
Table 3.4 : Material characteristics of school building	34
Table 3.5 : Torsional characteristics and the lateral stiffness of the regular and irregular case of school building in X direction.....	34
Table 4.1 : Ground types in Eurocode 8.	50
Table 4.2 : Selected records	55
Table 6.1 : Story mass of the studied buildings	70
Table 6.2 : Lateral load distribution values.....	70
Table 6.3 : Pushover and RSA results of SPEAR building in Y direction	75
Table 6.4 : Lateral load distribution values.....	77
Table 6.5 : Values of developed plastic hinges in SPEAR building.	81
Table 6.6 : Lateral load distribution values	83
Table 6.7 : Lateral force distribution values	87
Table 6.8 : Pushover and RSA results of ICON building in X direction	91
Table 6.9 : Values of developed plastic hinges in ICON building.....	93
Table 6.10 : Lateral load distribution values.....	95
Table 6.11 : Lateral load distribution values.....	99
Table 6.12 : Pushover and RSA results of school building in X direction	104
Table 6.13 : Values of developed plastic hinges in school building	106

LIST OF FIGURES

	<u>Page</u>
Figure 1.1 : 11 March 2011 Tohoku earthquake sequence [1]	26
Figure 1.2 : Shake maps of the October 23 Mw: 7.2 (left) and November 9 Ml: 5.6 (right) earthquakes in Van province [2].....	27
Figure 1.3 : Damage distribution of the investigated buildings in Van City [4].....	28
Figure 1.4 : After Mw 7.2 heavily damaged, after M 5.6 collapsed [4]	28
Figure 1.5 : After Mw 7.2 heavily damaged, after M 5.6 collapsed [4]	29
Figure 2.1 : Effects of aftershocks [7]	32
Figure 2.2 : Standard Takeda models (a) positive post-yield stiffness (b) negative post-yield stiffness [8]	32
Figure 2.3 : Modified Takeda model with pinching and strength degradation [8] ..	33
Figure 2.4 : Force-displacement response history of the oscillators having different prior damage with PDD = 0, 1, 4, 8 [8]	33
Figure 2.5 : Hysteretic models of the analyzed SDOF systems [9]	34
Figure 2.6 : q ratios of different hysteretic models for El Centro earthquake (a) non-degrading, (b) degrading stiffness [9].....	35
Figure 2.7 : Bilinear elasto-plastic model of SDOF used by Hatzigeorgiu et. al. [10]	35
Figure 2.8 : Seismic sequence [10]	36
Figure 2.9 : q-factor for moment resisting frames with rigid joints [11].....	37
Figure 2.10 : Hysteretic model for damaged welded connection [14].....	38
Figure 2.11 : Relationship between additional damage ratio by aftershock and the damage ratio by main shock of nine storey building, replicate aftershock (top), randomized aftershock (bottom) [12]	39
Figure 2.12 : Permanent displacements under multiple events [15].....	40
Figure 2.13 : Ratios of force reduction factor for Funehiki (left) and Hitachi (right) stations [16]	41
Figure 2.14 : Buckling and fracture in the degrading steel model [5]	41
Figure 2.15 : Degrading concrete model (a) tension and (b) compression [17]	42
Figure 2.16 : Comparison of displacement response of damaged and undamaged non-degrading gravity frame model [5]	43
Figure 2.17 : Comparison of displacement response of damaged and undamaged degrading gravity frame model [5].....	44
Figure 3.1 : Plan (top) and the elevation (bottom) of the SPEAR building.....	46
Figure 3.2 : Typical column and beam cross sections	47
Figure 3.3 : FE modeling of SPEAR building	48
Figure 3.4 : Regular plan of SPEAR building. Modified columns are marked with red circle.	49
Figure 3.5 : General view of the structure	51
Figure 3.6 : Plan of the ICON building.....	51
Figure 3.7 : Elevation of ICON building	52
Figure 3.8 : Column and beam cross sections.....	53
Figure 3.9 : FE modeling of ICON building.....	54

Figure 3.10 : Elevation (top) and plan (bottom) of ICON building	55
Figure 3.11 : FE modeling of the irregular case of ICON building	56
Figure 3.12 : Typical floor plan of the school building	57
Figure 3.13 : Typical column beam cross sections	58
Figure 3.14 : FE modeling of school building	58
Figure 3.15 : Irregular case of the school building	60
Figure 3.16 : Uniaxial constant confinement model (con2).....	61
Figure 3.17 : Numerical and experimental results of the concrete model tension (top) and compression (bottom)	62
Figure 3.18 : Stress-strain behavior of the concrete model (con5) [5].....	63
Figure 3.19 : Comparison of the concrete models [5].....	64
Figure 3.20 : Bilinear elasto-plastic steel model (stl1)	65
Figure 3.21 : Main characteristics of a steel stress-strain diagram [18].....	66
Figure 3.22 : Equilibrium of a buckled longitudinal steel bar [19].....	68
Figure 3.23 : Buckling and fracture in the steel model (stl4) [5].....	69
Figure 3.24 : Comparison of the steel models [5].....	70
Figure 3.25 : Fiber based models	71
Figure 3.26 : Effective flange width parameters [33]	72
Figure 3.27 : Definition of l_0 for calculation of effective width [33].....	72
Figure 3.28 : Rigid links at beam column connections.....	73
Figure 3.29 : Rigid diaphragm element in analytical modeling [23]	73
Figure 4.1 : Distribution of the main shock and aftershocks larger than M7.....	75
Figure 4.2 : E-W component of the IBR006 station	76
Figure 4.3 : N-S component of the IBR006 station	76
Figure 4.4 : PGA values and locations of the stations	77
Figure 4.5 : S_a and S_d - period graphs of selected ground motions.....	78
Figure 4.6 : PS_a and PS_v - period graphs of selected ground motions.	79
Figure 5.1 : Assumed displacement shapes for different types of buildings	82
Figure 5.2 : Bilinear force-displacement relationship [35]	83
Figure 5.3 : Approximate spectra for R-factor [46]	84
Figure 5.4 : Correction factors for the higher mode effects in plan [44]	85
Figure 6.1 : Periods and mode shapes of SPEAR structure (Zeus-NL).....	63
Figure 6.2 : Periods and mode shapes of SPEAR structure (SAP2000).....	64
Figure 6.3 : Periods and mode shapes of regular case of SPEAR structure (Zeus-NL)	65
Figure 6.4 : First two periods and mode shapes of ICON building (Zeus-NL)	66
Figure 6.5 : First two periods and mode shapes of ICON building (SAP2000)	66
Figure 6.6 : First two periods and mode shapes of irregular case of ICON building (Zeus-NL)	66
Figure 6.7 : Periods and mode shapes of school building (Zeus-NL).....	67
Figure 6.8 : Periods and mode shapes of school building (SAP2000).....	68
Figure 6.9 : Periods and mode shapes of irregular case of school building (Zeus-NL)	69
Figure 6.10 : Base shear-top displacement relationship of the SPEAR building in +Y direction.....	71
Figure 6.11 : Calculated values of R_μ and μ for SPEAR building in +Y direction ..	72
Figure 6.12 : Base shear-top displacement relationship of the SPEAR building in -Y direction.....	73
Figure 6.13 : Calculated values of R_μ and μ for SPEAR building in -Y direction ...	74
Figure 6.14 : Capacity curves of the SPEAR building in Y direction	74

Figure 6.15 : Correction factors (c_E) for displacements.....	75
Figure 6.16 : Correction factors (c_E) for drifts.....	76
Figure 6.17 : Correction factors (c_T) for plan	76
Figure 6.18 : Base shear-top displacement relationship of the remodeled SPEAR building in +Y direction	77
Figure 6.19 : Calculated values of R_μ and μ for remodeled SPEAR building in +Y direction.....	78
Figure 6.20 : Base shear-top displacement relationship of the remodeled SPEAR building in -Y direction	79
Figure 6.21 : Calculated values of R_μ and μ for remodeled SPEAR building in -Y direction.....	80
Figure 6.22 : Capacity curves of the SPEAR building for regular and irregular cases in Y direction.....	81
Figure 6.23 : Plastic hinge locations of the SPEAR building for regular (top) and irregular (bottom) cases in Y direction.....	82
Figure 6.24 : Base shear-top displacement relationship of the ICON building in +X direction.....	84
Figure 6.25 : Calculated values of R_μ and μ for ICON building in +X direction.....	85
Figure 6.26 : Base shear-top displacement relationship of the ICON building in -X direction.....	85
Figure 6.27 : Calculated values of R_μ and μ for ICON building in -X direction.....	86
Figure 6.28 : Capacity curves of the ICON building in X direction.....	87
Figure 6.29 : Base shear-top displacement relationship of the remodeled ICON building in +X direction	88
Figure 6.30 : Calculated values of R_μ and μ for remodeled ICON building in +X direction.....	89
Figure 6.31 : Base shear-top displacement relationship of the remodeled ICON building in -X direction	90
Figure 6.32 : Calculated values of R_μ and μ for remodeled ICON building in -X direction.....	91
Figure 6.33 : Correction factors (c_E) for displacements.....	92
Figure 6.34 : Correction factors (c_E) for drifts.....	92
Figure 6.35 : Capacity curves of the ICON building for regular and irregular cases in X direction.....	93
Figure 6.36 : Plastic hinge locations of the ICON building for regular (top) and irregular (bottom) cases in X direction.....	94
Figure 6.37 : Base shear-top displacement relationship of the school building in +X direction.....	95
Figure 6.38 : Calculated values of R_μ and μ for school building in +X direction	96
Figure 6.39 : Base shear-top displacement relationship of the school building in -X direction.....	97
Figure 6.40 : Calculated values of R_μ and μ for school building in -X direction.....	98
Figure 6.41 : Capacity curves of the school building in X direction	99
Figure 6.42 : Base shear-top displacement relationship of the remodeled school building in +X direction	100
Figure 6.43 : Calculated values of R_μ and μ for remodeled school building in +X direction.....	101
Figure 6.44 : Base shear-top displacement relationship of the remodeled school building in -X direction	102

Figure 6.45 : Calculated values of R_μ and μ for remodeled school building in -X direction	103
Figure 6.46 : Capacity curves of the school building for regular and irregular cases in X direction	103
Figure 6.47 : Correction factors (c_E) for displacements	104
Figure 6.48 : Correction factors (c_E) for drifts	105
Figure 6.49 : Correction factors (c_T) for plan	105
Figure 6.50 : Plastic hinge locations of the school building for regular case in X direction	107
Figure 6.51 : Plastic hinge locations of the school building for irregular case in X direction	108
Figure 6.52 : Top displacement-time history of the four different models in SPEAR building (IWT007EW record)	109
Figure 6.53 : Top displacement-time history of the four different models in ICON building (IWT012NS record)	110
Figure 6.54 : Top displacement-time history of the four different models in ICON building (FKS019NS record).....	110
Figure 6.55 : Top displacement-time history of the four different models in ICON building (IBR018EW record)	111
Figure 6.56 : Difference in residual displacement of the SPEAR building for IWT026NS record	112
Figure 6.57 : Mean residual top displacements ratio of SPEAR building	113
Figure 6.58 : Difference in residual displacement of the ICON building for IWT012NS record	113
Figure 6.59 : Mean residual top displacements ratio of ICON building	114
Figure 6.60 : Difference in residual displacement of the school building for IWT012EW record	114
Figure 6.61 : Mean residual top displacements ratio of school building	115
Figure 6.62 : Maximum top displacements of the degrading models for SPEAR building.....	117
Figure 6.63 : Maximum top displacements of the degrading models for ICON building.....	118
Figure 6.64 : Maximum top displacements of the degrading models for school building.....	119
Figure 6.65 : Mean drifts of SPEAR building.....	120
Figure 6.66 : Mean drifts of ICON building	121
Figure 6.67 : Mean drifts of school building.....	122
Figure 6.68 : Inter-storey drift ratio for SPEAR building (IWT007EW record)	123
Figure 6.69 : Inter-storey drift ratio for ICON building (FKS012EW record)	124
Figure 6.70 : Inter-storey drift ratio for school building (IWT026NS record)	124
Figure 6.71 : Number of developed plastic hinges in SPEAR building.....	125
Figure 6.72 : Mean number of developed plastic hinges in SPEAR building	126
Figure 6.73 : Number of developed plastic hinges in ICON building	127
Figure 6.74 : Mean number of developed plastic hinges in ICON building.....	127
Figure 6.75 : Number of developed plastic hinges in school building.....	128
Figure 6.76 : Base shear-time history and target shear value of the school building for FKS012EW record.....	129
Figure 6.77 : Mean number of developed plastic hinges in school building	130
Figure 6.78 : Plastic hinge locations of SPEAR building for regular-main shock case	131

Figure 6.79 : Plastic hinge locations of SPEAR building for regular-all sequence case	132
Figure 6.80 : Plastic hinge locations of SPEAR building for irregular-main shock case	133
Figure 6.81 : Plastic hinge locations of SPEAR building for irregular-all sequence case	134
Figure 6.82 : Plastic hinge locations of ICON building for original (left) and remodeled (right) case	135
Figure 6.83 : Plastic hinge locations of school building for regular case in main shock.....	136
Figure 6.84 : Plastic hinge locations of school building for regular case in all sequence	137
Figure 6.85 : Plastic hinge locations of school building for irregular case in main shock.....	138
Figure 6.86 : Plastic hinge locations of school building for regular case in all sequence	139

CAPACITY ASSESSMENT OF THREE DIMENSIONAL REINFORCED CONCRETE STRUCTURES UNDER MULTIPLE EARTHQUAKE EXCITATIONS

SUMMARY

Earthquakes that occurred in Turkey and in many other regions in the world showed that many foreshocks and aftershocks occur before and after an earthquake. According to conventional codes, one earthquake scenario is taken into consideration and related design is established. Experiences reveal that even if structures provide required performance level during main earthquake, they cannot provide required strength and rigidity during aftershocks. Moreover, as a result of carried studies, it's seen that materials of structures which were exposed to effects of an earthquake, don't show the same behavior as they did before the earthquake.

Within the context of this study, six buildings, three of which is regular and the three other of which are irregular, are evaluated under the effect of multiple earthquakes. Two of these buildings (ICON and SPEAR) were built in original scale in laboratory environment in Europe and subjected to various tests. SPEAR was built in ELSA laboratory, which states in Ispra / Italy under the name of Seismic Performance Assessment and Rehabilitation project. ICON, in a similar way, was also designed and built within the scope of Innovative Concepts for Seismic Design of New and Existing Structures and subjected to pseudo-dynamic test. Moreover, another one of these three buildings was built in Van /Turkey, and it is one of the school buildings, which was damaged during Van earthquake in 2011. ICON building is a four-storey, regular structure. SPEAR structure is three-storey and a irregular structure in plan according to Eurocode. School building is a three-storey building one of which is the basement and it is a regular structure according to TEC.

Three buildings are obtained that the regular building modified as irregular and the irregular ones modified as regular depending on the condition whether three building are regular and irregular. In ICON building, removing one of the frames, which located in top floor, setback limit in Eurocode 8 is exceeded and building classified as irregular in elevation. In SPEAR building, dimensions of three columns were changed while total lateral stiffness of the building remained as constant. Hence, the building was classified as regular in plan. Lastly, the eccentricity of the school building was increased, three shear wall located in center of rigidity shifting to external axis. According to Turkish Earthquake Code the building was modified as irregular in plan.

Zeus- NL, which is able to make 3D modeling, was used for modeling. Two different material models, which take into account stiffness degradation and strength deterioration, were used during the structural modeling. In addition, structures modeled with the material models, which have non-degrading effect.

In the first chapter of the study, which has seven subsections, introduction, objective and scope of the study are stated.

In the second chapter, recent important studies about multiple earthquake effect are mentioned. The material models, assessed structures and the results are summarized.

Characteristics of material types and the analysis program used in the analysis are referred in the third section of the thesis. Detailed information such as project information of three buildings, characteristics of the materials used in buildings, reinforced concrete details are included in the proceeded subsections. Also related information about modeling; determining of effective width of the beams related to structural modeling according to Eurocode, modeling diagonals which are defined for floor level to show diaphragm feature, connecting the beams which are attached to columns from different alignments to columns with rigid elements of frame element system is provided. Bilinear steel model is used and Mander model is used for concrete in the first stage of modeling. In second stage, Modified Menegotto-Pinto hysteric model, which have degradation effect and stiffness deterioration concrete model, which developed by Fenves, is used. In this section, related theories about these models are also mentioned.

To implement dynamic analysis, fourth chapter includes information about 11th March 2011 Tohoku/ Japan earthquake, selection of records related with prior earthquake and aftershocks from stations, considered points in record selection. Records are acquired from Japanese National Research Institute for Earth Science and Disaster Prevention (NIED) data bank. In record selection, distance between chosen stations and epicenter, characteristics of the ground on which the station is placed, the peak ground acceleration value of records are mentioned. In order not to consider any near fault effect, records are selected from at least 20 km further stations from epicenter. Moreover, it is another point, which is taken into consideration during record selection to have records from stations, which are placed on ground type B to avoid effects of soil amplification.

In fifth chapter analysis methods that are used are explained. N2 method, the situations appropriate for this analysis to be used and restrictions and extended N2 method, which used for irregular buildings, are presented.

Chapter six is reserved for analysis results. At first, periods and mode shapes of the buildings are represented using Zeus-NL and SAP2000 software. To check the accuracy of the models the results are compared. Then, the capacity curves of the buildings determined with N2 method. Extended N2 method is applied to irregular buildings, which are determined to be irregular according to Eurocode and TEC. In last phase, multiple earthquake records are applied to models, which have the degrading material properties. Story drifts, maximum top displacements, residual displacements, interstorey drifts and formation of plastic hinges are calculated through nonlinear dynamic time history analysis. The obtained results are summarized below.

- Degradation effect is seen clearly in residual displacements. The non-degrading models showed limited residual displacements compared to degrading models.
- Irregular structures showed more permanent displacements both for main-shock and all sequence case. However, increase in residual displacement ratios between the main shock and all sequence is almost same for both

regular and irregular in plan (SPEAR), irregular in elevation (ICON) buildings. This case is opposite for both plan and elevation irregular buildings (School building).

- Generally, the buildings experienced maximum top displacements during the main shock in degrading models.
- During the main shock, more plastic hinges are developed in irregular buildings compared to regular ones, therefore when the irregular structures experienced aftershocks, increase in plastic hinges is less than the regular case. Nevertheless, number of developed hinges are higher in irregular ones when the all sequence is finished.
- Conventional nonlinear static results differ from the nonlinear dynamic results, but when the relevant local quantities are multiplied by calculated factors, which are determined by using extended N2 method, similar results are captured with nonlinear dynamic analysis. Therefore, a good prediction can be made by the extended N2 method in terms of plastic hinge distribution.

In the light of this comparison, the nonlinear dynamic response of the selected buildings indicate that irregularity effects increase the dispersed damage on the buildings when structures are subjected to multiple ground motions. Consequently, more attention must be shown for multiple earthquake excitations during the design phase especially important buildings, which include the irregularity effects.

ÇOKLU DEPREM UYARIMLARI ALTINDA 3 BOYUTLU BETONARME YAPILARIN KAPASİTE DEĞERLENDİRMESİ

ÖZET

Türkiye’de ve dünyanın birçok bölgesinde meydana gelen depremler göstermektedir ki ana depremin öncesinde veya sonrasında birçok öncü deprem veya artçı depremler meydana gelmektedir. Yürürlükteki geleneksel yönetmeliklere göre tek bir deprem senaryosu göz önüne alınarak tasarım yapılmaktadır. Geçmişte yaşanan tecrübeler yapıların ana depremde hedeflenen performans seviyesini sağlasa bile artçı depremlerde gerekli dayanımı ve rijitliği gösteremediğini ortaya koymaktadır. Ayrıca yapılan çalışmalar sonucunda deprem etkilerine maruz kalan yapıların malzeme özellikleri deprem öncesinde gösterdiği davranışı göstermemektedir.

Bu çalışma kapsamında üçü düzenli üçü düzensiz altı adet binanın çoklu deprem etkileri altındaki değerlendirilmesi yapılmıştır. Bu binalardan ikisi (ICON ve SPEAR) daha önce Avrupa da laboratuvar ortamında birebir ölçekte inşa edilerek çeşitli testlere tabii tutulmuşlardır. SPEAR binası Ispra İtalya’da bulunan ELSA laboratuvarlarında sismik performans değerlendirilmesi ve iyileştirme projesi (Seismic Performance Assessment and Rehabilitation) adı altında inşa edilerek sözde-dinamik teste tabii tutulmuştur. Aynı şekilde ICON binası da yeni ve mevcut yapıların sismik tasarımı için yenilikçi yaklaşımlar projesi kapsamında (Innovative Concepts for Seismic Design of New and Existing Structures) 1999 yılında tasarlanıp inşa edilerek sözde-dinamik test uygulanmıştır. Binalardan diğeri ise Türkiye’nin Van ilinde yapılmış olup 2011 Van depreminde hasar almış okul binalarından bir tanesidir. Binalardan ICON 4 katlı olup düzenli bir yapıdır. SPEAR ise 3 katlıdır ve Eurocode’a göre planda düzensiz bir yapıdır. Okul binası bir bodrum kattan oluşmak üzere 3 katlıdır ve Türk Deprem Yönetmeliğine göre planda düzenli bir yapıdır.

Üç bina mevcut düzenlilik durumlarına göre düzenli binalar düzensiz, düzensiz binalar ise düzenli olarak yeniden modellenerek diğer üç bina elde edilmiştir. Yapıların yeniden modellenmesi sırasında yanal rijitlikleri korunmuştur. Bu binalardan ICON binasında üst kat çerçevelerinden biri kaldırılarak Eurocode’da belirtilen geri çekme sınırı aşılmış olup yapı düşeyde düzensiz yapılmıştır. SPEAR binasında ise binanın toplam yanal rijitliğinin değişmemesine dikkat edilerek 3 adet kolonun boyutları değiştirilmiştir. Böylece bina planda düzenli hale getirilmiştir. Son olarak okul binasında ise ritijlik merkezi üzerinde bulunan 3 adet perde dış aksa kaydırılarak binaya ek dışmerkezlilik verilmiştir. Yapı Türk Deprem Yönetmeliğine göre düzensiz duruma getirilmiştir.

Mevcut binaların modellenmesinde 3 boyutlu modelleme yapılabilen Zeus-NL programı kullanılmıştır. Binaların modellenmesinde rijitlikteki azalımı ve dayanımda ki bozunmayı göz önüne alan iki farklı malzeme kullanılmıştır. Doğrusal olmayan statik itme analizi sonuçları ve zaman tanım alanında doğrusal olmayan analiz sonuçlarından elde edilmiştir. Elde edilen sonuçlar kendi içlerinde değerlendirilerek

düşeyde ve yatayda düzensiz binaların düzenli binalara göre çoklu deprem uyarımları altındaki karşılaştırılması ve değerlendirilmesi yapılmıştır.

Yedi bölümden oluşan yüksek lisans tezinin birinci bölümünde giriş, tezin amacı ve yapılan çalışmanın kapsamı belirtilmiştir.

İkinci bölümde ise daha önce bu konuda yapılmış olan önemli çalışmalar anlatılmıştır. Bu çalışmalarda kullanılan malzeme özellikleri, değerlendirilen yapılar ve elde edilen sonuçlar açıklanmıştır.

Tezin üçüncü bölümünde kullanılan analiz programının özellikleri ve analizde kullanılan malzeme cinslerinin özelliklerine değinilmiştir. İlerleyen alt bölümlerinde üç binaya ait proje bilgileri, binalarda kullanılan malzemelerin özellikleri, betonarme detayları gibi yapılar hakkında detaylı bilgilere yer verilmiştir. Ayrıca yapısal modellemeye ile ilgili kirişlerin Eurocode'a göre tabla genişliklerinin belirlenmesi, kat düzeyinde yapıların diyafram özelliği göstermesi için tanımlanan yatay çapraz elemanların modellenmesi, farklı hizalardan kolonlara bağlanan kirişlerin çubuk eleman sisteminde rijit elemanlar ile kolonlara bağlanması gibi modelleme ile ilgili bilgiler bulunmaktadır. Modellemenin birinci aşamasında çelik için standart iki doğrulu çelik modeli ve beton içinse Mander modeli kullanılmıştır. İkinci aşamada ise azalımsal özelliği bulunan düzenlenmiş Menegotto-Pinto döngüsel gerilme-şekil değiştirme modeli ve kırılma-enerji esaslı ve rijitlik bozunumlu Fenves tarafından geliştirilen beton modeli kullanılmıştır. Bu bölümde ayrıca bu modellere ait teorilerde anlatılmıştır.

Dördüncü bölümde ise 11 Mart 2011 Tohoku Japonya depremine ait bilgiler verilmiş olup bu depreme ait belirli istasyonlardan ana ve artçı depremlere ait kayıtların seçilmesi, kayıt seçilmesinde göz önüne alınan konular anlatılmıştır. Kayıtlar Japonya Yer Bilimi ve Afetleri Önleme Ulusal Araştırma Enstitüsü (NIED) veri bankasından alınmıştır. Kayıt seçiminde seçilen istasyonların depremin merkez üssüne olan uzaklığı, istasyonun üzerinde bulunduğu zemine ait özellikler, kayıtların en büyük ivme değerleri gibi konulara değinilmiştir. Kayıt seçiminde herhangi bir yakın fay etkisini göz önüne almamak için depremin merkez üssüne 20 km'den daha uzak istasyonlardan kayıtlar seçilmiştir. Ayrıca seçilen kayıtlarda zemin büyütmesi gibi etkilerin olmaması için Eurocode'a göre B tipi zeminde yer alan istasyonlarda ki verilerin alınması diğer bir seçim özelliğidir.

Beşinci bölümde kullanılan analiz yöntemleri anlatılmıştır. N2 metodu ve kullanım sınırlamaları ile düzensiz binalar için genişletilmiş N2 metodu anlatılmıştır.

Tezin altıncı bölümü analiz sonuçlarına ayrılmıştır. İlk alt bölümde yapıların ana titreşim periyotları ve bu periyotlara ait titreşim genlikleri hem Zeus-NL hem de SAP2000 programları kullanılarak şekillerde gösterilmiştir. Modellerin doğruluğunun kontrol etmek için sonuçlar karşılaştırılmıştır. İkinci alt bölümde ise statik itme yöntemi kullanılarak her bir yapı için hem düzenli hem de düzensiz durumda kapasite eğrileri elde edilmiş olup N2 yöntemi kullanılarak yapıların hedef yerdeğiştirme talepleri hesaplanmıştır. Daha önceki bölümlerde düzensizlik durumu belirlenmiş olan binalara genişletilmiş N2 metodu uygulanmıştır.

Takip eden son alt bölümde ise azalımsal ve azalımsal olmayan malzeme özelliklerine sahip modellere zaman tanım alanında doğrusal olmayan analiz ile çoklu deprem kayıtları uygulanmıştır. Yapılarda oluşan kat ötelenmeleri, en büyük tepe yerdeğiştirmeleri, kalıcı ötelenmeler, göreceli kat ötelenmeleri, plastik mafsallı oluşumu gibi sonuçlar elde edilmiştir. Elde edilen sonuçlar düzenli ve düzensiz

binalarda karşılıklı olarak hem ana deprem hem de artçı depremleri içeren bütün seri olarak irdelenmiştir. Elde edilen sonuçlar aşağıda özetlenmiştir.

- Kalıcı yerdeğişimler azalımsal özelliğe sahip modellerde etki açıkça görülmektedir. Azalımsal olmayan modellerde kalıcı yerdeğişimler ya hiç görülmemektedir ya da çok sınırlı kalmaktadır.
- Düzensiz binalarda hem ana deprem hem de bütün seri için düzenli binalara göre daha fazla kalıcı yerdeğiştirme oluşmaktadır. Ancak ana deprem ile bütün seri arasındaki kalıcı yerdeğişimlerdeki artış oranı düzenli ve sadece planda ya da sadece düşeyde düzensiz binalar için neredeyse aynıdır. Bu durum hem planda hem de düşeyde düzensiz olan okul binası içinse tam tersidir.
- Genellikle, azalımsal özelliğe sahip malzeme modeli kullanılan yapılarda bütün seri depremler boyunca en büyük tepe yerdeğiştirmesi ana deprem sırasında olmaktadır.
- Ana deprem sırasında düzensiz binalarda düzenli binalara oranla daha fazla plastik mafsall oluşmaktadır. Artçı depremler sırasında ise, ana depremde daha fazla hasar almış düzensiz binalardaki plastik mafsall artışı düzenli kadar fazla olmamaktadır. Yinede bütün seri bittiğinde oluşan plastik mafsall sayısı düzensiz yapılarda daha fazladır.
- Plastik mafsall dağılımı karşılaştırıldığında doğrusal olmayan analiz sonuçları ile N2 yöntemi sonuçları farklıdır. Fakat genişletilmiş N2 yöntemi uygulanarak ilgili bölgesel nicelikler hesaplanan katsayılar ile arttırıldığında doğrusal olmayan analiz ile benzer sonuçlar elde edilmektedir. Bu sebepten genişletilmiş N2 yöntemi ile düzensiz yapılarda iyi yaklaşım yapılabilmektedir.

Bu karşılaştırmalar sonucunda çoklu deprem uyarılarına maruz kalan yapılardaki düzensizlik etkilerinden dolayı hasar artışı dikkat çekmektedir. Sonuç olarak sık deprem etkilerine maruz kalan bölgelerde özellikle yapısal düzensizlik içeren önemli yapıların, hizmette kaldıkları süre boyunca oluşabilecek çoklu deprem uyarılarına, tasarımı sırasında dikkat edilmesi gerektiği belirlenmiştir.

1. INTRODUCTION

Before or after the most damaging earthquake, prior or aftershocks occur in Turkey and many parts of the world. Multiple earthquakes cause damage accumulation in buildings. In design, conventional single earthquake scenarios are performed according to applicable codes. The stiffness and strength degradation in the materials due to multiple earthquake excitations affect the behavior of the buildings, which is not taken into account during repair and strengthening or determining the situation of damaged structures.

Multiple earthquakes occur in two ways. One of them is main shock and subsequent aftershocks sequence or foreshock and following main shock sequence, the other one is independent earthquakes on different faults with close epicenter to each other or on the same fault with different segments. 11 March 2011 Tohoku and 22 February 2011 Christchurch earthquakes are example of significant main and after-shock sequences. The foreshocks and the aftershocks in Tohoku earthquake sequence can be seen in Figure 1.1.

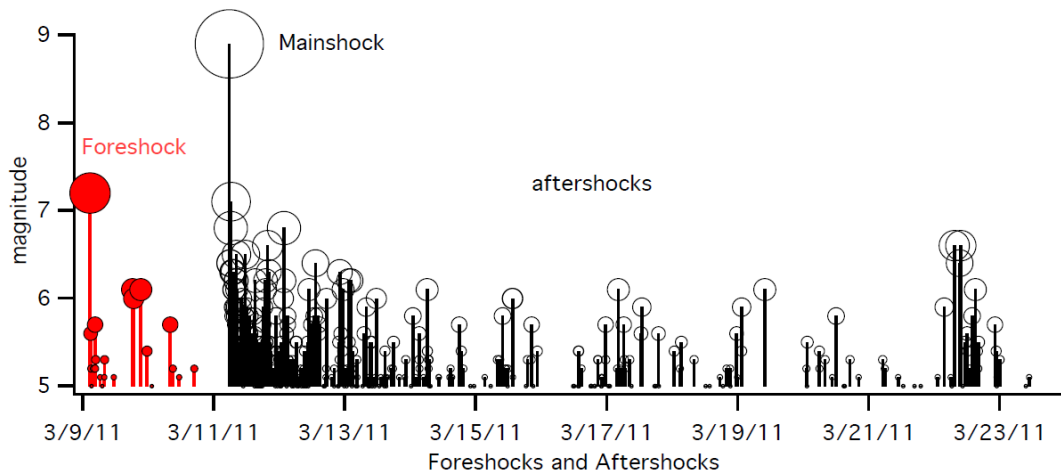


Figure 1.1 11 March 2011 Tohoku earthquake sequence [1]

23 October 2011 Van earthquake and the following 09 November 2011 Edremit-Van earthquake are significant independent earthquakes on different faults close rupture locations. In Figure 1.2, the shake maps of the two earthquakes are represented. 1999 Kocaeli

earthquake and few months later 1999 Düzce earthquake are the significant independent earthquake sequence on same fault but different fault segments.

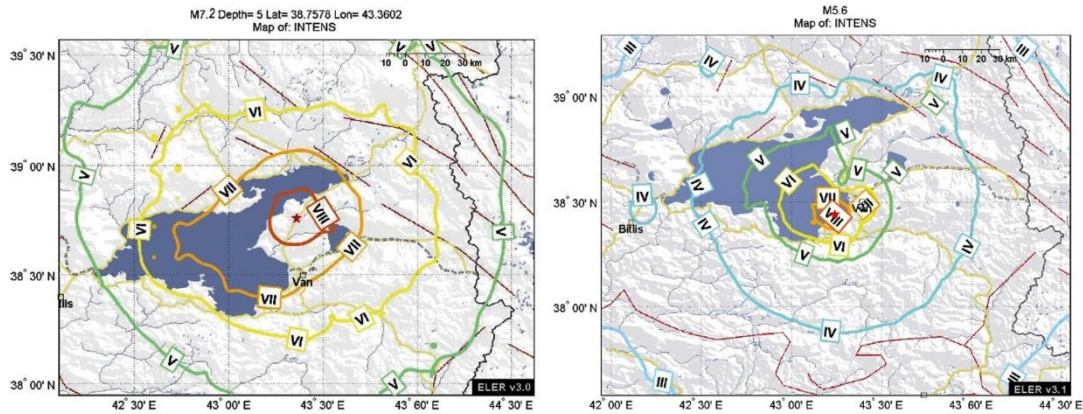


Figure 1.2 Shake maps of the October 23 Mw: 7.2 (left) and November 9 Ml: 5.6 (right) earthquakes in Van province [2]

Field investigations indicated that the collapse of buildings during the after-shocks are caused by damage accumulation under repeated shaking. Recently, failure of the buildings due to multiple earthquake excitations was observed in Van earthquake clearly [3] [4].

On October 23, 2011 an earthquake of magnitude M_w 7.2 occurred in Van province. Few days later, an earthquake of magnitude M 5.6 occurred in Edremit-Van. 128 buildings were investigated after the first earthquake in Van city by researchers in METU [3]. Many buildings received different levels of damage on the first earthquake. The buildings are categorized in five damage level. The buildings which reach the failure mechanism are classified as collapse, the buildings which included of plastic hinges in columns categorized as heavily damaged, the buildings which had major cracks on infill walls and structural system classified as moderate damage, the buildings which had minor cracks on infill walls and structural system categorized as slightly damage and the buildings which had no damage in any structural system are classified as no damage. After the second earthquake, same buildings were investigated to find out the effect of second excitation. Researchers report that three buildings which were heavily damaged under first earthquake, were collapsed after the second earthquake. One of the collapsed buildings categorized as medium level after the first shaking. Also damage level of two buildings, which categorized as heavily damaged during the first earthquake, were not changed after the second earthquake.

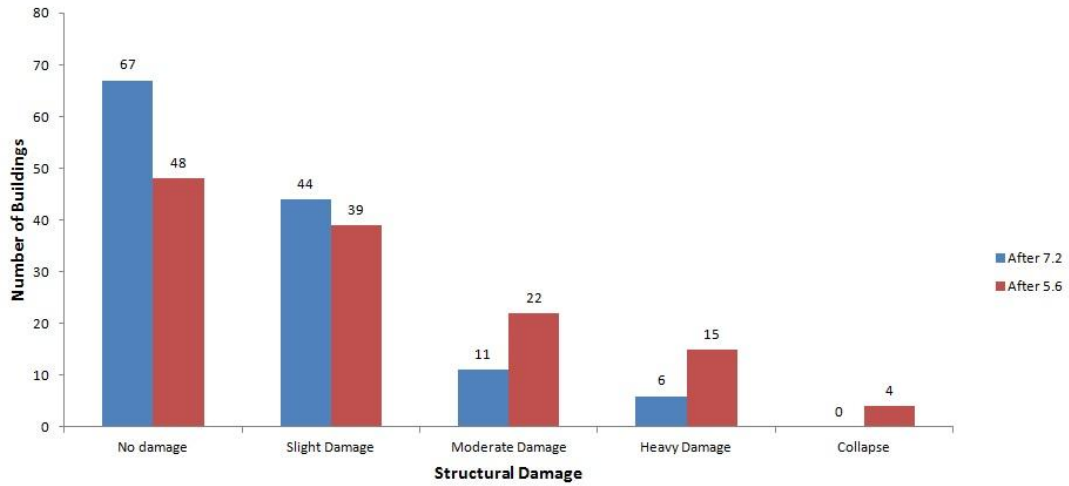


Figure 1.3 Damage distribution of the investigated buildings in Van City [4]

Figure 1.3 represents that change of damage level of buildings between first and second earthquake. Researchers also report that among the 111 buildings, which undamaged or slightly damaged buildings in first earthquake, had decreased by 20 percent and number of damaged ones had increased by about 20 percent after the second earthquake. Some of the collapsed buildings after the second earthquake in Van city are showed in following figures.



Figure 1.4 After M_w 7.2 heavily damaged, after M 5.6 collapsed [4]



Figure 1.5 After M_w 7.2 heavily damaged, after M 5.6 collapsed [4]

1.1 Purpose of Thesis

Multiple earthquake effects has been investigated on SDOF system by many researchers. Studies are represented behavior of SDOF in system level with hysteretic force displacement relationship. Moreover, in these studies many studies were established on MDOF system with component level based models under repeated earthquake sequences. These models can cover moment-rotation relationships, which can consider both the stiffness and strength degradation. Moreover, plasticity is assumed to be concentrated on the pre-defined plastic hinges on beam-column connections. The system level and component level based models have many insufficient features and leads to inaccurate assessment of the response of structures under multiple earthquake excitation.

Recently, a comprehensive study was conducted by Abdelnaby [5] to capture the multiple earthquake effect on the two dimensional structures considering the stiffness and strength degradation in material level. The response of the degrading and non-degrading models based on material level under multiple earthquake excitations is not fully studied in three-dimensional structures.

The object of the this thesis is investigating the response of the 3D structures under multiple earthquake effects. The material models, which were explained by Abdelnaby and Elnashai [6] is used to take into account the degradation features in material.

In addition, the effect of irregularity of the degrading and non-degrading models under multiple earthquake excitations is not compared properly yet. One of the purpose of the thesis aims to fulfill this lack. In this study, behavior of buildings, among which two of three are irregular in plan and one is irregular in elevation, were represented under multiple earthquake sequence.

2. LITERATURE REVIEW

This chapter presents on general review of the previous studies. The literature review focuses on the effect of the earthquake sequences and the degrading material models. Multiple earthquake effects has been studied by many researchers in system level based models, component level based models and rarely in material level based models. In this section firstly, the previous researches and the results were summarized on SDOF systems, which were studied in system level followed by component level based model studies on MDOF system which are described in terms of hysteretic modeling, record usage and structural modeling and finally researches on the material based models were summarized. In the last chapter of the MDOF systems, the study on the material deterioration under multiple events was represented.

2.1 Single Degree of Freedom Systems

SDOF systems were investigated such as Mahin [7], Aschheim and Black [8], Amadio et al. [9] and Hatzigeorgiu et al [10].

Mahin investigated effects of duration and aftershocks on inelastic design earthquakes [7]. Elasto-perfectly plastic model was used and P- Δ effect was considered during the analysis. Main shock and two effective aftershocks of 1972 Managua were used in this study. PGA of the main shock is 351 gal and PGA of the aftershocks are 120 and 227 gal respectively. In this study, maximum displacement ductility and energy dissipation ductility were presented with different η values, which defines the system's yield resistance divided by the product of the systems mass and peak ground acceleration.

It was observed that the first aftershock had little effect on maximum displacement ductility on the other hand, was affected more than twice on the second aftershock on maximum displacement ductility especially in low η values. The results of the study can be seen in Figure 2.1.

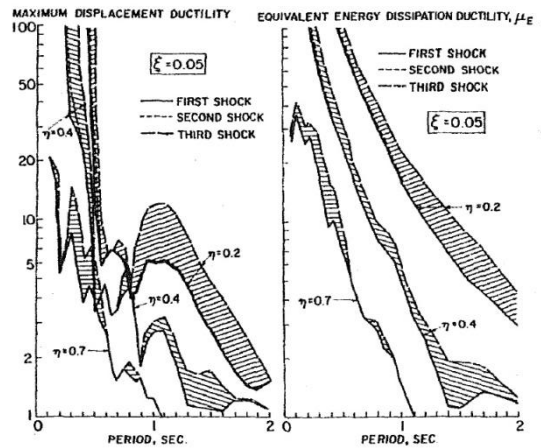


Figure 2.1 : Effects of aftershocks [7]

Aschheim and Black were the first researchers who studied the degrading systems. They examined “effects of prior earthquake damage on response of simple stiffness degrading structures” [8].

In this study, the effect of damage was investigated for three load-deformation relations. Over 20,000 SDOF oscillators were analyzed to capture the effect of prior earthquake damage on peak displacement response. First load-deformation model used in the study was standard Takeda model. The second model was standard Takeda model with negative post-yield stiffness and the last model is modified Takeda model, which considered pinched hysteretic response. The models which are considered in study were shown in Figure 2.2 and 2.3.

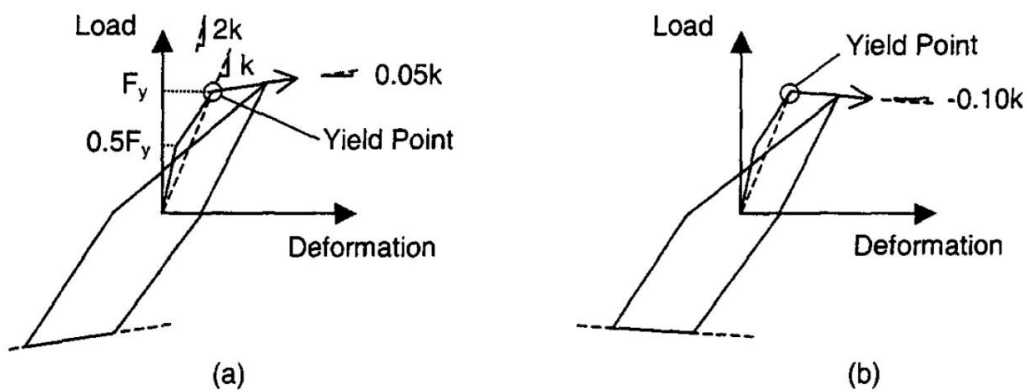


Figure 2.2 : Standard Takeda models (a) positive post-yield stiffness (b) negative post-yield stiffness [8]

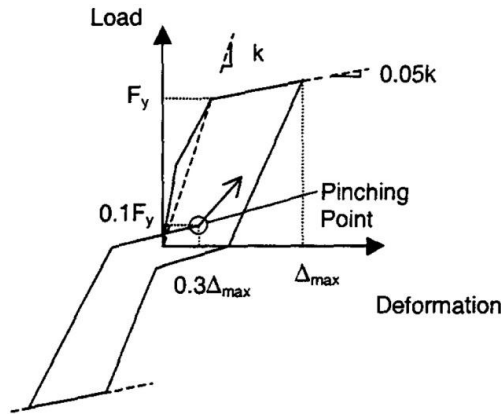


Figure 2.3 : Modified Takeda model with pinching and strength degradation [8]

The prior damage was reflected by the slope of the initial loading curve which adjusting pre-specified level of prior displacement ductility. Different prior displacement ductility values were used including 1,2,3,4 and 8. Aschheim and Black concluded that the prior damage usually has a minor effect on peak displacement response. Residual displacement resulting from the prior shaking was negligible [8]. This conclusion was observed in positive-post yield stiffness and modified Takeda model. The displacement history of the oscillators with different degrees of prior damage in modified Takeda model, was shown in Figure 2.4.

During the first five seconds, prior damage has influenced on displacement response but after the peak displacements response, the rest of the displacement history was showed that prior damage has little effect on displacement response.

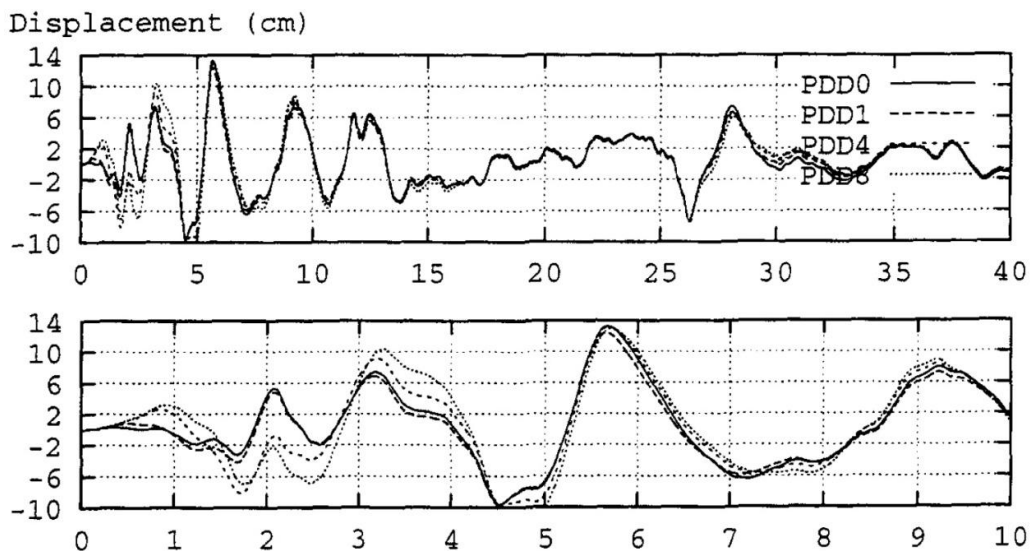


Figure 2.4 : Force-displacement response history of the oscillators having different prior damage with PDD = 0, 1, 4, 8 [8]

Amadio et al. studied the response of the SDOF system under multiple events with nonlinear behavior. Three hysteretic models including Non-degrading, degrading stiffness and degrading stiffness and strength model was considered as shown in following figure.

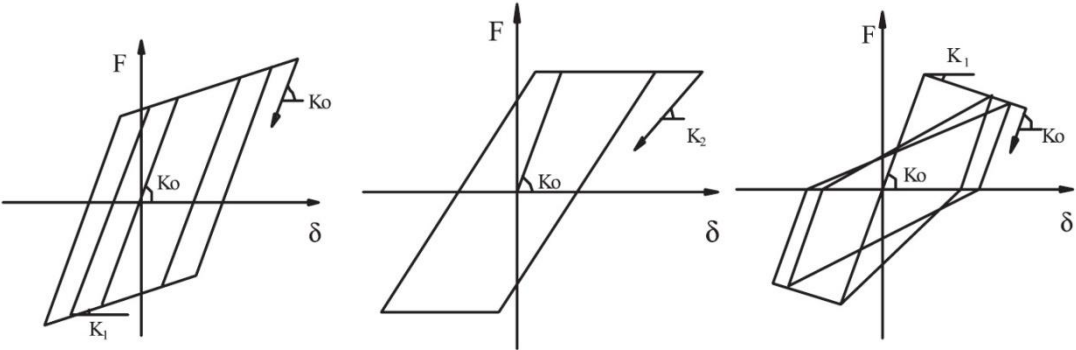


Figure 2.5 : Hysteretic models of the analyzed SDOF systems [9]

The elastic-perfectly plastic model was used with zero stiffness and strength degradation, which represents the non-degrading behavior, two degrading stiffness model were used without pinching effect and the last model considers stiffness and strength degradation on the inelastic response [9].

Two generated records, which were compatible with the Eurocode 8 spectra for stiff and soft soil respectively and El Centro earthquake record, were considered in the study. The q factor, which is defined as the ratio between the maximum accelerogram structures can withstand without collapse and first yielding on any component of structure used for the inelastic response of the models.

Amadio et al. observed that multiple excitations are induced damage accumulation and significant reduction in the q factor. Furthermore, the non-degrading model is the most vulnerable system in terms of q factor respect to degrading stiffness and degrading stiffness and strength models. Whereas reduction is more than 60% in non-degrading model, the reduction is about 53% in degrading model in terms of q factor on high ductile systems. The q3 represents the third sequence in the Figure 2.6.

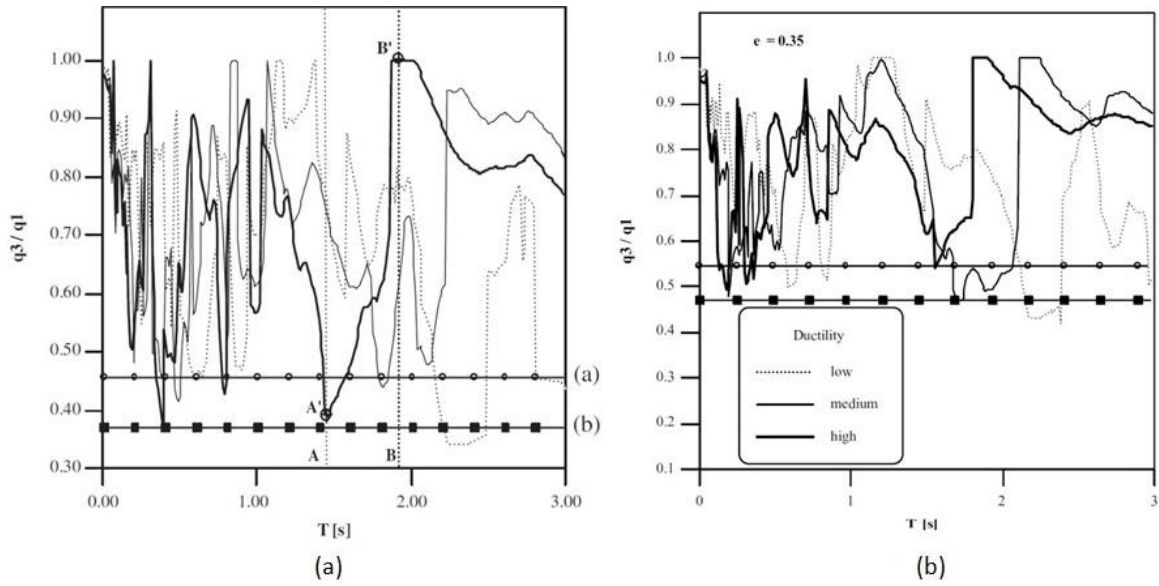


Figure 2.6 : q ratios of different hysteretic models for El Centro earthquake (a) non-degrading, (b) degrading stiffness [9]

Hatzigeorgiu et al. investigated inelastic displacement ratios for SDOF systems under repeated earthquake excitations. Effect of period of vibration, the viscous damping ratio, the post-yield stiffness ratio, the force reduction factor and the soil class on inelastic displacement ratios of SDOF were obtained with extensive parametric studies. Bilinear elasto-plastic model with hardening or softening was used in study. The considered hysteretic model is represented Figure 2.7.

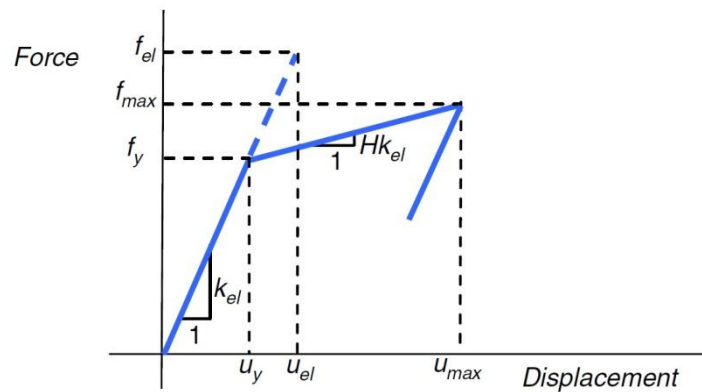


Figure 2.7 : Bilinear elasto-plastic model of SDOF used by Hatzigeorgiu et al. [10]

Four earthquake scenarios were implemented. 112 records were applied one, two and three times which can be seen in Figure 2.8 as case 1, case 2 and case 3, respectively. A result of this study demonstrated that inelastic displacement ratio is not affected significantly by

viscous damping ratio and the local soil class. Decrease of the strain-hardening ratio leads to higher inelastic displacement ratio and also, increase of force reduction factor leads to increase inelastic displacement under multiple earthquake excitations.

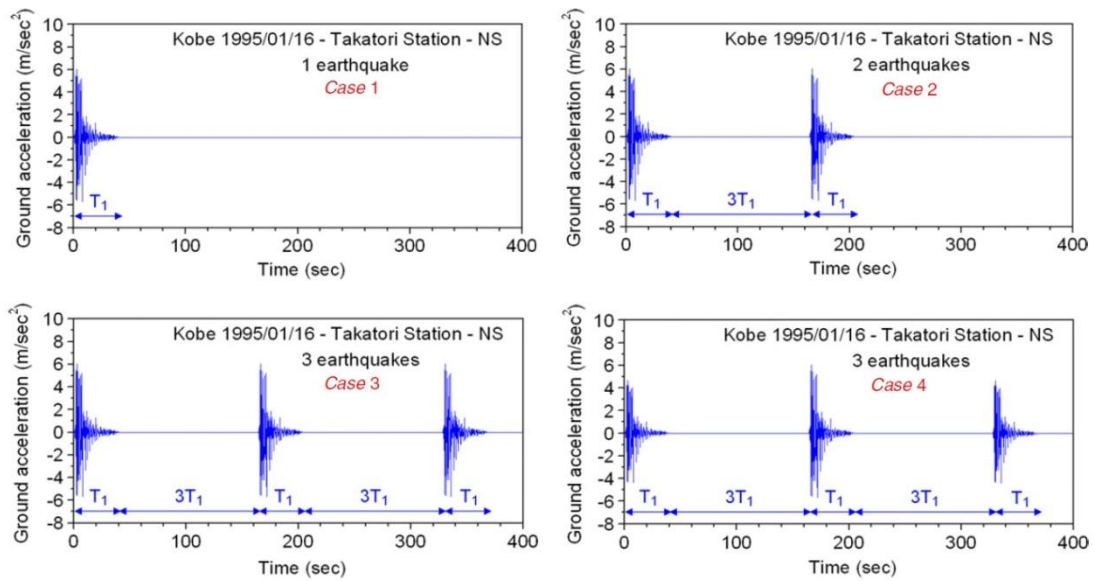


Figure 2.8 : Seismic sequence [10]

2.2 Multi Degree of Freedom Systems

The SDOF systems, which were presented in above were not represent the variation of axial load distribution on vertical load bearing components, effect of higher modes and complex behavior of the plastic hinges [5]. Researchers also added that the SDOF systems were not capable of estimating the actual response of structures under multiple excitations [9]. Therefore, component level based models in MDOF systems under multiple earthquake excitations have been widely examined. These models can cover moment-rotation relationships, which can consider both stiffness and strength degradation. Furthermore, plasticity is assumed to be concentrated on the pre-defined plastic hinge locations on beam column connections which is a disadvantage to these models.

Fragiacomo et al. examined the seismic response of steel frames under repeated earthquake ground motions [11]. In this study, three types of steel frames which are moment resisting frames with rigid joints without bracings, moment resisting frames with semi-rigid joints without bracings and a concentrically braced frames with tension-only bracing systems and hinge joints were studied. The q factor, which defined as the ratio between the maximum

accelerogram structures can withstand without collapse and first yielding on any component of structure used for the inelastic response of the models. El Centro 1940, Romania 1977 and Mexico City 1985 were considered as a recorded earthquake ground motions.

It was evaluated that the concentrically braced frames with tension only bracing systems are the most vulnerable steel structures. Reduction of the q factor in this type of frames was up to 60%. Reductions in the moment resisting frames with rigid joints were about 40% and in the semi-rigid moment resisting frames, reductions were up to 30% as seen in Figure 2.9.

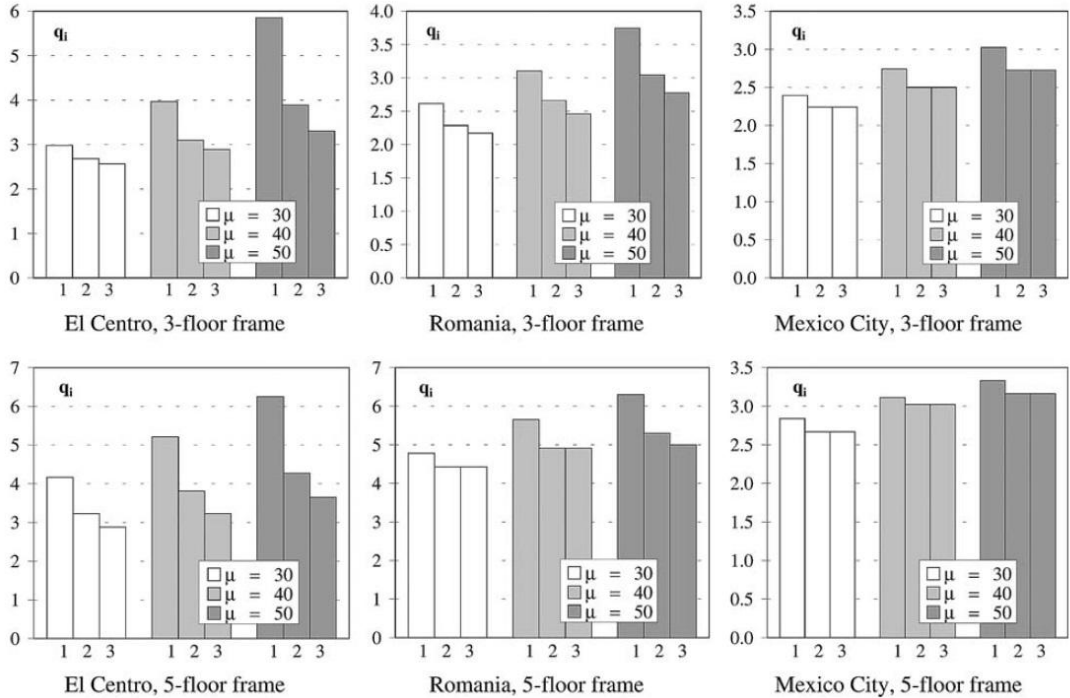


Figure 2.9 : q-factor for moment resisting frames with rigid joints [11]

Ellingwood et al. investigated the performance evaluation and damage assessment of steel frame buildings under main shock-aftershock earthquake sequences [12]. The Gutenberg/Richter formula was used to estimate main shock-aftershock sequences. Enhanced uncoupled modal response history analysis was used in the analysis of the frame [13]. SAC 20-storey building and SAC 9-storey buildings were used to evaluate the response of the steel frames. Moment rotation relationship which has been proposed by Gross [14] was used in the model of welded connections. Hysteretic model for welded connections is shown in Figure 2.10. Damage accumulation is represented as a normalized damage ratio, which is defined as the number of fractured connections divided by the total number of connections.

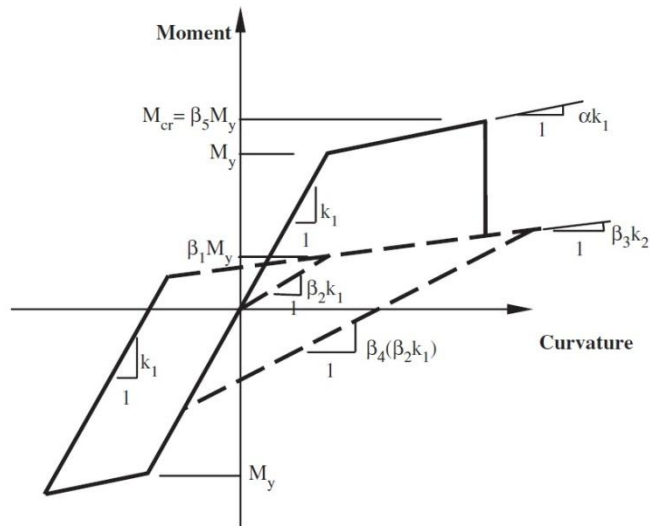


Figure 2.10 : Hysteretic model for damaged welded connection [14]

In this study, it was shown that the amplitude and frequency content of the aftershocks have a significant effect on the damage accumulation. As seen in Figure 2.11, in a replicate sequence, the additional damage ratio, which induced the main shock, was not altered due to aftershock. In randomized sequence, additional damage ratio was altered due to aftershock.

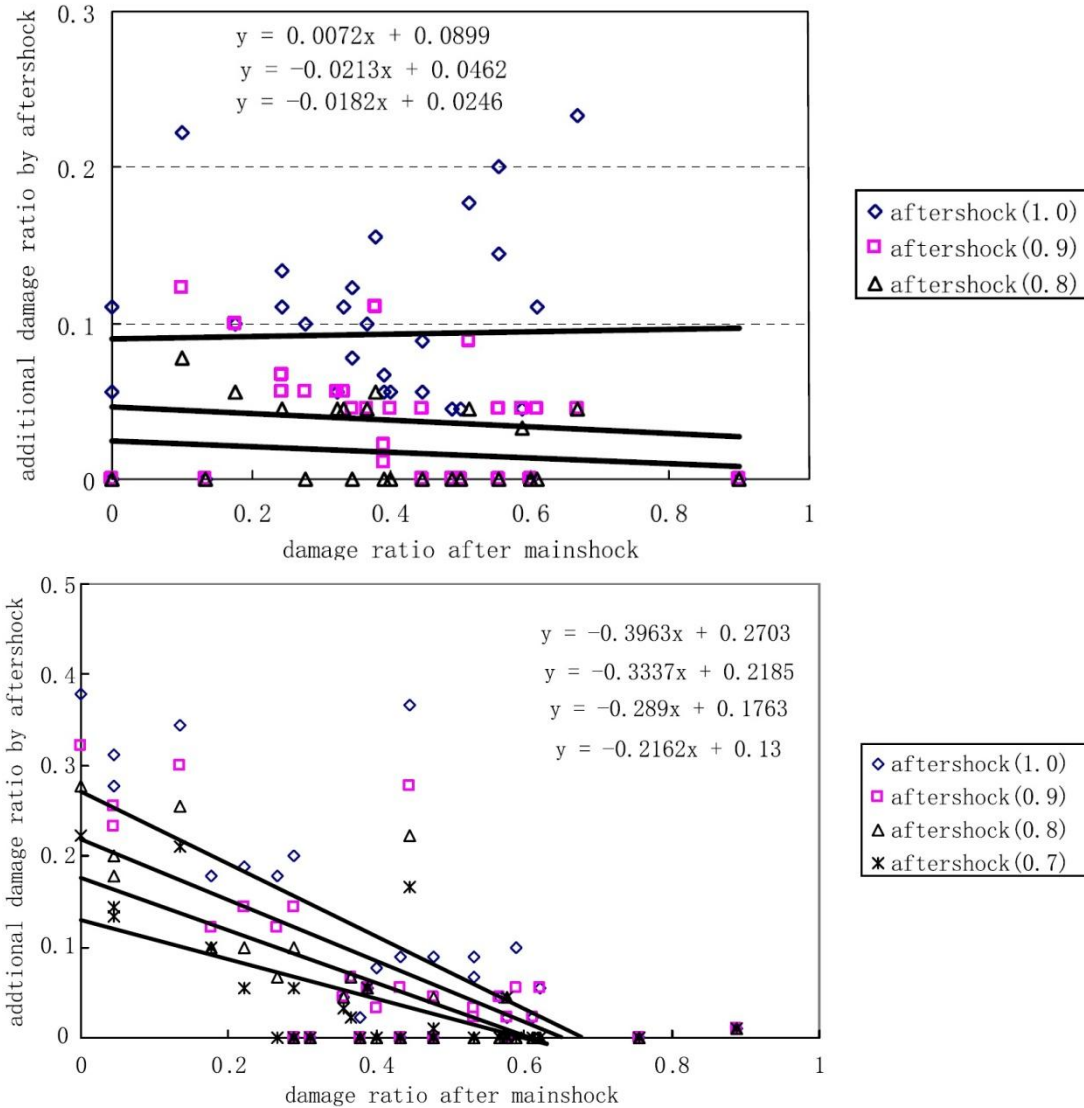


Figure 2.11 : Relationship between additional damage ratio by aftershock and the damage ratio by main shock of nine storey building, replicate aftershock (top), randomized aftershock (bottom) [12]

Hatzigeorgiu et al. studied on nonlinear behavior of reinforced concrete frames under repeated strong ground motions [15]. In this article, regular and irregular structures were examined under five real and forty artificial ground motions, which were compatible with EC 8 Type 1 Soil B spectrum. An empirical expression was proposed to estimate the ductility demand of structures under multiple earthquake sequence.

It was evaluated that the multiple earthquakes require increased displacement demand as seen in Figure 2.12 .This phenomenon should be considered to design of structures.

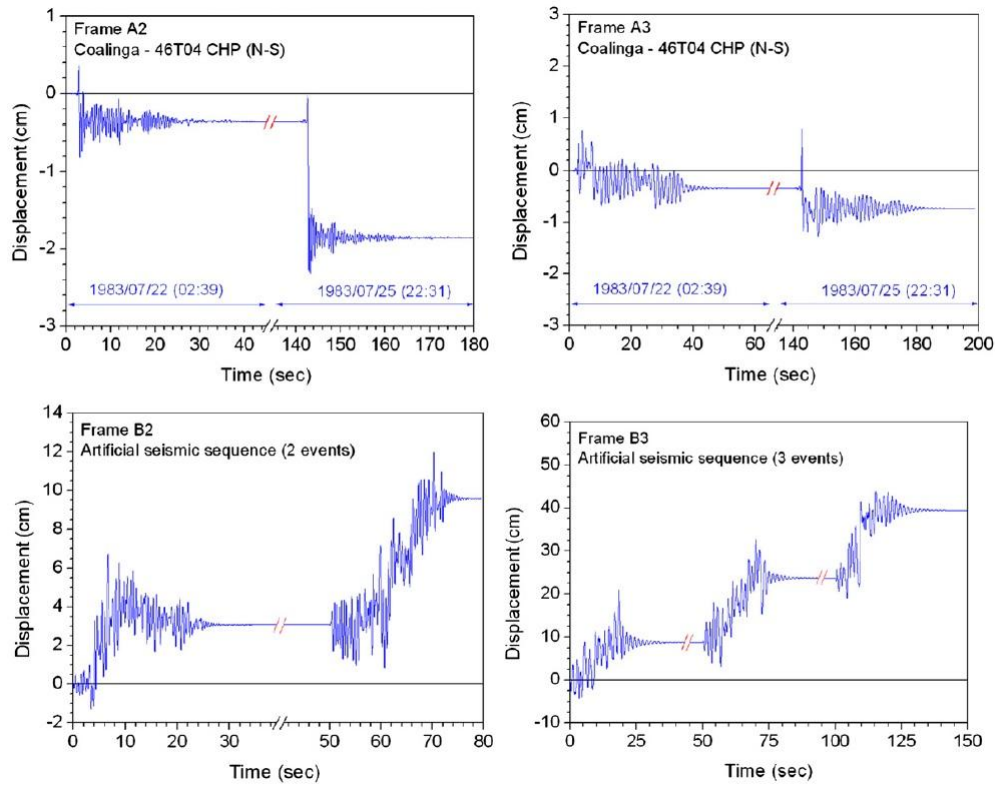


Figure 2.12 : Permanent displacements under multiple events [15]

L. Di Sarno examined the effects of earthquake sequences on inelastic response [16]. In this reference, two-storey two-bay reinforced concrete frame was used with polygonal hysteretic model (PHM). PHM was employed to model stiffness degradation, strength deterioration and pinching behavior for evaluate to inelastic response in terms of force reduction factor ratio, inelastic drift ratio and roof displacement. Force reduction factor is a ratio between elastic spectral acceleration and inelastic spectral acceleration. 11 March 2011 Tohoku earthquake sequence was selected in the study due to the existence of the many sets of records.

It was concluded that the force reduction factors for multiple excitations were 56% lower than the single excitation for FKS010 station. Ratio of force reduction factor-time graph for different stations is shown in Figure 2.13. L. Di Sarno demonstrated that the stiffness degradation, strength deterioration and moderate pinching effects should be considered to evaluate accurate inelastic response parameters [16].

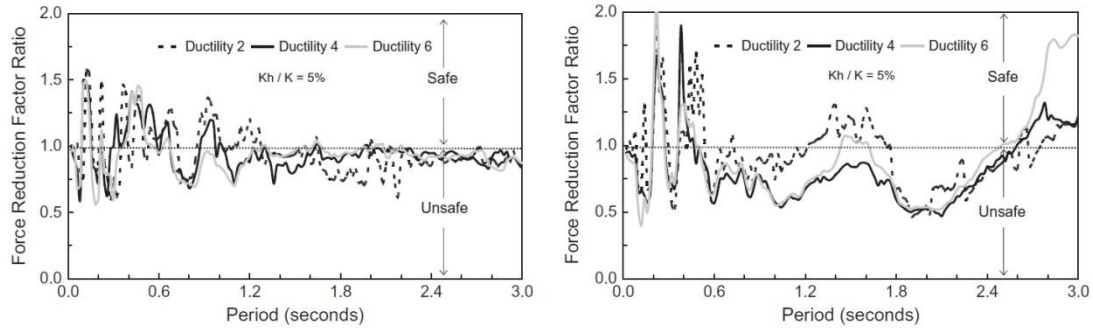


Figure 2.13 : Ratios of force reduction factor for Funehiki (left) and Hitachi (right) stations [16]

A comprehensive study was investigated in 2D structures in material level based under multiple earthquakes by Abdelnaby [5][6]. In this study, non-degrading and degrading material models were used in analysis. The non-degrading material models used in the study were bilinear stress strain relationship for steel and Mander model for concrete. Stiffness degradation and strength deterioration were considered in both steel and concrete in degrading material models. Plastic damage model [17] was used for concrete and modified Menegotto-Pinto Model [18][19] was used for reinforcing bars to consider the material deterioration. Degradation effect of the steel and concrete materials can be seen in Figure 2.14 and 2.15, respectively.

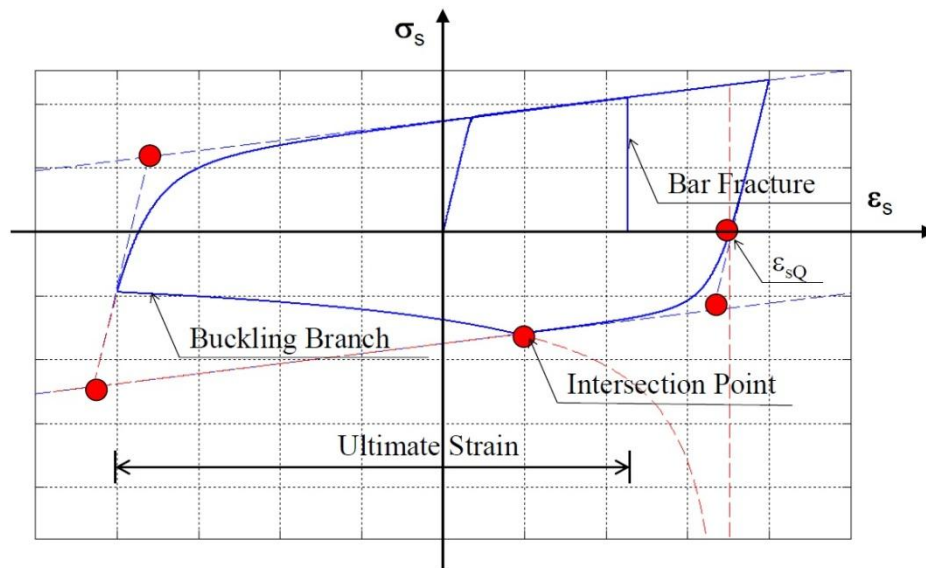


Figure 2.14 : Buckling and fracture in the degrading steel model [5]

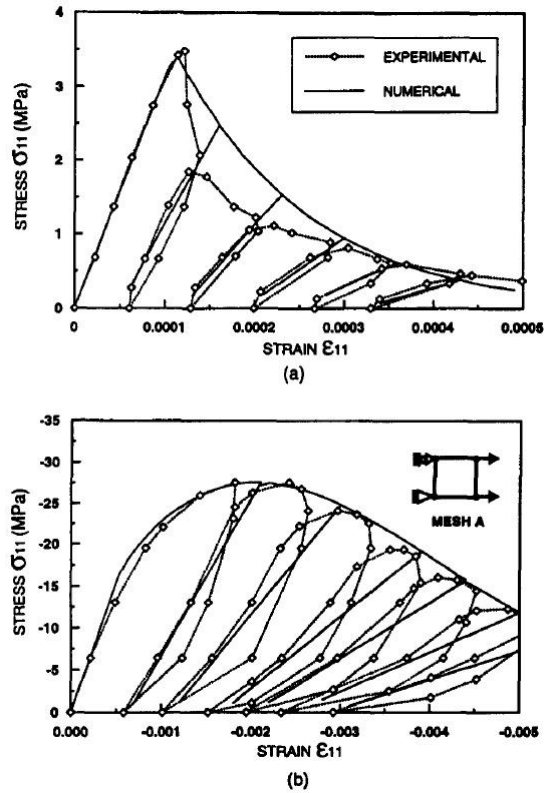


Figure 2.15 : Degrading concrete model (a) tension and (b) compression [17]

In this study, one building, which is designed with three design approaches, namely gravity, direct and capacity, was taken into account for assessment.

Random earthquake sequence and real time earthquake sequence (Tohoku earthquake and Christchurch earthquake) were used in the analyses.

It was concluded that the degrading response was not accurately specified by system level based model and component level based models [5]. Also buckling and fracture of reinforcing bars, crushing of concrete effected the deterioration of reinforced concrete structures significantly compared with yielding of steel and cracking of concrete under repeated earthquakes. As seen in following figures, response of the building was strongly influenced by stiffness degradation and strength deterioration. In Figure 2.16 and 2.17, the displacement responses of the buildings with degrading and non-degrading materials were represented.

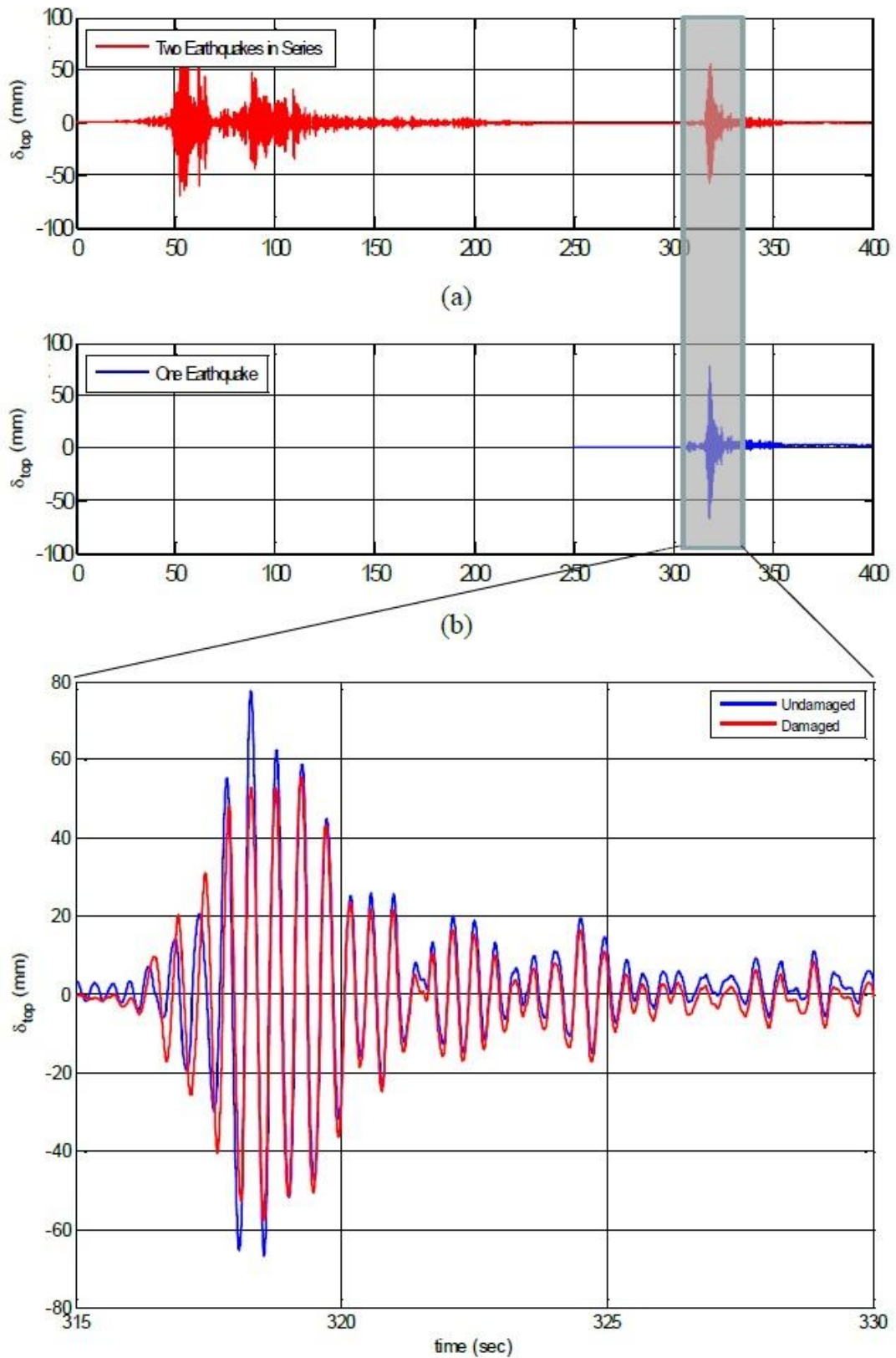


Figure 2.16 : Comparison of displacement response of damaged and undamaged non-degrading gravity frame model [5]

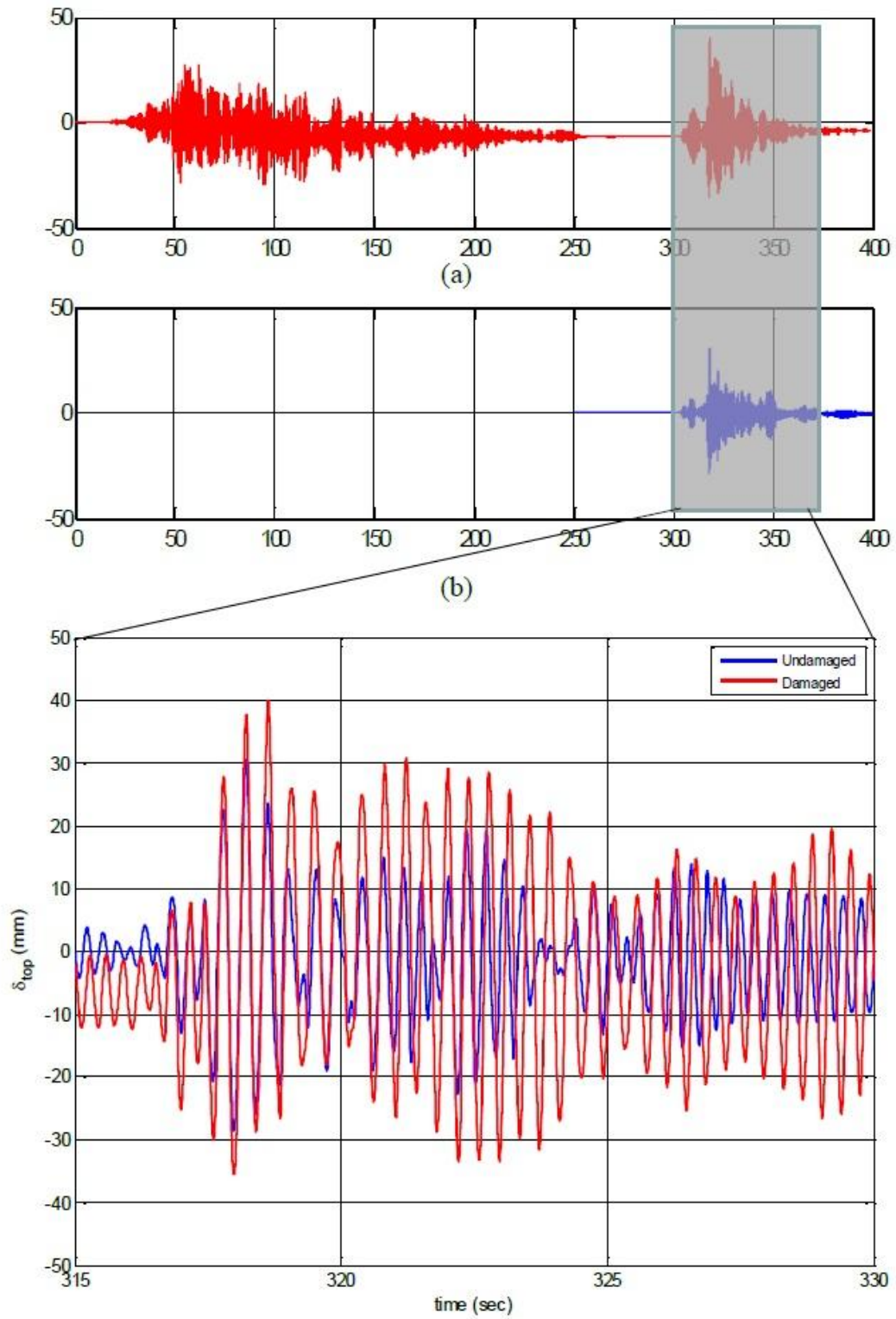


Figure 2.17 : Comparison of displacement response of damaged and undamaged degrading gravity frame model [5]

3. MODELING

3.1.1 Description of the studied buildings

In this study, three RC buildings are considered. Effects of multiple excitations are investigated on Seismic Performance Assessment and Rehabilitation of Existing Building (SPEAR), Innovative Concepts for Seismic Design of New and Existing Structures (ICON) and a real school building established in Van, Turkey.

In order to consider the seismic response of irregular RC buildings under multiple earthquake excitations, the structures are analyzed for two cases. First case corresponds where the structures are assumed to be in their original condition and the second case corresponds where the geometry is modified without altering their stiffness to achieve irregular behavior for ICON and school building, regular behavior for SPEAR building.

3.1.1.1 SPEAR building

The SPEAR structure is a full-scale building and it has been built for pseudo dynamic testing the European Laboratory for Structural Assessment (ELSA) in Ispra, Italy.

Structure was designed by Fardis [20]. It represents the buildings, which designed in 1970 Mediterranean region, without considering earthquake effect. The structure has been designed for the gravity loads alone, using the concrete design code applying in Greece between 1954 and 1995, with construction practice and materials used in Greece in early 1970's [21].

The structure is asymmetric in plan. It has three stories and two spans in both direction. All stories are 3 meter height. Design loads are 0.5 kN/m^2 for finishing and 2 kN/m^2 for live load. The plan and the elevation of the building are represented in Figure 3.1.

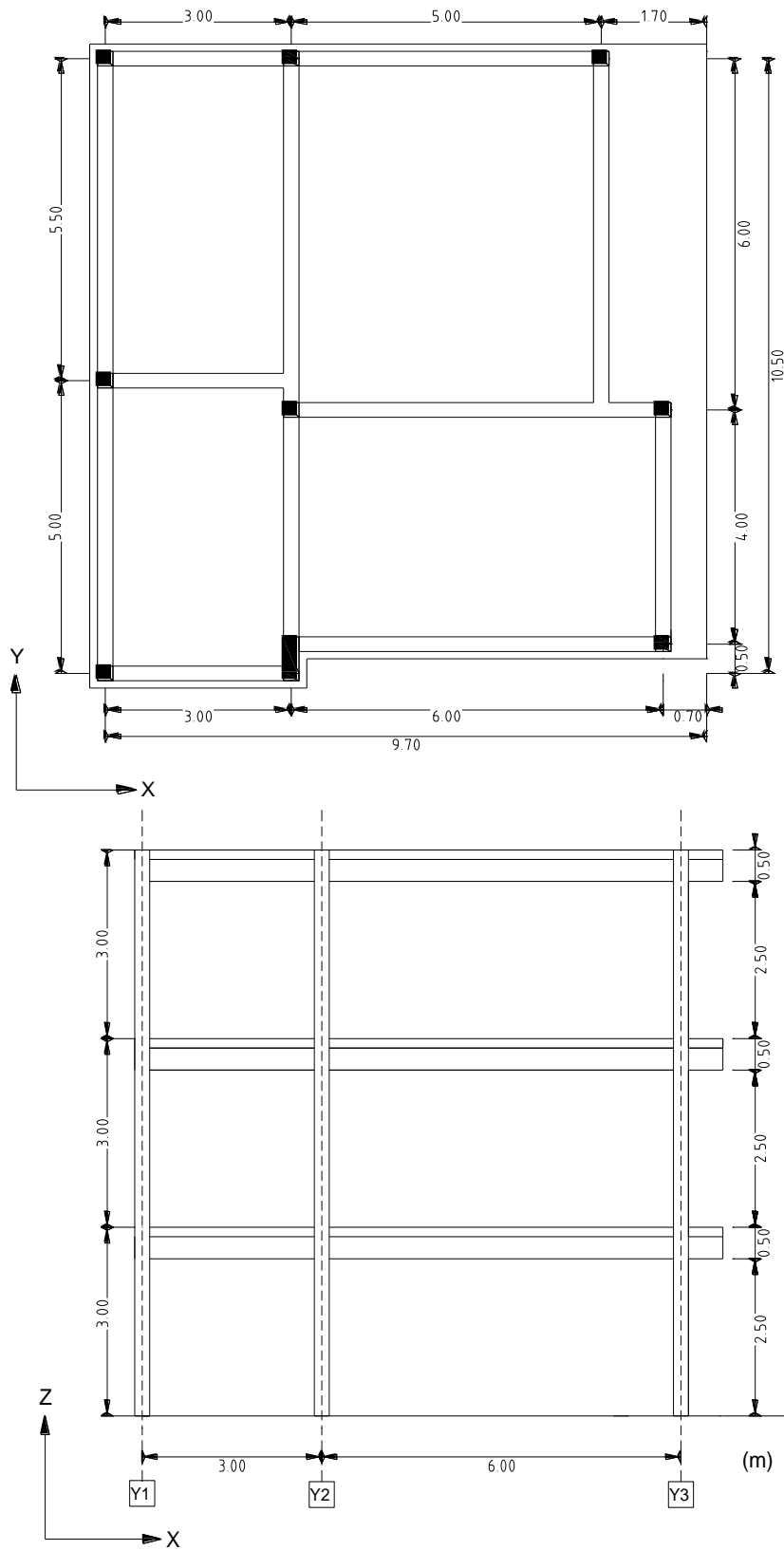


Figure 3.1 : Plan (top) and the elevation (bottom) of the SPEAR building

Slabs are 150 mm thick, cast in place monolithically and reinforced with 8 mm bars at 200 mm in both directions. The dimensions of the C6 column is 750x250 mm and all other columns are 250x250 mm. Diameter of the reinforcement bars in the columns are 12 mm and lap splice is 400 mm at floor levels. Column stirrups are 8 mm diameter and distance between the bars are 250 mm, closed with 90° hooks and not exist in the joints. All beams are 250 mm width and 500 mm depth. The top beam reinforcement consists two 12 mm bars, reinforcement bars continuously throughout beam until the end of the column and anchored with 180° hooks. On the bottom of the beam, consist two bending reinforcement bar continuously throughout the beam whereas others are bent up bar. The bottom bars could be either 12 mm or 20 mm diameter. Beam stirrups are 8 mm diameter and distance between the stirrups are 200 mm, closed with 90° hooks. All bars used in building is smooth. A complete description of the structure is presented in Appendix A. Typical column and beam cross sections are represented in Figure 3.2. Finite element (FE) model of the considered building is represented in Figure 3.3.

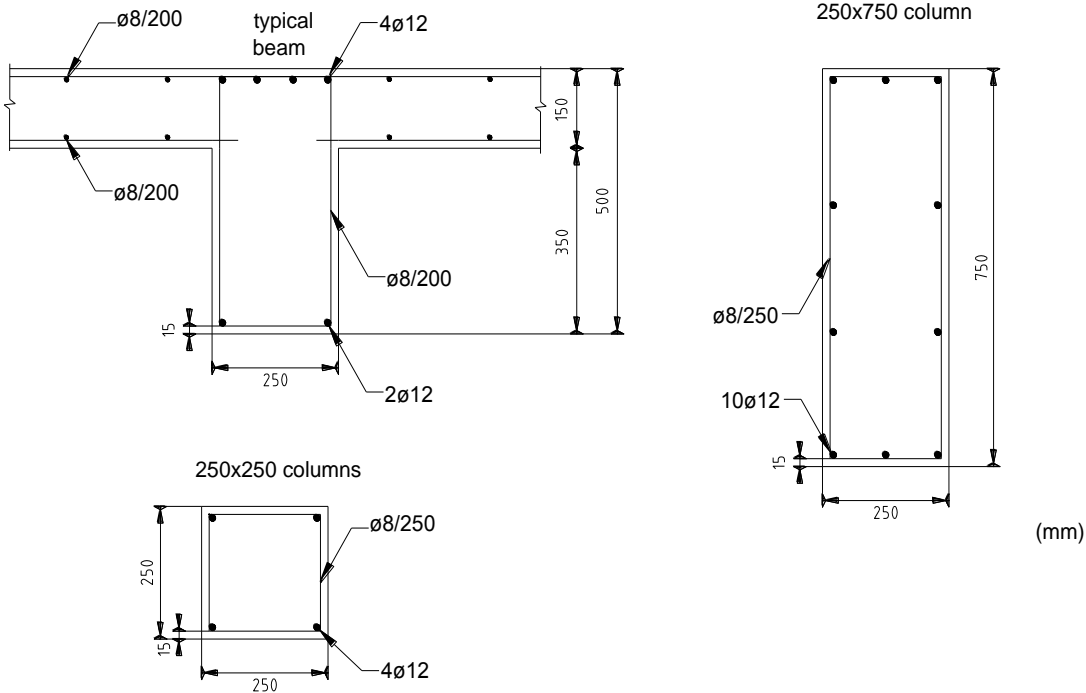


Figure 3.2 : Typical column and beam cross sections

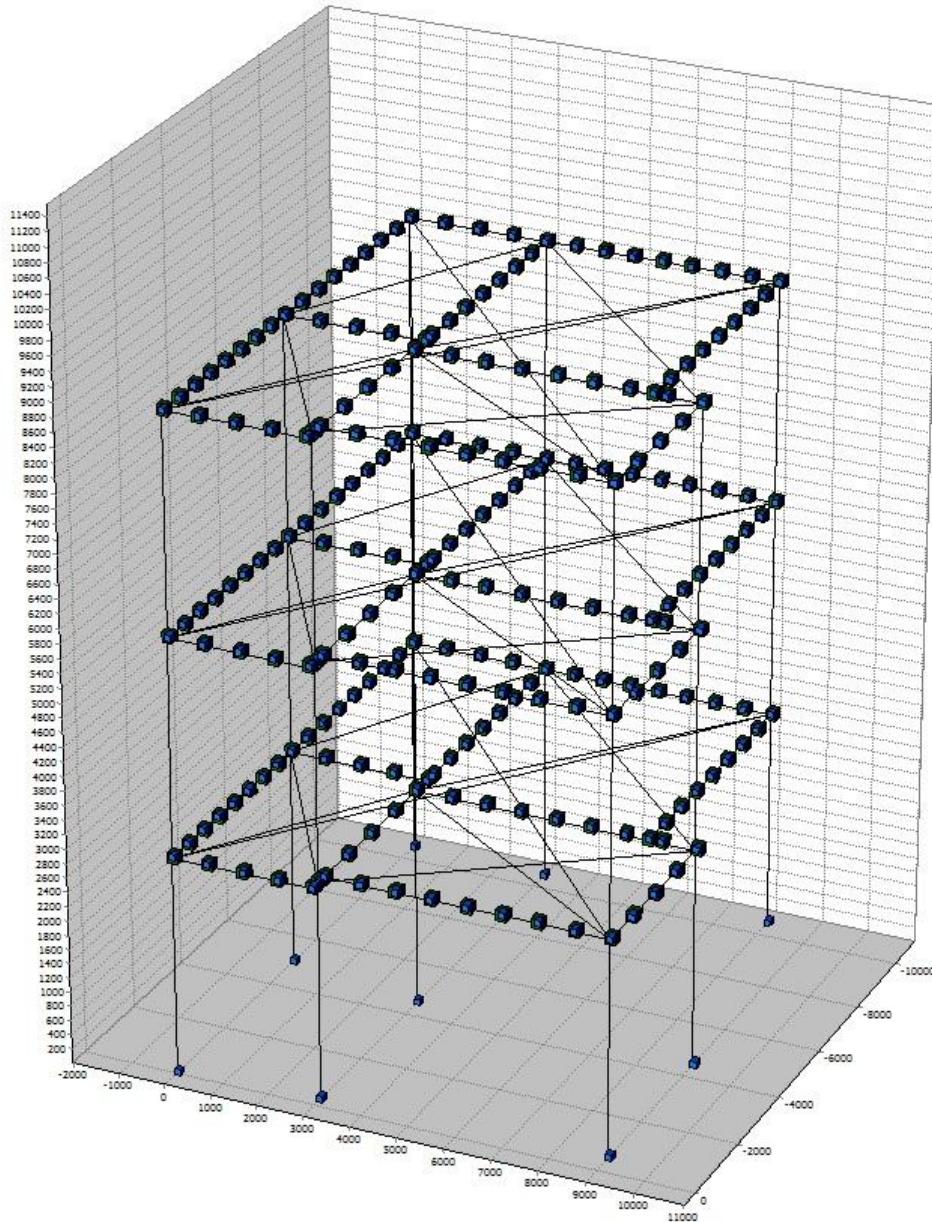


Figure 3.3 : FE modeling of SPEAR building

Compressive strength of the concrete is 25 MPa and yield strength of the reinforcement rebar is 400 MPa [22][23].

Table 3.1 : Material characteristics of SPEAR building

Compressive strength of concrete (f_c)	Yield strength of steel (f_y)
25 N/mm ²	400 N/mm ²

3.1.1.2 Regular case of SPEAR building

According to EC 8, the structural eccentricity e_0 and the torsional radius r shall be in accordance with the two conditions [24].

$$e_{ox} \leq 0.30 \cdot r_x \tag{3.1}$$

$$r_x \geq l_s \tag{3.2}$$

Three column dimensions were modified to classify the structure as regular in plan. The column C6 dimensions of which is 25x75 cm, C7 dimensions of which is 25x25 and C8 dimensions of which is 25x25 were modified to 25x65 cm, 25x50 cm and 25x35 cm, respectively. The locations of the replaced columns are shown in Figure 3.4.

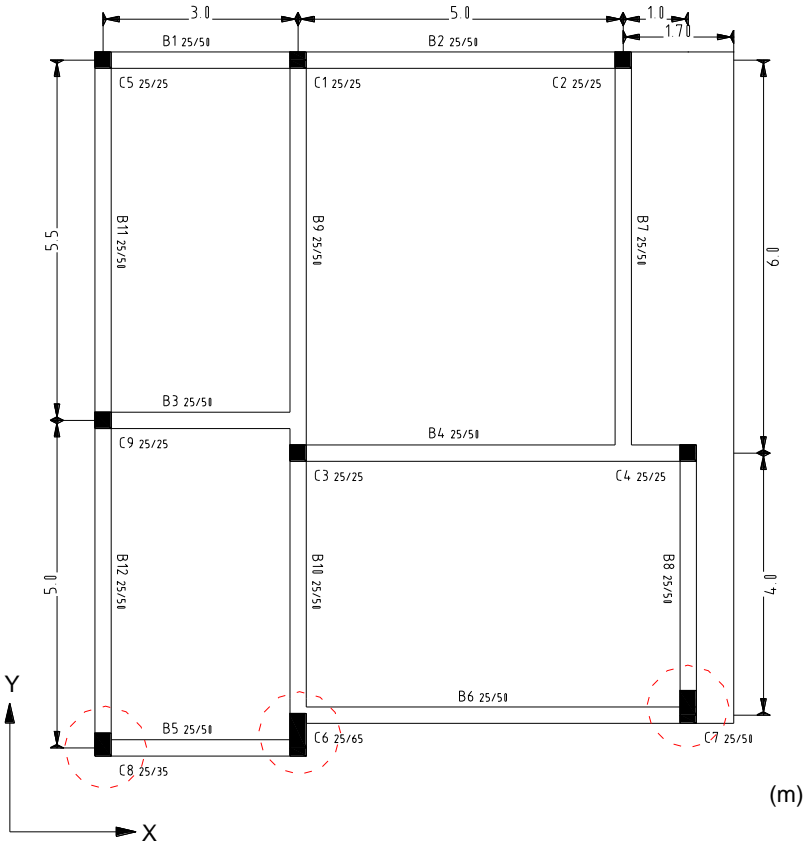


Figure 3.4 : Regular plan of SPEAR building. Modified columns are marked with red circle.

While the building modified to the regular case to determine the irregularity effect, the lateral stiffness of the building did not change. The total lateral stiffness ratio of the regular to irregular buildings in y direction was 2 percent. The structural eccentricity e_{0x} is reduced to 0.23 m and it is lower than the $0.3 r_x$.

The torsional radius is not greater than the radius of gyration of the floor mass in plan hence it does not provide the formula 4.1b in EC8. To provide formula 4.1b in EC8, lateral stiffness of the building is needed to increase substantially however any variance of the lateral stiffness is not requested. This situation was ignored depending on actual lateral stiffness of the building. Characteristics of the regular and irregular case of SPEAR building can be seen in Table 3.2

Table 3.2 : Torsional characteristics and the lateral stiffness of the regular and irregular case of SPEAR building in Y direction

	$e_{o,x}(m)$	$r_x(m)$	$l_s(m)$	$0.3r_x(m)$	$k_y(kN/m)$
Regular	0.23	1.86	4.38	0.55	148958
Irregular	1.31	1.45	4.38	0.43	151909

3.1.2 ICON structure

The ICON (Innovative Concepts for Seismic Design of New and Existing Structures) structure is a full-scale reinforced concrete frame, have been built for pseudo dynamic testing the European Laboratory for Structural Assessment in Ispra, Italy. General view of the building, which is constructed, was shown in Figure 3.5.

Structure was designed for gravity loads by Carvalho et al. [25] and represented the typical design and construction practice in most South-European countries in 1950's. Structure has four stories and three bays in one direction. Two of the bay are 5 meter span and one of it is 2.5 meter span. Story height is 2.7 meter. Slab thickness is 150 mm. All the main beams are 250 mm width and 500 mm depth while the transverse beams are 200 mm width and 500 mm depth [26]. One of the columns is lying on its stronger axis while the others are lying on their weak axis. Detailed description of the building is represented in Figure 3.6 and 3.7.



Figure 3.5 : General view of the structure

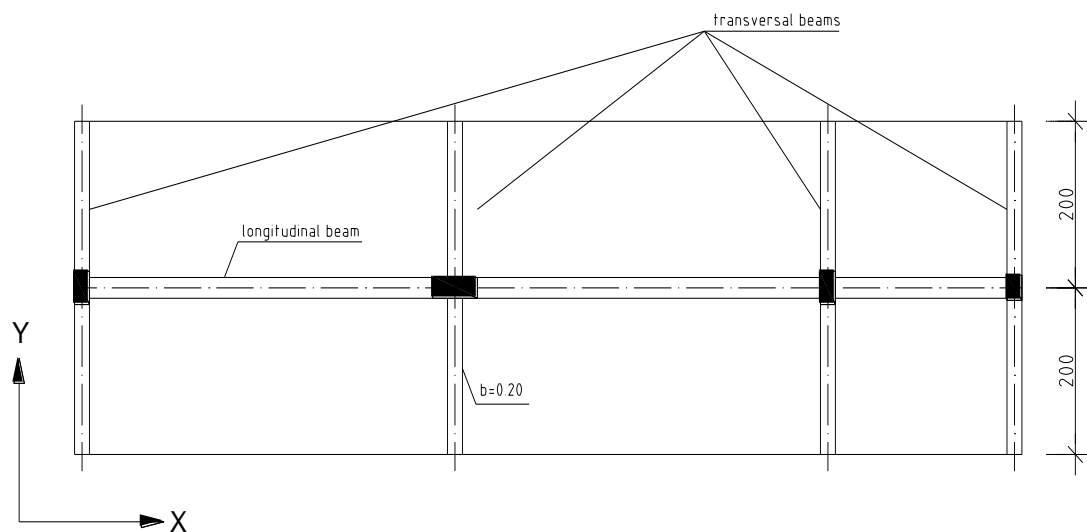


Figure 3.6 : Plan of the ICON building

The column lap splice is 700 mm in all stories. Column stirrups are 6mm diameter and distance between bars are 150 mm, closed with 90° hooks and not exist in the joints. Main beam stirrups are 8 mm diameter and distance between bars 200 mm, closed with 90° hooks. All bars used in building are smooth. Detailed column and beam cross sections are represented Figure 3.8. A complete description of the structure is presented in Appendix B.

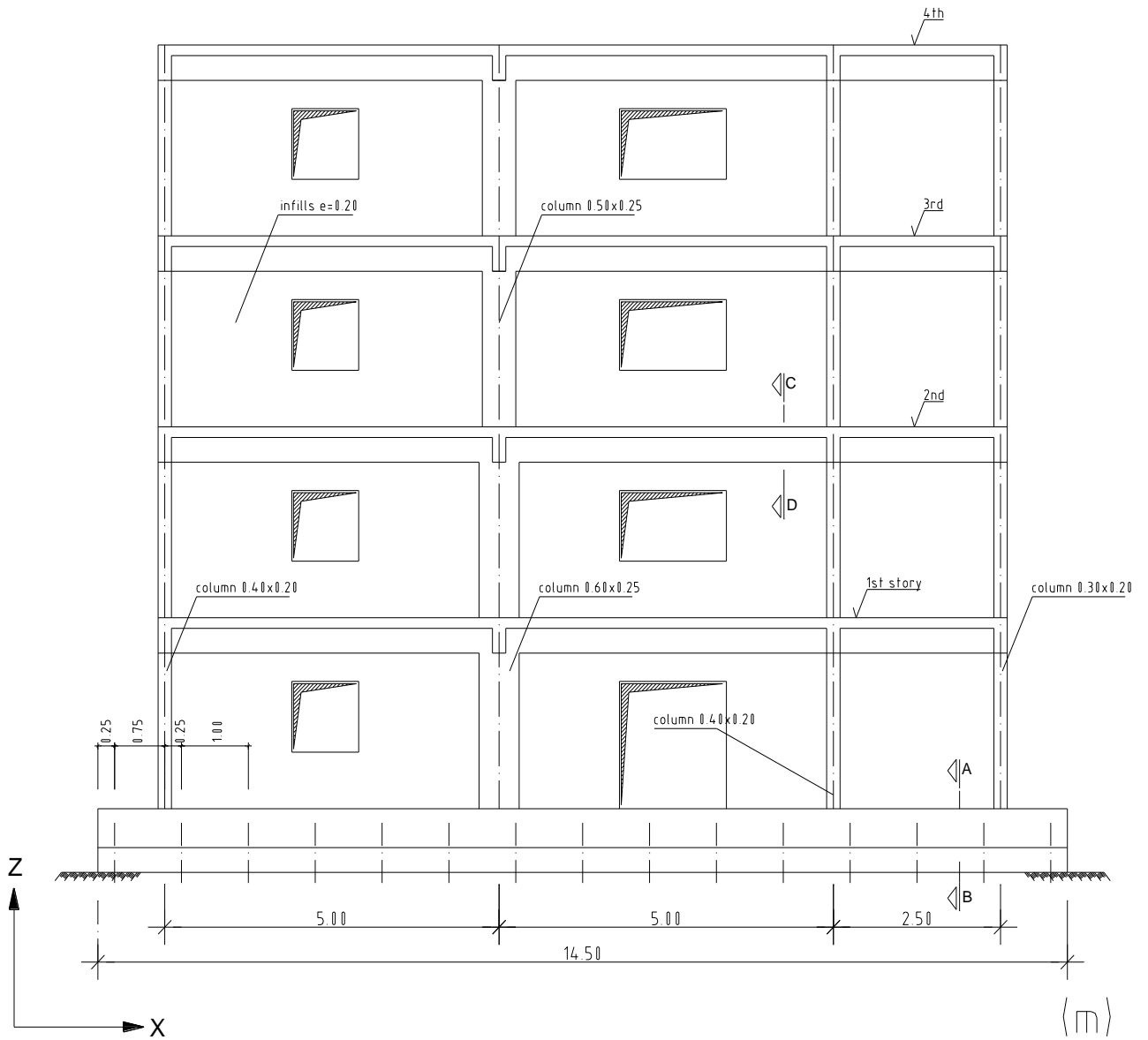


Figure 3.7 : Elevation of ICON building

Finite element model of the considered building, which is formed using Zeus-NL, is represented in Figure 3.9.

Story	1	2	3	4
4	<p>6Ø12 0.40 0.20 stir.Ø6//0.15</p>	<p>4Ø16+2Ø12 0.25 0.50 stir.Ø6//0.15</p>	<p>6Ø12 0.40 0.20 stir.Ø6//0.15</p>	<p>6Ø12 0.30 0.20 stir.Ø6//0.15</p>
2	<p>6Ø12 0.40 0.20 stir.Ø6//0.15</p>	<p>8Ø16+2Ø12 0.25 0.60 stir.Ø6//0.15</p>	<p>8Ø12 0.40 0.20 stir.Ø6//0.15</p>	<p>6Ø12 0.30 0.20 stir.Ø6//0.15</p>
0				

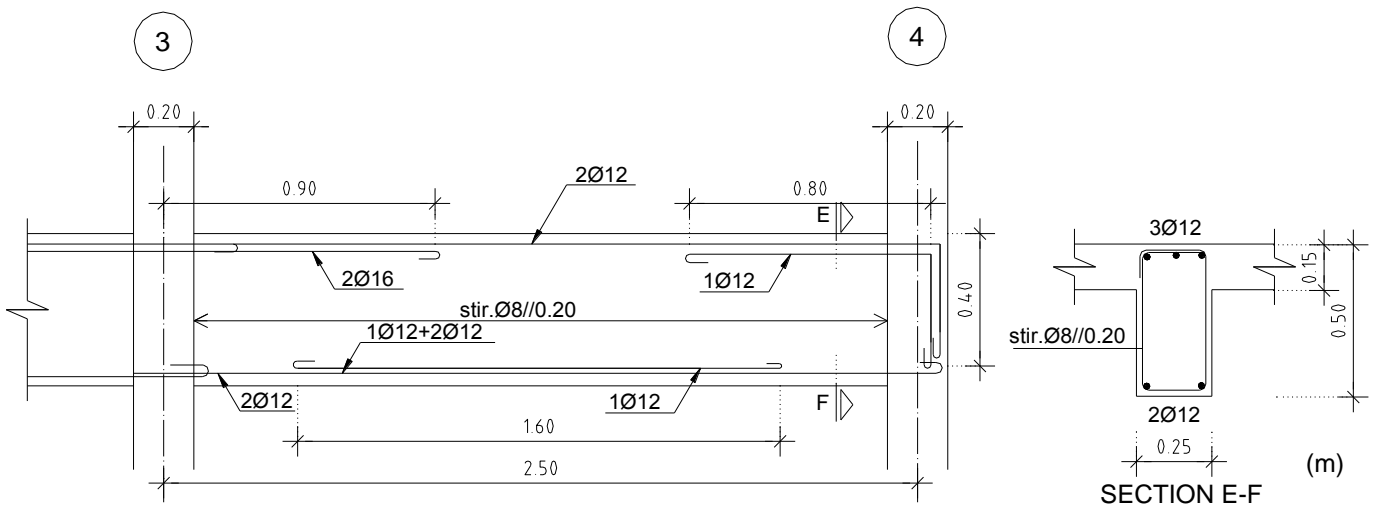


Figure 3.8 : Column and beam cross sections

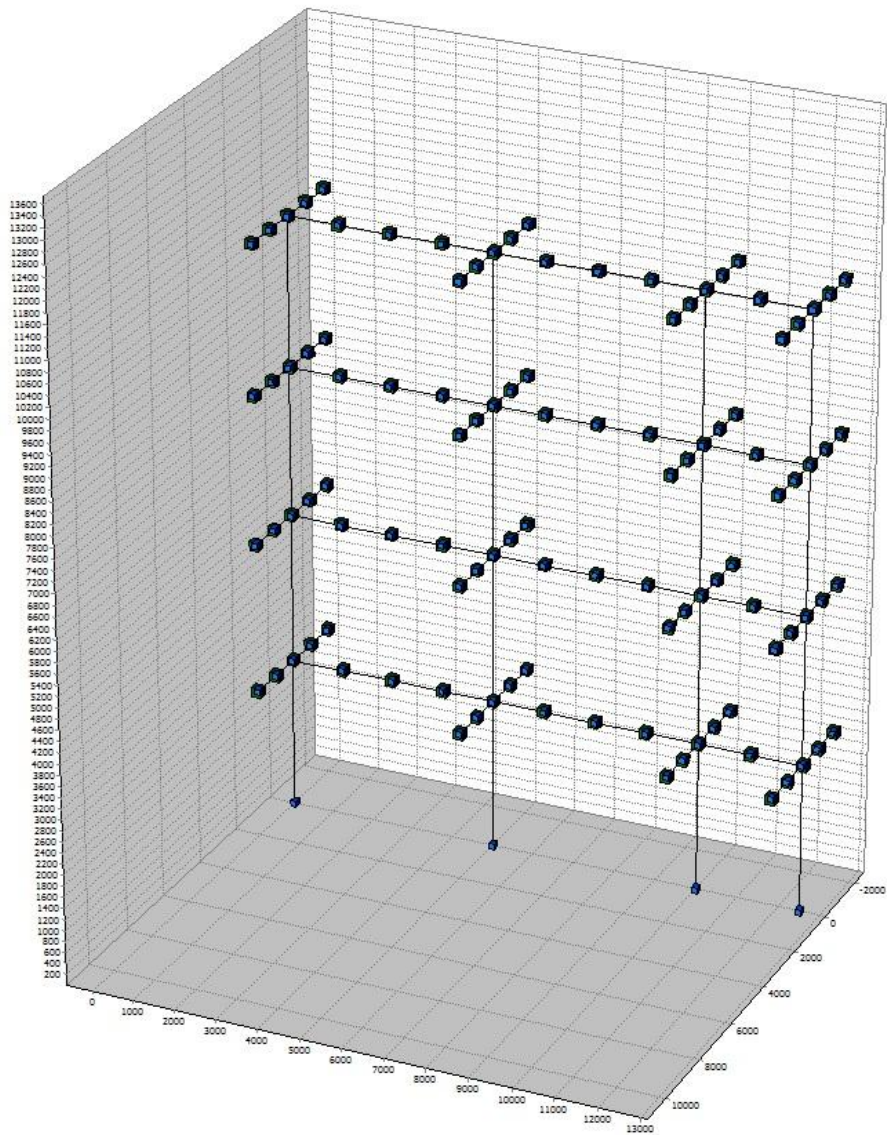


Figure 3.9 : FE modeling of ICON building

Compressive strength of the concrete is 16.3 MPa and yield strength of the reinforcement rebar is 343 MPa [27].

Table 3.3 : Material characteristics of ICON building

Compressive strength of concrete (f_c)	Yield strength of steel (f_y)
16.3 N/mm ²	343 N/mm ²

3.1.2.1 Irregular case of ICON building

ICON structure was modified as irregular in elevation. The individual setbacks shall not be greater than 10% of the previous plan dimension according to EC8 [24]. Top column in 1 axis, beams and slabs between the 1 and 2 axis were removed to provide the irregularity in elevation. The setback of the building was 40% in fourth story. The elevation, plan and FE model of the remodeled building were represented in Figure 3.10 and 3.11, respectively.

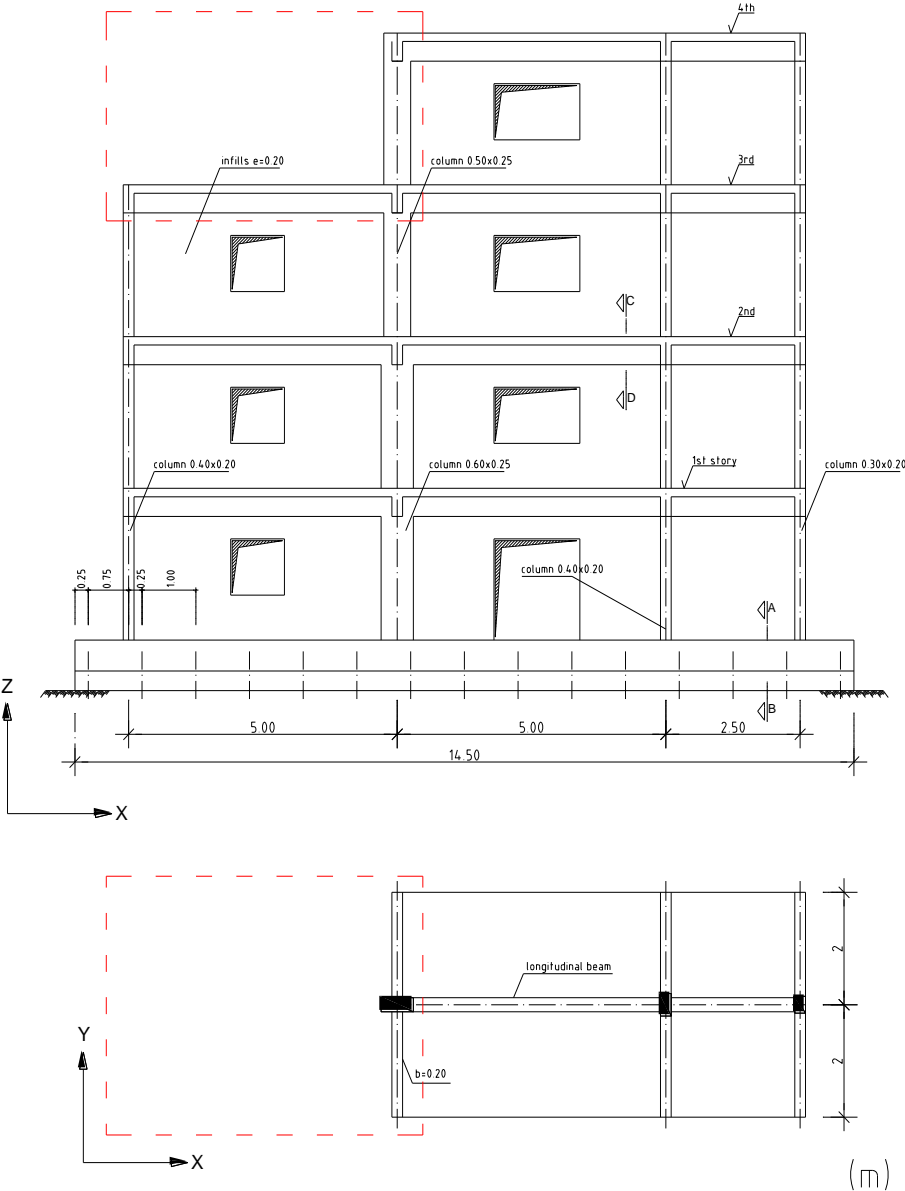


Figure 3.10 : Elevation (top) and plan (bottom) of the fourth story of ICON building

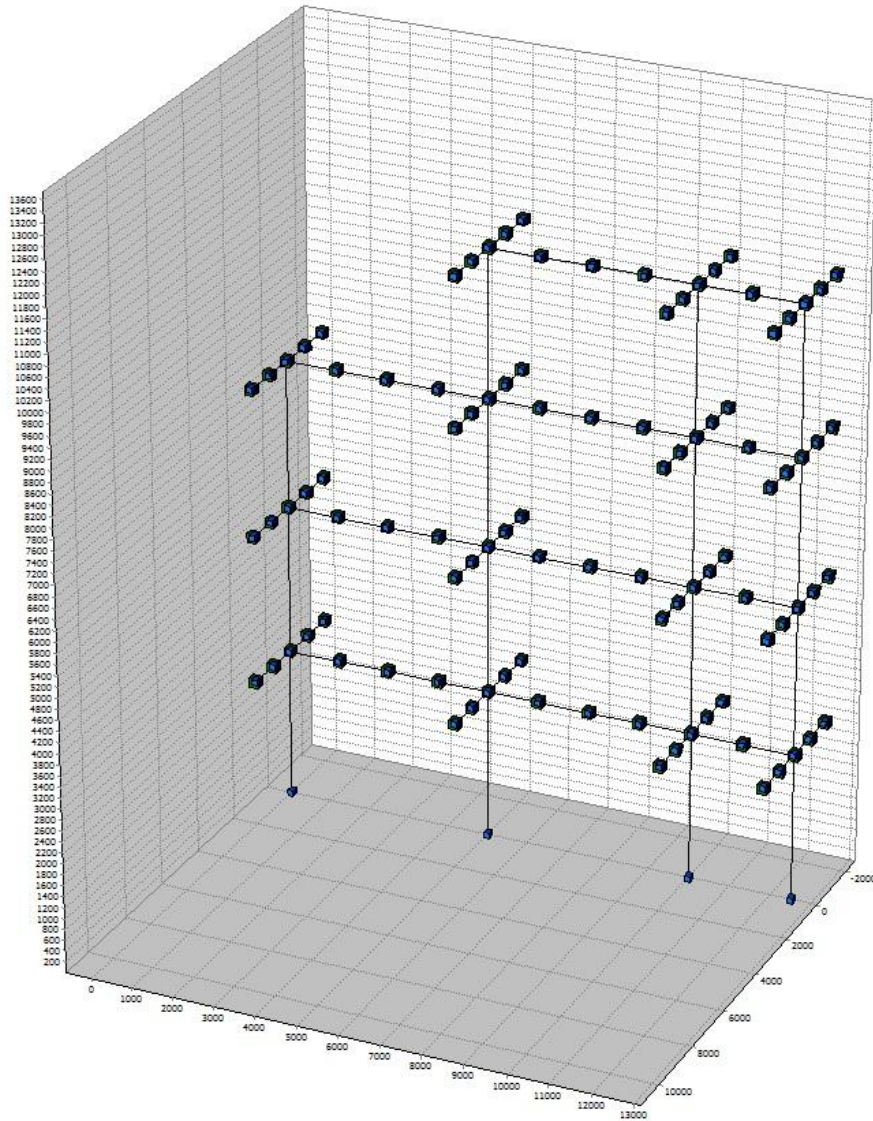


Figure 3.11 : FE modeling of the irregular case of ICON building

3.1.3 School building

Structure was designed according to TEC 1975 and built in 1995. The structure was built in Van province in Turkey. It was damaged during the 2011 Van Earthquake. The structure has three stories. While the basement floor is 3.5 meter height, the upper ones are 3 meter height. Slab thickness is 150 mm. All the beams are 300 mm width and 600 mm depth. Typical floor plan of the structure represented Figure 3.12.

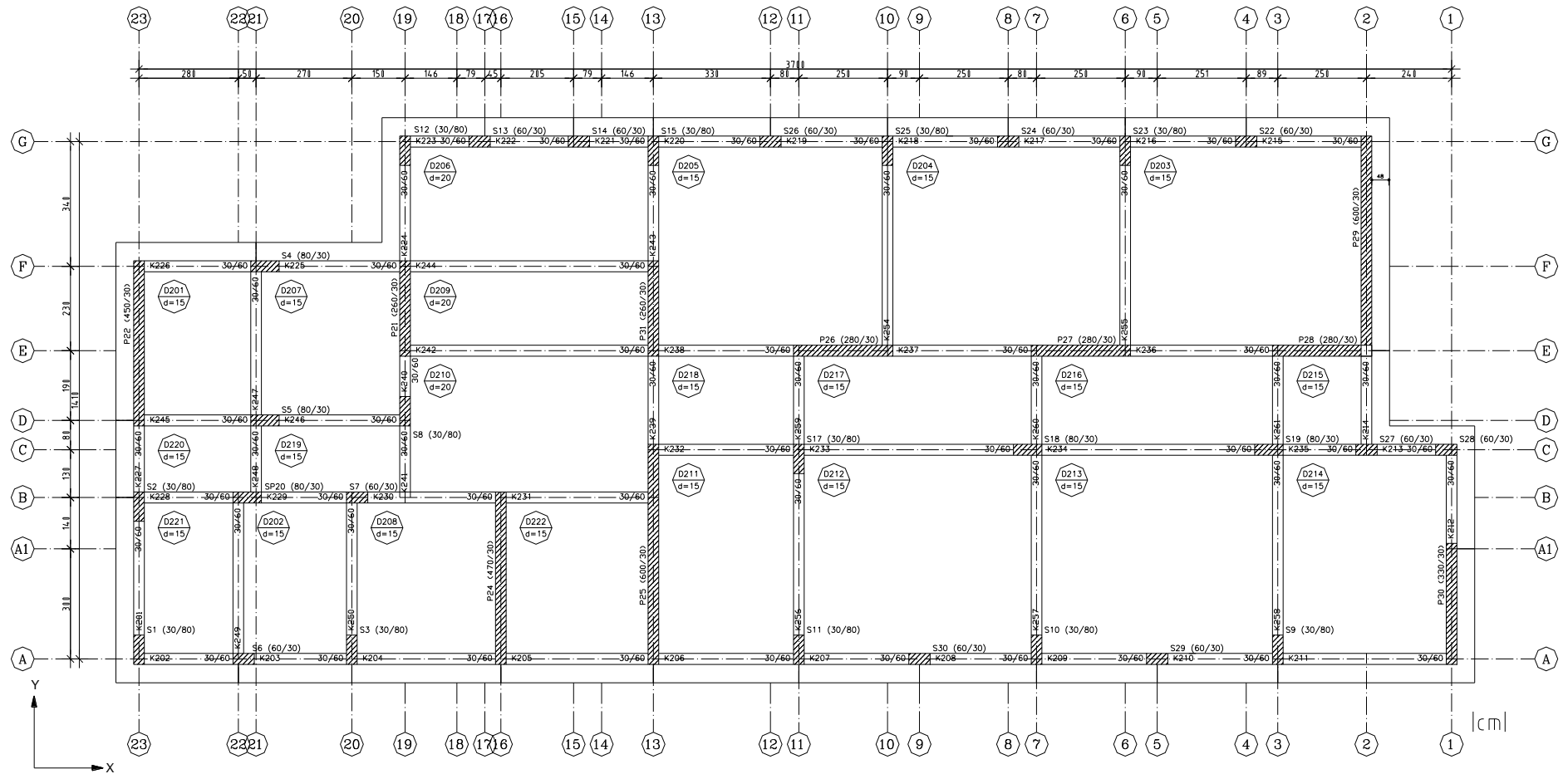


Figure 3.12 : Typical floor plan of the school building

Stirrups exist in the joints and also confinement zone exists in the reinforcement elements. All the stirrups in elements are closed with 135° hooks. All the bars used in building are deformed reinforcing steel rebars. Typical column-beam cross sections and the FE model of the building are shown in Figure 3.13 and 3.14.

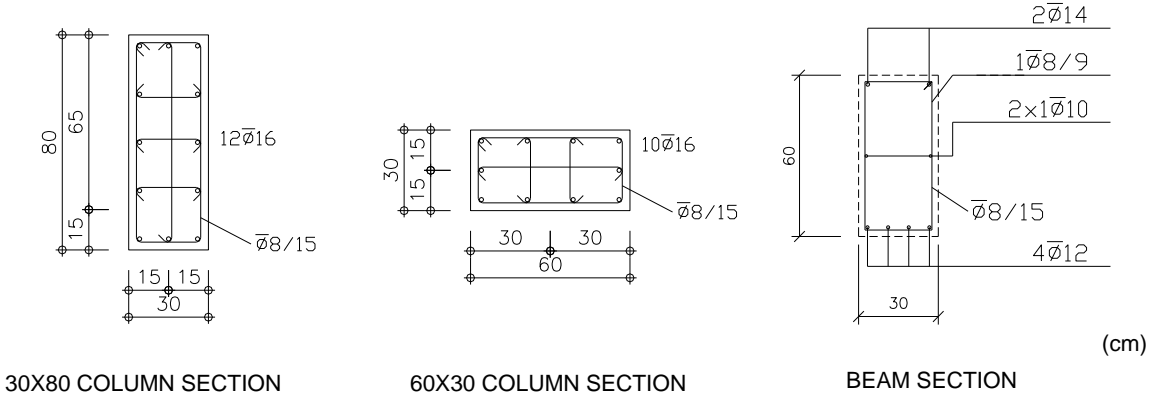


Figure 3.13 : Typical column beam cross sections

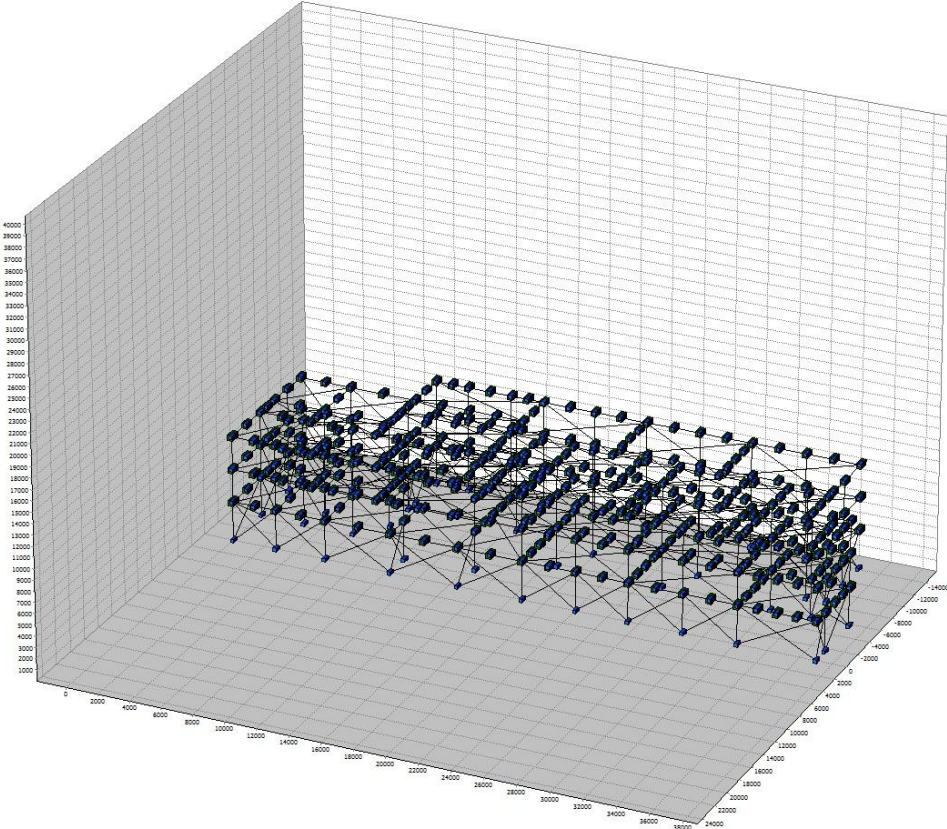


Figure 3.14 : FE modeling of school building

Compressive strength of the concrete is 20 MPa and yield strength of the reinforcement rebar is 420 MPa.

Table 3.4 : Material characteristics of school building

Compressive strength of concrete (f_c)	Yield strength of steel (f_y)
20 N/mm ²	420 N/mm ²

3.1.3.1 Irregular case of the School building

School building is regular in plan. According to TEC 2007, torsional irregularity factor η_{bi} which is defined for any of the two orthogonal earthquake directions as the ratio of the maximum relative storey drift at any storey to average relative storey drift at the same storey in the same direction, is provide following formula [28].

$$n_{bi} = (\Delta_i)_{\max} / (\Delta_i)_{avr} > 1.2 \quad (3.3)$$

Three shear walls, which are located in E axis, was replaced to columns which are located in G axis and the eccentricity of the building was increased. The η_{bi} value calculated as 1.21 in remodeled case. Hence, the structure was classified as irregular in plan according to TEC 2007. Locations of the replaced shear walls and columns are shown in Figure 3.15.

Table 3.5 : Torsional characteristics and the lateral stiffness of the regular and irregular case of school building in X direction

	η_{bi}	$k_x(kN/m)$
Regular	1.06	23074178
Irregular	1.21	23074178

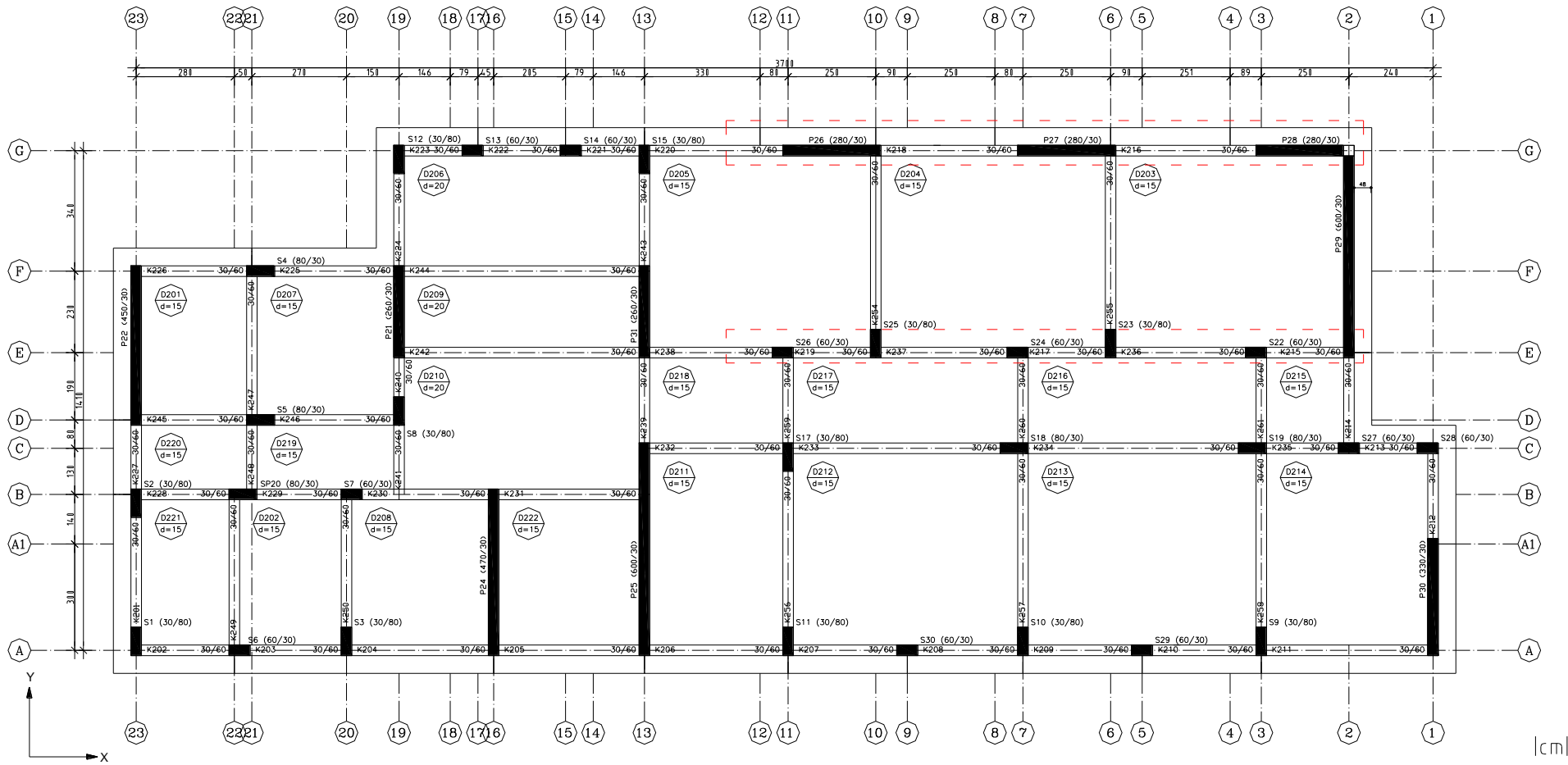


Figure 3.15 : Irregular case of the school building

3.2 Material Models

Two different material models are presented in this chapter. These are degrading and non-degrading material models. The non-degrading models are used Mander [29] (con2) for concrete and bilinear stress-strain relationship (stl1) for steel. Modified Menegotto-Pinto steel model [18] [19] (stl4) and plastic concrete model [17] (con5) is used for degrading features. Detailed description of the models is represented in the following chapters.

3.2.1 Concrete models

3.2.1.1 Uniaxial constant confinement concrete model

Uniaxial constant confinement concrete model is based on the Mander model [29]. The model is defined by compressive strength of unconfined concrete, tensile strength, crushing strain and a confinement factor. This model assumes that constant confinement is in concrete. The model is employed for the represent the behavior of non-degrading concrete. Figure 3.16 simulates the characteristic of the model (con2). Characteristics of Mander model are determined with compressive strength (f_c), tensile strength (f_t), crushing strain (ϵ_{cu}) and confinement factor. The characteristics of the con2 model were represented in the Figure 3.16.

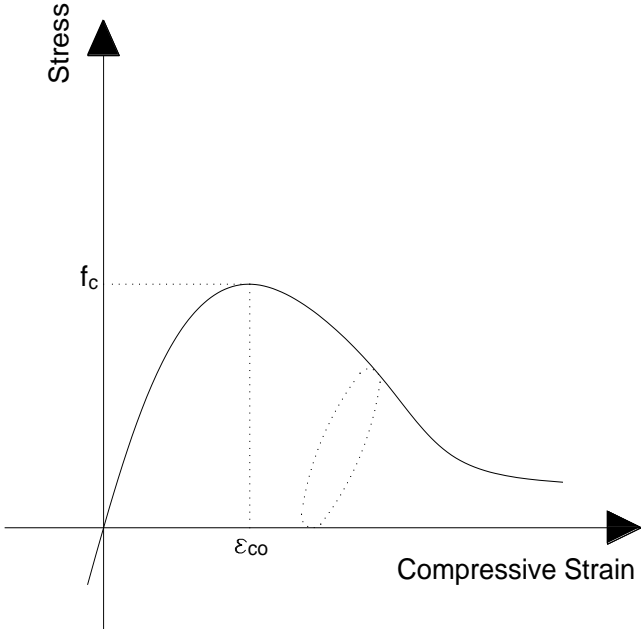


Figure 3.16 : Uniaxial constant confinement model (con2)

3.2.1.2 Plastic damage concrete model

This model was implemented by Abdelnaby [5] into the ZEUS-NL source code with using the concepts of fracture-energy-based damage and stiffness degradation in continuum damage mechanics developed by Fenves et al [18]. Different two variables were defined for damage stages under tensile and compressive stress independently. A thermodynamically consistent scalar model is used to determine the stiffness degradation. It indicates the pinching effect (crack opening and closure). The elasto-plastic response is identify effective stress and damage variable. The experimental and numerical results of the concrete model were shown in Figure 3.17.

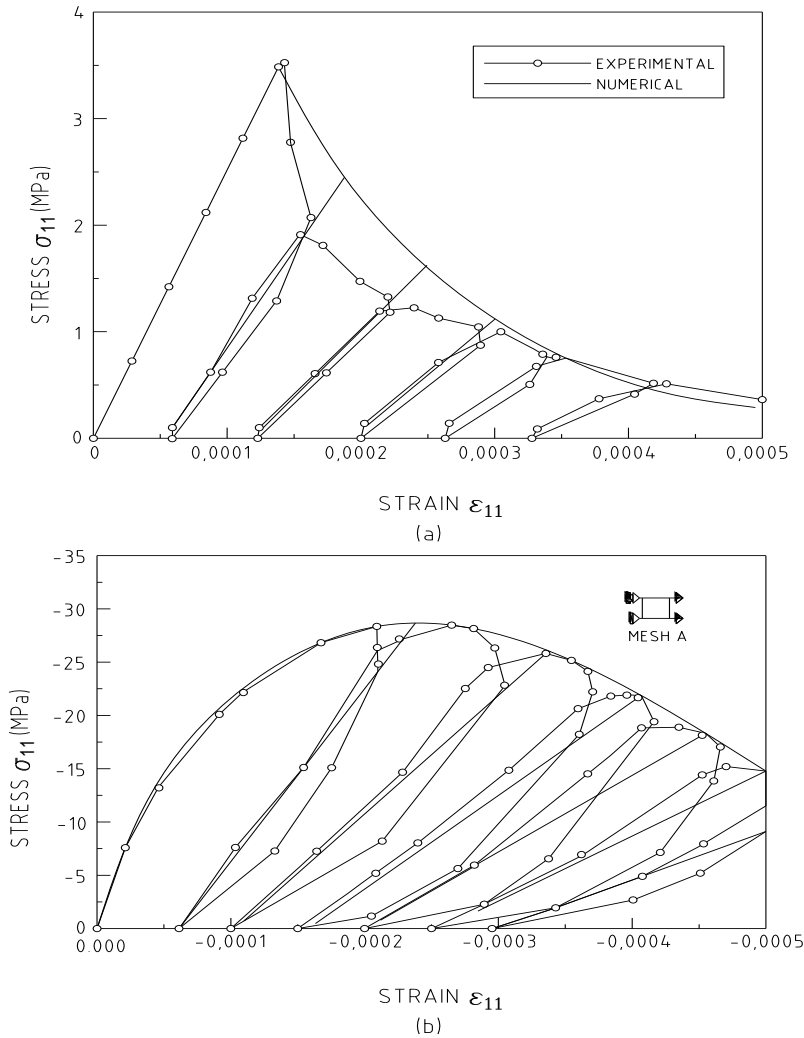


Figure 3.17 : Numerical and experimental results of the concrete model tension (top) and compression (bottom) [18]

The results obtained from experimental data showed that after the tensile loading, the compressive strength is not degraded. Hence, the yield surface was determined by the compressive damage. However, the stiffness degradation caused by compressive strength affect the tensile strength the reason is that dilatancy.

In con5 model, the uniaxial stress-strain relationship is determined by

$$\sigma_g = f_{g0} [(1 + a_g) \exp(-b_g \varepsilon^p) - a_g \exp(-2b_g \varepsilon^p)] \quad (3.4)$$

$$1 - D_g = \exp(-d_g \varepsilon^p) \quad (3.5)$$

$$\bar{\sigma}_g = f_{g0} [(1 + a_g) (\exp(-b_g \varepsilon^p))^{1 - (\frac{d_g}{b_g})} - a_g (\exp(-2b_g \varepsilon^p))^{2 - (\frac{d_g}{b_g})}] \quad (3.6)$$

$$k_g = \frac{1}{g_g} \int_0^{\varepsilon_p} \sigma_g(\varepsilon^p) d\varepsilon^p \quad (3.7)$$

$$g_g = \int_0^{\infty} \sigma_g(\varepsilon^p) d\varepsilon^p \quad (3.8)$$

Figure 3.18 shows the behaviour of the concrete model

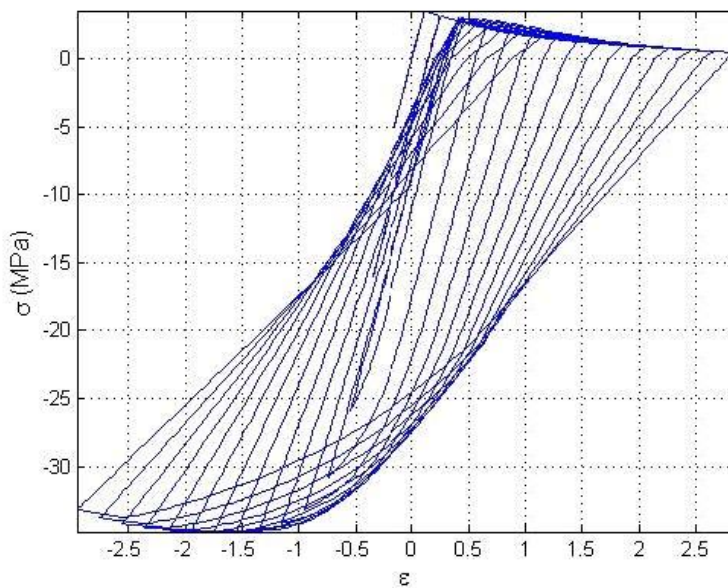


Figure 3.18 : Stress-strain behavior of the concrete model (con5) [5]

As seen in the figure, pinching effect due to the crack opening and closure is reflected in the behavior of the concrete where the unloading branches from tension to compression or the opposite direction. In addition, the stiffness degradation is clear when stiffness at any point compared with initial stiffness at zero stress-strain values. Characteristics of plastic damage concrete model are determined by two values, which are concrete compressive strength (f_c) and modulus of elasticity (E). Comparison of the con2 and con5 can be seen in following figure.

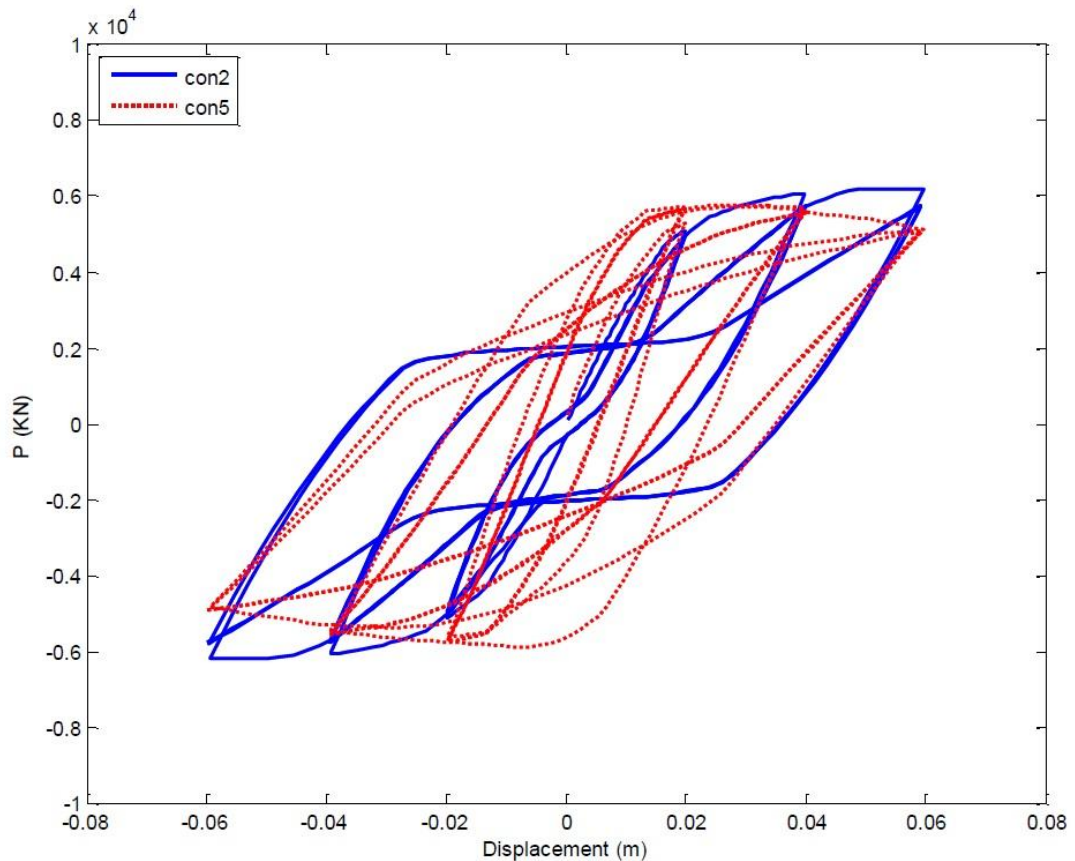


Figure 3.19 : Comparison of the concrete models [5]

As seen in the Figure 3.19, strength deterioration is obvious between con5 and con2 model with the same displacement values.

3.2.2 Steel models

3.2.2.1 Bilinear elasto-plastic steel model

The bilinear elasto-plastic steel model simulates the following characteristics, in the first branch, stress-strain remains elastic until the yield point. After the yield point, stress-strain increases with factor of strain hardening parameter. Figure 3.20 shows

the material characteristics. Bilinear elasto-plastic steel characteristics are determined by young modulus (E), yield strength (f_y) and the strain-hardening parameter (μ) in ZEUS-NL.

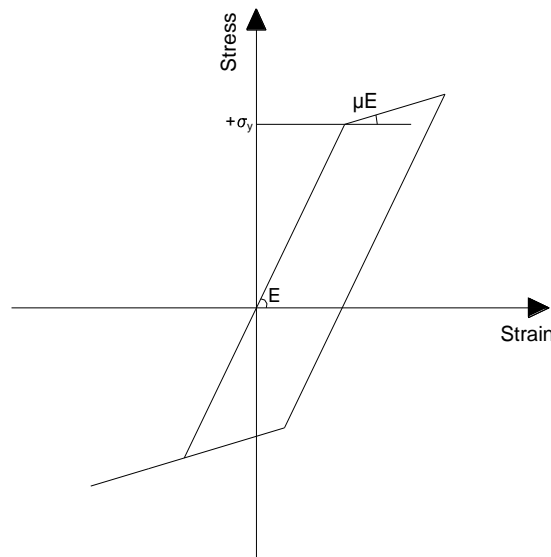


Figure 3.20 : Bilinear elasto-plastic steel model (st11)

As shown in Figure 3.20 bilinear elasto-plastic model properties have not degradation effect.

3.2.2.2 Modified Menegotto-Pinto model

The model was developed in 1973 [19]. The first modification was proposed by Filippou et al to simulate the isotropic strain-hardening [30]. In 1996, Gomes et al proposed new modification [19]. The modification was developed to take into account the effect of inelastic buckling of the reinforcing bars. The steel model indicates following characteristics [5]:

- a) Elastic, yielding and hardening branches in the first excursion
- b) Baushinger effect which consist of reduction of the yield stress after a reverse which increases with the enlargement of the plastic strain component of the last excursion and decrease of the curvature in the transition zone between the elastic and the plastic branches
- c) Isotropic strain hardening which consists of an increase of the envelope curve, proportional to the plastic strain component of the last excursion

- d) Inelastic buckling of reinforcing bars after crushing of concrete cover
- e) Fracture of reinforcing bars when the ultimate strain is exceeded under any excursion

Characteristics of the model is shown in Figure 3.21

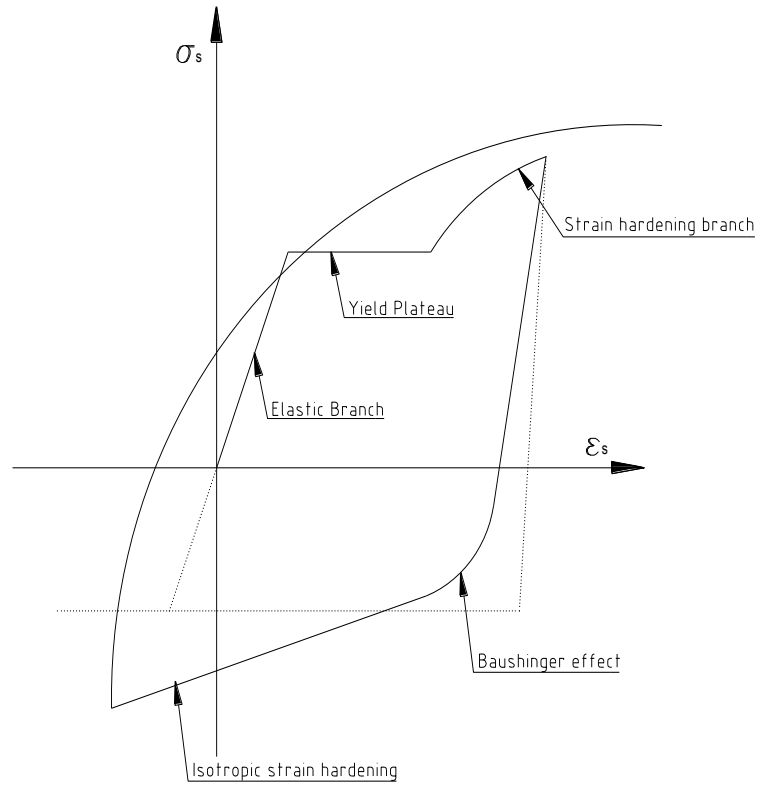


Figure 3.21 : Main characteristics of a steel stress-strain diagram [18]

In the model the loading and unloading paths shown in following formula

$$\sigma_s^* = \beta \varepsilon_s^* + (1 - \beta) \frac{\varepsilon_s^*}{[1 + (\varepsilon_s^*)^R]^{1/R}} \quad (3.9)$$

The normalized strain and stress are obtained by

$$\varepsilon_s^* = \varepsilon_s / \varepsilon_{s0} \quad (3.10)$$

$$\sigma_s^* = \sigma_s / \sigma_{s0} \quad (3.11)$$

After the first load is reversed by

$$\varepsilon_s^* = \varepsilon_s - \varepsilon_{sa} / 2\varepsilon_{so} \quad (3.12)$$

$$\sigma_s^* = \sigma_s - \sigma_{sa} / 2\sigma_{so} \quad (3.13)$$

After the loading direction is reversed, stress-strain relationship becomes unloading path until the stress becomes compressive. The material starts flowing plastically before it reach yield stress. This effect is called as Baushenger effect. Baushenger effect is the decrease of the yield stress between elastic and plastic zones. Baushenger effect is defined by the formula which is stated below

$$R = R_o - \frac{a_1 \xi}{a_2 + \xi} \quad (3.14)$$

The Menegotto-Pinto model cannot take into account isotropic strain hardening. Hence Filippou et al. proposed two modifications of this model. The purpose of the first modification improves the accuracy of the model. Proposed new variables are determined by these;

$$\varepsilon_s^* = \frac{\varepsilon_s - \varepsilon_{sa}}{\varepsilon_{s1} - \varepsilon_{sa}} \quad (3.15)$$

$$\sigma_s^* = \frac{\sigma_s - \sigma_{sa}}{\sigma_{s1} - \sigma_{sa}} \quad (3.16)$$

The second modification considers the isotropic strain hardening. A yield stress is determined in the following formula after the load converse the opposite value

$$\sigma_{so}^e = \sigma_{so} a_3 \left(\frac{\varepsilon_{s \max}}{\varepsilon_{so}} - a_4 \right) \quad (3.17)$$

In extreme loading conditions, if confinement is not adequate, first the concrete cover crushes and consequently the longitudinal bars buckle.

Gomes et al proposed the buckling effect and adopted into the model. Model was calibrated with the experimental results. The isotropic strain hardening modification

is not taken into account proposed buckling effect because the experimental results were not adequate to indicate that effect [19].

The simple model was developed to consider the buckling effect. The longitudinal bars limited with two consecutive transverse bars. The equilibrium of the buckled rebars are determined by

$$P = \frac{2M_p}{w} \quad (3.18)$$

In the previous formula, bars are in deformed condition as shown in Figure 3.22

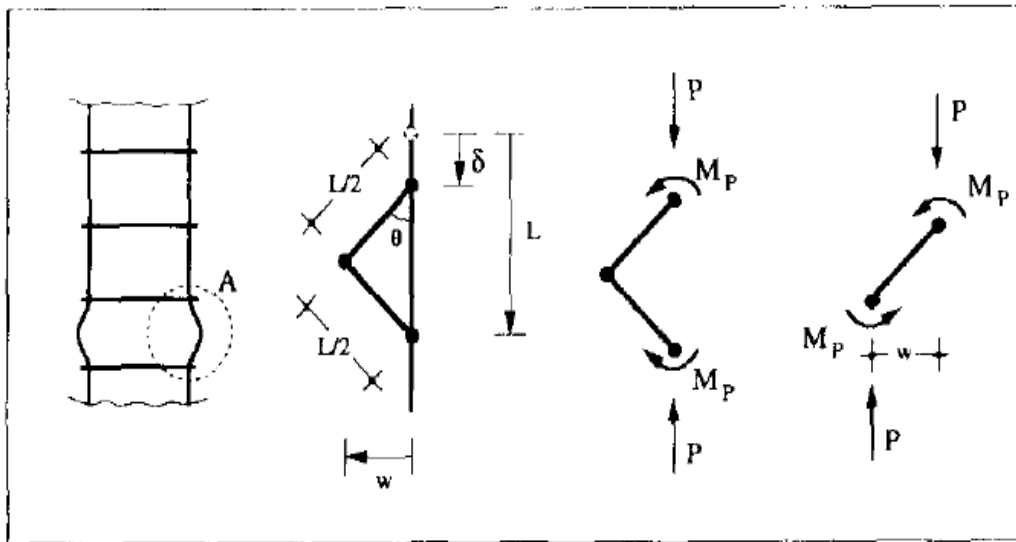


Figure 3.22 : Equilibrium of a buckled longitudinal steel bar [19]

The relation between transversal displacement w , the longitudinal displacement δ and the rigid body rotation θ are determined by

$$w = L/2 \sin \theta \quad (3.19)$$

$$\delta = L(1 - \cos \theta) \quad (3.20)$$

According to previous formulas

$$w = \sqrt{\frac{\delta L}{2}} \quad (3.21)$$

$$P = \frac{2\sqrt{2}M_p}{\sqrt{L}} \frac{1}{\sqrt{\delta}} \quad (3.22)$$

The average strain between two transverse rebar is determined by

$$\varepsilon_s = \delta / L \quad (3.23)$$

The stress in the bar is given by

$$\sigma_s = P / A_s \quad (3.24)$$

Hence, the equation 3.22 becomes

$$\sigma_s = \frac{2\sqrt{2}M_p}{\sqrt{L}} \frac{1}{\sqrt{\varepsilon_s}} \quad (3.25)$$

Equation 3.25 simulates the relation between the stress and the strain of a buckled steel bar. It should be noted that the proposed model does not consider the interaction between the bending moment and axial force.

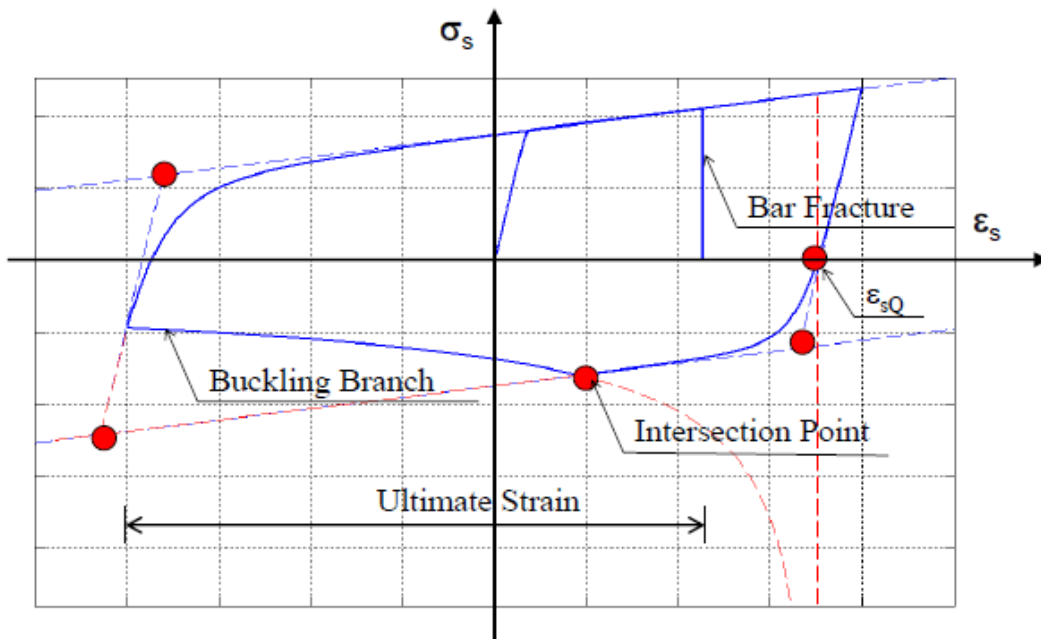


Figure 3.23 : Buckling and fracture in the steel model (stl4) [5]

The fracture of reinforcing bars under large strains occurs when steel exceed ultimate strain. In the steel model, which implemented into Zeus-NL also the bar fractures is taken into account. Figure 3.23 shows the buckling and fracture of the steel model.

Modified Menegotto-Pinto steel model characteristics are determined with modulus of elasticity(E), yield strength(f_y), yield strain (ϵ_y), ultimate strain (ϵ_u), parameter R which simulates the Baushinger effect and the material constants (a_1, a_2, a_3, a_4) in ZEUS-NL.

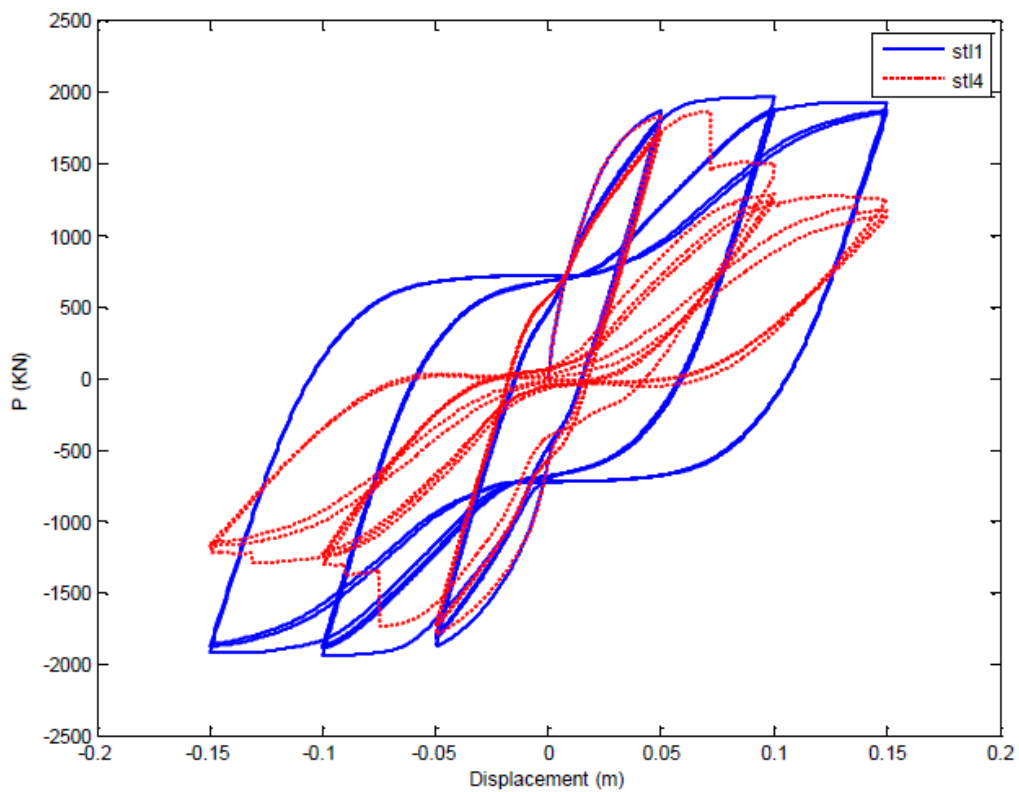


Figure 3.24 : Comparison of the steel models [5]

As seen in Figure 3.24, strength and stiffness degradation are obvious between stl4 and stl1 model with the same displacement values. The difference is due to buckling effect and fracture in reinforcing bar.

3.3 Structural Modeling

3.4 Analysis Software

The software used in analytical modeling is ZEUS-NL developed at the University of Illinois at Urbana Champaign [31]. The program is capable of representing spread of inelasticity along the member length and across the section utilizing the fiber analysis approach. In addition, it can represent geometrical nonlinearity and P-Δ effects.

3.4.1 Analytical modeling of members

The software allows to establish a detailed fiber based finite element model. It is an efficient and accurate tool for simulating the response of a complete structural system under static and dynamic loading conditions [5]. Section subdivision into fibers in reinforced concrete was shown in Figure 3.25. Structural members were modeled as using 3D cubic elasto-plastic beam-column element. These elements follow the Euler-Bernoulli formulation.

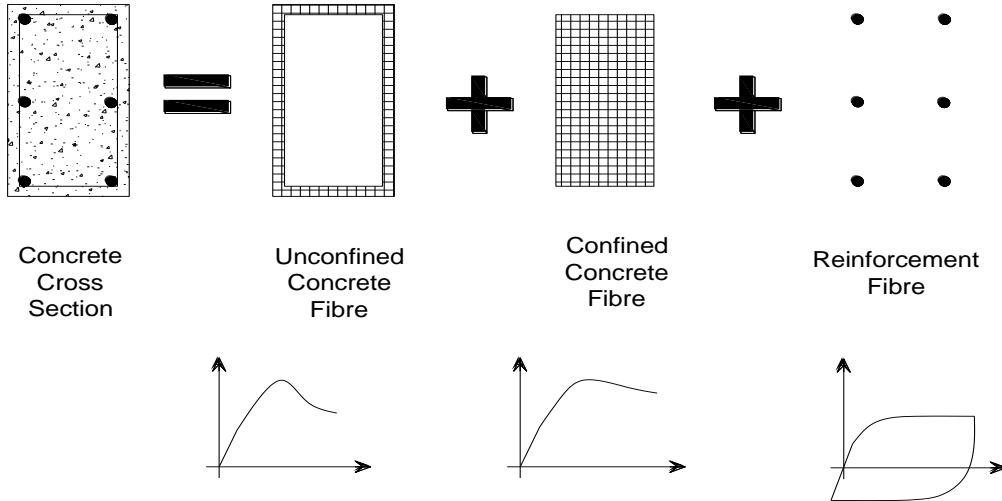


Figure 3.25 : Fiber based models

The members were divided into smaller sizes to determine the high inelasticity accurately near the beam column joints. In the analytical models, the slabs are omitted and their contribution to beam stiffness and strength is reflected by effective

width of the T-section [32]. The effective widths of the beams were determined according to Eurocode 2 [33]. The effective flange width b_{eff} for beams is derived as equation (3.26).

$$b_{eff} = \sum b_{eff,i} + b_w \leq b \quad (3.26)$$

$b_{eff,i}$ is defined according to equation (3.27). Effective flange width parameters were represented in Figure 3.26.

$$b_{eff,i} = 0.2b_i + 0.1l_0 \leq 0.2l \quad (3.27)$$

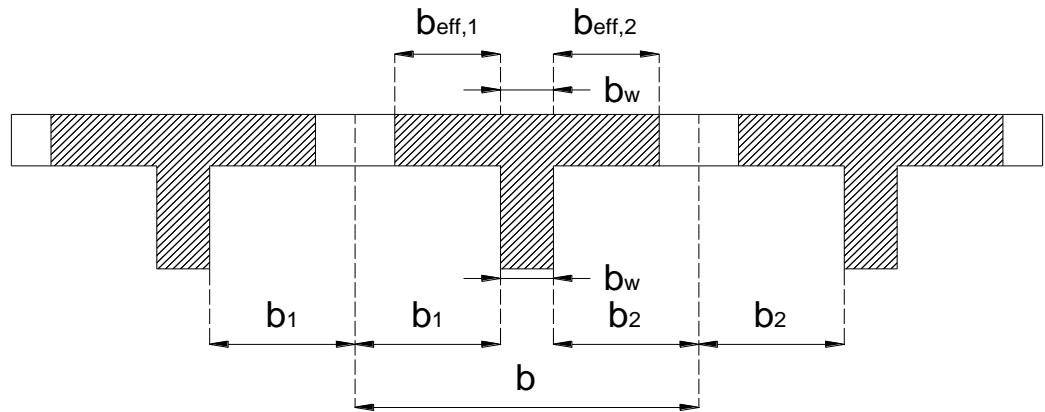


Figure 3.26 : Effective flange width parameters [33]

l_0 is the distance between points of zero moment. It was obtained from Figure 3.27.

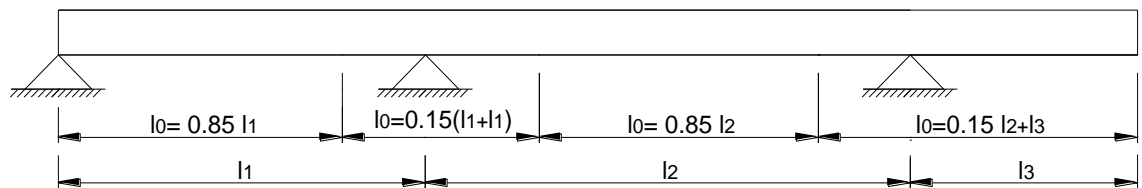


Figure 3.27 : Definition of l_0 for calculation of effective width [33]

The certain beams adjacent to columns or walls not in alignment hence the rigid links are used in order to model force transverse as shown in Figure 3.28.

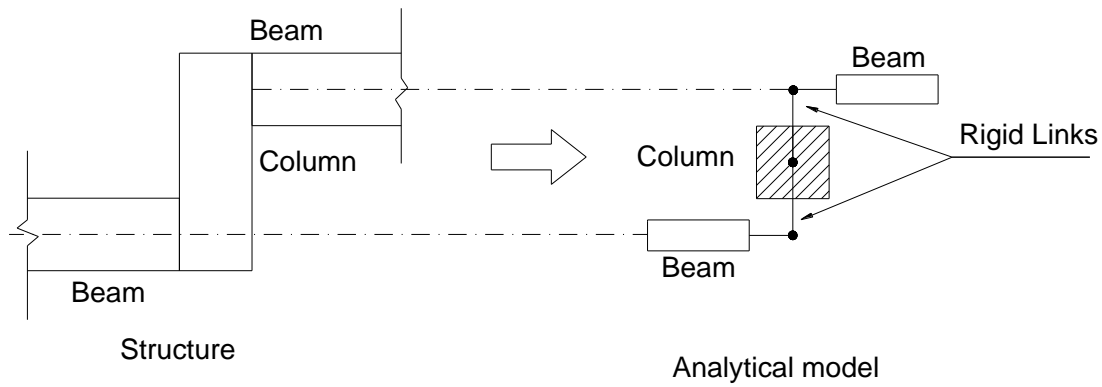


Figure 3.28 : Rigid links at beam column connections.

Diagonal elements were defined in the floor level to reflect the diaphragm behavior. The thickness of the diaphragm elements was determined in accordance of the purpose that vertical stiffness is ineffective however, horizontal stiffness is large-scale to indicate the diaphragm behavior. Hence, as shown in Figure 3.29 members were used with quite thin and wide cross-section.



Figure 3.29 : Rigid diaphragm element in analytical modeling [23]

4. EARTHQUAKE SEQUENCES

A devastating earthquake with moment magnitude (M_w) 9.0 occurred at 14:46 (JST, GMT+9) on March 11, 2011 in Japan. This recorded moment magnitude value is categorized among the most powerful earthquakes in the world since 1900's when the modern record keeping began [34]. The focal mechanism of the excitation reported as a reverse fault with a compressional axis in east-to-west direction at a depth of 24km by JMA [35]. The earthquake occurred on the plate boundary between the North American and the Pacific plates [36].

It should be noted that this earthquake is unique due to its foreshocks and aftershocks. It is noted in Zhao [37] the sequence started with a foreshock having a magnitude of 7.3 two days before the main shock and triggered vigorous aftershocks. Kazama and Noda [38] indicated 593 aftershock activities within three months period between March 11 and June 11, among which, of five had 5 events had a magnitude of 7 or greater. Indeed the M_w 9.0 Tohoku excitation had greatly increased the seismic activity in broad regions in and around the Japan Islands. More than 10,000 aftershocks with magnitude ≥ 3.0 occurred in the forearc area [39]. The epicenter of the above mentioned ground excitation, the foreshock and the aftershocks higher than 7 are marked on a map with green and blue bookmark respectively in Figure 4.1.

4.1 Record Selection Criteria

Selection criteria of earthquake records are described in this section. The record selection is the important issue to obtain accurate the time history analysis. Recorded motions are affected many cases such as soil characteristics of the recording site, source to site distance etc. [40].

The distance between the epicenter to recorded site is a strong influence on the ground motion amplitude. In order to eliminate the near fault effect, records are taken from stations that are at least 20 km away from the epicenter.

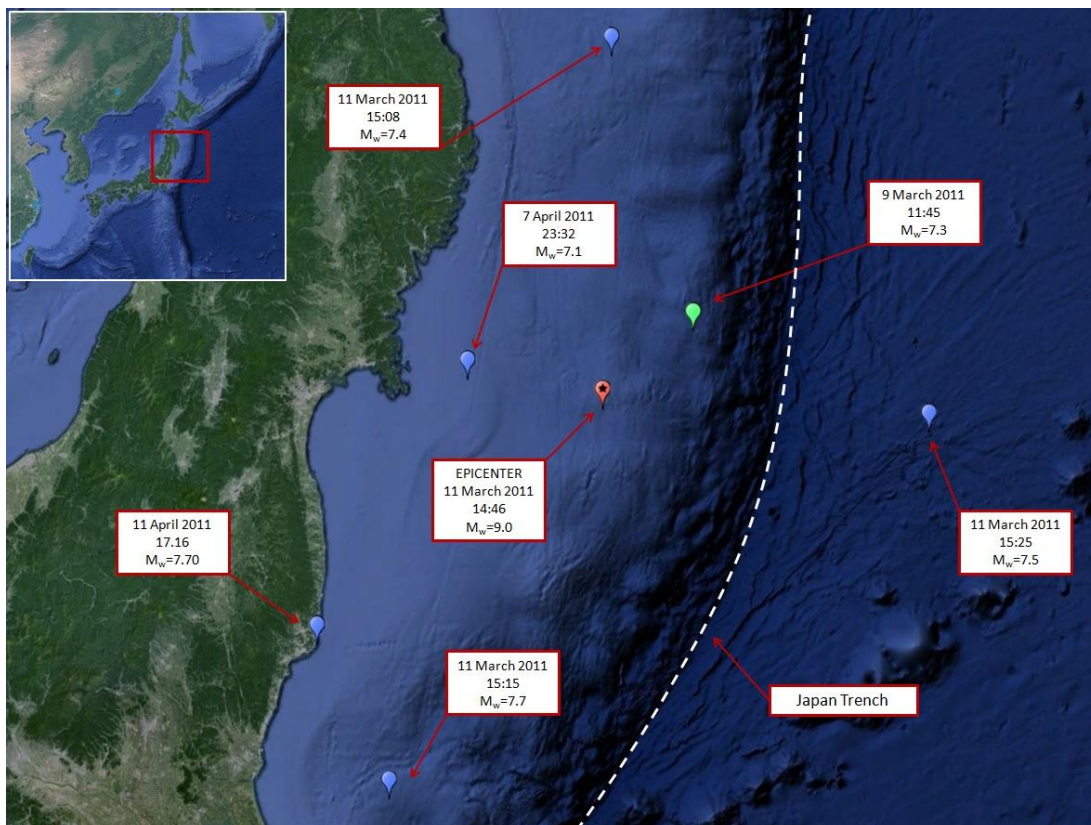


Figure 4.1 : Distribution of the main shock and aftershocks larger than M7

Soft soils can amplify the ground motion. Therefore, characteristic of the soil type, where the station is placed, is significant. The records which recorded at site having average shear wave velocity of the upper 30 meter layer of the ground ($V_{s,30}$) is between 800-360 m/sec are selected according to Eurocode ground type classification to avoid the influence of subsoil characteristics. The ground type classification in Eurocode 8 is listed in Table 4.1

Table 4.1 : Ground types in Eurocode 8

Ground Types	A	B	C	D	E
$V_{s,30}$ (m/s)	>800	800-360	360-180	<180	-

Since ground motions with a PGA value less than 0.2g are not expected to cause any significant damage and ground motions with a PGA value more than 0.8g are expected partial or complete collapse these events are excluded the selection criteria. Therefore, fortythree records were selected out of the 240 record from NIED strong motion data bank [41], which meets the criteria listed above. Only the K-Net stations was used since the $V_{s,30}$ values of ground, which stations located was available.

Acceleration–time history of the station IBR006 station is showed in Figure 4.2 and Figure 4.3.

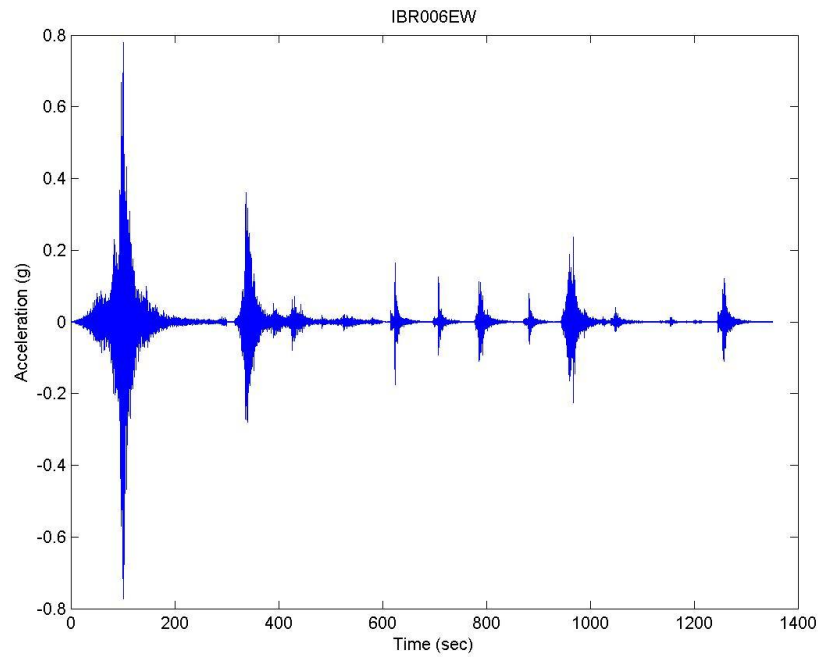


Figure 4.2 : E-W component of the IBR006 station

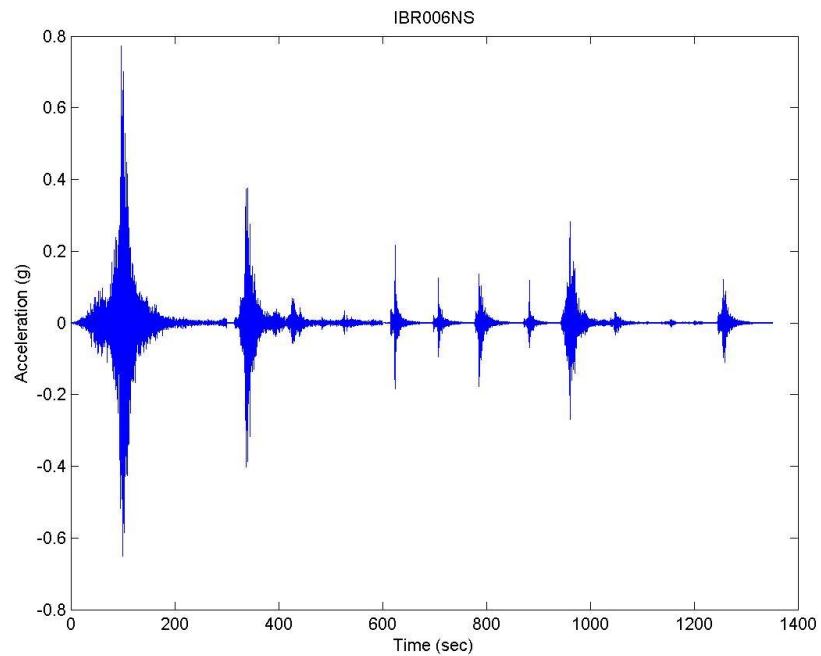


Figure 4.3 : N-S component of the IBR006 station

The stations locations and measured PGA are shown in Figure 4.4. The recorded stations, record direction, measured PGA, the shear wave velocity of the first 30

meter of the soil layer and the distance from the epicenter are shown on Table 4.3. Acceleration – time history of the records are given in appendix C.



Figure 4.4 : PGA values and locations of the stations

Spectral Displacement (Sd), Spectral Acceleration (Sa), Pseudo-Spectral Velocity (PSv) and Pseudo-Spectral Acceleration (PSa) graphs of the sequences are plotted in Figure 4.5 and Figure 4.6. Furthermore, the mean, mean + standard deviation (σ) and mean – standard deviation (σ) are given in figures. Besides, response spectrum regarding soil type B of EC8 is also plotted on the Sa and PSa for to make a comparison. As it can be inferred from the mentioned figure that the mean response spectra of the selected earthquake ground motions are found to be in accordance with EC8 for low period values.

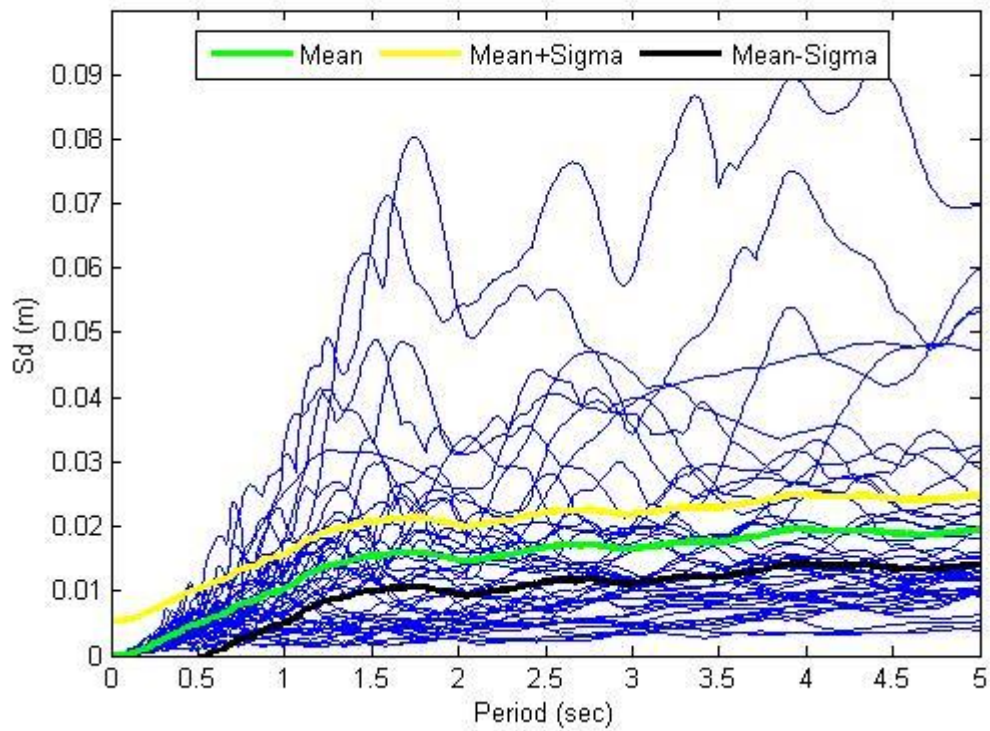
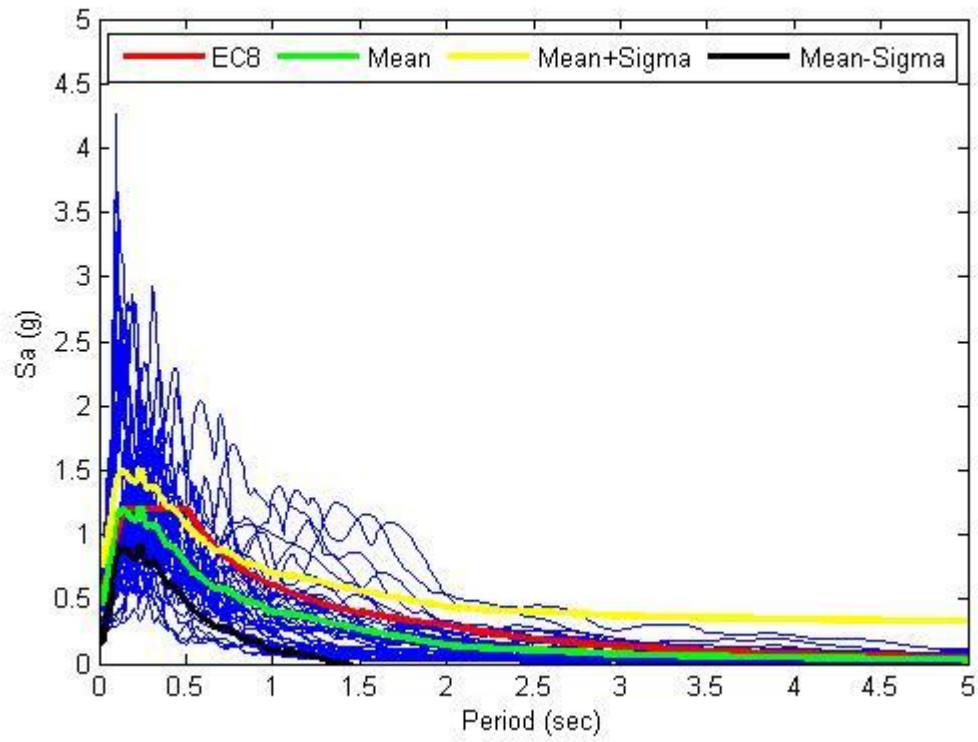


Figure 4.5 : S_a and S_d – period graphs of selected ground motions.

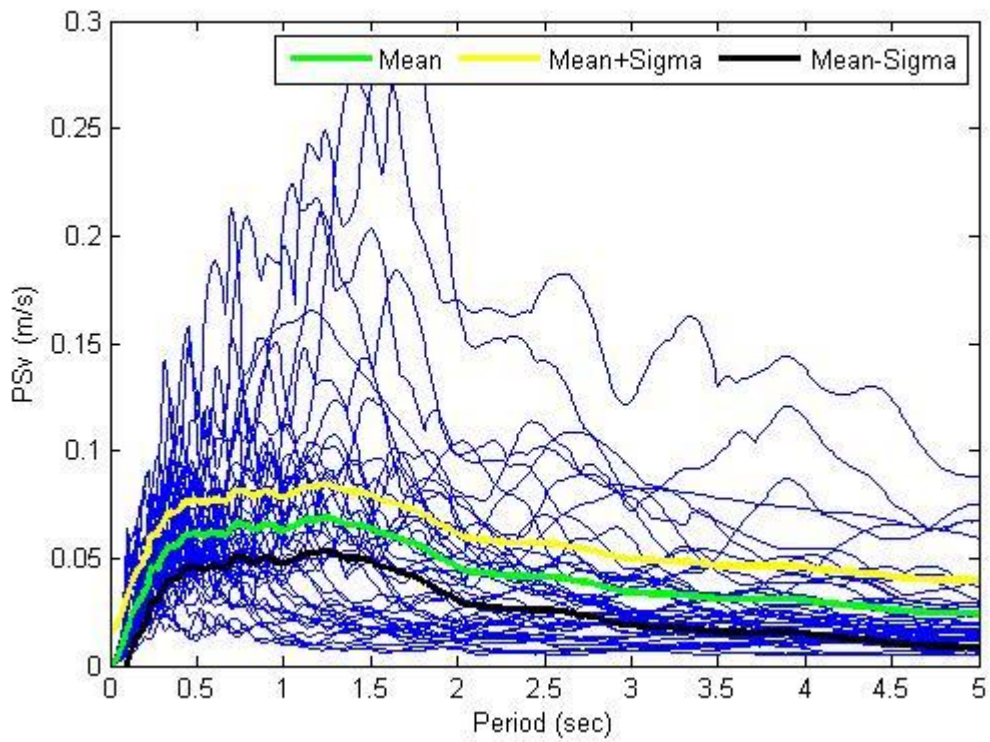
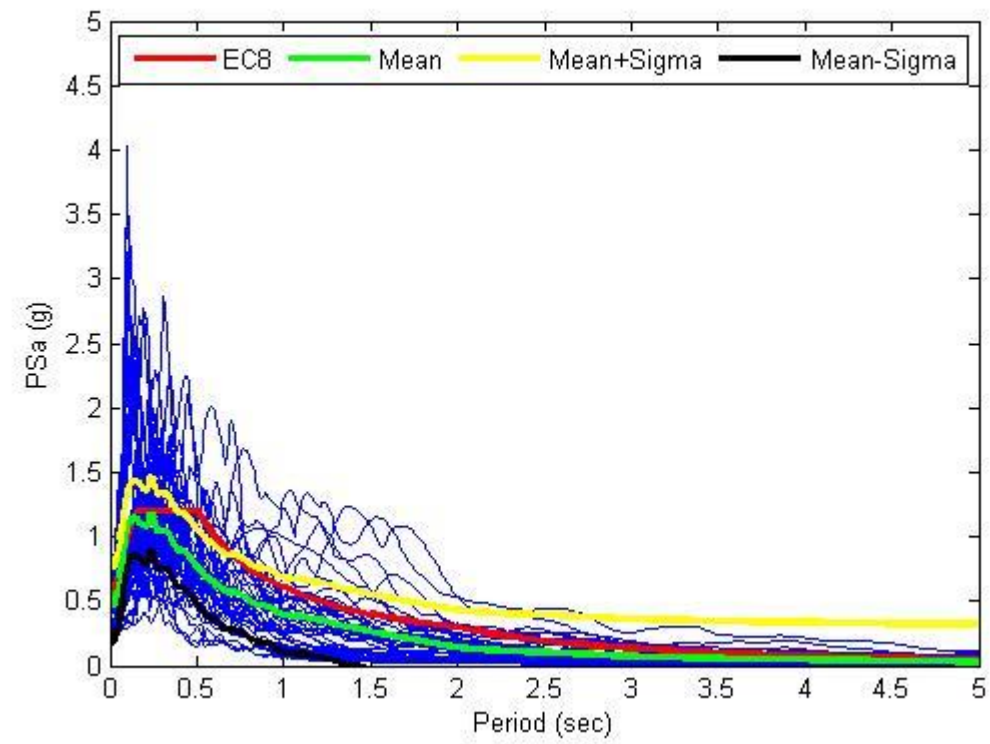


Figure 4.6 : PSa and PSv - period graphs of selected ground motions.

Table 4.2 : Selected records

Station	Direction	PGA (g)	$V_{s,30}$ (m/sn)	Distance from the epicenter (km)
AOM007	NS	0.26569	676	369
FKS002	EW	0.5801	525	200
FKS002	NS	0.49133	525	200
FKS003	EW	0.2831	402	213
FKS003	NS	0.34372	402	213
FKS008	EW	0.71595	747	215
FKS012	EW	0.24393	636	226
FKS012	NS	0.34197	636	226
FKS018	NS	0.78267	407	234
FKS019	EW	0.41696	497	220
FKS019	NS	0.4054	497	220
IBR006	EW	0.77947	540	287
IBR006	NS	0.77197	540	287
IBR012	EW	0.3149	593	312
IBR012	NS	0.28737	593	312
IBR018	EW	0.67336	625	308
IBR018	NS	0.50063	625	308
IWT001	EW	0.24758	645	274
IWT001	NS	0.23009	645	274
IWT007	EW	0.66206	750	156
IWT007	NS	0.61903	750	156
IWT011	EW	0.34916	429	188
IWT011	NS	0.2184	429	188
IWT012	EW	0.48137	419	202
IWT012	NS	0.59914	419	202
IWT016	EW	0.24721	559	195
IWT016	NS	0.2309	559	195
IWT019	EW	0.24901	609	214
IWT019	NS	0.32181	609	214
IWT026	EW	0.41094	469	200
IWT026	NS	0.33064	469	200
MYG002	EW	0.65929	457	137
MYG002	NS	0.6829	457	137
MYG006	EW	0.52143	657	174
MYG006	NS	0.46963	657	174
MYG007	EW	0.64744	405	151
MYG007	NS	0.57759	405	151
MYG009	EW	0.55828	389	177
MYG009	NS	0.46531	389	177
MYG010	EW	0.37229	371	143
MYG010	NS	0.4464	371	143
TCG012	EW	0.44363	416	338
TCG012	NS	0.30217	416	338

5. ANALYSIS PROCEDURES

5.1 Nonlinear Static Procedures

In this section, nonlinear static procedures are described. Nonlinear static analysis (NSA) procedures utilize SDOF representations of MDOF systems to relate story drifts and component actions to a global displacement demand parameter through a pushover curve [42]. In a recent research conducted by National Institute of Standards and Technology concluded that NSP procedures for regular and low-rise structures the N2 procedure first proposed by Fajfar and Gaspersic [43] and later implemented to Eurocode 8 gives good correlation with the nonlinear dynamic analyses results. Therefore, in this study the capacity of the regular structures is assessed using N2 method.

Despite the fact that when irregularities arise on the structure to take into account the multi modal effects extended N2 [44] procedure is applied to derive the pushover curves.

5.1.1 N2 method

N2 method was proposed by Fajfar and Gaspersic, where N stands for non-linear and 2 for two mathematical models [43]. The basic idea came from the Q model developed by Saiidi and Sozen [45]. The procedure uses two separate mathematical models for determining target displacement of structures.

In the method, the time-independent displacement shape $\{\phi\}$ is assumed for determining the lateral load distribution. Assumed shape is normalized to the top displacement equal to 1 ($\phi_n = 1$). Researchers have shown that the results are not affected significantly from the small and moderate changes in displacement shape. Assumed displacement shapes are given in the Figure 5.1. Vertical distribution of the lateral load is achieved by equation 5.1.

$$\{P\} = [M]\{\Phi\} \quad (5.1)$$

As a result of the loading acting on the building, push-over curve is obtained in terms of base shear-top displacement.

After this step, second mathematical model is needed for determining the target displacement. The second mathematical model is obtained by the converting the first model (MDOF) quantities to equivalent SDOF quantities.

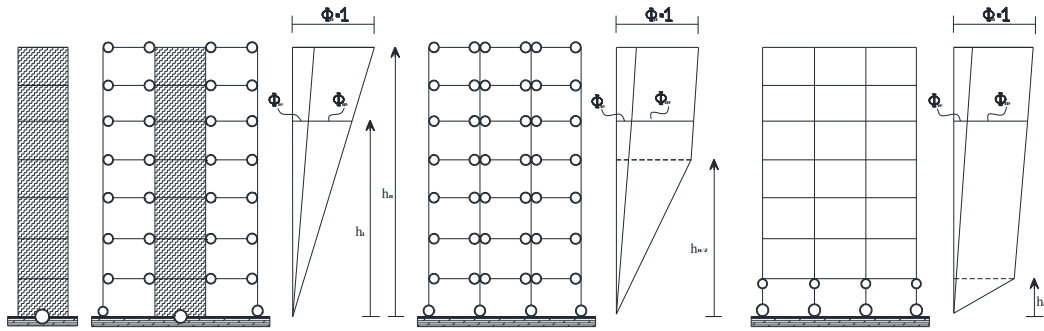


Figure 5.1 : Assumed displacement shapes for different types of buildings

Coefficient c is used for the convert MDOF quantities to SDOF quantities.

$$c = \frac{\{\Phi\}^T [M] \{\Phi\}}{\{\Phi\}^T [M] \{1\}} = \frac{\sum m_i \Phi_i^2}{\sum m_i \Phi_i} \quad (5.2)$$

In the formula 5.2, $\{\Phi\}^T [M] \{\Phi\}$ represents the generalized mass value of the i th mode and $\{\Phi\}^T [M] \{1\}$ represents the mass of the equivalent SDOF system. The pushover curve of MDOF values are multiplied by c to determining the SDOF pushover curve. The transformation can be written as following formula

$$R^* = cR \quad (5.3)$$

R^* represents the quantities of the equivalent SDOF system and R represents the quantities of the MDOF system. Obtained force-displacement curve, which belongs to the SDOF system, brought to bilinear case as seen in Figure 5.2.

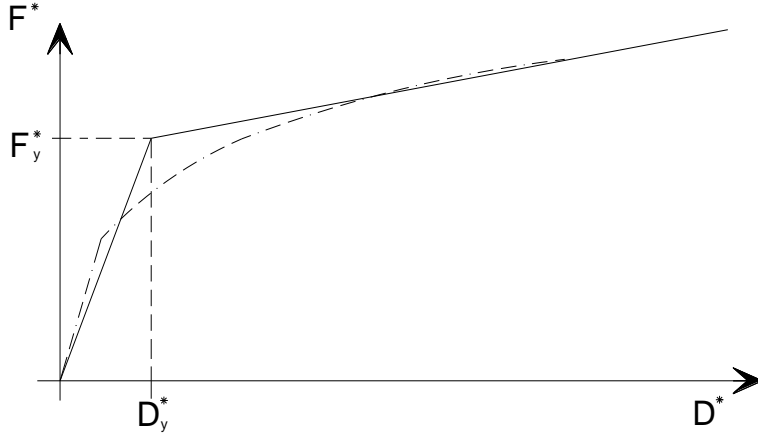


Figure 5.2 : Bilinear force-displacement relationship [35]

The yield strength (F_y^*) and the yield displacement (D_y^*) are determined from the bilinear curve. Hence, the stiffness and the period of the SDOF are determined by

$$k^* = F_y^* / D_y^* \quad (5.4)$$

$$T^* = 2\pi\sqrt{m^* / k^*} \quad (5.5)$$

The relationship between strength and ductility defined as

$$F_y = \frac{mA_e}{R_\mu} \quad (5.6)$$

The ductility factor (μ) is determined according to reduction factor (R_μ) spectrum or the following formulas. R_μ spectrum can be seen in Figure 5.3.

$$T^* < T_1 \longrightarrow \mu = (R_\mu - 1) \frac{T_1}{T^*} + 1 \quad (5.7)$$

$$T^* > T_1 \longrightarrow R_\mu = \mu \quad (5.8)$$

T_1 is transition period where the constant acceleration segment of the response spectrum intersects to constant velocity segment of the spectrum. If period of the SDOF (T^*) is higher than the corner period (T_1) $R_\mu = \mu$ due to equal displacement rule.

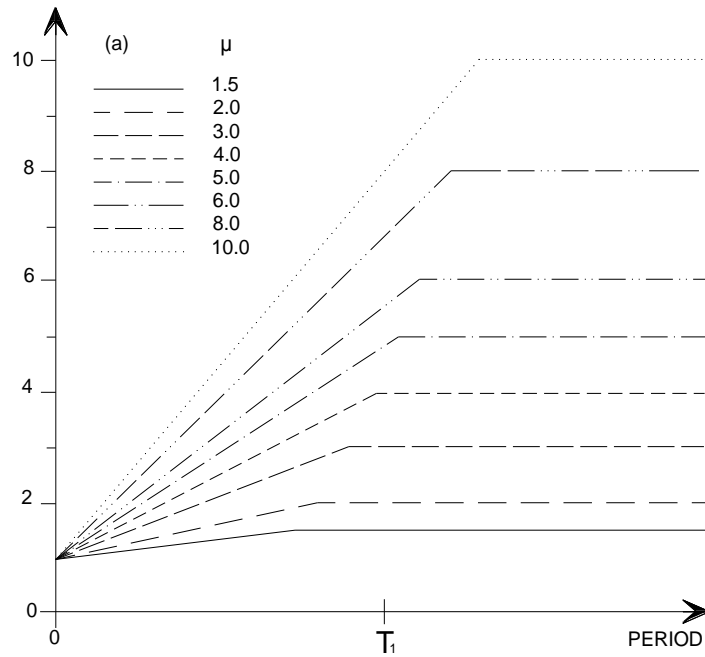


Figure 5.3 : Approximate spectra for R-factor [46]

In addition, displacement demand of equivalent SDOF system is determined by

$$D^* = \mu D_y^* = \frac{mA_e}{R_\mu W^2} \quad (5.9)$$

Displacement demand of SDOF is transformed by dividing c coefficient to determine displacement demand of MDOF.

$$D_t = D^* / c \quad (5.10)$$

Pushover analysis is reperformed up to the displacement demand and the assessment of the building can be determined.

5.1.2 Extended N2 metod

The basic N2 method cannot take into account the higher mode effects in plan and elevation. Hence, its use is limited. Therefore, basic N2 method developed and extended to consider higher modes effect in both plan and elevation [44].

The development of the method is based on the structure remains elastic when vibrating in the higher modes hypothesis. The higher mode effects are considered combining the basic N2 method and standard elastic modal analysis (RSA).

Two correction factors was proposed to determine the higher mode effects. One of two is for elevation and the other is for plan. The target displacement ratio between the pushover analysis and elastic modal analysis is obtained in centre of mass for normalize the RSA results.

$$c_{NORM} = \frac{d_{t,PUSH}}{d_{t,RSA}} \quad (5.11)$$

The RSA results are multiplied by c_{NORM} and all the related results that are obtained by RSA, are compared with pushover results.

Normalized results ratio, between which is obtained by elastic modal analysis and the absolute values of the results obtained by conventional pushover analysis in the center of mass is specified the correction factor c_E for higher modes effects in elevation. If the ratio is less than 1, the value is taken as 1. Normalized results ratio between which is obtained by elastic modal analysis and the absolute values of the results obtained by conventional pushover analysis, is specified the correction factor c_T for higher modes effects in plan. If the ratio is less than 1, the value is taken as 1.

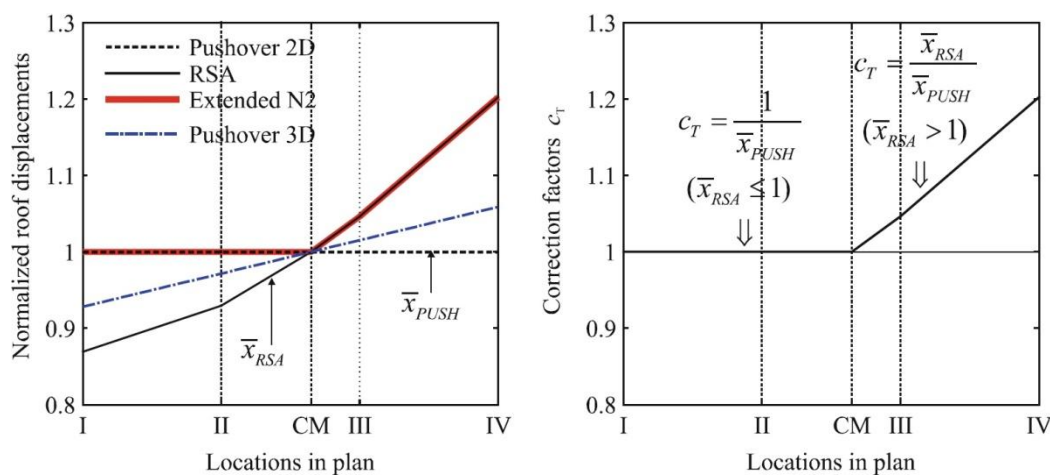


Figure 5.4 : Correction factors for the higher mode effects in plan [44]

While the higher mode effects are assumed to constant any location in plan for c_E . c_T depends on the location in plan. Hence, for c_E , same correction factor is used for any position in the plan. Meanwhile, c_T factors are assumed to independent from elevation. Hence, same c_T is used for any storey in elevation. In the Figure 5.4, the correction factors for plan were shown for studied building by Kreslin and Fajfar.

The assessment of the structure is performed multiplying by the determined correction factors with all local quantities results of basic N2 method.

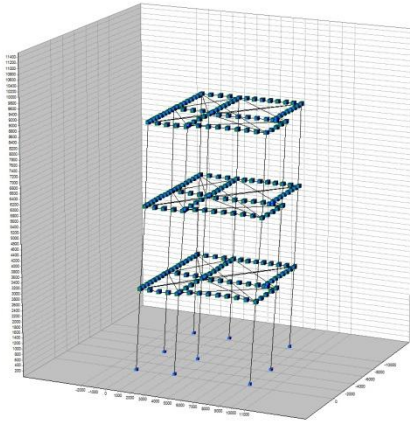
6. ANALYSIS RESULTS

Conventional pushover analyses are carried out to indicate the response of the buildings. In addition, dynamic time history analysis performed to capture the multiple earthquake sequence between models which have the degrading and non-degrading material characteristics both regular and irregular case. The procedures are applied buildings in only one direction. The Y direction is selected for SPEAR building because of the torsional eccentricities are larger in Y direction. For school building, X direction is selected for school building. Total lateral rigidity in X direction is smaller than the Y direction. Hence, more damage is expected in X direction.

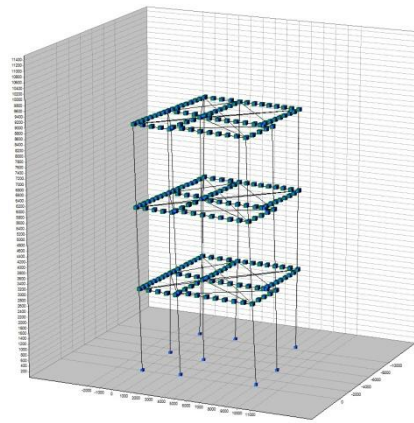
6.1 Eigen-value Analyses and Mode Shapes

Eigen-value analyses are conducted to derive the fundamental periods and vibration modes of the considered structures both for regular and irregular cases. Lumped masses were assigned at the nodes of beam elements. Mass values are determined by taking into account both dead load (D) and live load (Q). Live loads are reduced by live load reduction factor (n) which changes according to structural type. For SPEAR and ICON buildings this reduction factor is taken as 0.3, whereas 0.6 for the school building.

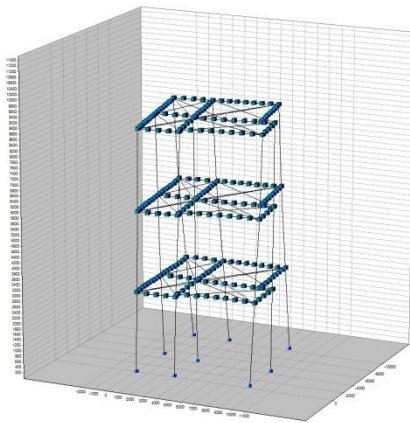
The mode shapes which belongs to original buildings, are obtained with using both ZEUS-NL and SAP2000 [47] to compare the results and make sure the models are compatible with each other. In remodeled case, only the Zeus-NL results are given. The mode shapes are given through Figure 6.1 to Figure 6.9 for SPEAR, ICON and school building, respectively.



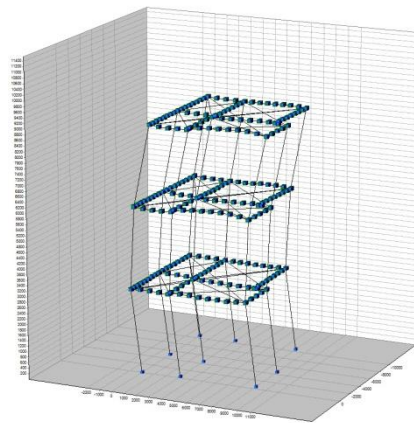
$T_1=0.66$ sec



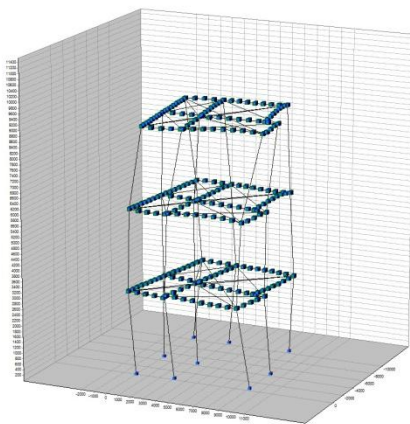
$T_2=0.61$ sec



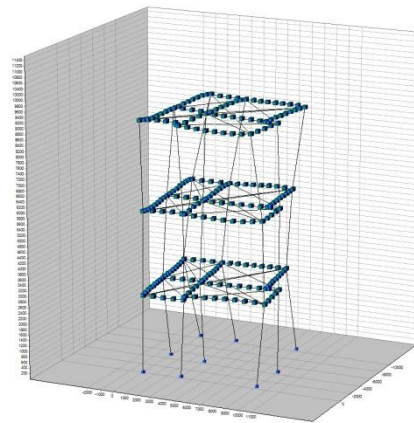
$T_3=0.50$ sec



$T_4=0.22$ sec



$T_5=0.20$ sec



$T_6=0.16$ sec

Figure 6.1 : Periods and mode shapes of SPEAR structure (Zeus-NL)

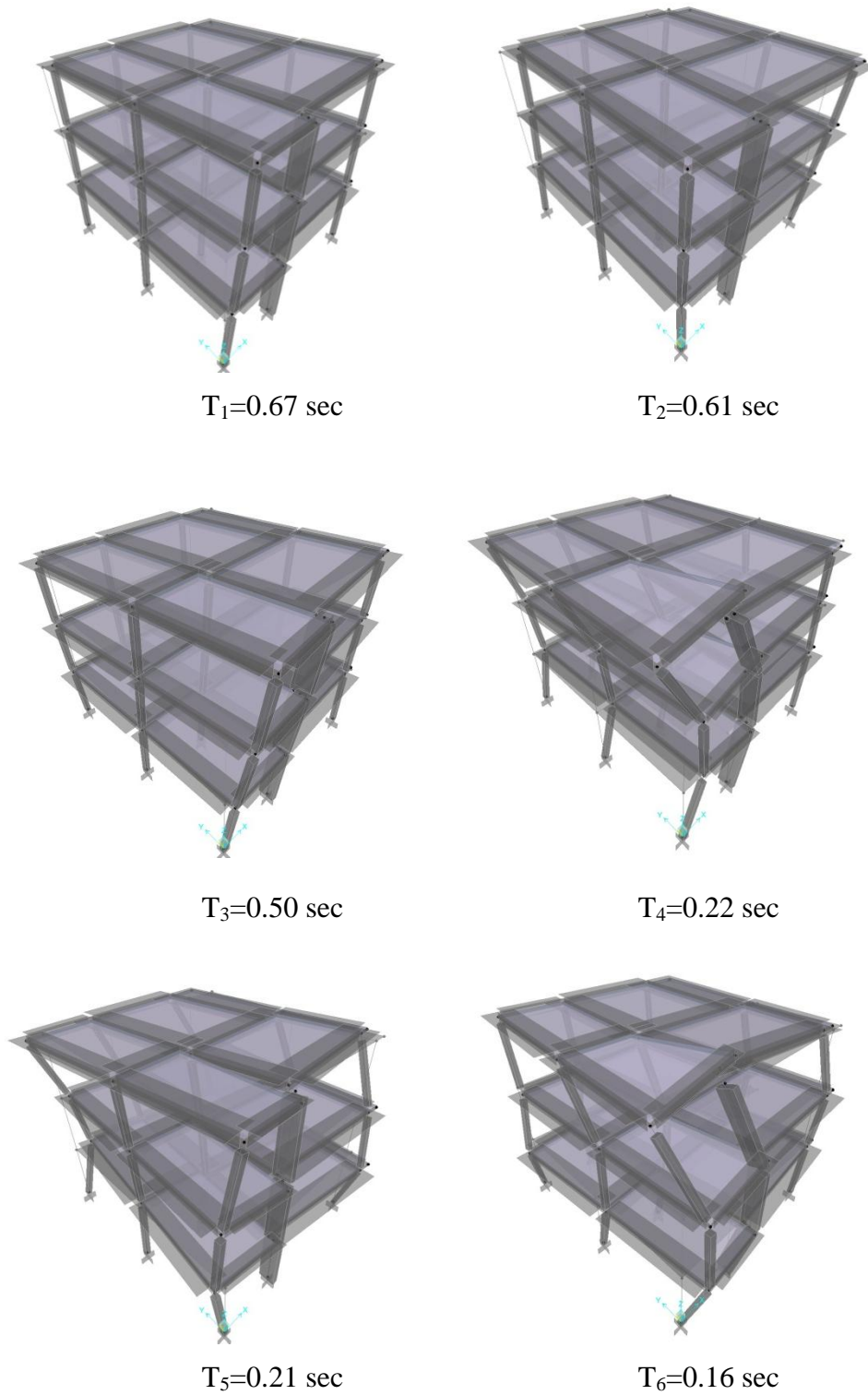
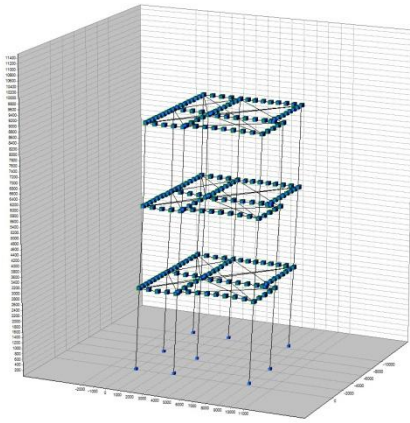
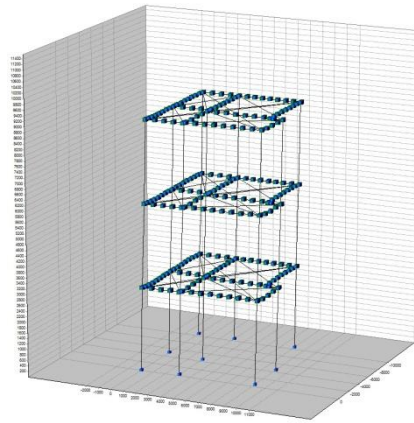


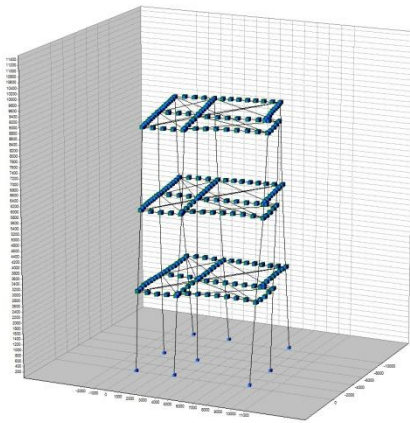
Figure 6.2 : Periods and mode shapes of SPEAR structure (SAP2000)



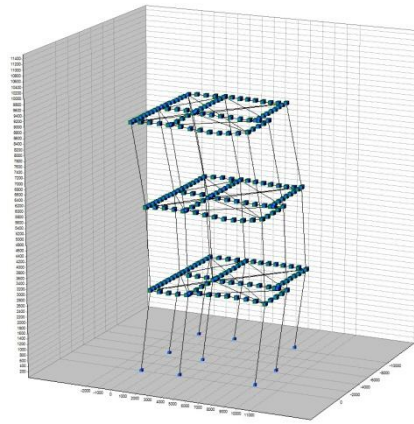
$T_1=0.63$ sec



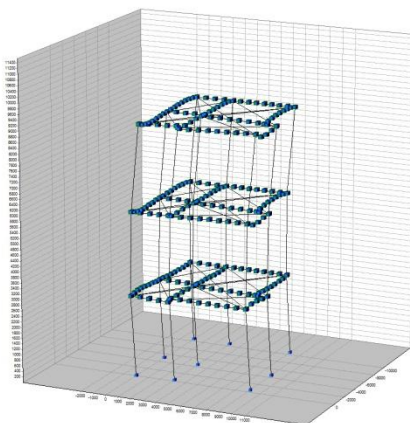
$T_2=0.52$ sec



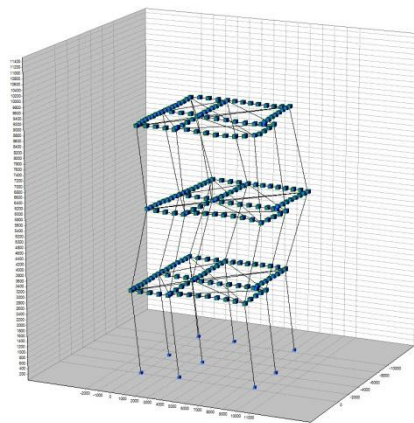
$T_3=0.46$ sec



$T_4=0.21$ sec



$T_5=0.16$ sec



$T_6=0.13$ sec

Figure 6.3 : Periods and mode shapes of regular case of SPEAR structure (Zeus-NL)

Icon building has no span on the y direction. Hence, only the mode shapes which are belong to the x direction are given.

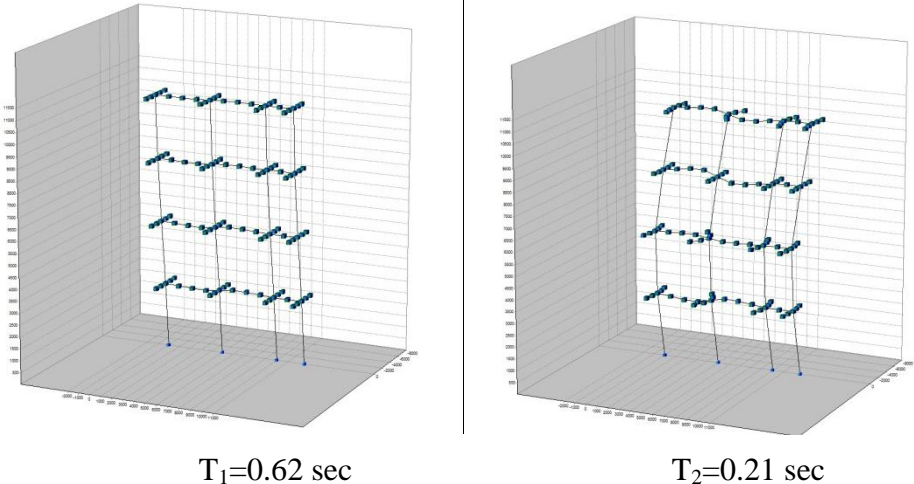


Figure 6.4 : First two periods and mode shapes of ICON building (Zeus-NL)

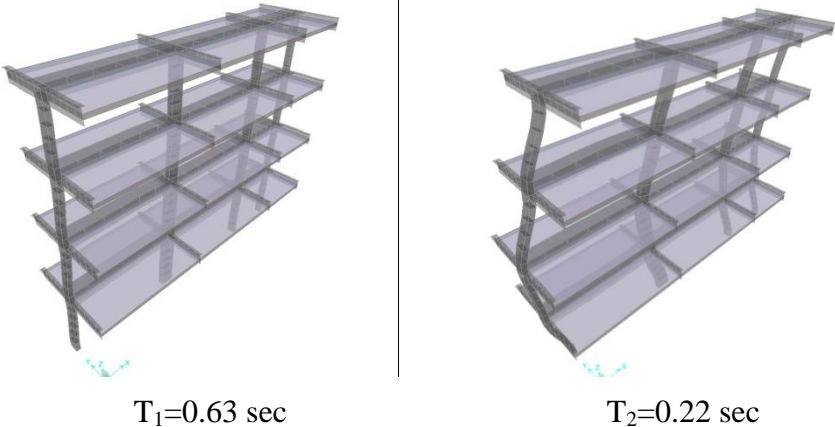


Figure 6.5 : First two periods and mode shapes of ICON building (SAP2000)

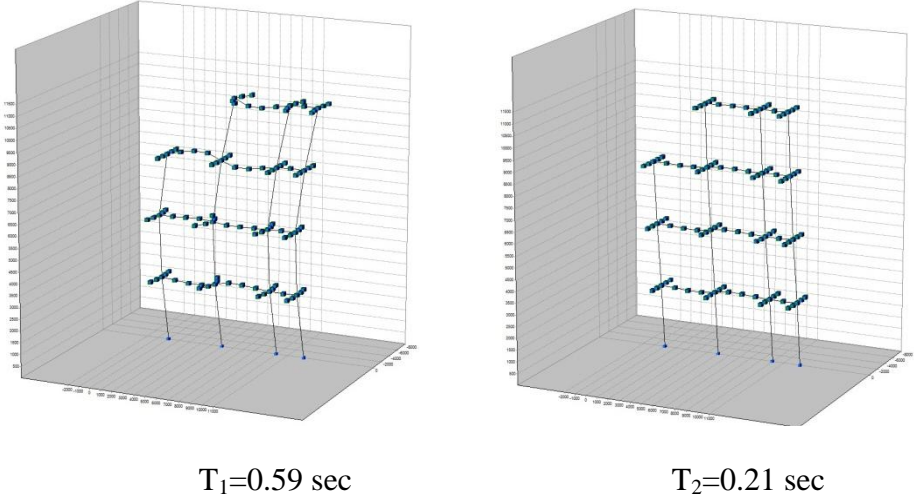
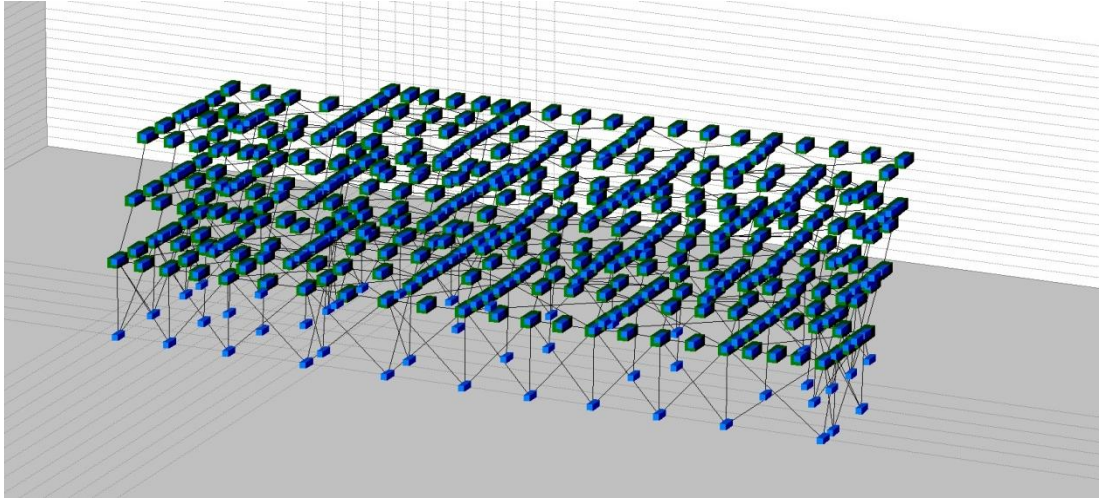
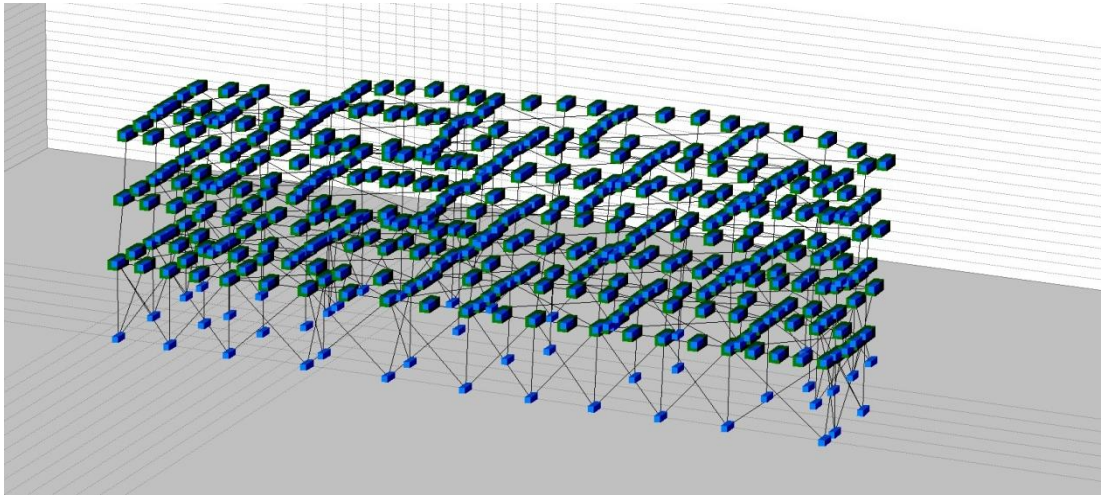


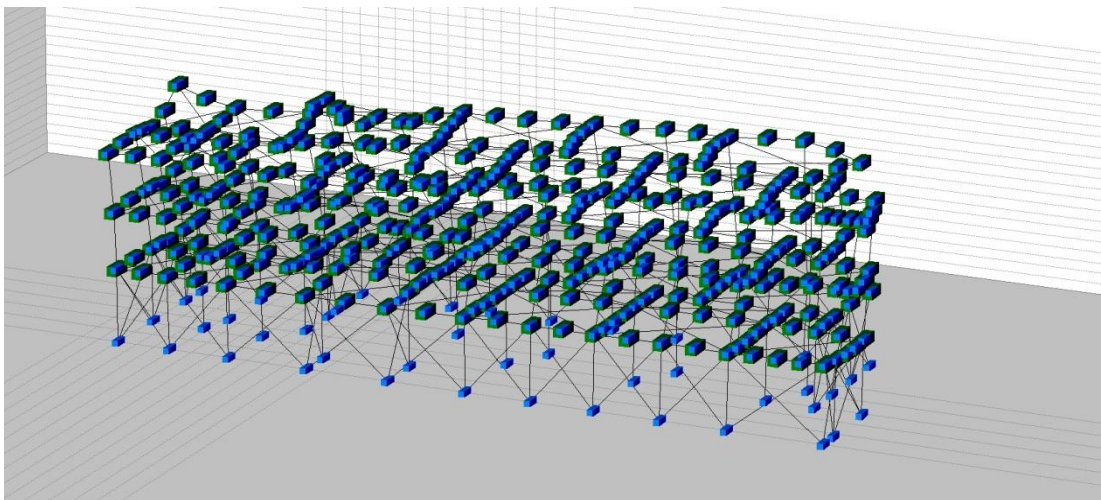
Figure 6.6 : First two periods and mode shapes of irregular case of ICON building



$T_1=0.19$ sec

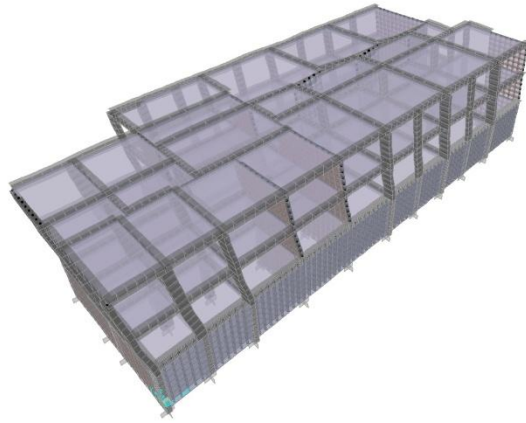


$T_2=0.13$ sec

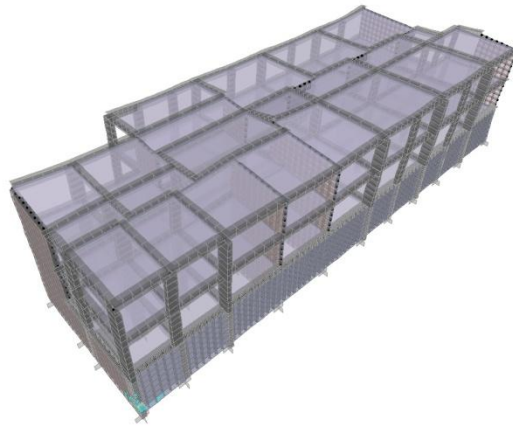


$T_3=0.09$ sec

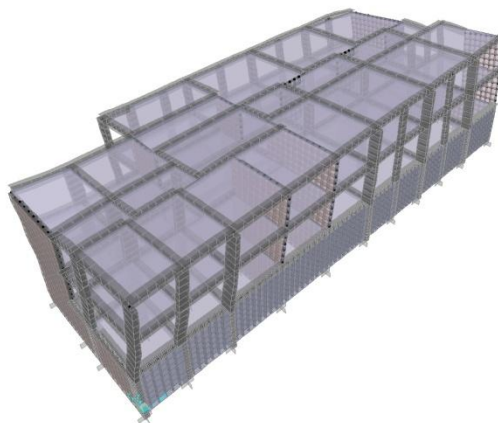
Figure 6.7 : Periods and mode shapes of school building (Zeus-NL)



$T_1=0.19$ sec

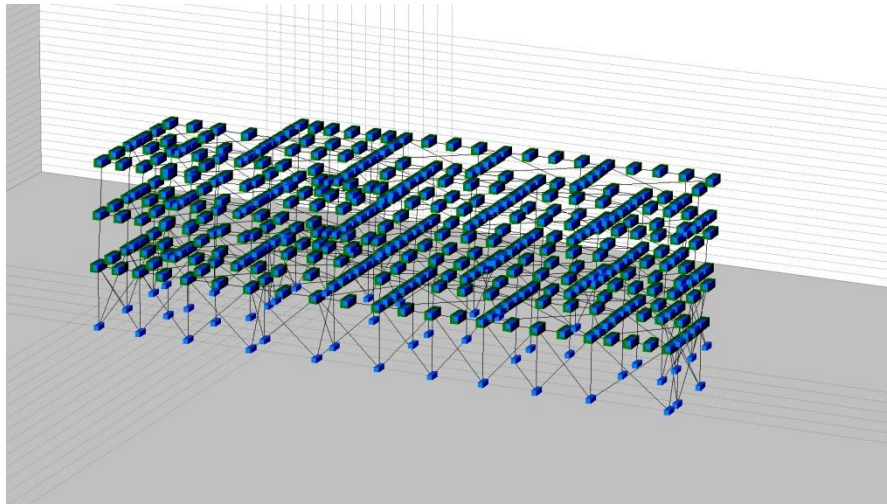


$T_2=0.13$ sec

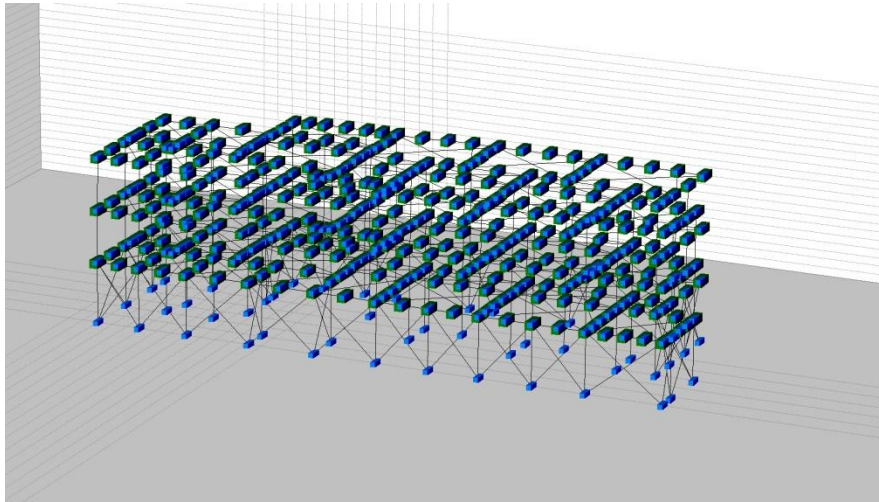


$T_3=0.10$ sec

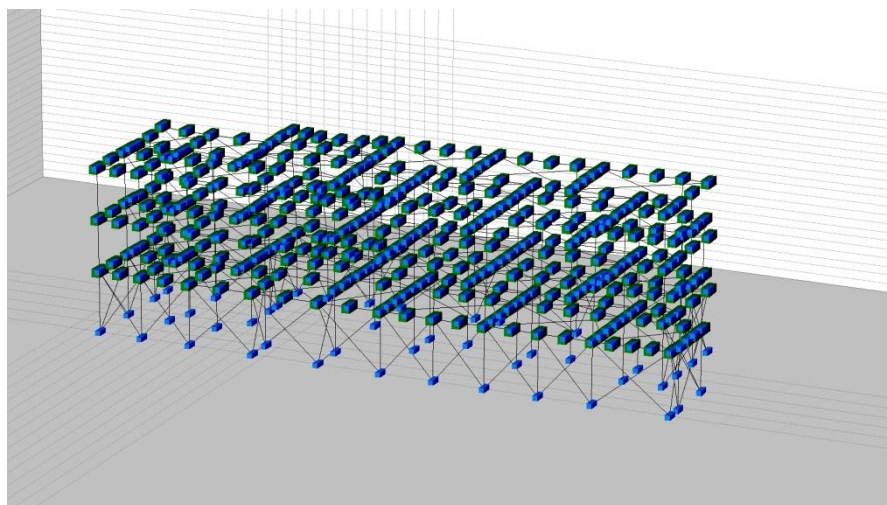
Figure 6.8 : Periods and mode shapes of school building (SAP2000)



$T_1=0.18$ sec



$T_2=0.12$ sec



$T_3=0.09$ sec

Figure 6.9 : Periods and mode shapes of irregular case of school building (Zeus-NL)

While the structures are remodeled in order to achieving regular or irregular behavior, there are some change occurred in total mass of the buildings. Total mass of the SPEAR building is increased about 7.36% due to changed column dimensions. In ICON building, total mass of the structure is decreased about 0.95% due to removed one span in fourth storey. There is not alter any mass in school building. Story mass and total mass of the buildings are given in Table 6.1.

Table 6.1 : Story mass of the studied buildings

Regularity	Name	Story 1 Mass (kN)	Story 2 Mass (kN)	Story 3 Mass (kN)	Story 4 Mass (kN)	Total Mass (kN)
Irregular	SPEAR	629.8	629.8	619.0	-	1878.6
	ICON	400.7	400.7	399.1	320.8	1521.3
	School Building	8048.8	7830.0	5944.9	-	21823.7
Regular	SPEAR	675.9	675.9	665.1	-	2016.9
	ICON	400.7	400.7	399.1	245.2	1445.7
	School Building	8048.8	7830.0	5944.9	-	21823.7

6.2 Nonlinear Static Procedure Results

6.2.1 SPEAR building

Nonlinear static procedures were applied the SPEAR structure in Y direction for negative and positive direction.

6.2.2 N2 method for original case of SPEAR building

The fundamental mode of the considered structure in Y direction is second mode. The mode shape and lateral load distribution are given in Table 6.2.

Table 6.2 : Lateral load distribution values

Storey	Mode Shape	Normalized Mode Shape	Weight (kN)	Lateral Load (kN)
3	0.0208	0.286	629.8	180.46
2	0.0513	0.704	629.8	443.97
1	0.0728	1.000	619.0	619.06

The generalized mass of the considered mode and the mass of the equivalent SDOF system are given below for Y direction.

$$\{\Phi\}^T [M] \{\Phi\} = 100.28$$

$$\{\Phi\}^T [M] \{1\} = m^* = 126.75t$$

Therefore, coefficient c is calculated as below.

$$c = \frac{100.28}{126.75} = 0.7911$$

+Y direction

Base shear-top displacement of the equivalent SDOF model and the bilinear curve is given in Figure 6.10.

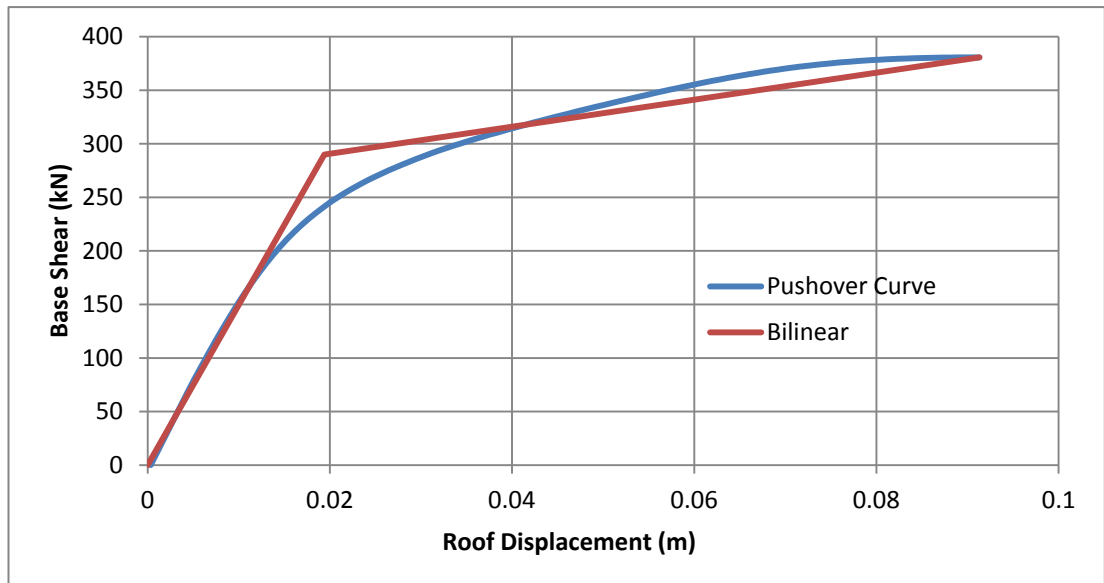


Figure 6.10 : Base shear-top displacement relationship of the SPEAR building in +Y direction

Yield strength, yield displacement, rigidity and period of the equivalent SDOF model are determined from the bilinear curve as

$$F_y^* = 290kN$$

$$D_y^* = 0.0194m$$

$$k^* = \frac{290}{0.0194} = 14948kN/m$$

$$T^* = 2 \cdot 3.14 \cdot \sqrt{\frac{126.75}{14498.4}} = 0.58 \text{sec}$$

According to EC 8 soil type B spectrum acceleration value is determined as 1.03 g for T^*

$$R_\mu = \frac{126.75 \cdot 1.03 \cdot 9.81}{290} = 4.417$$

Transition period where the constant acceleration segment of the response spectrum passes to constant velocity segment of the spectrum (T_1) = 0.5. Hence, according to R-spectrum (as seen in Figure 6.11) R_μ is equal to μ due to equal displacement rule.

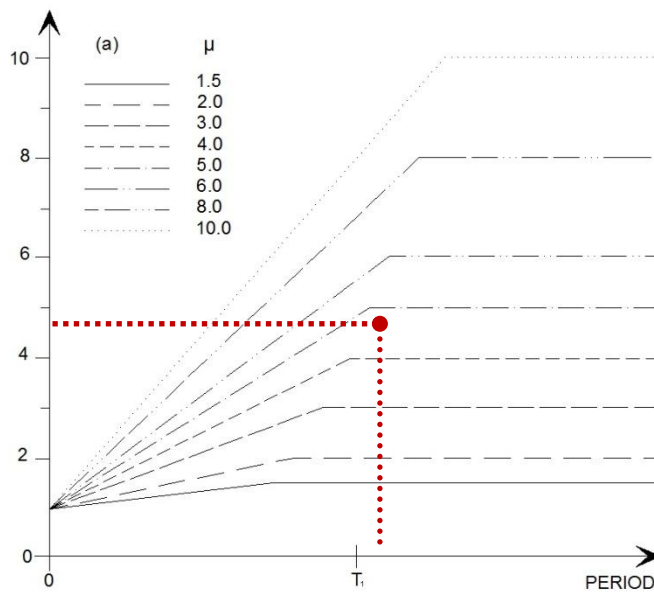


Figure 6.11 : Calculated values of R_μ and μ for SPEAR building in +Y direction

$$D^* = 0.0194 \cdot 4.417 = 0.086m$$

Finally, target displacement is determined with following formula

$$D = \frac{0.086}{0.7911} = 0.108m$$

-Y direction

Base shear-top displacement of the equivalent SDOF model and the bilinear curve is given in Figure 6.12.

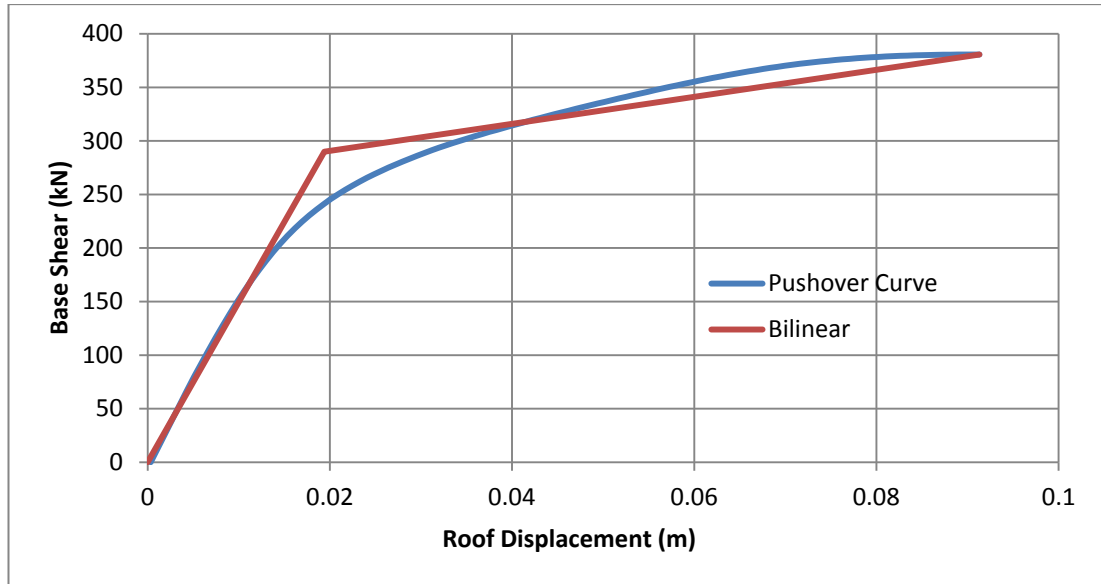


Figure 6.12 : Base shear-top displacement relationship of the SPEAR building in -Y direction

Yield strength, yield displacement, rigidity and period of the equivalent SDOF model are determined from the bilinear curve as

$$F_y^* = 287 \text{ kN}$$

$$D_y^* = 0.0178 \text{ m}$$

$$k^* = \frac{287}{0.0178} = 16123 \text{ kN/m}$$

$$T^* = 2 \cdot 3.14 \cdot \sqrt{\frac{126.75}{16123}} = 0.56 \text{ sec}$$

According to EC 8 soil type B spectrum acceleration value is determined as 1.07 g for T^*

$$R_\mu = \frac{126.75 \cdot 1.07 \cdot 9.81}{287} = 4.636$$

Transition period where the constant acceleration segment of the response spectrum passes to constant velocity segment of the spectrum (T_1) = 0.5. Hence, according to R-spectrum (as seen in Figure 6.13) R_μ is equal to μ due to equal displacement rule.

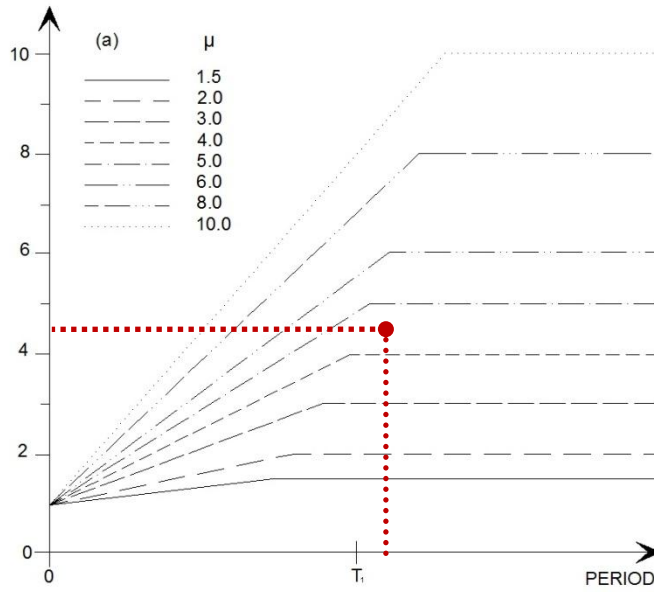


Figure 6.13 : Calculated values of R_μ and μ for SPEAR building in -Y direction

$$D^* = 0.0178 \cdot 4.636 = 0.083m$$

Finally, target displacement is determined with following formula

$$D = \frac{0.083}{0.7911} = 0.104m$$

Capacity curves of the SPEAR building were plotted in Figure 6.14 for positive and negative sign.

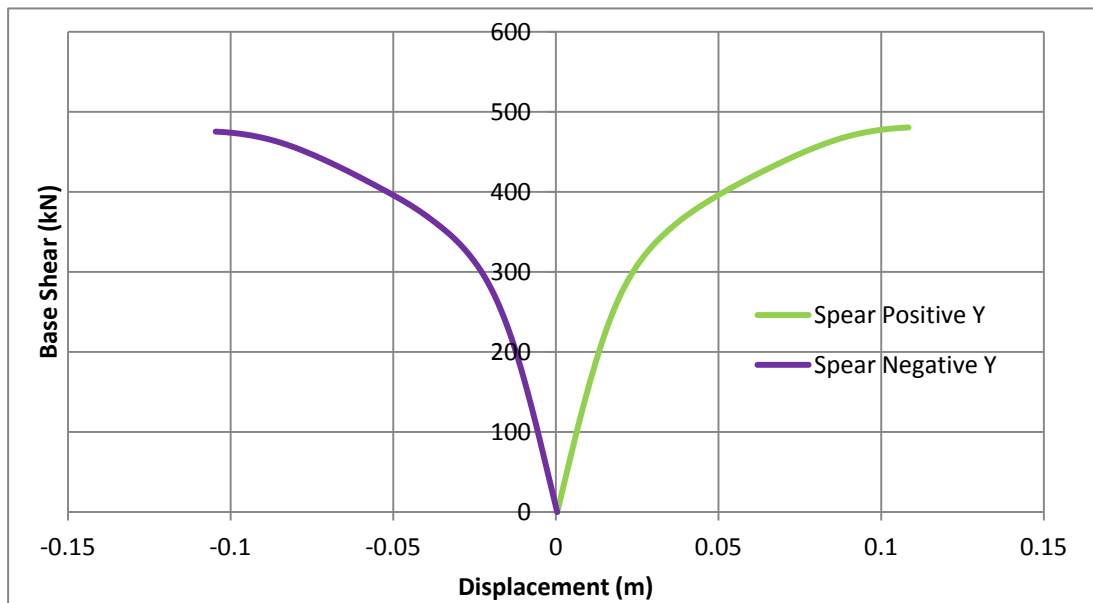


Figure 6.14 : Capacity curves of the SPEAR building in Y direction

6.2.3 Extended N2 Method for original case of SPEAR building

Extended N2 method is applied the SPEAR building due to irregularity in plan. Elastic modal response analysis (RSA) is performed to capture the deformed shape of the building in centre of mass. For normalized the elastic modal analysis results, a factor is calculated as,

$$c_{NORM} = \frac{0.108}{0.075} = 1.43$$

Table 6.3 : Pushover and RSA results of SPEAR building in Y direction

Pushover		RSA	
Displacement (m)	Storey Drift (%)	Displacement (m)	Storey Drift (%)
0.026	0.9	0.030	1.01
0.070	1.5	0.074	1.45
0.108	1.3	0.108	1.13

Correction factors for along the elevation for building (c_E) are calculated 1, 1.05 and 1.16 for displacements and 1, 1 and 1.17 for drifts in story 3, story 2 and story 1, respectively as seen in Figure 6.15 and 6.16. In addition, as seen in Figure 6.17, Y3 axis of the building is flexible edge. Correction factor for plan (c_T) is calculated as 1.23 for Y3 axis.

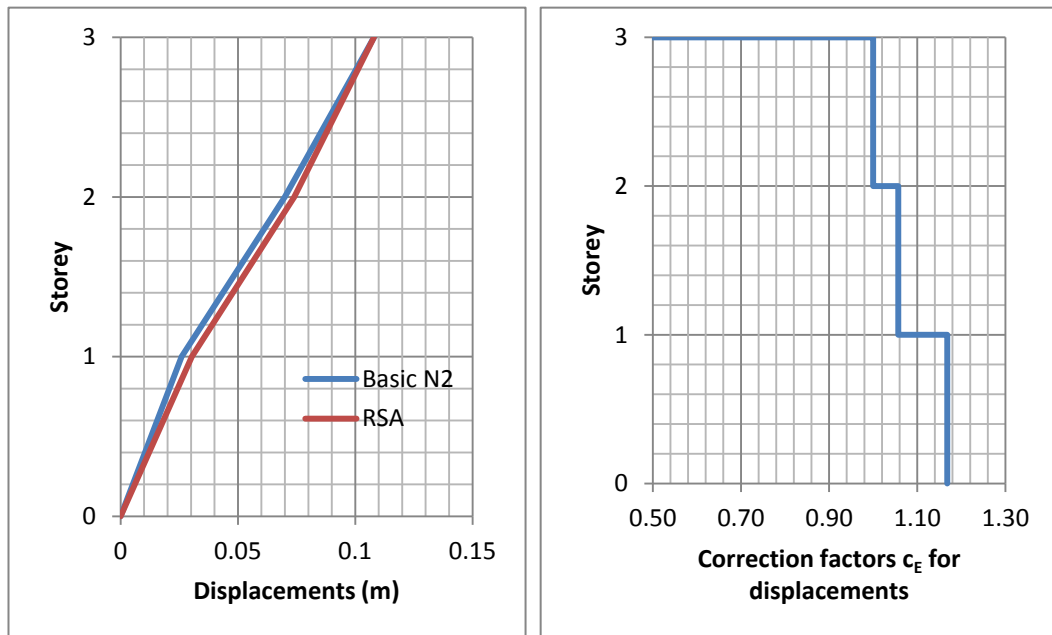


Figure 6.15 : Correction factors (c_E) for displacements

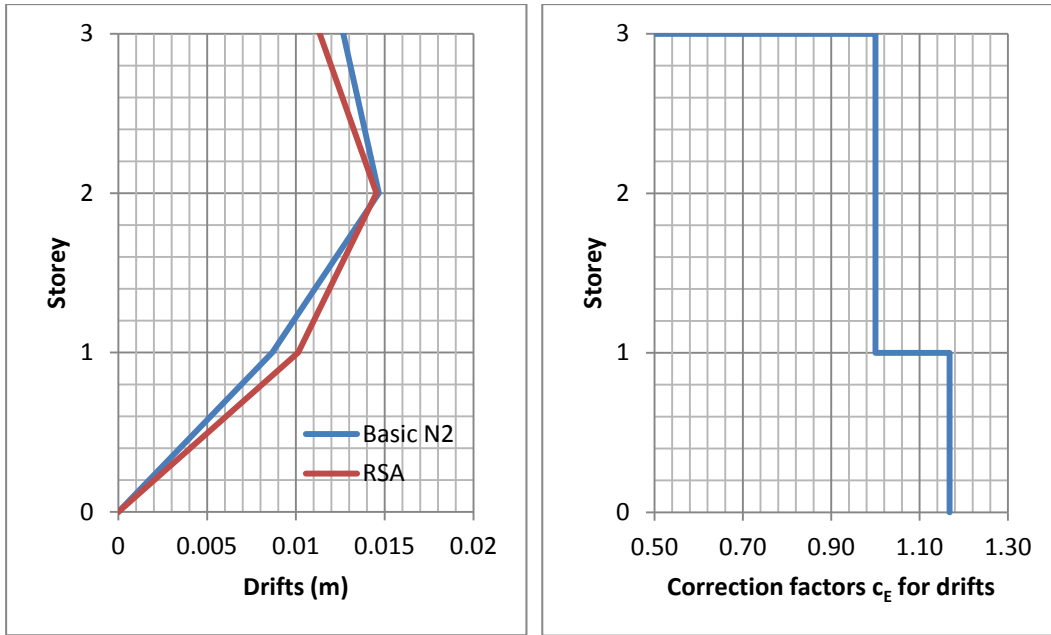


Figure 6.16 : Correction factors (c_E) for drifts

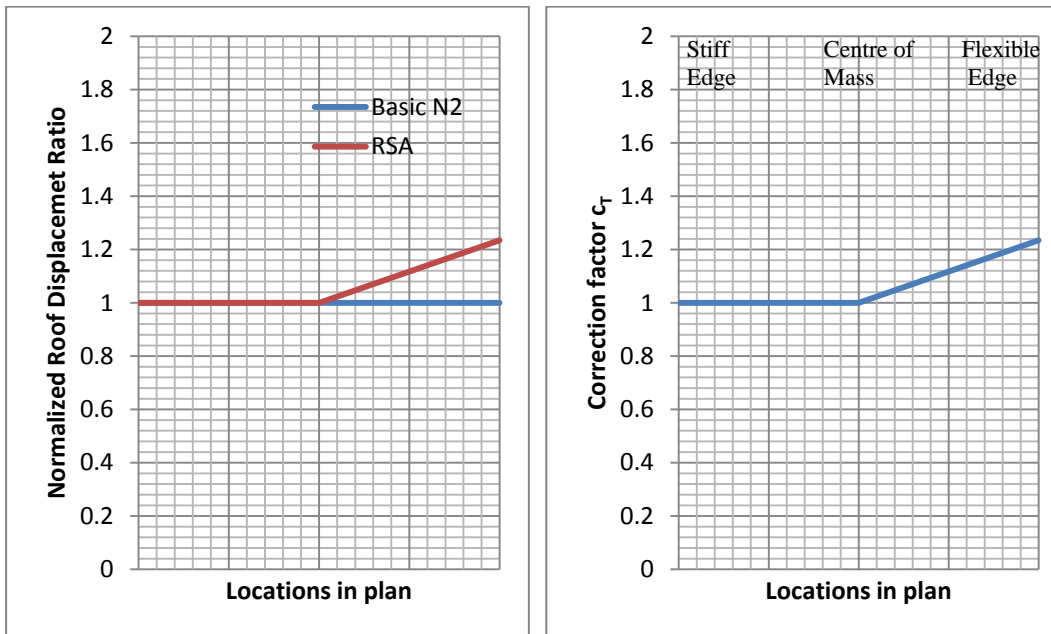


Figure 6.17 : Correction factors (c_T) for plan

6.2.4 N2 method for remodeled case of SPEAR building

The fundamental mode and force distribution is altered due to remodeled case. The mode shape and lateral load distribution are given in Table 6.4.

Table 6.4 : Lateral load distribution values

Storey	Mode Shape	Normalized Mode Shape	Weight (kN)	Lateral Load (kN)
3	0.0297	0.302	629.8	190.39
2	0.0699	0.710	629.8	447.17
1	0.0984	1	619.0	619.06

The generalized mass of the considered mode and the mass of the equivalent SDOF system are given below for Y direction.

$$\{\Phi\}^T [M] \{\Phi\} = 101.34$$

$$\{\Phi\}^T [M] \{1\} = m^* = 128.09t$$

Therefore, coefficient c is calculated as below.

$$c = \frac{101.34}{128.09} = 0.7911$$

+Y direction

Base shear-top displacement of the equivalent SDOF model and the bilinear curve is given in Figure 6.18.

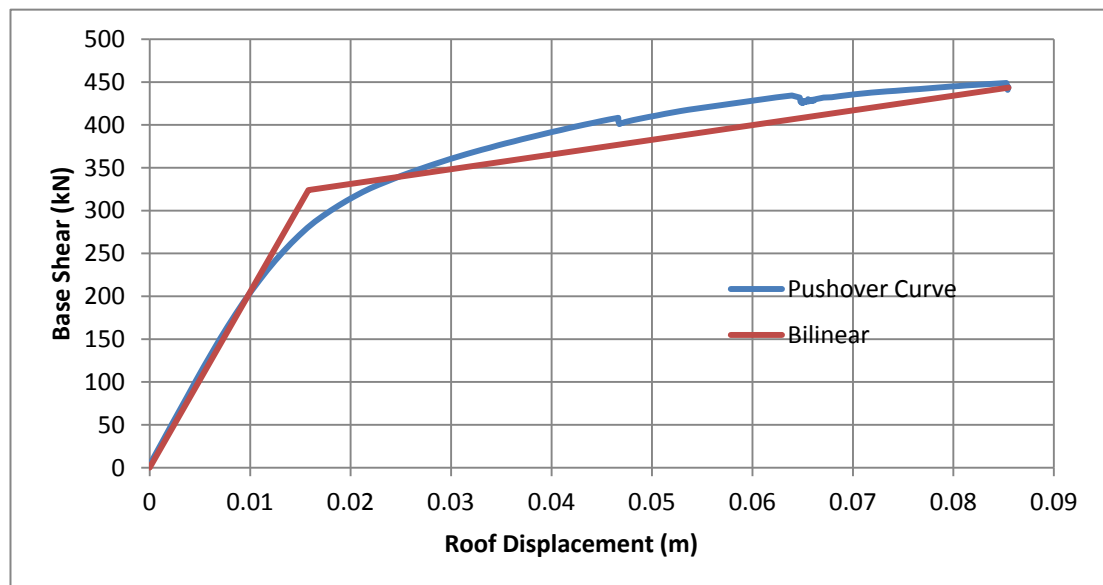


Figure 6.18 : Base shear-top displacement relationship of the remodeled SPEAR building in +Y direction

Yield strength, yield displacement, rigidity and period of the equivalent SDOF model are determined from the bilinear curve as

$$F_y^* = 324kN$$

$$D_y^* = 0.0158m$$

$$k^* = \frac{324}{0.0158} = 20506kN/m$$

$$T^* = 2 \cdot 3.14 \cdot \sqrt{\frac{128.09}{20506}} = 0.50sec$$

According to EC 8 soil type B spectrum acceleration value is determined as 1.2 g for T^*

$$R_\mu = \frac{128.09 \cdot 1.2 \cdot 9.81}{324} = 4.654$$

Transition period where the constant acceleration segment of the response spectrum passes to constant velocity segment of the spectrum (T_1) = 0.5. Hence, according to R-spectrum (as seen in Figure 6.19) R_μ is equal to μ due to equal displacement rule.

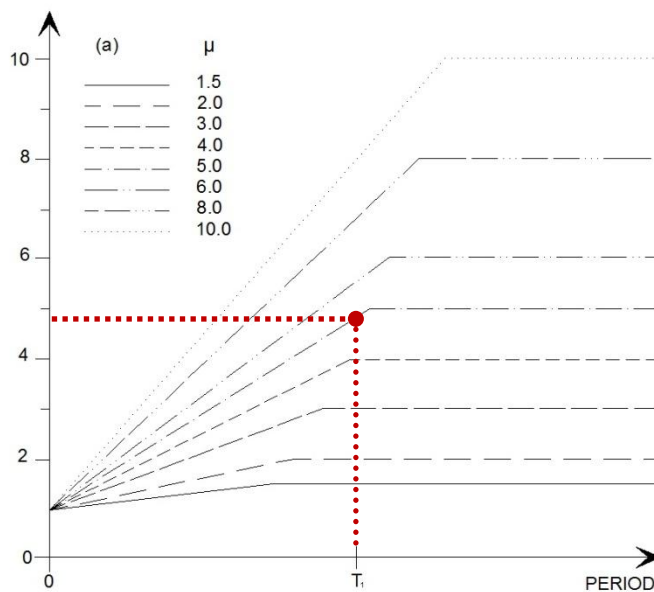


Figure 6.19 : Calculated values of R_μ and μ for remodeled SPEAR building in +Y direction

$$D^* = 0.0158 \cdot 4.654 = 0.074m$$

Finally, target displacement is determined with following formula

$$D = \frac{0.074}{0.7911} = 0.093m$$

-Y direction

Base shear-top displacement of the equivalent SDOF model and the bilinear curve is given in Figure 6.20.

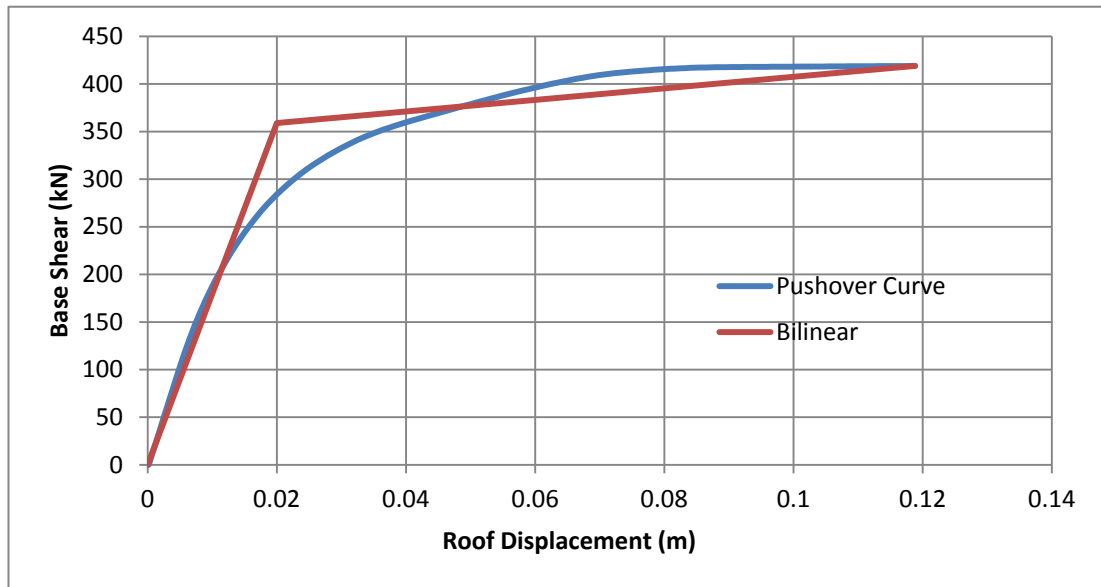


Figure 6.20 : Base shear-top displacement relationship of the remodeled SPEAR building in -Y direction

Yield strength, yield displacement, rigidity and period of the equivalent SDOF model are determined from the bilinear curve as

$$F_y^* = 359kN$$

$$D_y^* = 0.02m$$

$$k^* = \frac{359}{0.02} = 17950kN/m$$

$$T^* = 2 \cdot 3.14 \cdot \sqrt{\frac{128.09}{17950}} = 0.53sec$$

According to EC 8 soil type B spectrum acceleration value is determined as 1.13 g for T^*

$$R_\mu = \frac{128.09 \cdot 1.13 \cdot 9.81}{359} = 3.955$$

Transition period where the constant acceleration segment of the response spectrum passes to constant velocity segment of the spectrum (T_1) = 0.5. Hence, according to R-spectrum (as seen in Figure 6.19) R_μ is equal to μ due to equal displacement rule.

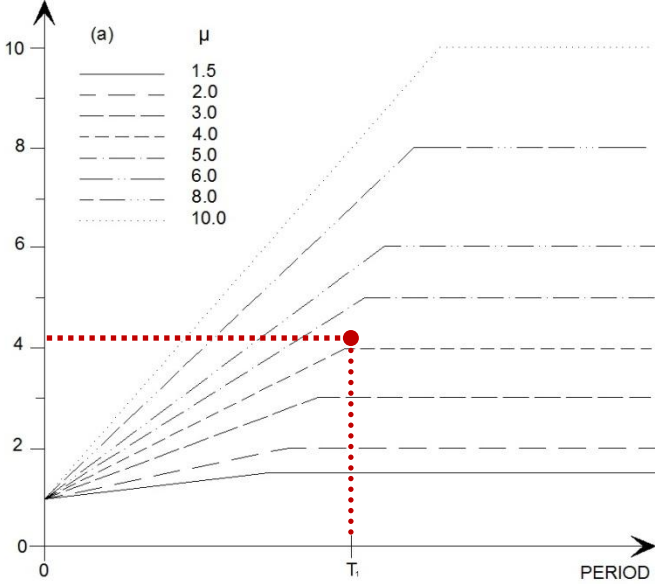


Figure 6.21 : Calculated values of R_μ and μ for remodeled SPEAR building in -Y direction

$$D^* = 0.02 \cdot 3.955 = 0.079m$$

Finally, target displacement is determined with following formula

$$D = \frac{0.079}{0.7911} = 0.1m$$

The capacity curves of the SPEAR building for regular and irregular cases are given in Figure 6.22. For positive and negative direction, the capacity of the regular structure are higher compared to irregular case. The capacity of the +Y direction larger than the -Y direction. For +Y direction, large columns are in compression and the sections of the mentioned columns are fully resists the external forces however for -Y direction, large columns are in tension. Capacity curves of the SPEAR building for regular and irregular case are plotted in Figure 6.22.

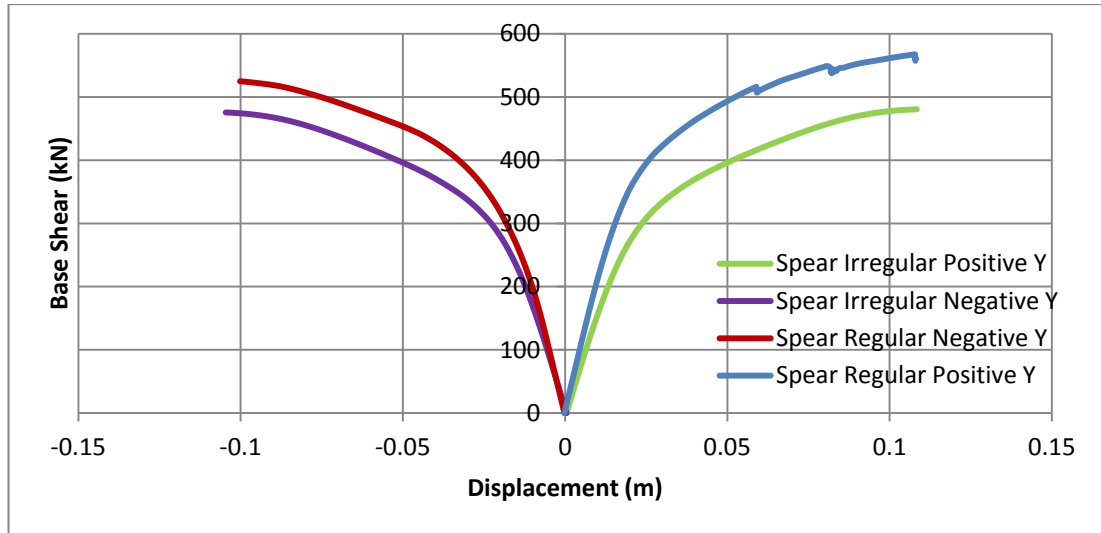


Figure 6.22 : Capacity curves of the SPEAR building for regular and irregular cases in Y direction

Number of plastic hinges and the location of the hinges are given in following table and figure. Number of developed plastic hinges are more than for irregular case compared to regular case.

Table 6.5 : Values of developed plastic hinges in SPEAR building

Regular		Irregular	
+Y	-Y	+Y	-Y
14	25	33	34

As seen in Figure 6.23, number of plastic hinges are more than the in Y3 axis compared to Y1 and Y2 axis for irregular case. Due to torsional characteristics, Y3 axis of the building is flexible edge. Hence, the local quantities are multiplied by 1.23, which is calculated according to extended N2 method. After the using extended N2 method, number of plastic hinges are increased in flexible edge. While the increasing of the hinges are three for +Y direction, it is eight for -Y direction. In addition, for the regular structure, locations of the plastic hinges are distributed more uniform along the building.

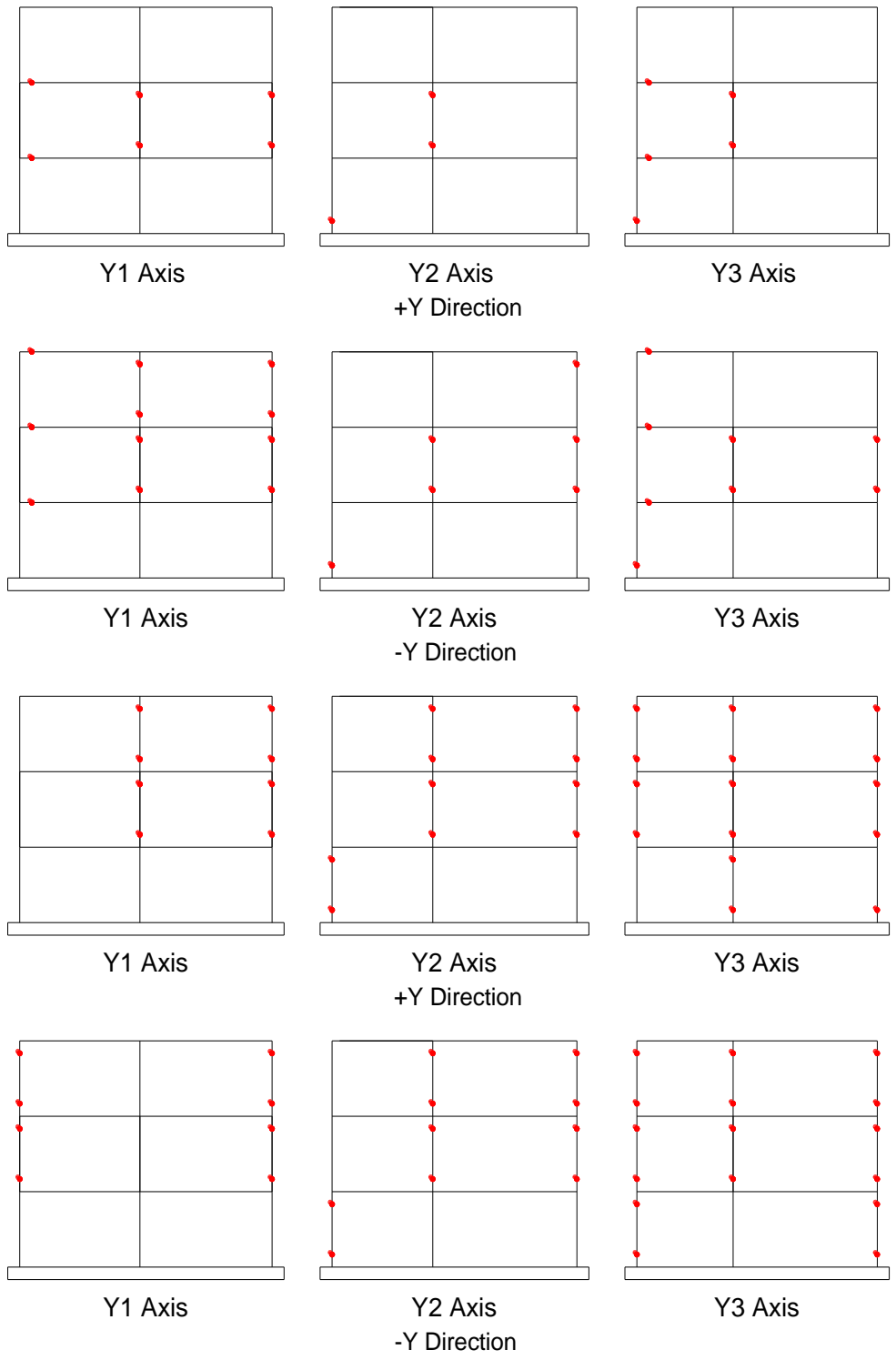


Figure 6.23 : Plastic hinge locations of the SPEAR building for regular (top) and irregular (bottom) cases in Y direction

6.2.5 ICON building

Nonlinear static procedures were applied the ICON structure in X direction for negative and positive direction.

6.2.6 N2 method for original case of ICON building

The fundamental mode of the considered structure in X direction is first mode. The mode shape and lateral load distribution are given in Table 6.6.

Table 6.6 : Lateral load distribution values

Storey	Mode Shape	Normalized Mode Shape	Weight (kN)	Lateral Load (kN)
4	0.110	0.246	40.85	98.91
3	0.261	0.586	40.85	235.00
2	0.380	0.851	40.68	339.71
1	0.446	1.000	32.70	320.78

The generalized mass of the considered mode and the mass of the equivalent SDOF system are given below for X direction.

$$\{\Phi\}^T [M] \{\Phi\} = 78.71$$

$$\{\Phi\}^T [M] \{1\} = m^* = 101.36t$$

Therefore, coefficient c is calculated as below.

$$c = \frac{78.71}{101.36} = 0.7765$$

+X direction

Base shear-top displacement of the equivalent SDOF model and the bilinear curve is given in Figure 6.24.

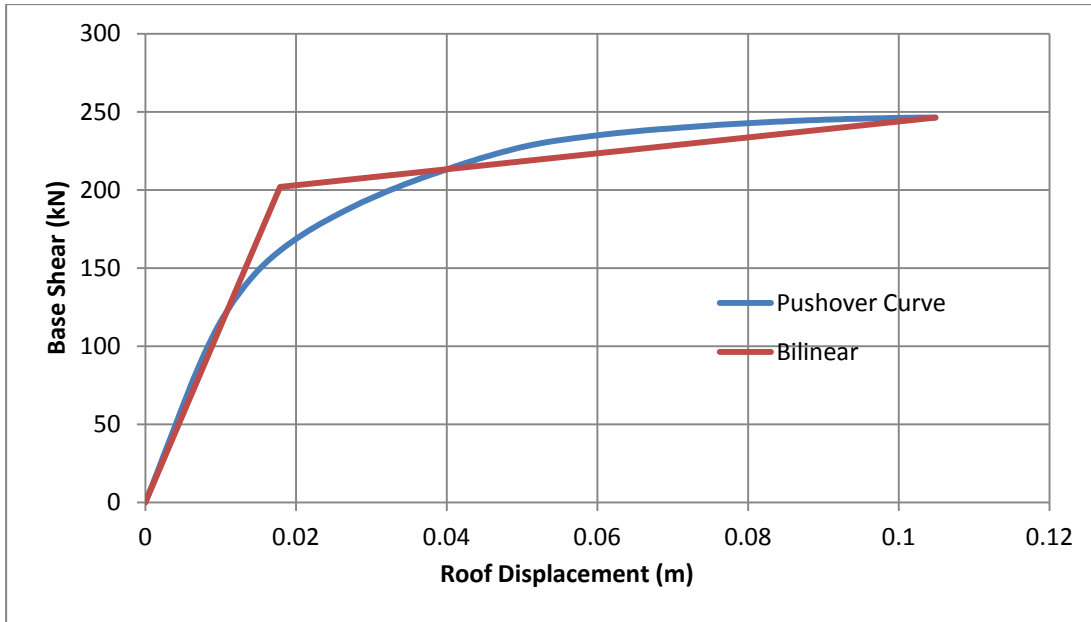


Figure 6.24 : Base shear-top displacement relationship of the ICON building in +X direction

Yield strength, yield displacement, rigidity and period of the equivalent SDOF model are determined from the bilinear curve as

$$F_y^* = 202kN$$

$$D_y^* = 0.0178m$$

$$k^* = \frac{202}{0.0178} = 11303kN/m$$

$$T^* = 2 \cdot 3.14 \cdot \sqrt{\frac{101.36}{11303}} = 0.59 \text{ sec}$$

According to EC 8 soil type B spectrum acceleration value is determined as 1.016 g for T^*

$$R_\mu = \frac{101.36 \cdot 1.016 \cdot 9.81}{202} = 5.002$$

Transition period where the constant acceleration segment of the response spectrum passes to constant velocity segment of the spectrum (T_1) = 0.5. Hence, according to R-spectrum (as seen in Figure 6.25) R_μ is equal to μ due to equal displacement rule.

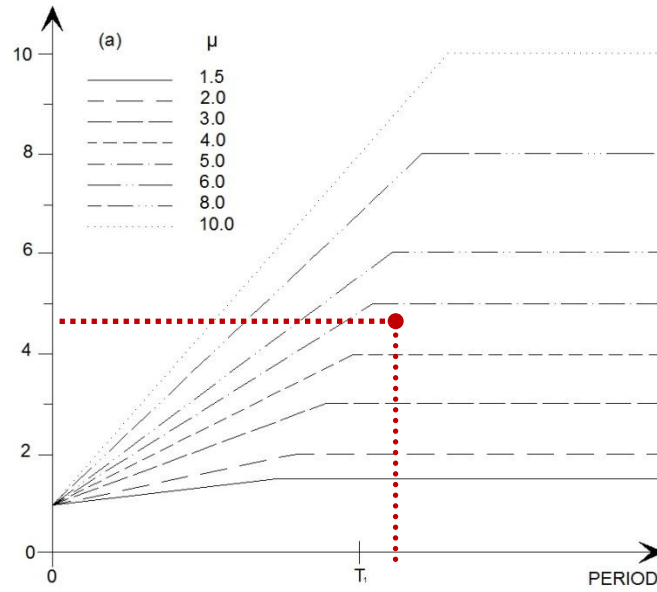


Figure 6.25 : Calculated values of R_μ and μ for ICON building in +X direction

$$D^* = 0.0178 \cdot 5.002 = 0.089m$$

Finally, target displacement is determined with following formula

$$D = \frac{0.089}{0.7765} = 0.115m$$

-X direction

Base shear-top displacement of the equivalent SDOF model and the bilinear curve is given in Figure 6.26.

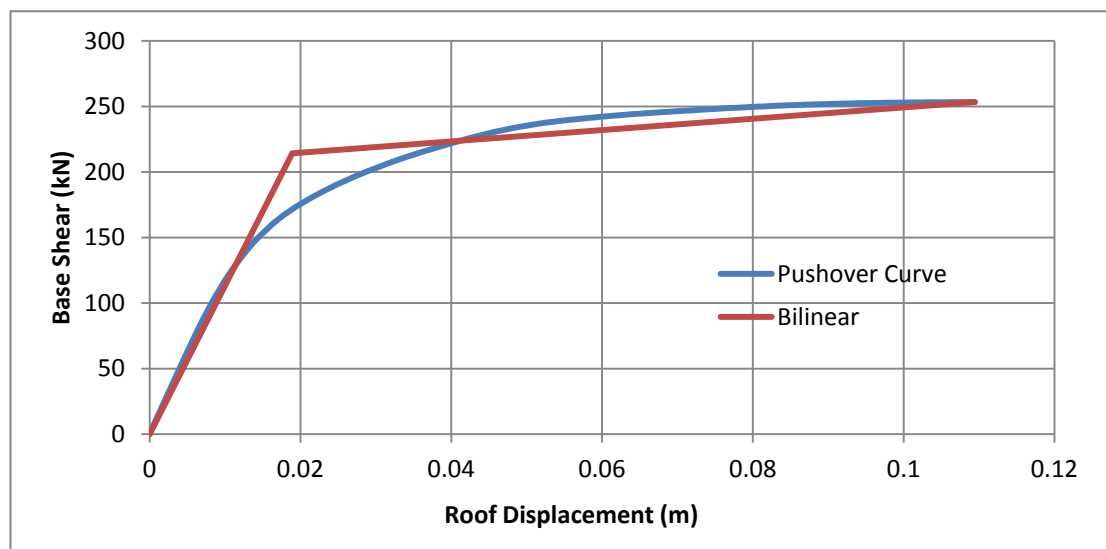


Figure 6.26 : Base shear-top displacement relationship of the ICON building in -X direction

Yield strength, yield displacement, rigidity and period of the equivalent SDOF model are determined from the bilinear curve as

$$F_y^* = 214kN$$

$$D_y^* = 0.0189m$$

$$k^* = \frac{214}{0.0189} = 11333kN/m$$

$$T^* = 2 \cdot 3.14 \cdot \sqrt{\frac{101.36}{11333}} = 0.59sec$$

According to EC 8 soil type B spectrum acceleration value is determined as 1.016 g for T^*

$$R_\mu = \frac{101.36 \cdot 1.016 \cdot 9.81}{214} = 4.717$$

Transition period where the constant acceleration segment of the response spectrum passes to constant velocity segment of the spectrum (T_1) = 0.5. Hence, according to R-spectrum (as seen in Figure 6.27) R_μ is equal to μ due to equal displacement rule.

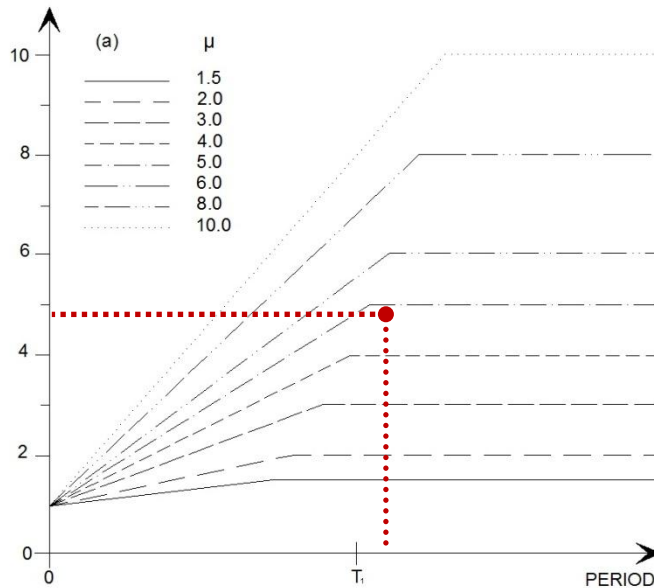


Figure 6.27 : Calculated values of R_μ and μ for ICON building in -X direction

$$D^* = 0.0189 \cdot 4.717 = 0.089m$$

Finally, target displacement is determined with following formula

$$D = \frac{0.089}{0.7765} = 0.115m$$

Capacity curves of the ICON building are plotted for negative and positive sign in Figure 6.28.

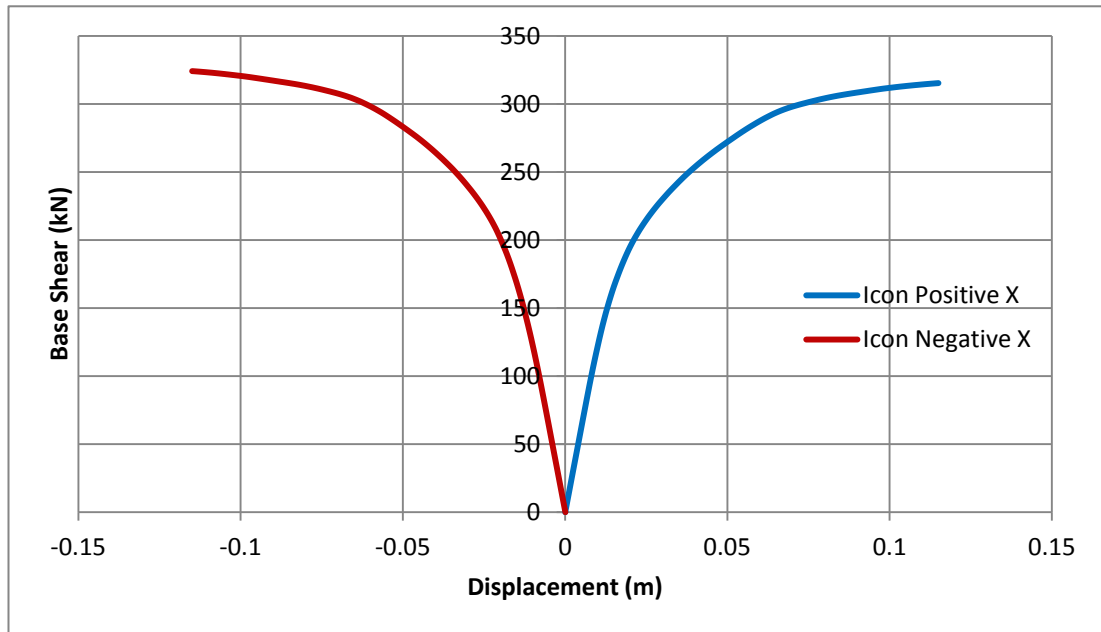


Figure 6.28 : Capacity curves of the ICON building in X direction

6.2.7 N2 method for remodeled case of ICON building

The fundamental mode and force distribution is altered due to remodeled case. The mode shape and lateral load distribution are given in Table 6.7.

Table 6.7 : Lateral force distribution values

Storey	Mode Shape	Normalized Mode Shape	Weight (kN)	Lateral Load (kN)
4	0.116	0.325	40.85	130.30
3	0.275	0.767	40.85	307.75
2	0.398	1.11	40.68	443.08
1	0.358	1.00	25.00	245.22

The generalized mass of the considered mode and the mass of the equivalent SDOF system are given below for X direction.

$$\{\Phi\}^T [M] \{\Phi\} = 103.55$$

$$\{\Phi\}^T [M] \{1\} = m^* = 114.81t$$

Therefore, coefficient c is calculated as below.

$$c = \frac{103.55}{114.81} = 0.9019$$

+X direction

Base shear-top displacement of the equivalent SDOF model and the bilinear curve is given in Figure 6.29.

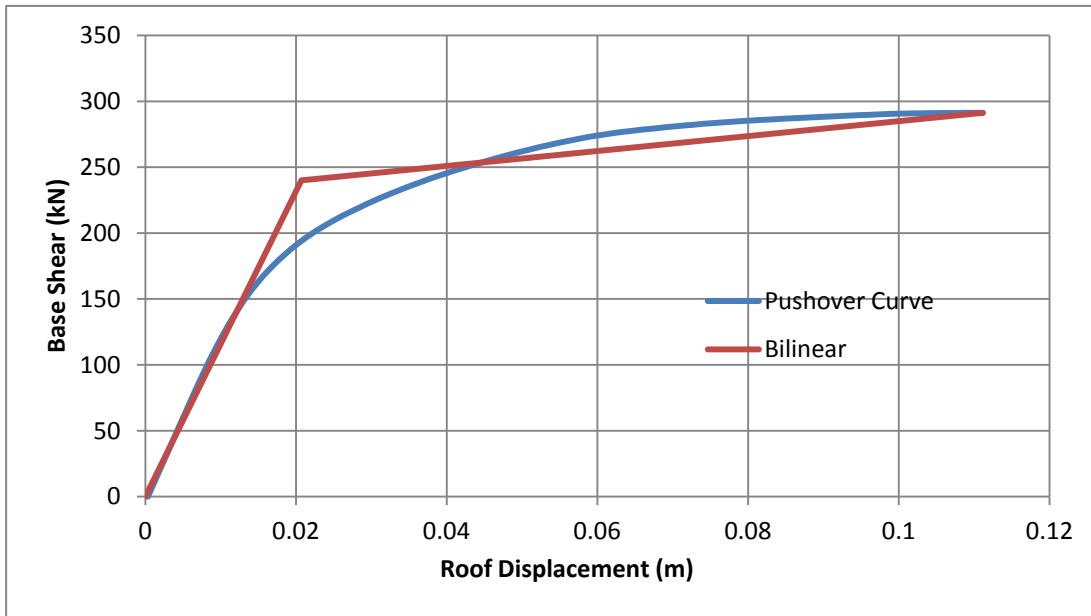


Figure 6.29 : Base shear-top displacement relationship of the remodeled ICON building in +X direction

Yield strength, yield displacement, rigidity and period of the equivalent SDOF model are determined from the bilinear curve as

$$F_y^* = 240kN$$

$$D_y^* = 0.0207m$$

$$k^* = \frac{240}{0.0207} = 11594kN/m$$

$$T^* = 2 \cdot 3.14 \cdot \sqrt{\frac{114.81}{11594}} = 0.62 \text{ sec}$$

According to EC 8 soil type B spectrum acceleration value is determined as 0.952 g for T^*

$$R_{\mu} = \frac{114.81 \cdot 0.968 \cdot 9.81}{240} = 4.543$$

Transition period where the constant acceleration segment of the response spectrum passes to constant velocity segment of the spectrum (T_1) = 0.5. Hence, according to R-spectrum (as seen in Figure 6.30) R_{μ} is equal to μ due to equal displacement rule.

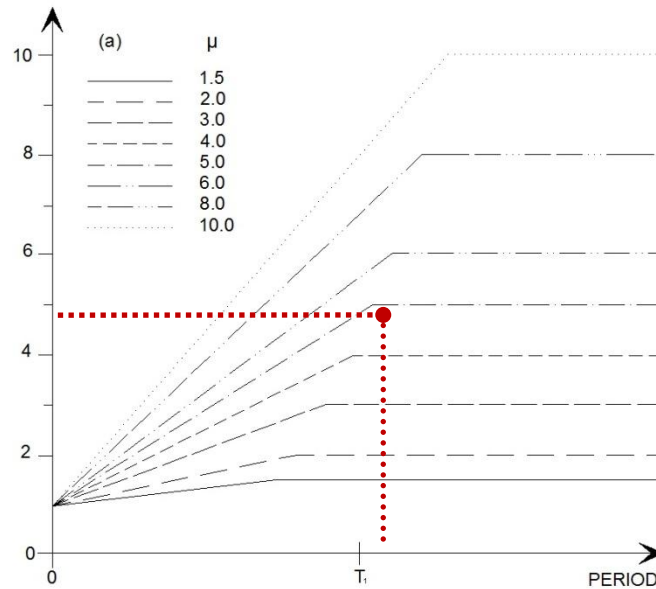


Figure 6.30 : Calculated values of R_{μ} and μ for remodeled ICON building in +X direction

$$D^* = 0.0207 \cdot 4.543 = 0.094m$$

Finally, target displacement is determined with following formula

$$D = \frac{0.094}{0.901} = 0.104m$$

-X direction

Base shear-top displacement of the equivalent SDOF model and the bilinear curve is given in Figure 6.31.

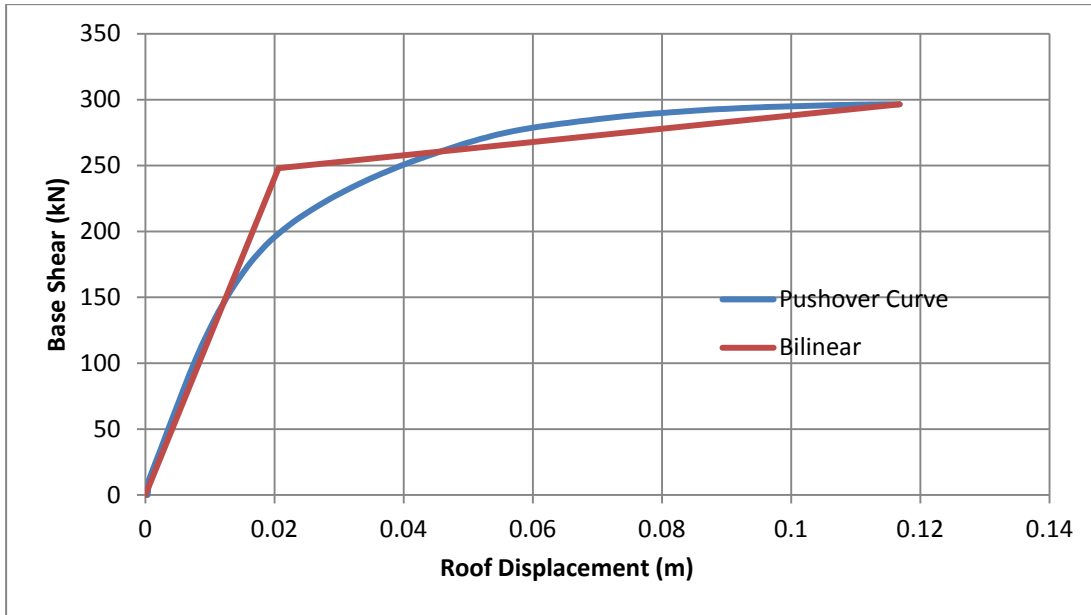


Figure 6.31 : Base shear-top displacement relationship of the remodeled ICON building in -X direction

Yield strength, yield displacement, rigidity and period of the equivalent SDOF model are determined from the bilinear curve as

$$F_y^* = 248kN$$

$$D_y^* = 0.0206m$$

$$k^* = \frac{248}{0.0206} = 12038kN/m$$

$$T^* = 2 \cdot 3.14 \cdot \sqrt{\frac{114.81}{12038}} = 0.61sec$$

According to EC 8 soil type B spectrum acceleration value is determined as 0.983 g for T^*

$$R_\mu = \frac{114.81 \cdot 0.983 \cdot 9.81}{248} = 4.465$$

Transition period where the constant acceleration segment of the response spectrum passes to constant velocity segment of the spectrum (T_1) = 0.5. Hence, according to R-spectrum (as seen in Figure 6.32) R_μ is equal to μ due to equal displacement rule.

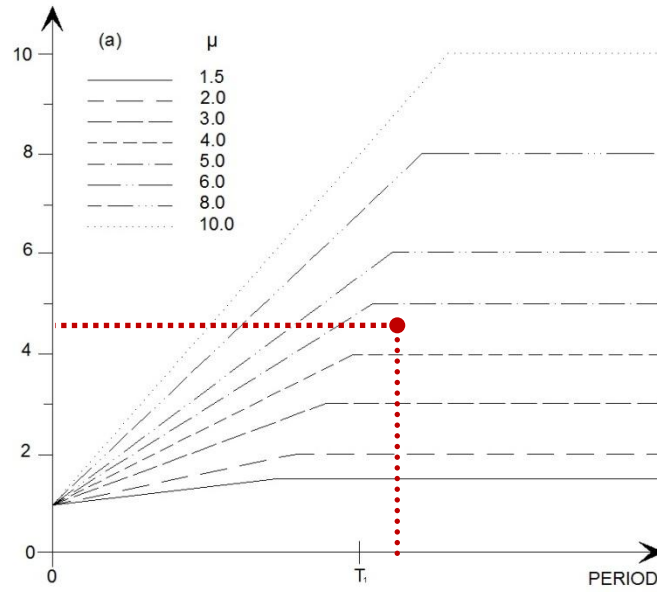


Figure 6.32 : Calculated values of R_μ and μ for remodeled ICON building in -X direction

$$D^* = 0.0206 \cdot 4.465 = 0.092m$$

Finally, target displacement is determined with following formula

$$D = \frac{0.092}{0.901} = 0.102m$$

6.2.8 Extended N2 Method for remodeled case of ICON building

Extended N2 method is applied the ICON building due to irregularity in elevation. Elastic modal response analysis (RSA) is performed to capture the deformed shape of the building in centre of mass. For normalized the elastic modal analysis results, a factor is calculated as,

$$c_{NORM} = \frac{0.104}{0.00989} = 10.52$$

Table 6.8 : Pushover and RSA results of ICON building in X direction

Pushover		RSA	
Displacement (m)	Storey Drift (%)	Displacement (m)	Storey Drift (%)
0.031	0.0114	0.029	0.0107
0.066	0.0130	0.061	0.0121
0.090	0.0089	0.090	0.0104
0.104	0.0052	0.104	0.0053

Due to the ICON building being 2D system, correction factor for plan is not calculated. As seen in Figure 6.33, correction factor for plan (c_E) is calculated as 1 for displacements along the elevation of the considered building. In addition, in Figure 6.34, same correction factors (c_E) are calculated 1.02, 1.17 in story 4 and story 3, respectively.

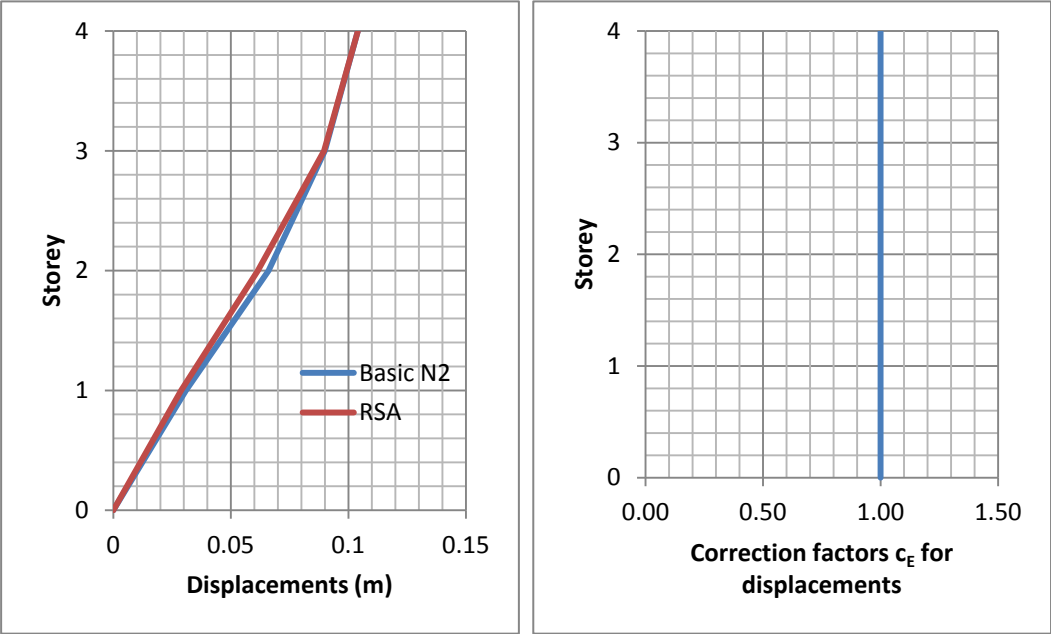


Figure 6.33 : Correction factors (c_E) for displacements

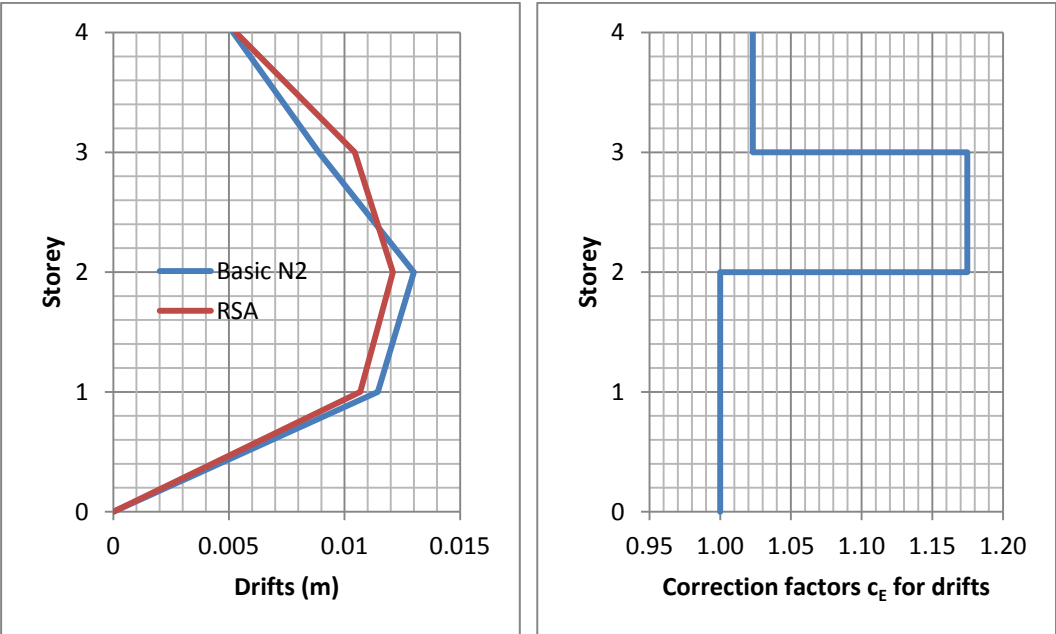


Figure 6.34 : Correction factors (c_E) for drifts

The capacity curves of the ICON building for regular and irregular cases are given in Figure 6.35. Although the capacity of the structures are close to each other, irregular structure are a bit more higher than irregular case, for positive and negative direction.

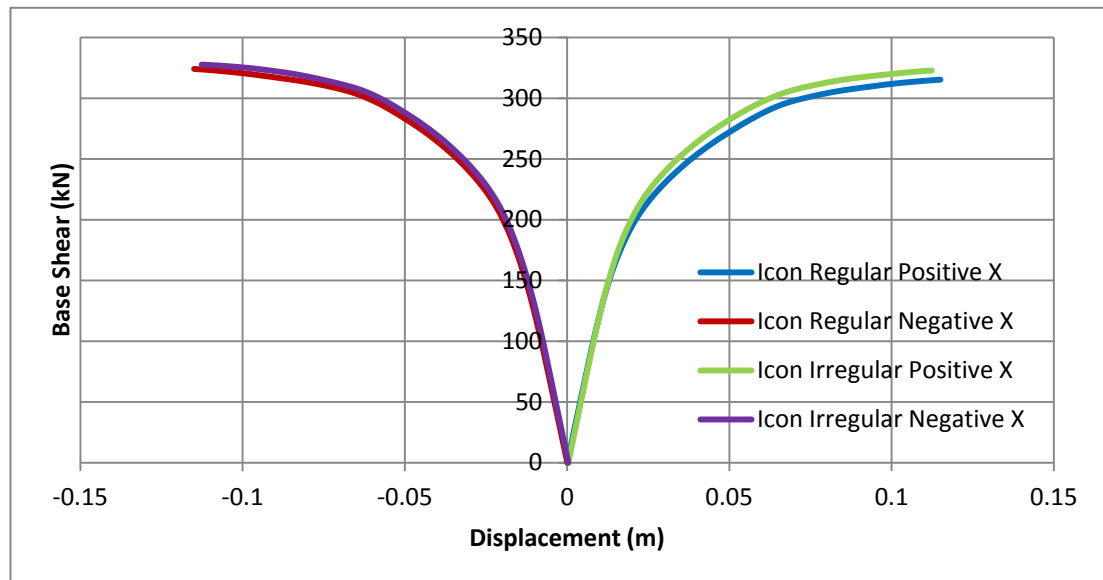


Figure 6.35 : Capacity curves of the ICON building for regular and irregular cases in X direction

Number of plastic hinges and the location of the hinges are given in following table and figure. Number of developed plastic hinges are more than for regular case compared to irregular case. Changing of the modal shape and load distribution, decreasing of the number of the elements and decreasing of the axial loads on columns are affected to capacity of the frame.

Table 6.9 : Values of developed plastic hinges in ICON building

Regular		Irregular	
+X	-X	+X	-X
12	12	11	7

As seen in Figure 6.36, removing the one axis from the top of the building is effected +X direction.

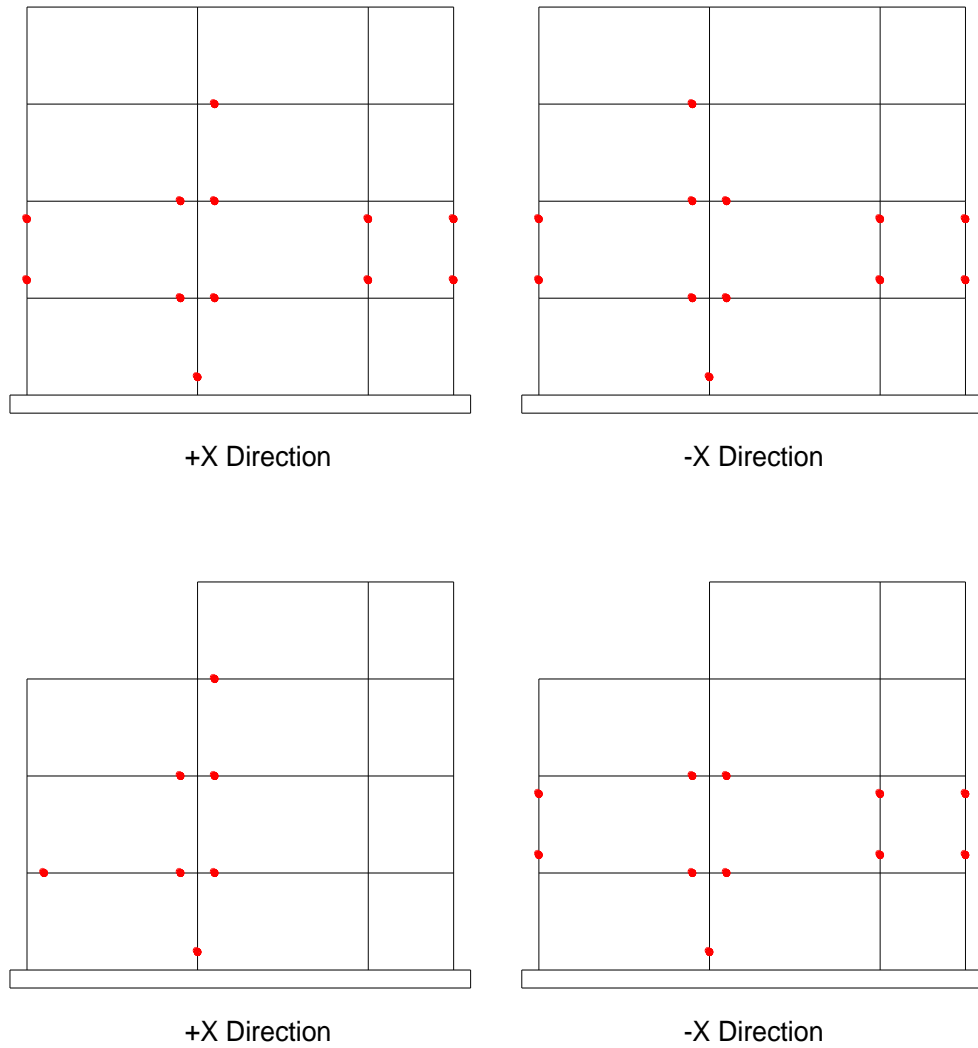


Figure 6.36 : Plastic hinge locations of the ICON building for regular (top) and irregular (bottom) cases in X direction

6.2.9 School building

Nonlinear static procedures were applied the school building in X direction for negative and positive direction.

6.2.10 N2 method for original case of school building

The fundamental mode of the considered structure in X direction is first mode. The mode shape and lateral load distribution are given in Table 6.10.

Table 6.10 : Lateral load distribution values

Storey	Mode Shape	Normalized Mode Shape	Weight (kN)	Lateral Load (kN)
3	0.0032	0.089	820.47	721.46
2	0.0195	0.546	798.19	4277.02
1	0.0357	1	606.08	5945.63

The generalized mass of the considered mode and the mass of the equivalent SDOF system are given below for X direction.

$$\{\Phi\}^T [M] \{\Phi\} = 850.81$$

$$\{\Phi\}^T [M] \{1\} = m^* = 1115.61t$$

Therefore, coefficient c is calculated as below.

$$c = \frac{850.81}{1115.61} = 0.7626$$

+X direction

Base shear-top displacement of the equivalent SDOF model and the bilinear curve is given in Figure 6.37.

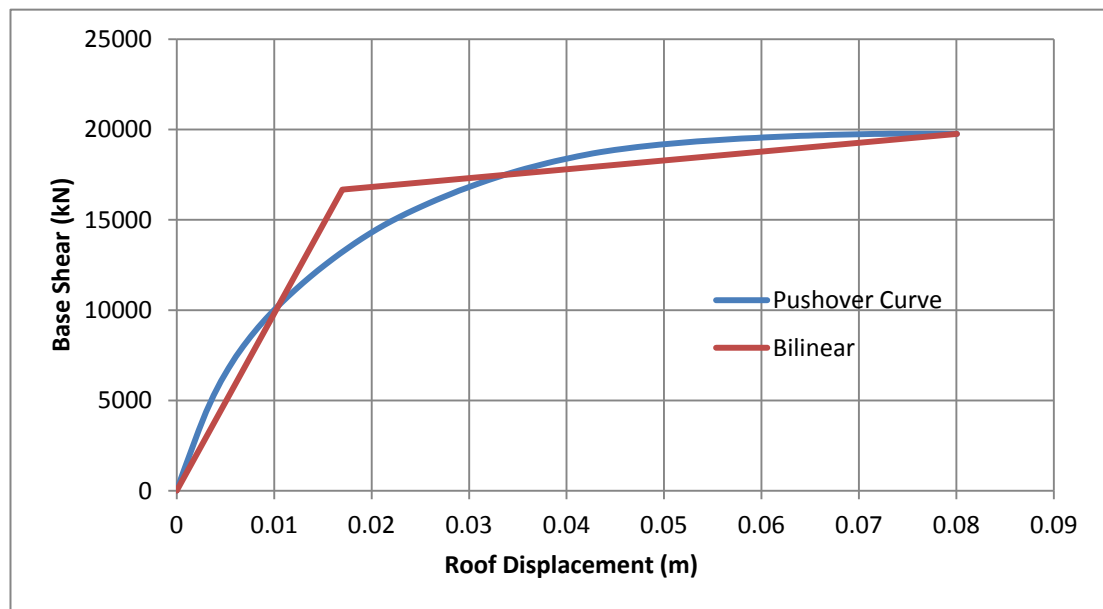


Figure 6.37 : Base shear-top displacement relationship of the school building in +X direction

Yield strength, yield displacement, rigidity and period of the equivalent SDOF model are determined from the bilinear curve as

$$F_y^* = 16670kN$$

$$D_y^* = 0.017m$$

$$k^* = \frac{16670}{0.017} = 980588kN/m$$

$$T^* = 2 \cdot 3.14 \cdot \sqrt{\frac{1115}{980588}} = 0.21sec$$

According to EC 8 soil type B spectrum acceleration value is determined as 1.2 g for T^*

$$R_\mu = \frac{1115 \cdot 1.2 \cdot 9.81}{16670} = 0.788$$

According to mentioned reference in section 5.1.1, the reduction factor (R_μ) starts at 1. Therefore, R_μ is taken as 1 and according to equation 5.7, μ is calculated as

$$\mu = (1 - 1) \frac{0.5}{0.21} + 1 = 1$$

Calculated values are marked with red point in Figure 6.38.

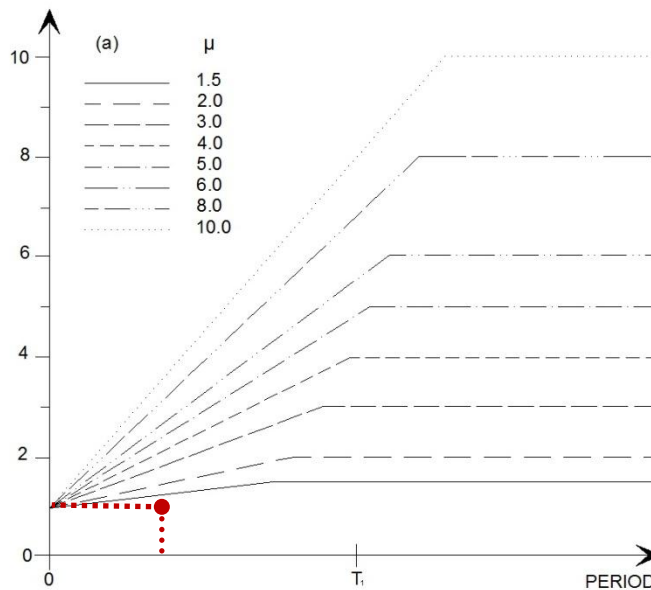


Figure 6.38 : Calculated values of R_μ and μ for school building in +X direction

$$D^* = 0.017 \cdot 1 = 0.017m$$

Finally, target displacement is determined with following formula

$$D = \frac{0.017}{0.7626} = 0.022m$$

-X direction

Base shear-top displacement of the equivalent SDOF model and the bilinear curve is given in Figure 6.39.

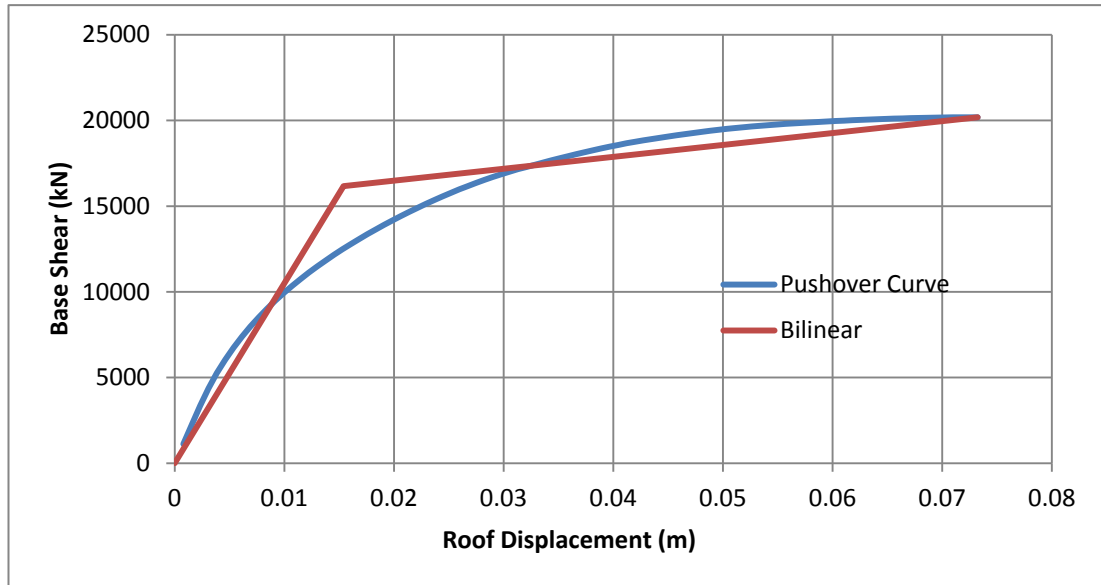


Figure 6.39 : Base shear-top displacement relationship of the school building in -X direction

Yield strength, yield displacement, rigidity and period of the equivalent SDOF model are determined from the bilinear curve as

$$F_y^* = 16166kN$$

$$D_y^* = 0.0154m$$

$$k^* = \frac{16166}{0.0154} = 1049740kN/m$$

$$T^* = 2 \cdot 3.14 \cdot \sqrt{\frac{1115}{1049740}} = 0.20sec$$

According to EC 8 soil type B spectrum acceleration value is determined as 1.2 g for T^*

$$R_{\mu} = \frac{1115 \cdot 1.2 \cdot 9.81}{16166} = 0.812$$

According to mentioned reference in section 5.1.1, the reduction factor (R_{μ}) starts at 1. Therefore, R_{μ} is taken as 1 and according to equation 5.7, μ is calculated as

$$\mu = (1-1) \frac{0.5}{0.20} + 1 = 1$$

Calculated values are marked with red point in Figure 6.40.

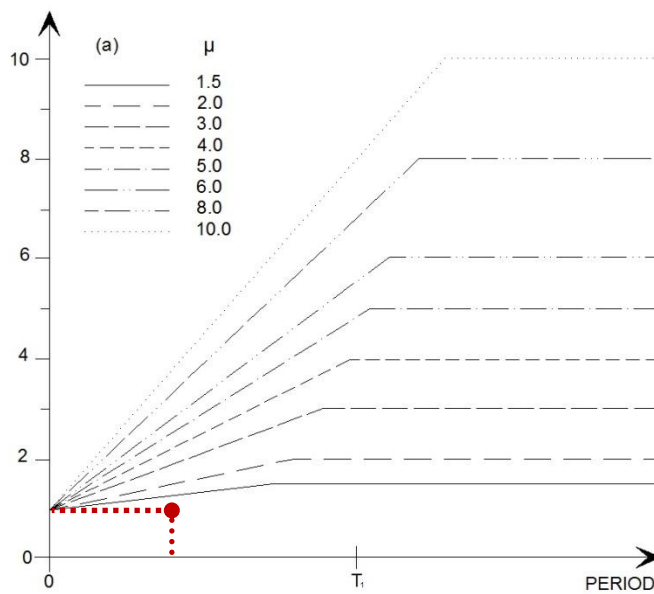


Figure 6.40 : Calculated values of R_{μ} and μ for school building in -X direction

$$D^* = 0.0154 \cdot 1 = 0.0154m$$

Finally, target displacement is determined with following formula

$$D = \frac{0.0154}{0.7626} = 0.02m$$

Capacity curves of the school building was plotted in Figure 6.41 for positive and negative sign.

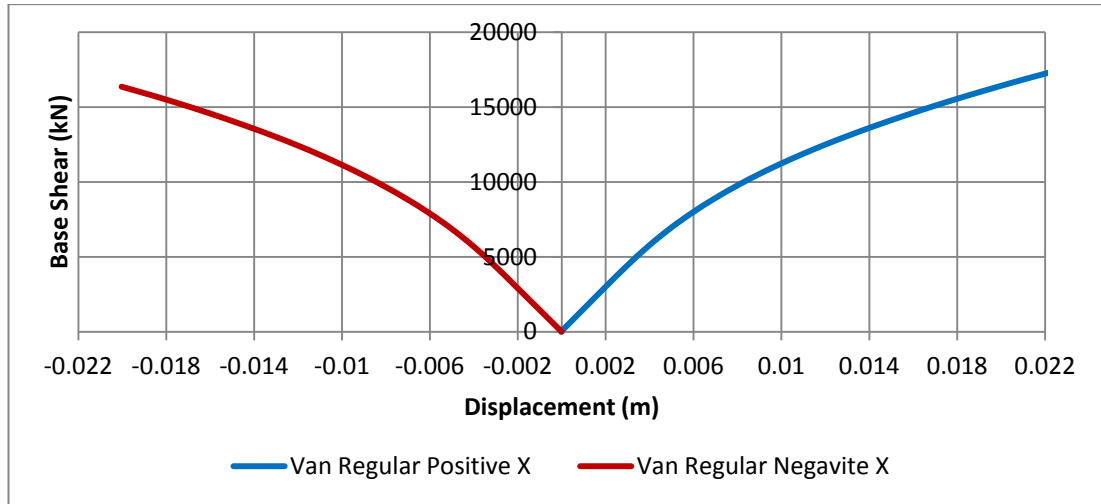


Figure 6.41 : Capacity curves of the school building in X direction

6.2.11 N2 method for remodeled case of school building

The fundamental mode and force distribution is altered due to remodeled case. The mode shape and lateral load distribution are given in Table 6.11.

Table 6.11 : Lateral load distribution values

Storey	Mode Shape	Normalized Mode Shape	Weight (kN)	Lateral Load (kN)
3	0.00182	0.052	820.47	418.06
2	0.02027	0.578	798.19	4529.6
1	0.03504	1	606.08	5945

The generalized mass of the considered mode and the mass of the equivalent SDOF system are given below for X direction.

$$\{\Phi\}^T [M] \{\Phi\} = 875.40$$

$$\{\Phi\}^T [M] \{1\} = m^* = 1110.43t$$

Therefore, coefficient c is calculated as below.

$$c = \frac{875.40}{1110.43} = 0.7883$$

+X direction

Base shear-top displacement of the equivalent SDOF model and the bilinear curve is given in Figure 6.42.

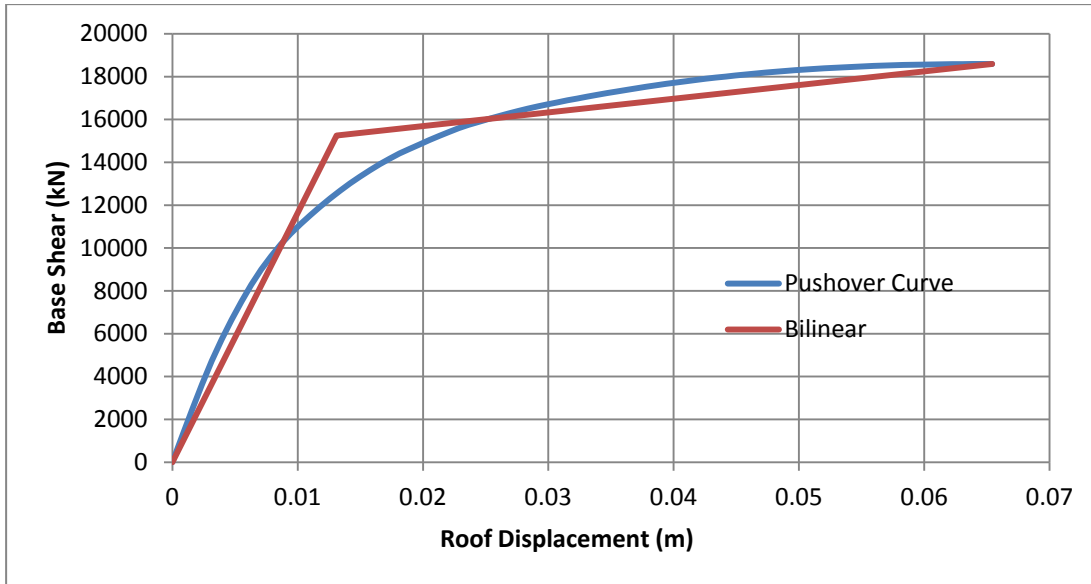


Figure 6.42 : Base shear-top displacement relationship of the remodeled school building in +X direction

Yield strength, yield displacement, rigidity and period of the equivalent SDOF model are determined from the bilinear curve as

$$F_y^* = 15250 \text{ kN}$$

$$D_y^* = 0.0121 \text{ m}$$

$$k^* = \frac{15250}{0.0121} = 1260330 \text{ kN/m}$$

$$T^* = 2 \cdot 3.14 \cdot \sqrt{\frac{1110}{1260330}} = 0.19 \text{ sec}$$

According to EC 8 soil type B spectrum acceleration value is determined as 1.2 g for T^*

$$R_\mu = \frac{1110 \cdot 1.2 \cdot 9.81}{15250} = 0.857$$

According to mentioned reference in section 5.1.1, the reduction factor (R_μ) starts at 1. Therefore, R_μ is taken as 1 and according to equation 5.7, μ is calculated as

$$\mu = (1-1) \frac{0.5}{0.19} + 1 = 1$$

Calculated values are marked with red point in Figure 6.43.

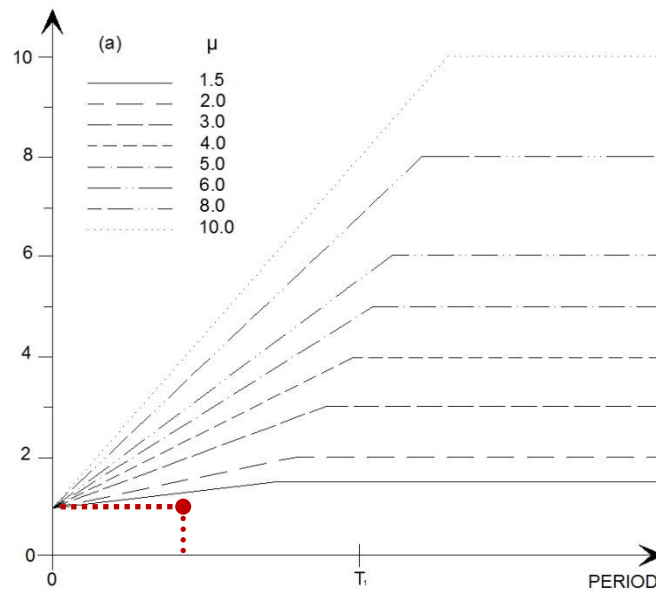


Figure 6.43 : Calculated values of R_μ and μ for remodeled school building in +X direction

$$D^* = 0.0121 \cdot 1 = 0.0121m$$

Finally, target displacement is determined with following formula

$$D = \frac{0.0121}{0.7883} = 0.019m$$

-X direction

Base shear-top displacement of the equivalent SDOF model and the bilinear curve is given in Figure 6.44.

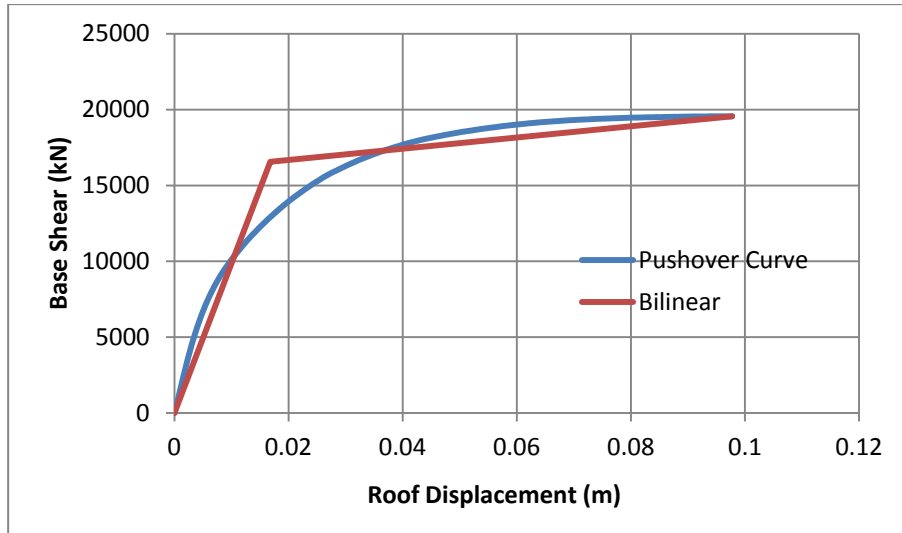


Figure 6.44 : Base shear-top displacement relationship of the remodeled school building in -X direction

Yield strength, yield displacement, rigidity and period of the equivalent SDOF model are determined from the bilinear curve as

$$F_y^* = 16565 \text{ kN}$$

$$D_y^* = 0.0168 \text{ m}$$

$$k^* = \frac{16565}{0.0168} = 986011 \text{ kN/m}$$

$$T^* = 2 \cdot 3.14 \cdot \sqrt{\frac{1110}{986011}} = 0.21 \text{ sec}$$

According to EC 8 soil type B spectrum acceleration value is determined as 1.2 g for T^*

$$R_\mu = \frac{1110 \cdot 1.2 \cdot 9.81}{16565} = 0.789$$

According to mentioned reference in section 5.1.1, the reduction factor (R_μ) starts at 1. Therefore, R_μ is taken as 1 and according to equation 5.7, μ is calculated as

$$\mu = (1-1) \frac{0.5}{0.21} + 1 = 1$$

Calculated values are marked with red point in Figure 6.45.

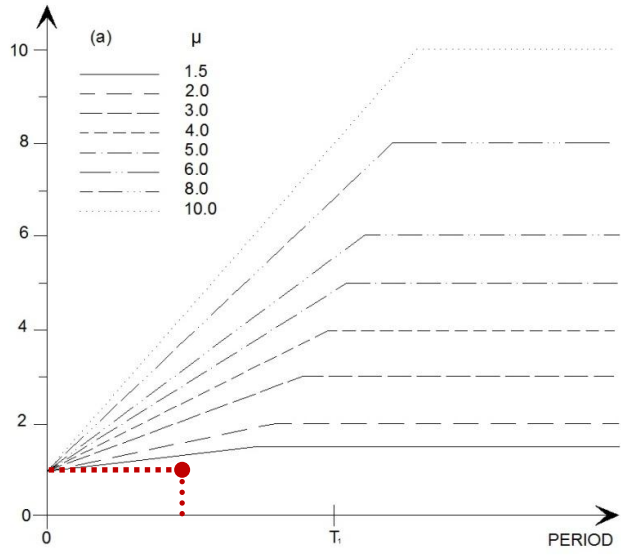


Figure 6.45 : Calculated values of R_μ and μ for remodeled school building in -X direction

$$D^* = 0.017 \cdot 1 = 0.017m$$

Finally, target displacement is determined with following formula

$$D = \frac{0.017}{0.7883} = 0.021m$$

The capacity curves of the school building for regular and irregular cases are given in Figure 6.46. For positive and negative direction, the capacity of the regular structure are higher compared to irregular case.

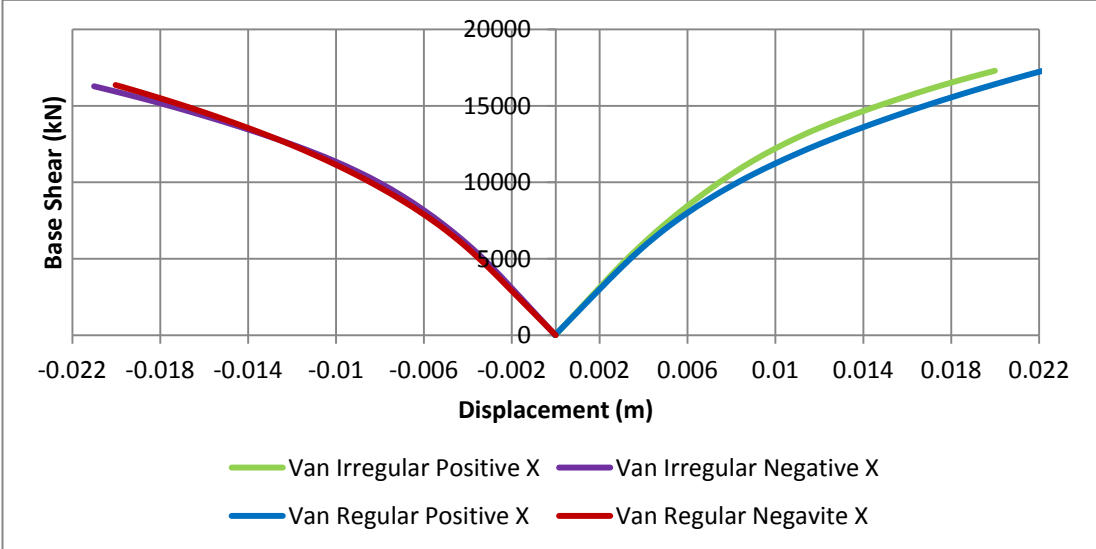


Figure 6.46 : Capacity curves of the school building for regular and irregular cases in X direction

6.2.12 Extended N2 Method for original case of school building

Extended N2 method is applied the school building due to irregularity in plan. Elastic modal response analysis (RSA) is performed to capture the deformed shape of the building in centre of mass. For normalized the elastic modal analysis results, a factor is calculated as,

$$c_{NORM} = \frac{0.021}{0.010} = 2.01$$

Table 6.12 : Pushover and RSA results of school building in X direction

Pushover		RSA	
Displacement (m)	Storey Drift	Displacement (m)	Storey Drift
0.001	0.0002	0.001	0.0002
0.012	0.0038	0.001	0.0003
0.021	0.0031	0.002	0.0002

Correction factors for along the elevation for building (c_E) are calculated 1.02, 1 and 1 for displacements and 1.02, 1 and 1 for drifts in story 3, story 2 and story 1, respectively as seen in Figure 6.47 and 6.48. In addition, as seen in Figure 6.49, A axis of the building is flexible edge. Correction factor for plan (c_T) is calculated as 1.12 for A axis.

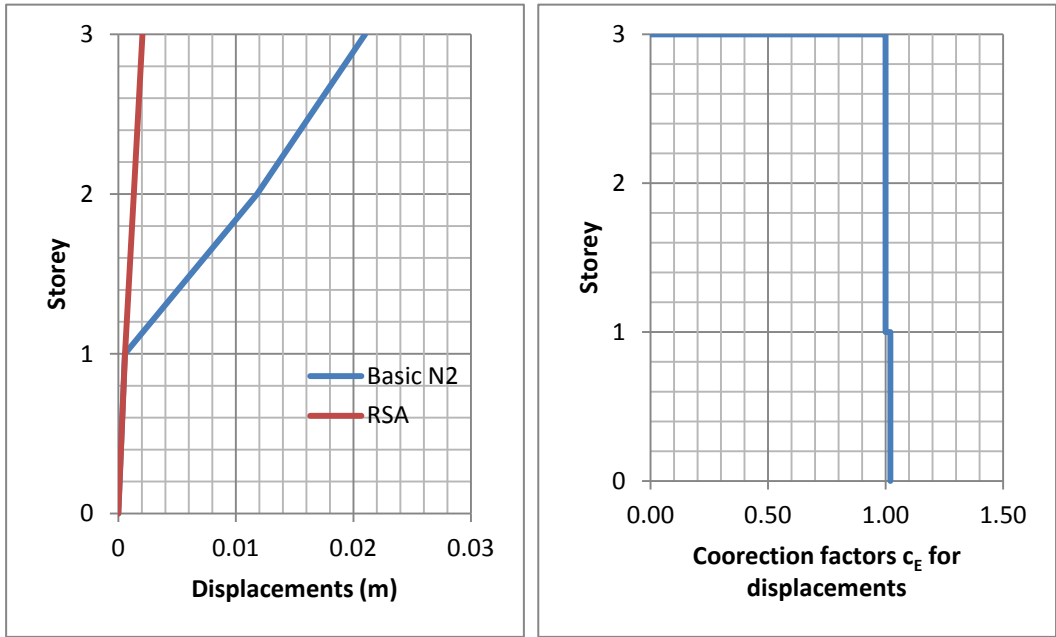


Figure 6.47 : Correction factors (c_E) for displacements

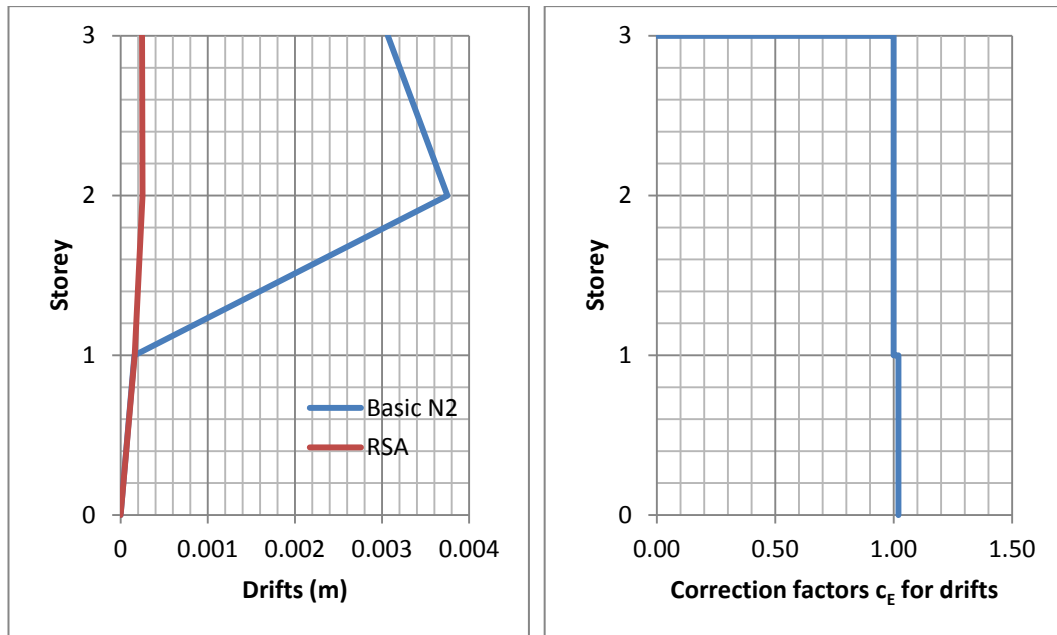


Figure 6.48 : Correction factors (c_E) for drifts

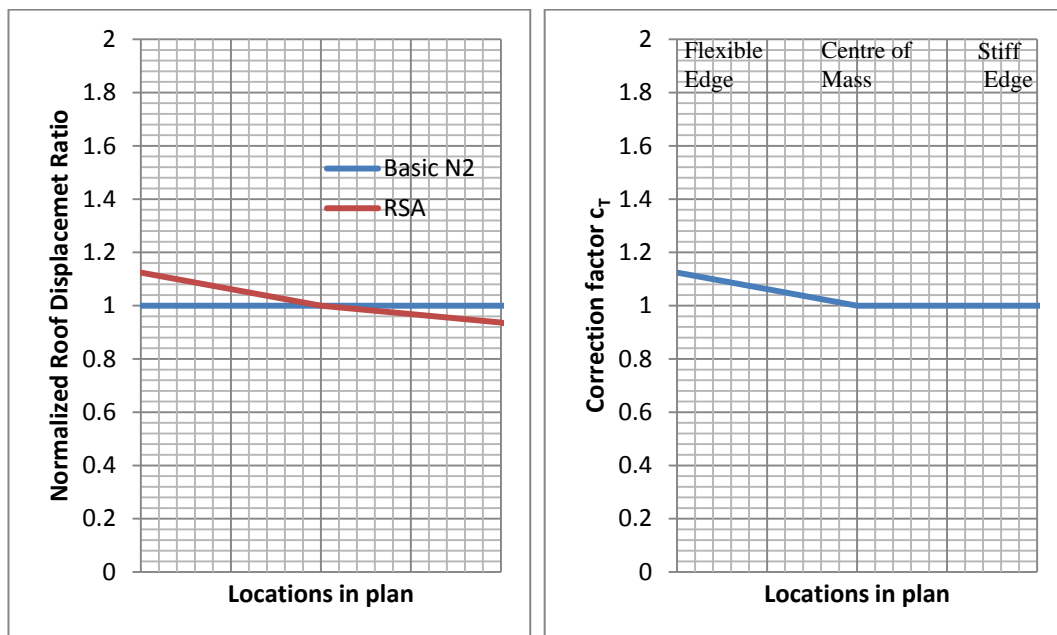


Figure 6.49 : Correction factors (c_T) for plan

Number of plastic hinges and the location of the hinges are given in following table and figure. Number of developed plastic hinges are more than for regular case compared to irregular case. After the using extended N2 method, number of plastic hinges are increased in flexible edge. The increasing of the hinges is two for both +X and -X direction.

Table 6.13 : Values of developed plastic hinges in school building

Regular		Irregular	
+X	-X	+X	-X
29	25	26	25

As seen in Figure 6.50 and Figure 6.51, while the number of plastic hinges are more in D-E axis for regular buildings, it is more in G axis for irregular buildings. The shear walls are located in D-E axis for regular and G axis for irregular cases and that is the reason developments of the plastic hinges in this axis.

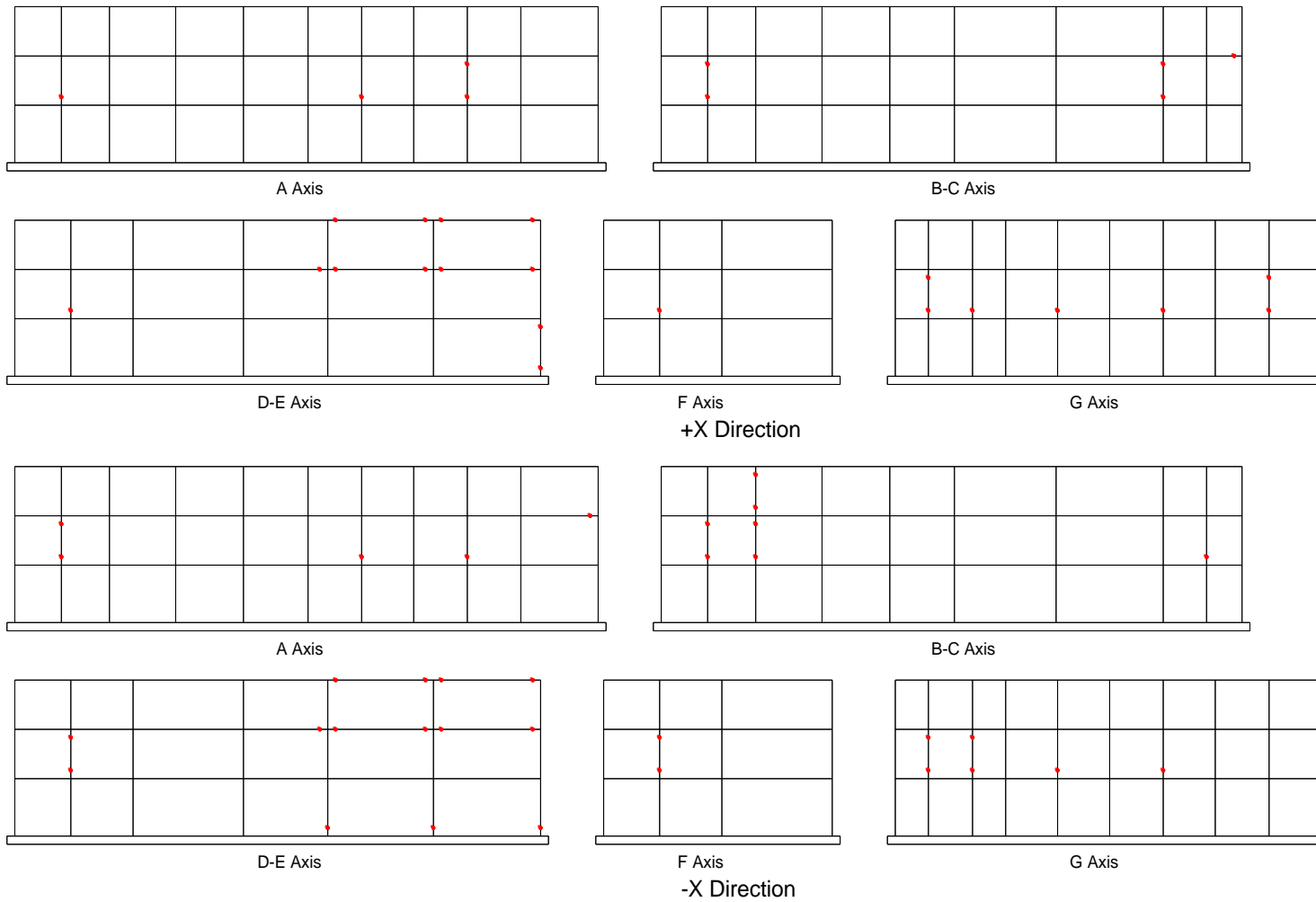


Figure 6.50 : Plastic hinge locations of the school building for regular case in X direction

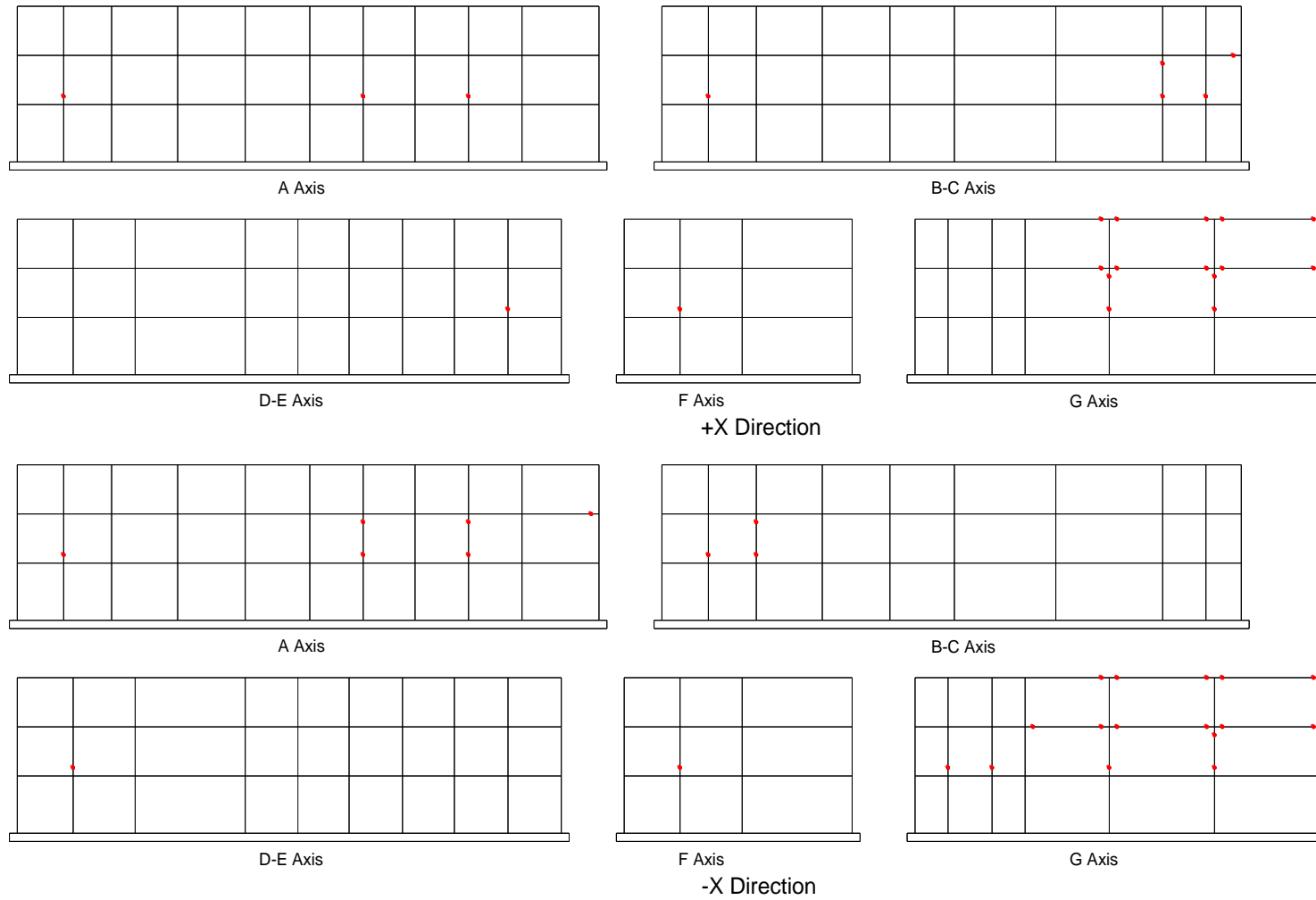


Figure 6.51 : Plastic hinge locations of the school building for irregular case in X direction

6.3 Seismic Response of Regular and Irregular Models

This chapter presents time history analysis results. Regular and irregular buildings were compared in terms of top displacement, drifts, residual displacements, formation of plastic hinges and interstory drifts for main shock and following aftershocks. 43 time history analysis were conducted for each building and each case which are named as degrading regular, degrading irregular, non-degrading regular and non-degrading irregular. Totaly 516 analysis were performed.

Limited residual displacements were observed in non-degrading models. However, the increment of residual displacements is clearly observed in degrading models due to aftershocks in lots of analysis as seen in Figure 6.52 and 6.53.

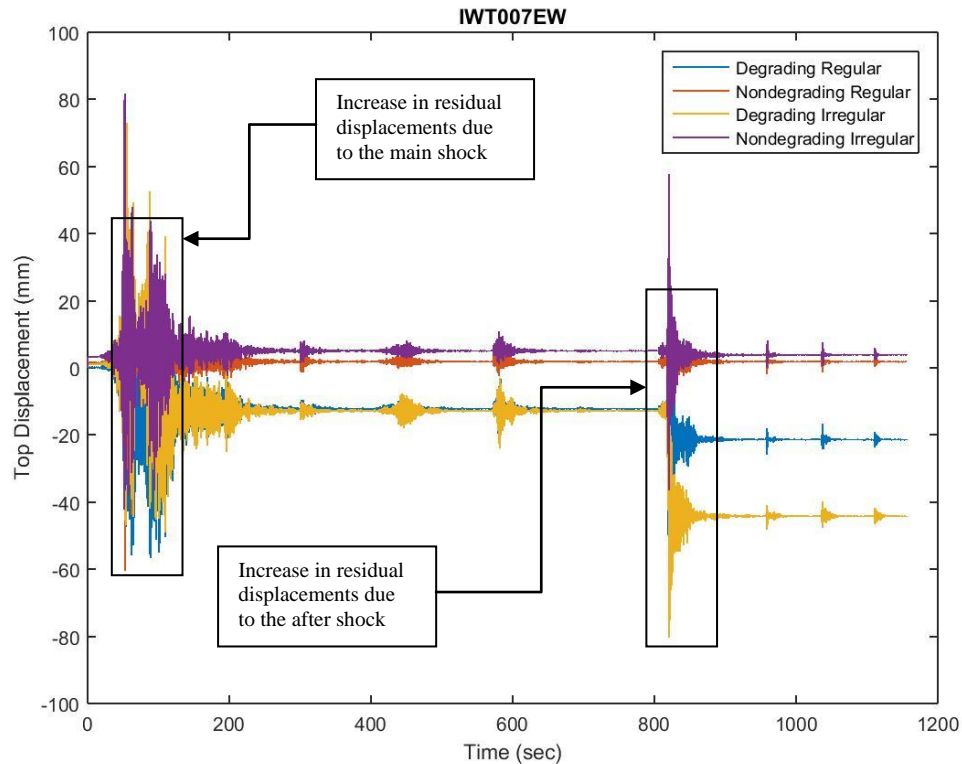


Figure 6.52 : Top displacement-time history of the four different models in SPEAR building (IWT007EW record)

However, as seen in Figure 6.54, aftershocks does not always cause increment of residual displacements. Residual displacements are formed in 42 of the 43 analyses for both regular and irregular case in SPEAR building. This values are 31/37 and

34/37 for regular and irregular cases, respectively in ICON building and 26/43 and 33/43 for regular and irregular cases, respectively in school building.

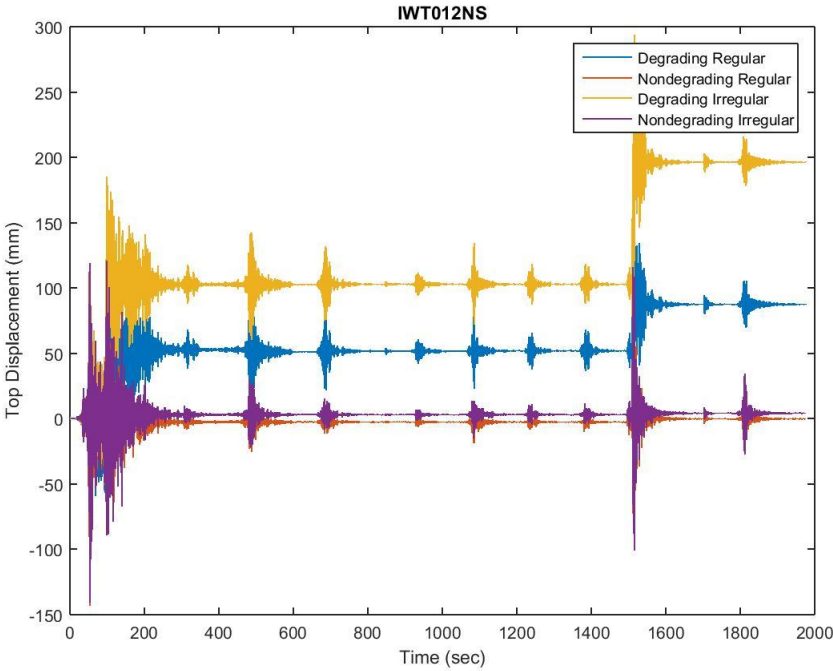


Figure 6.53 : Top displacement-time history of the four different models in ICON building (IWT012NS record)

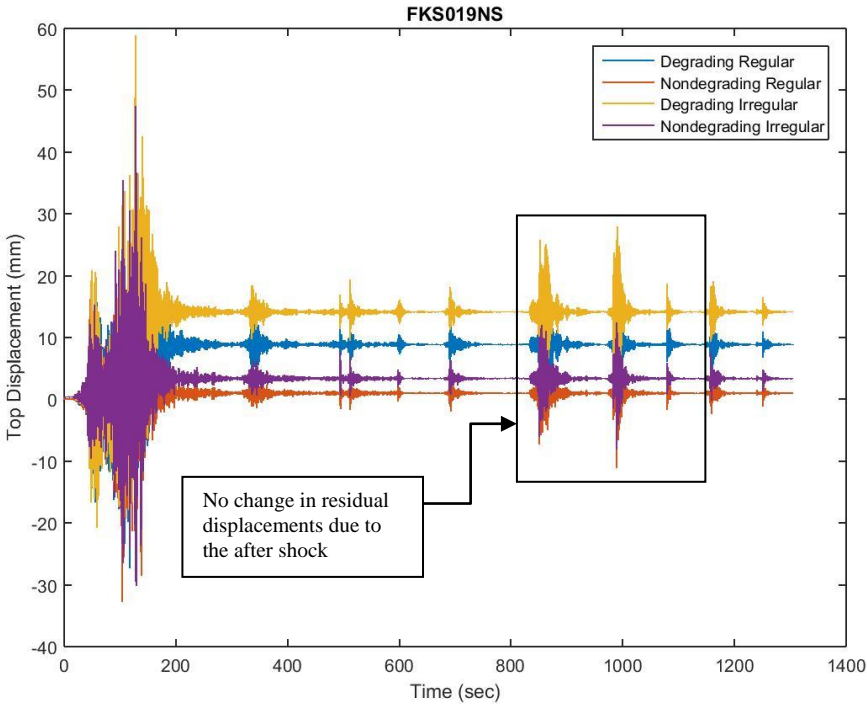


Figure 6.54 : Top displacement-time history of the four different models in ICON building (FKS019NS record)

Even if it is so rarely, in some situations residual displacement is reversed during the aftershocks as seen in Figure 6.55. In addition, number of the residual displacements that reversed during the aftershocks are 9 and 8 times for regular and irregular case, respectively in SPEAR building. While the reversal effect on residual displacements is formed in 6 and 8 times in ICON building, they are formed in 4 and 3 times for regular and irregular case in school building, respectively.

No residual displacement or limited residual displacement is seen in non-degrading models. This case is observed in each building. It consists of more damage in irregular buildings than regular ones according to time.

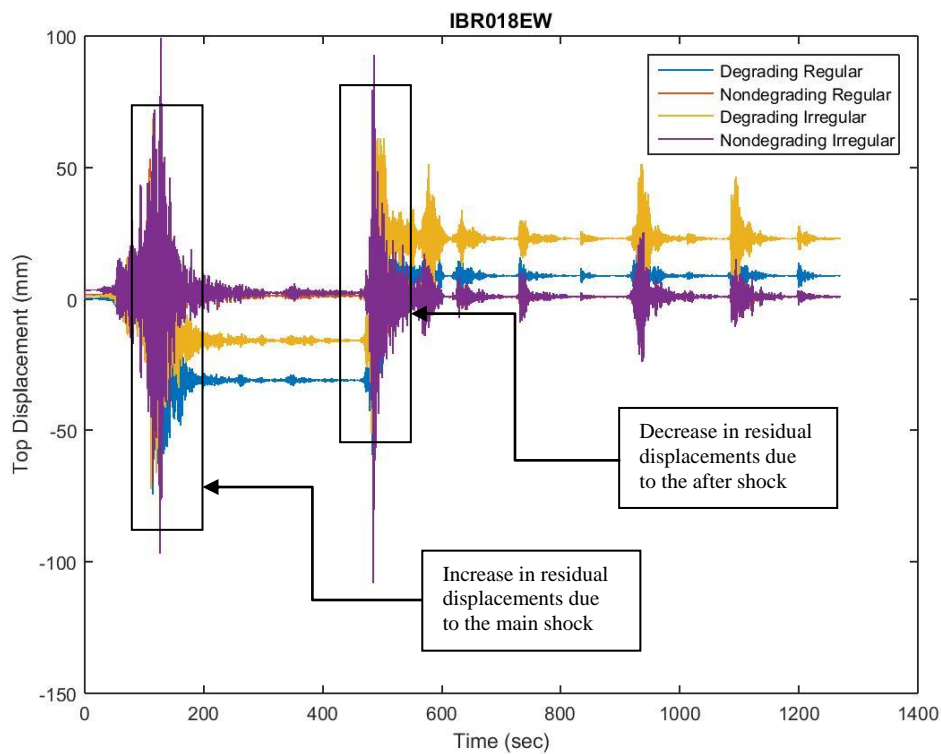


Figure 6.55 : Top displacement-time history of the four different models in ICON building (IBR018EW record)

6.3.1 Permanent Displacements

Comparisons of the mean residual displacements are represented for the main shock–all sequence, degrading – non-degrading models both for regular and irregular cases. It is observed that the irregular structures showed more permanent displacements compared to the regular ones. It is obvious for degrading models but it is very limited in non-degrading models.

When the main shocks are considered for the SPEAR building in degrading models, it is found that the residual displacement values of the irregular cases is 27% higher than regular cases. In addition, the difference in the residual displacement values for all sequences is determined to be increased by 28% in degrading models. The same ratios are 10% and 8% for non-degrading models, respectively. Mean residual displacements have small values as the ratios between the regular and irregular cases for both main shock and all sequence. The difference in residual displacement between the main shock and following aftershocks is marked for IWT026NS record on the Figure 6.56 and the differences in mean residual displacements are given in Figure 6.57.

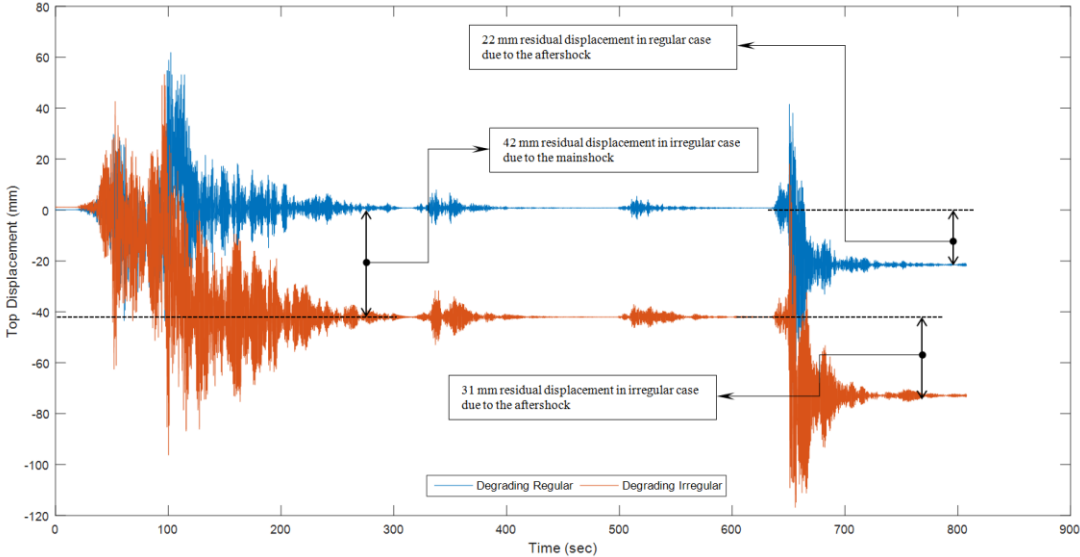


Figure 6.56 : Difference in residual displacement of the SPEAR building for IWT026NS record

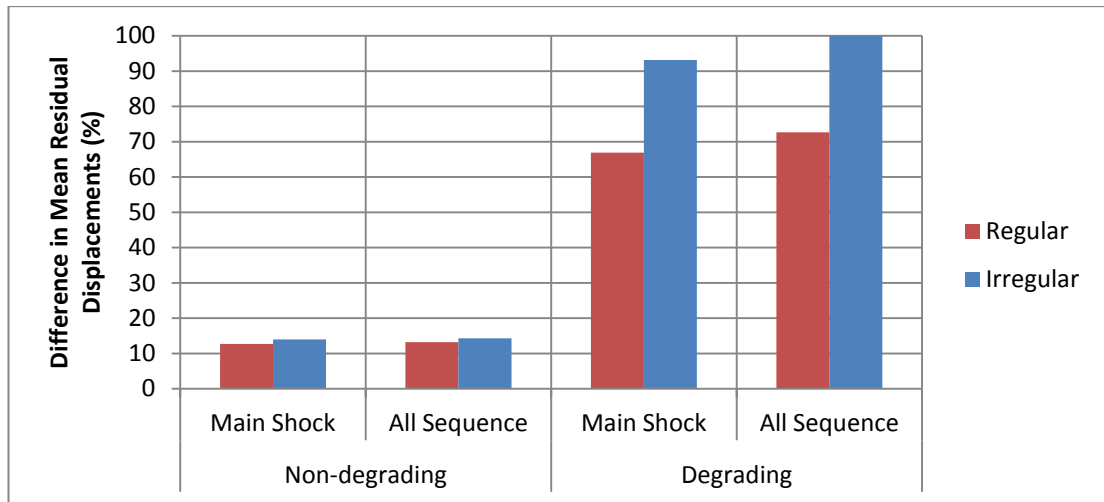


Figure 6.57 : Mean residual top displacements ratio of SPEAR building

When the main shocks are considered for the ICON building in degrading models, it is found that the residual displacement values of the irregular cases is 35% higher than regular cases. Moreover, the difference in the residual displacement values for all sequences is determined to be increased by 36% in degrading models. In ICON building, ratio of permanent displacements increased compared to the SPEAR building in non-degrading models but irregular-all sequence case is barely reach the regular-main shock case in degrading models. The difference in residual displacement between the main shock and following aftershocks is marked for IWT012NS record on the Figure 6.58 and the differences in mean residual displacements are given in Figure 6.59 for ICON building.

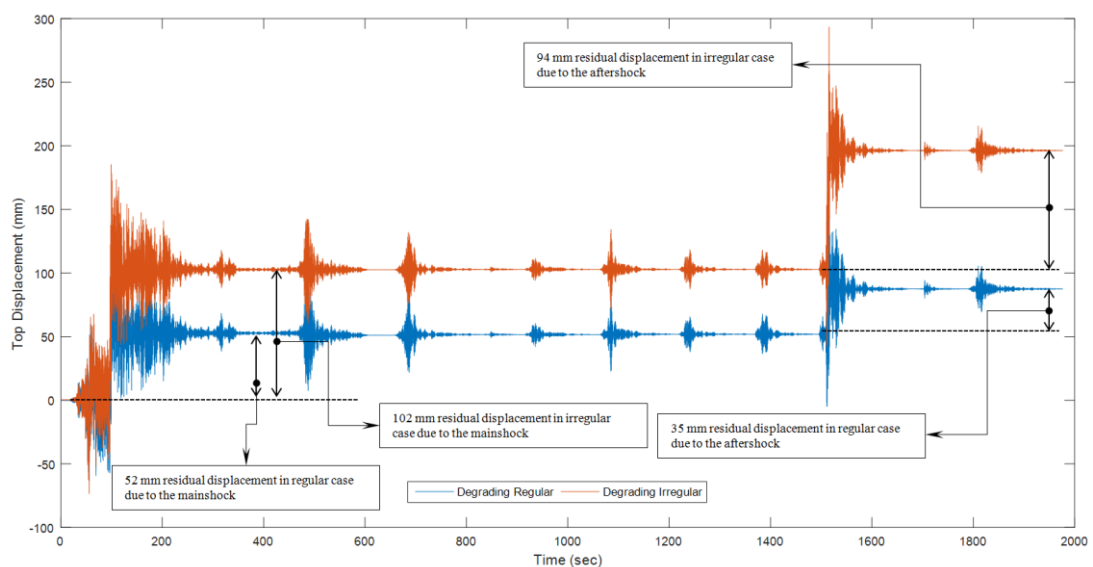


Figure 6.58 : Difference in residual displacement of the ICON building for IWT012NS record

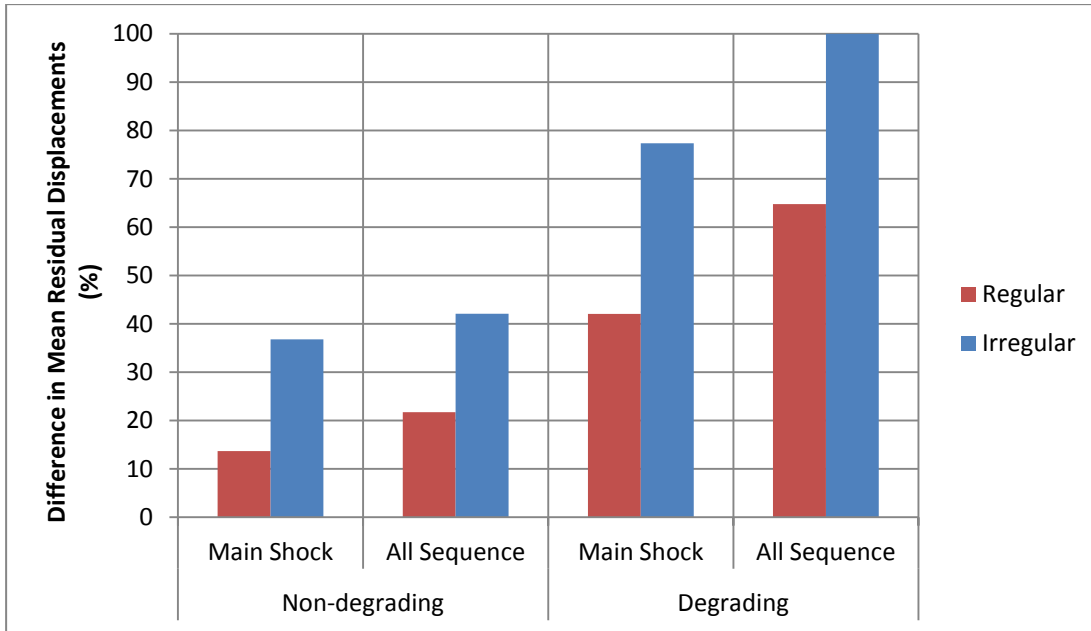


Figure 6.59 : Mean residual top displacements ratio of ICON building

When the main shocks are considered for the school building in degrading models, it is found that the residual displacement values of the irregular cases is 29% higher than regular cases. In addition, the difference in the residual displacement values for all sequences is determined to be increased by 35% in degrading models. The difference in residual displacement between the main shock and following aftershocks is marked for IWT012EW record on the Figure 6.60 and the differences in mean residual displacements are given in Figure 6.51 for school building.

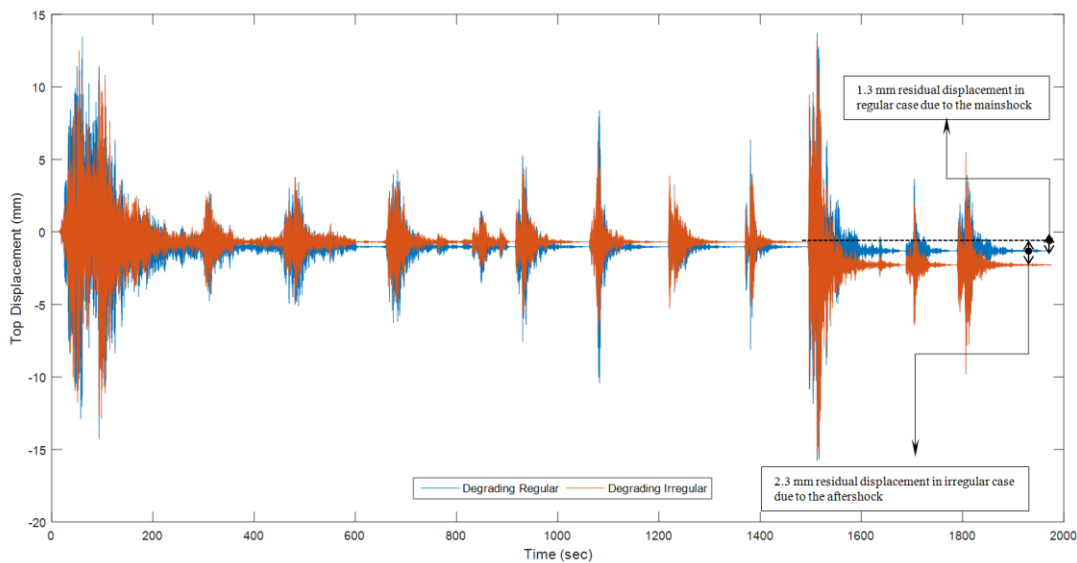


Figure 6.60 : Difference in residual displacement of the school building for IWT012EW record

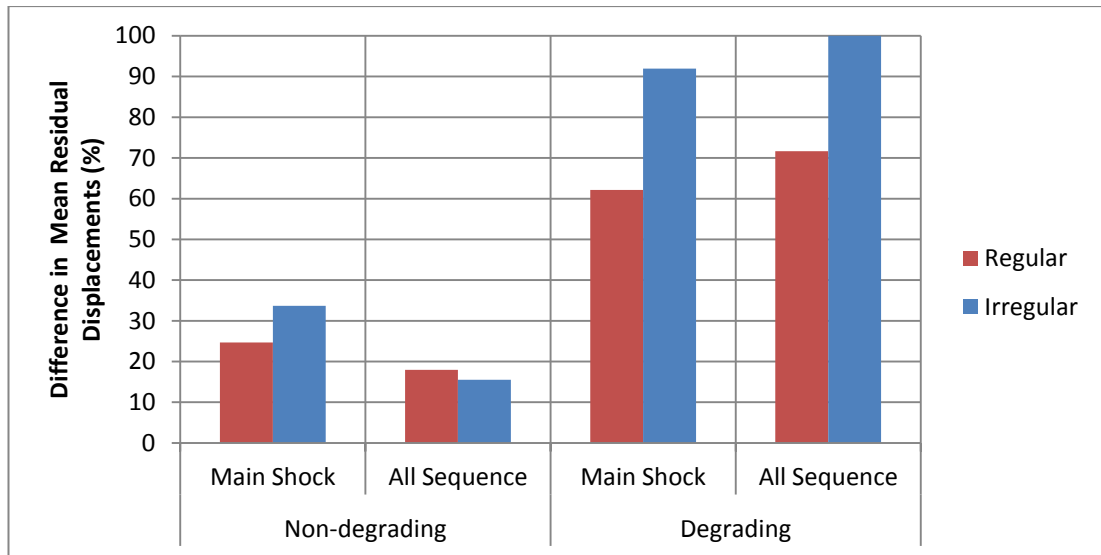


Figure 6.61 : Mean residual top displacements ratio of school building

It is also concluded that taking into account the aftershock sequences increase the residual displacement difference by 6%, 22% and 3% for the regular cases and 7%, 23% and 9% for the irregular cases. For SPEAR (irregular in plan) and ICON (irregular in elevation) buildings increase in ratio of residual displacements are not significant but it is opposite for school building (irregular in plan and elevation). Moreover, as seen in figures the permanent displacements are not reflected the structures actual behavior in non-degrading models.

6.3.2 Maximum top displacements

The maximum top displacements of the degrading models for 43 individual records were represented for considered buildings. Maximum top displacements were compared in only degrading models.

Top displacement of the SPEAR building monitored at the top of the C7 column for all analysis. When the maximum displacements are compared between the main shock and all sequence for each analysis, mostly (32/43 analyses) aftershocks did not affect the maximum top displacements both regular and irregular models.

In ICON building, 37 records were used in assessment. 6 analyses were not completed due to convergence problems. Excessive displacements caused convergence problems, hence results of the six records are not proper for assessment. When the maximum displacements are compared between the main shock and all

sequence for each analysis, in most of analysis aftershocks did not affect of the maximum top displacements both regular and irregular models. Same results were observed with SPEAR building.

As seen in through Figure 6.62 to 6.63, about 75% of the 43 analyses, there aren't any increment in maximum displacements between the main and all sequence case both for regular and irregular models. This ratio is higher in school building. Even if aftershocks have greater PGA, maximum top displacements of the buildings did not exceed the displacements, which were experienced during the main shock due to the strength deterioration and stiffness degradation in material.

When the average results were compared between the main shock and all sequence case, SPEAR building showed 5% and 7% increment for regular and irregular cases, respectively. While these ratios are 10% and 13% for ICON building, 4% and 5% for school building.

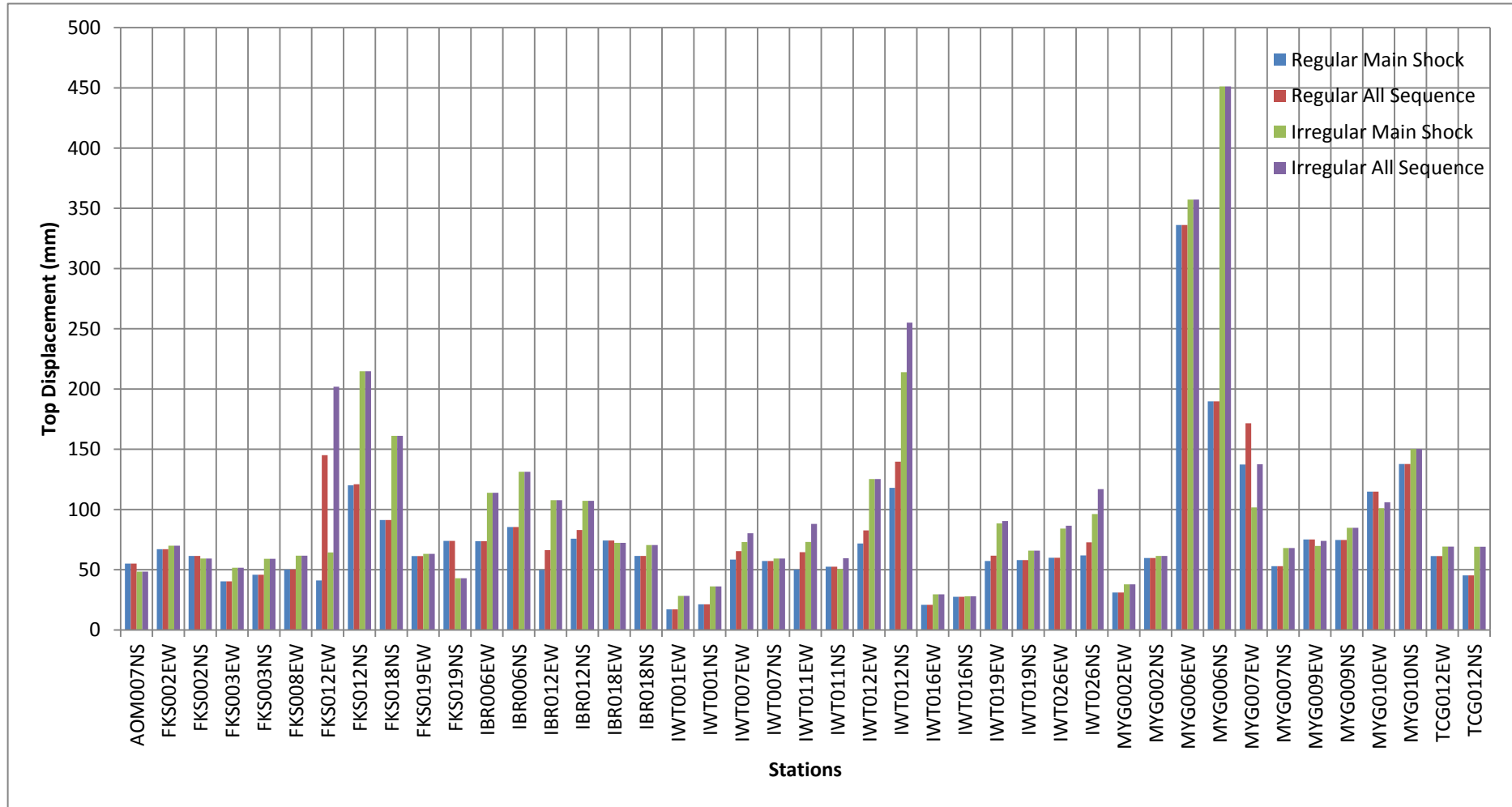


Figure 6.62 : Maximum top displacements of the degrading models for SPEAR building

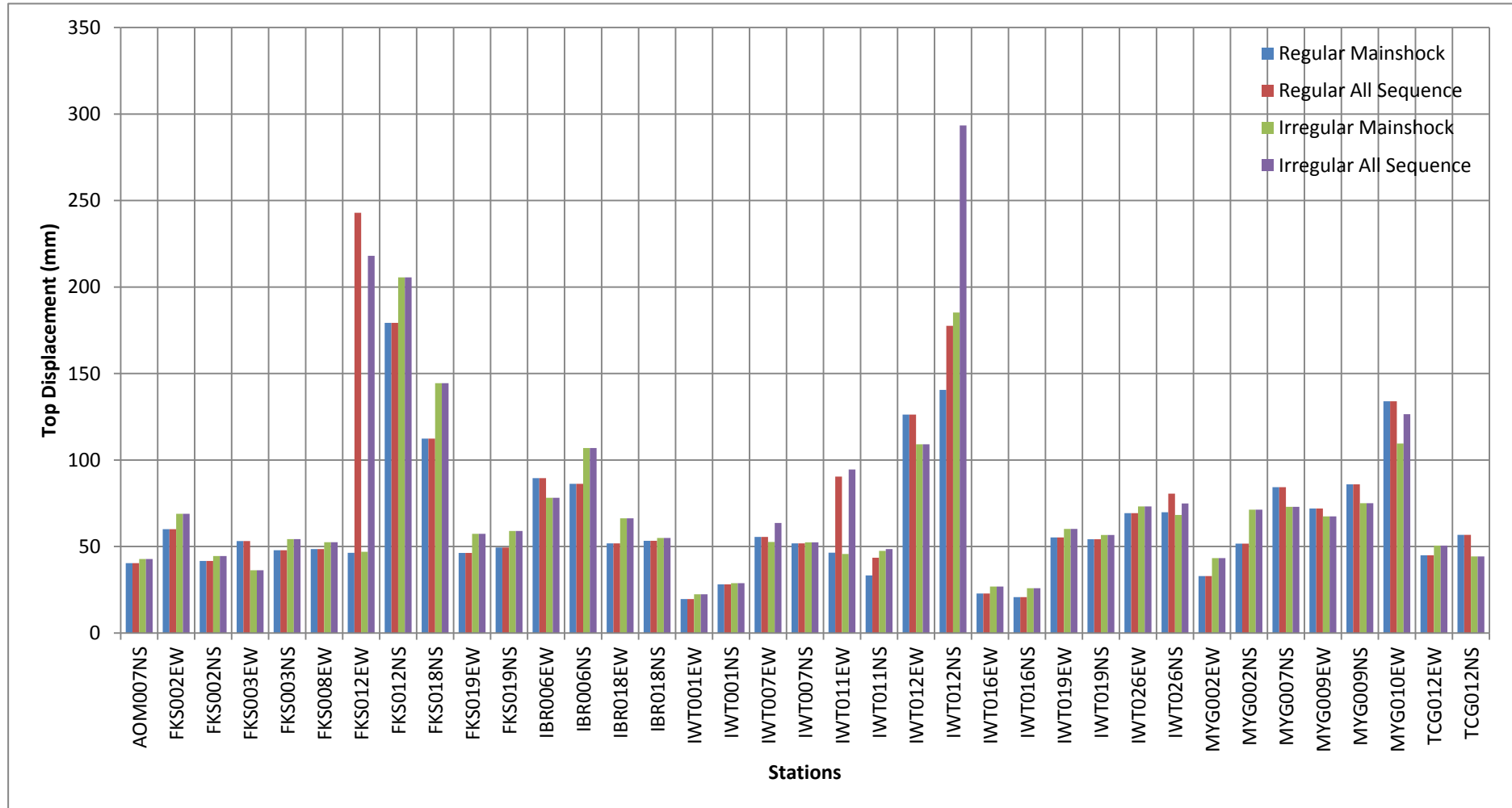


Figure 6.63 : Maximum top displacements of the degrading models for ICON building

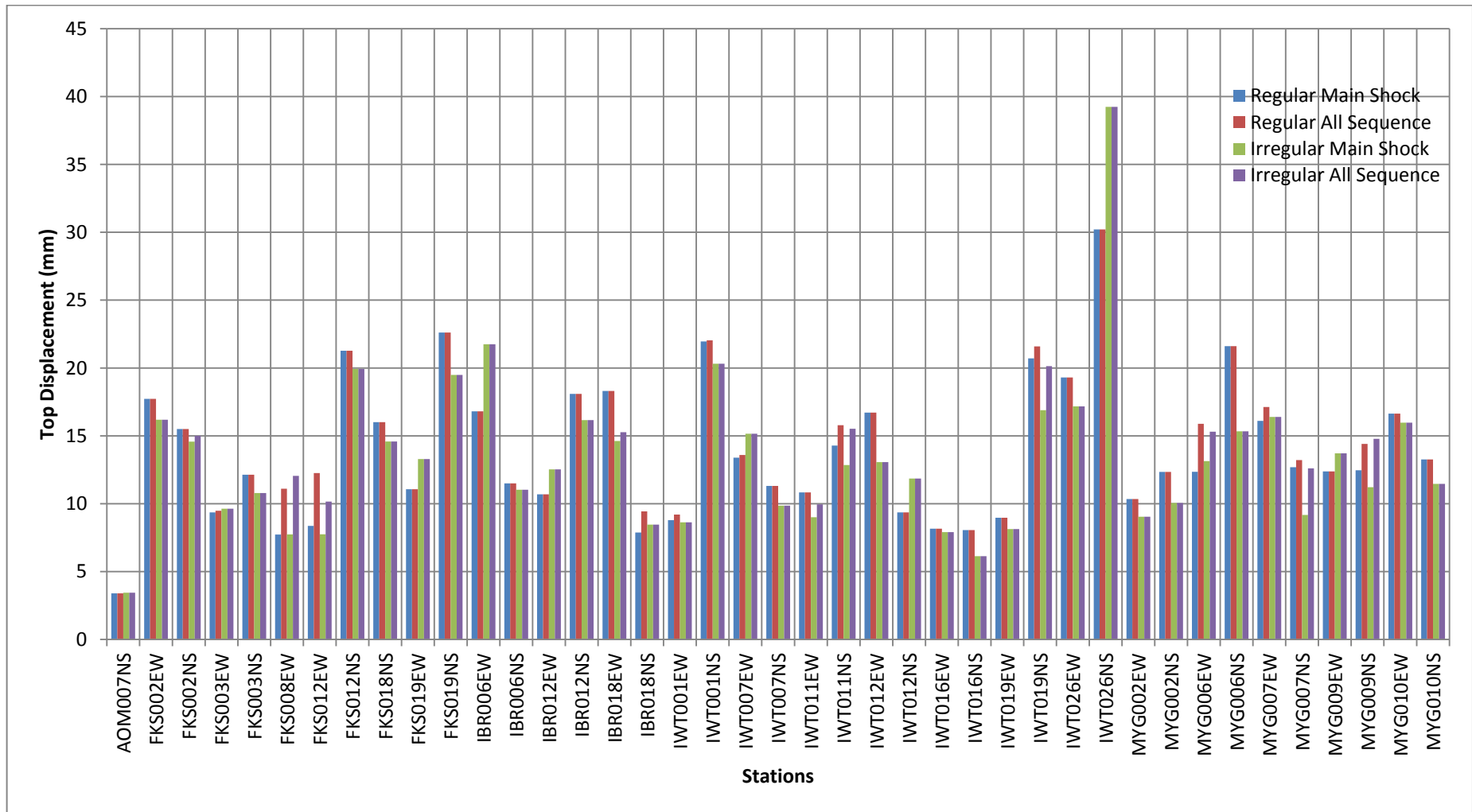


Figure 6.64 : Maximum top displacements of the degrading models for school building

6.3.3 Drifts

Drift profiles regarding the considered structures for degrading models are plotted in Figure 6.65, Figure 6.66 and Figure 6.67. To check the accuracy of the applied nonlinear static pushover procedures, comparisons in terms of drift results are also evaluated. The calculated drift values from the N2 and extended N2 methods for the regular and irregular cases of the degrading models are also marked in the Figures. It is concluded that the nonlinear static results were in good correlation with the implemented time history analyses especially for the lower stories. For the higher stories, the difference in the results can be correlated due to the higher mode effects. Further, the drift results belonging to the irregular cases were found to be more than the regular case for the considered structures.

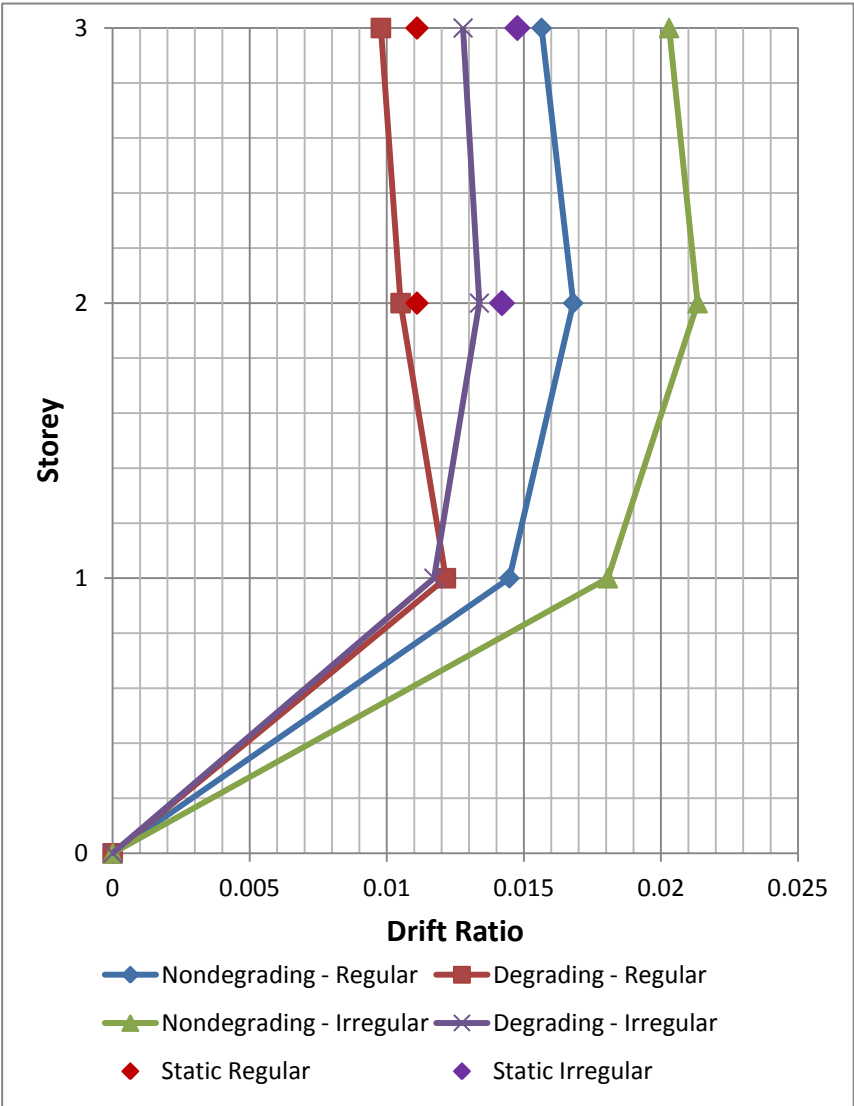


Figure 6.65 : Mean drifts of SPEAR building

In SPEAR building, maximum mean drifts occurred in second story. Non-degrading models showed more drifts compared with degrading models. Moreover, irregular models showed more drift compared with regular models.

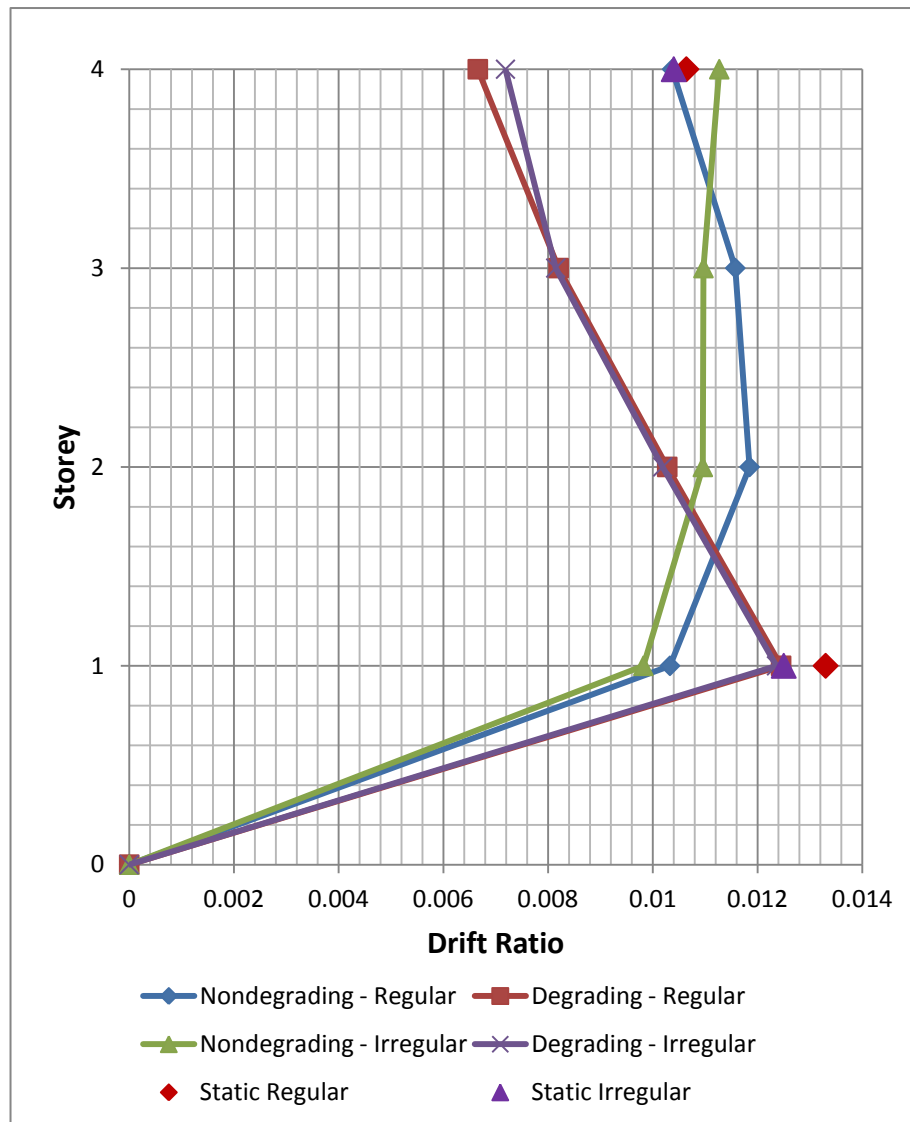


Figure 6.66 : Mean drifts of ICON building

In ICON building, while the maximum average drifts occurred on first story in degrading models, maximum average drifts was formed on second story in non-degrading ones. Unlike the SPEAR building, degrading models performed more mean of maximum drifts compared to non-degrading models. Moreover, on the fourth story where the setback consists, drift of the irregular models was higher than the regular models.

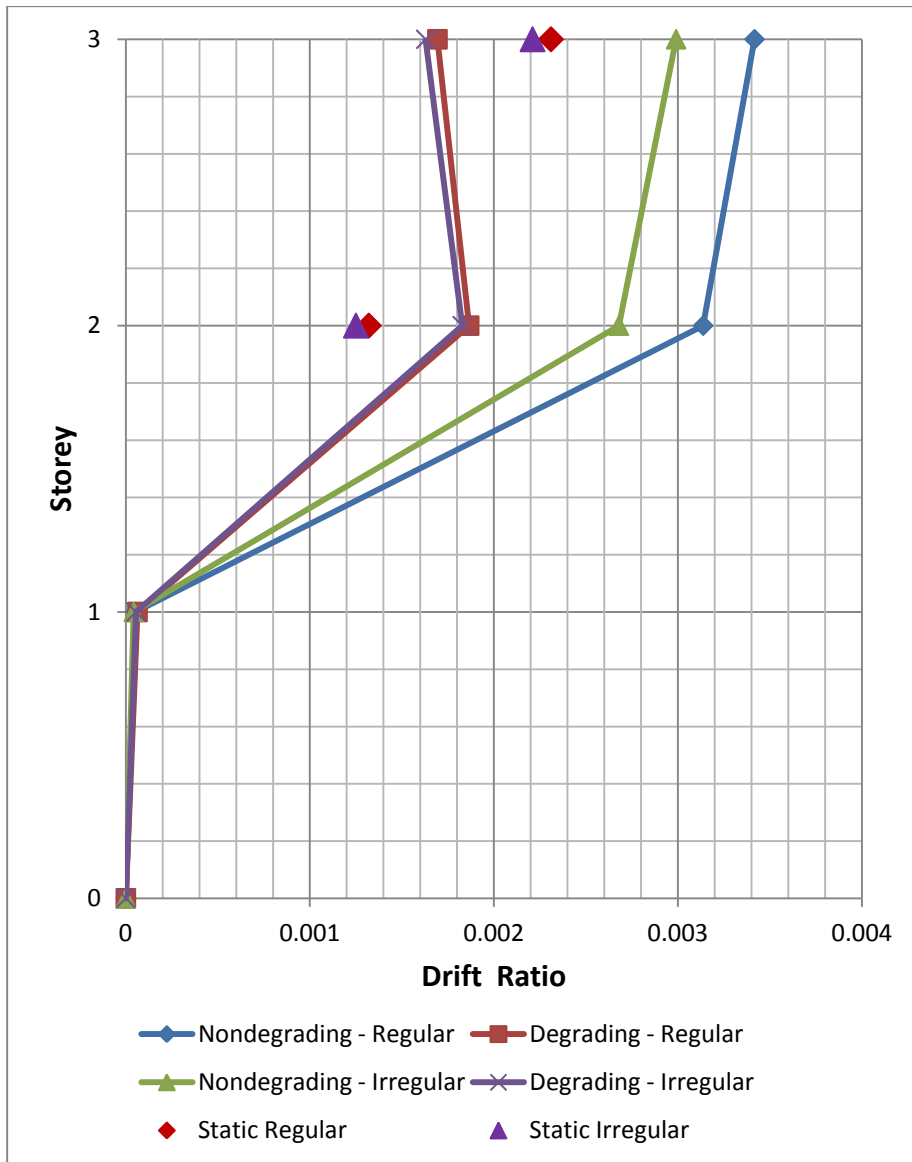


Figure 6.67 : Mean drifts of school building

In school building, while the maximum average drifts occurred on second story in degrading models, maximum average drifts was formed on third story in non-degrading ones. Drifts limited in the first story due to rigid basement walls. Degrading-irregular case shows less drifts compared to degrading- regular one due to the fact that irregularity effect cannot be seen clearly in school building.

6.3.4 Inter-storey Drifts

The inter-story drifts are plotted for critical stories, which are determined from the drift profiles at previous section. Inter-story drifts are plotted for second, first and second story for SPEAR, ICON and school building through in Figure 6.68 to Figure 6.70, respectively. Code threshold limit corresponding to the damageability limit

state is also plotted on the same graphs. As it can be easily inferred from the given plots, the residual displacements increased due to the aftershocks for SPEAR and ICON frames and the Code threshold limit is exceeded both for regular and irregular cases. However, the results regarding the irregular case was much more than the regular ones. Furthermore, when it is the case for school building, the aftershock sequence did not alter the residual displacement values since the building had shear walls surrounding the bottom storey. The capability of degrading material models on the shear wall structures has not been tested before. It is believed that the model should be calibrated taking into account the shear wall behavior.

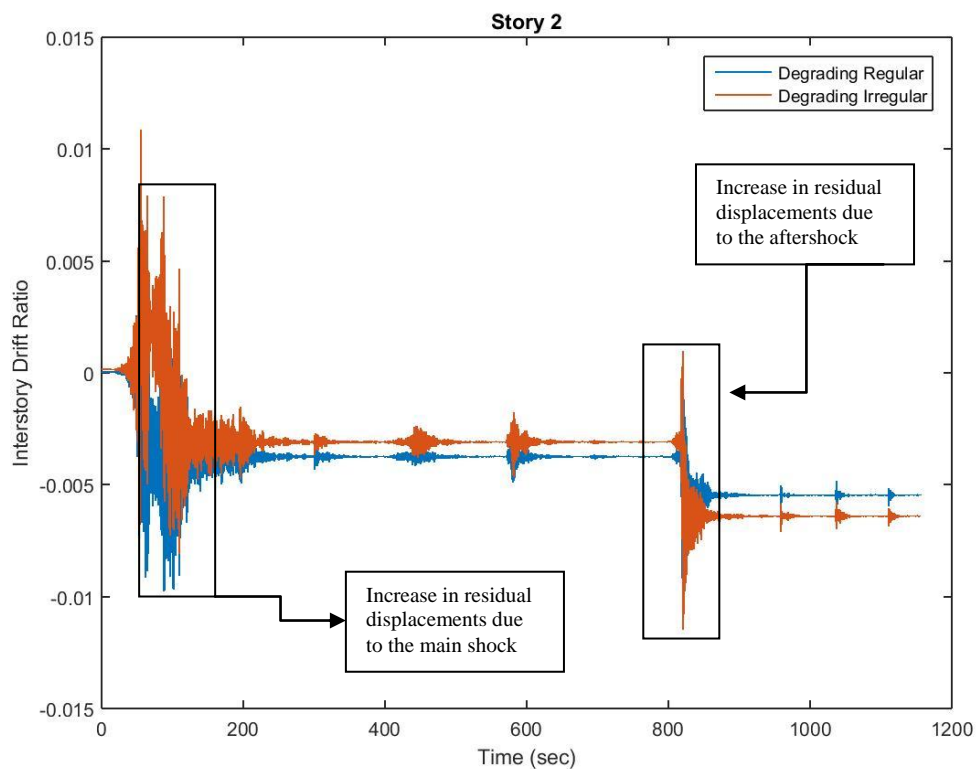


Figure 6.68 : Inter-storey drift ratio for SPEAR building (IWT007EW record)

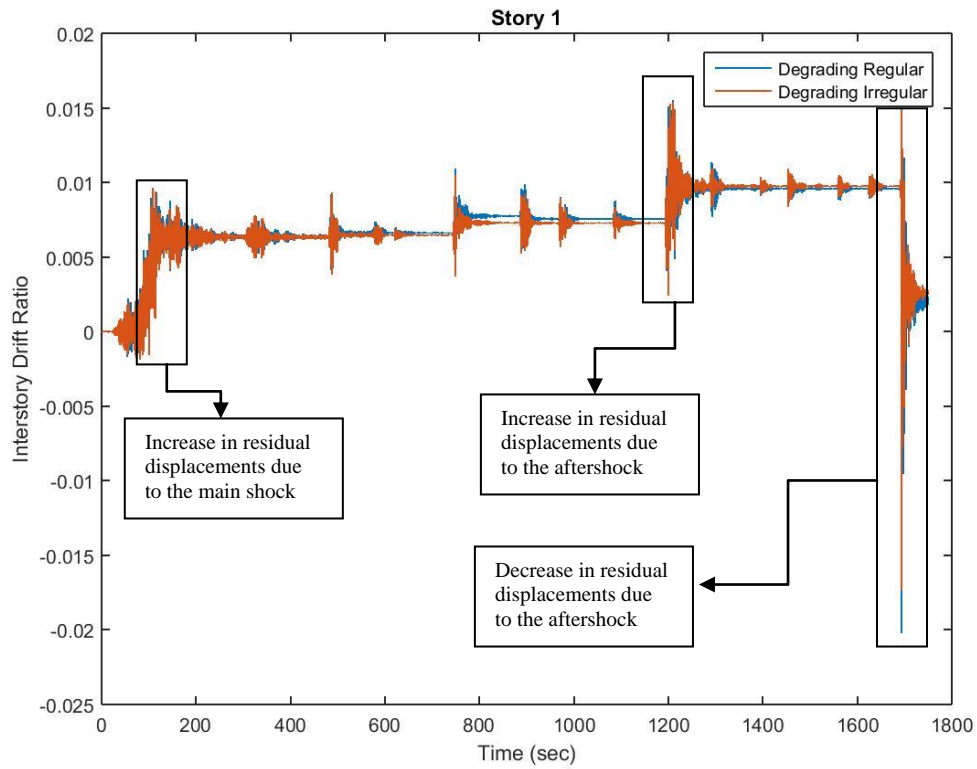


Figure 6.69 : Inter-storey drift ratio for ICON building (FKS012EW record)

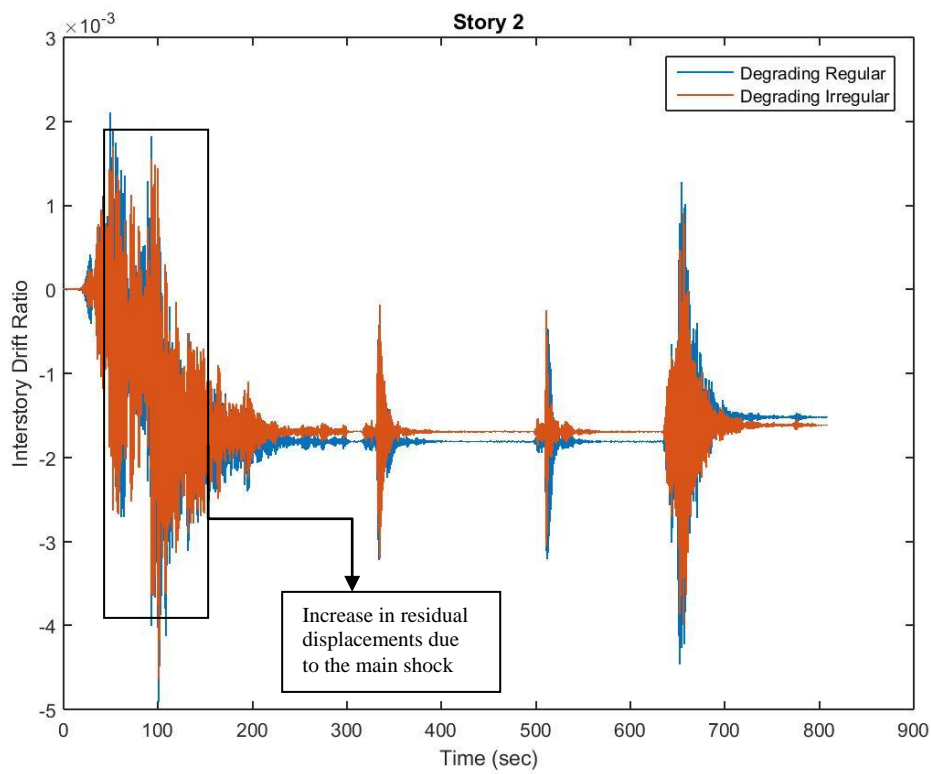


Figure 6.70 : Inter-storey drift ratio for school building (IWT026NS record)

6.3.5 Plastic Hinges

The number of developed plastic hinges for individual records and the mean of the five records were represented for SPEAR, ICON and school building, respectively. Plastic hinge mechanism was determined at the ends of the beams and columns. Five earthquake results, which include larger residual displacements than the mean residual displacements for main and aftershock in degrading models, were selected for the monitored hinges. Number of plastic hinges were compared for four cases, which are regular main shock, regular all sequence, irregular main shock and irregular all sequence.

In SPEAR building, number of plastic hinges increased in irregular case compared to the regular case in both main shock and all sequence in three records as seen in Figure 6.71. In one record which named as FKS012NS, was vice versa because of top displacement of the structure was reversed while the aftershocks in irregular case. In the other record, number of plastic hinges showed little change.

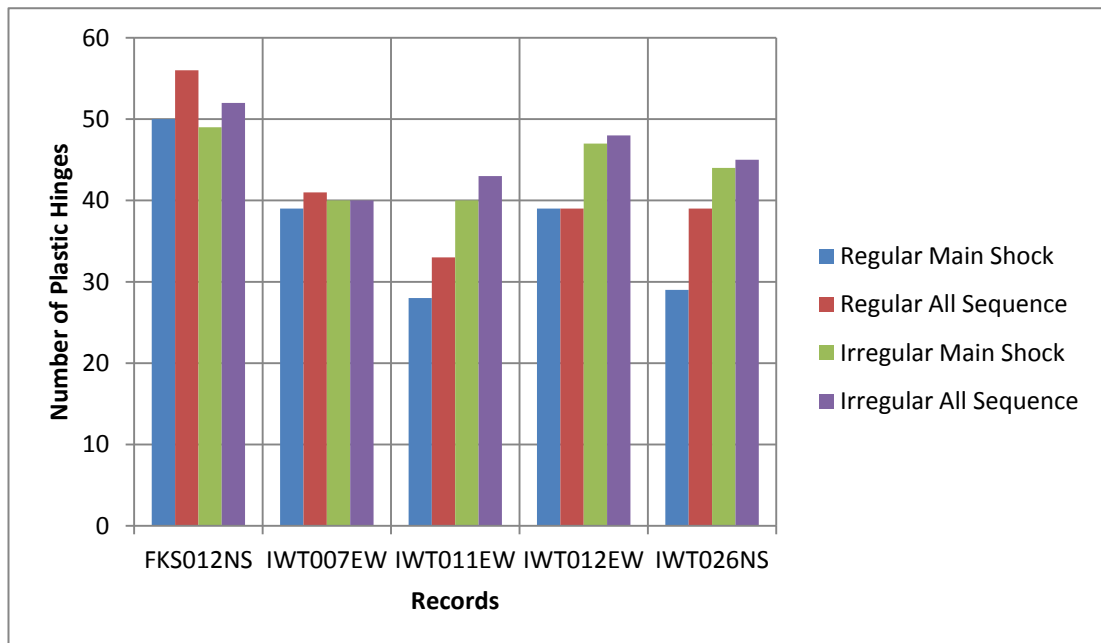


Figure 6.71 : Number of the developed plastic hinges in SPEAR building

In the Figure 6.72, the average results show that highest number of plastic hinges were developed in irregular-all sequence case. It is also observed that increase in the plastic hinges between the main shock and all sequence are 1.12 and 1.04 times for

regular and irregular case, respectively. Moreover, the differences between the regular and irregular cases are same for main shock and all sequence, respectively.

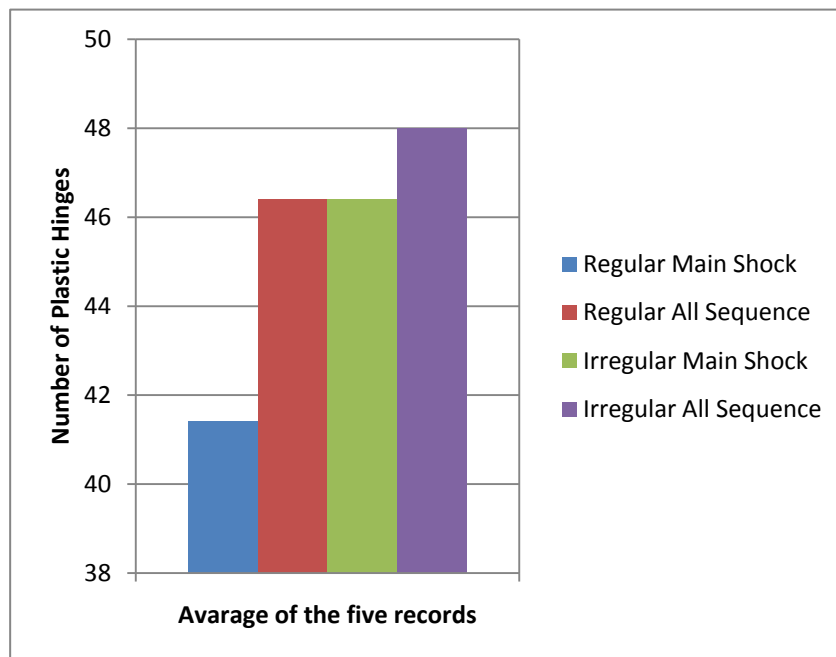


Figure 6.72 : Mean number of the developed plastic hinges in SPEAR building

Formations of plastic hinges are plotted in Figure 6.78, 6.79, 6.80 and 6.82 for SPEAR building. As seen in mentioned figure, the values of hinges are more in flexible edge compared to other axis for irregular case. Same situation was seen in nonlinear static case so it can be said that a good prediction was made with the extended N2 method.

In ICON building, the number of plastic hinges increased in irregular case compared to the regular case in both main shock and all sequence in three records. In one record, which named as FKS012EW, number of the plastic hinges are same with regular and irregular case in both main and all sequence case as seen in Figure 6.73.

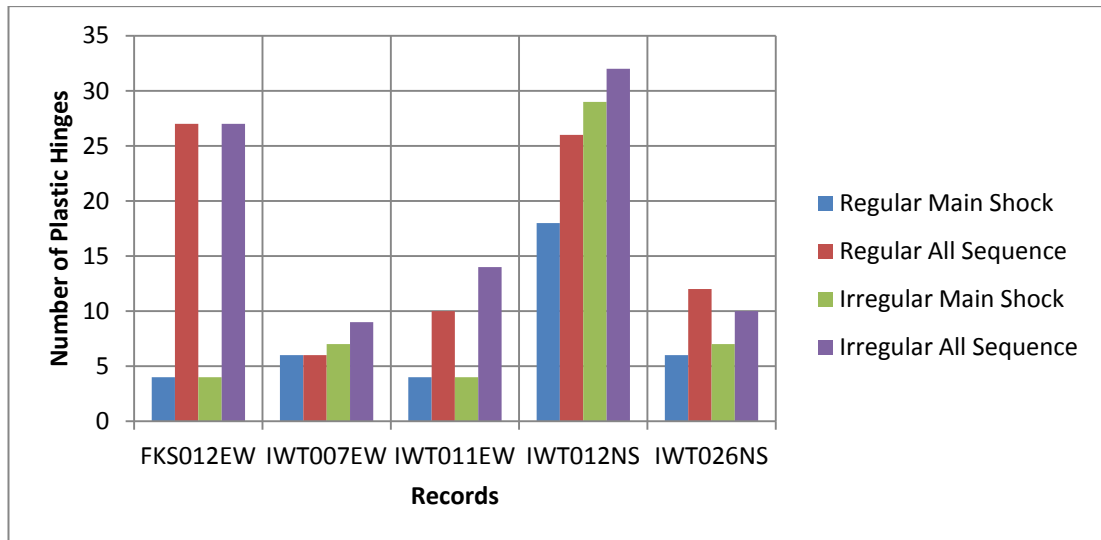


Figure 6.73 : Number of the developed plastic hinges in ICON building

In the Figure 6.74, the average results show that highest number of plastic hinges were developed in irregular all sequence case. It is also concluded that increase in the plastic hinges between the main shock and all sequence are 1.92 and 1.79 times for regular and irregular case, respectively. Moreover, the differences between the regular and irregular cases are 1.09 times and 1.05 times for main shock and all sequence, respectively. Distributions of plastic hinges are plotted in Figure 6.82.

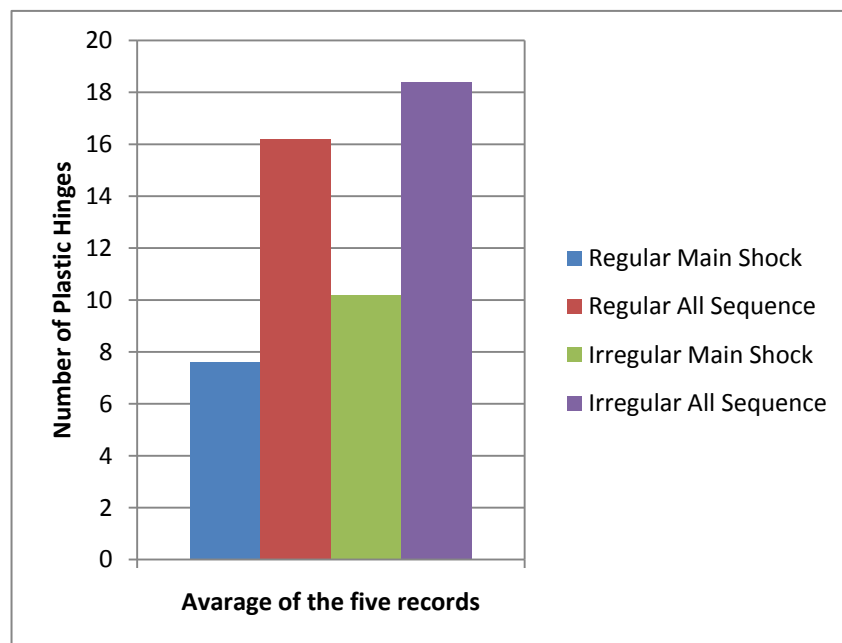


Figure 6.74 : Mean number of the developed plastic hinges in ICON building

In school building, the number of plastic hinges increased in irregular case compared to the regular case in both main shock and all sequence in three records as seen in

Figure 6.75. One record, which named as FKS012EW, plastic hinges are not developed. When the base shear of the building which obtained from the FKS012EW record, is compared to the shear which corresponds to the target displacement, it is observed that, formed base shear which belongs to FKS012EW record, remained extremely under the target shear as seen in Figure 6.76.

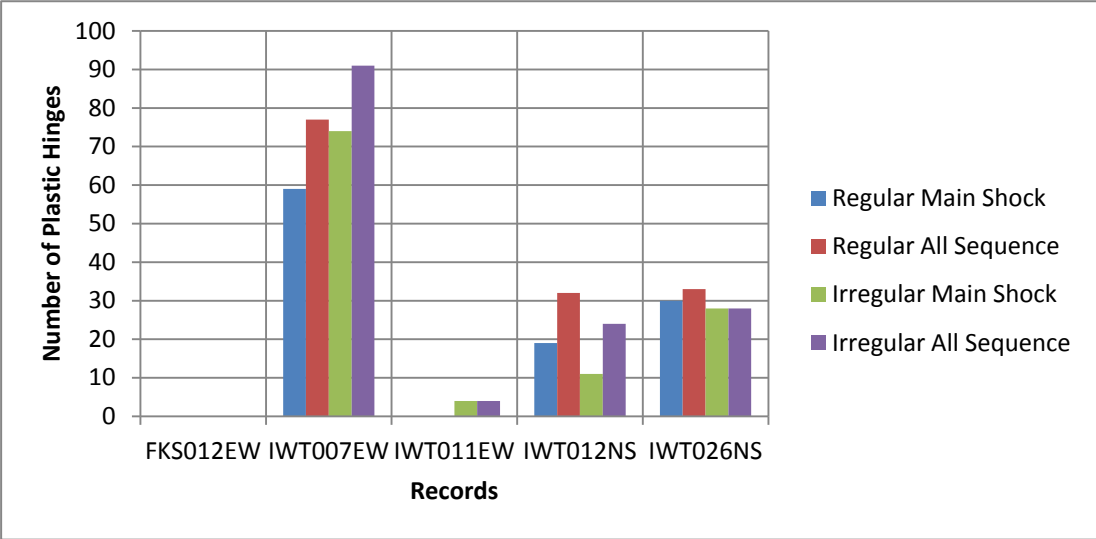


Figure 6.75 : Number of the developed plastic hinges in school building

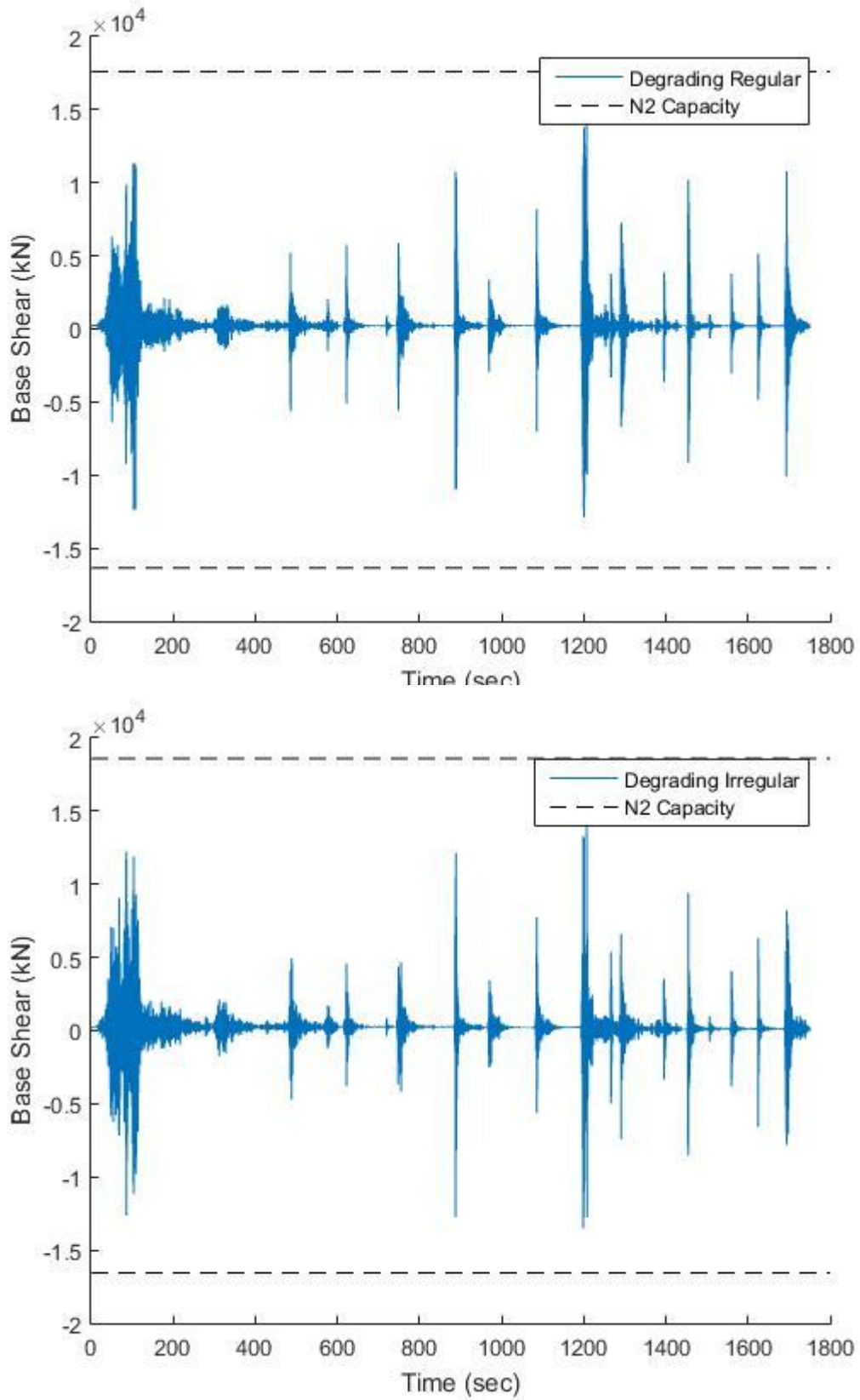


Figure 6.76 : Base shear-time history and target shear value of the school building for FKS012EW record

In the Figure 6.77, the average results show that highest number of plastic hinges were developed in irregular all sequence case. It is also concluded that increase in plastic hinges between the main shock and all sequence are 1.31 and 1.25 times for regular and irregular case, respectively. Moreover, the differences between the regular and irregular cases are 1.08 times and 1.04 times for main shock and all sequence, respectively.

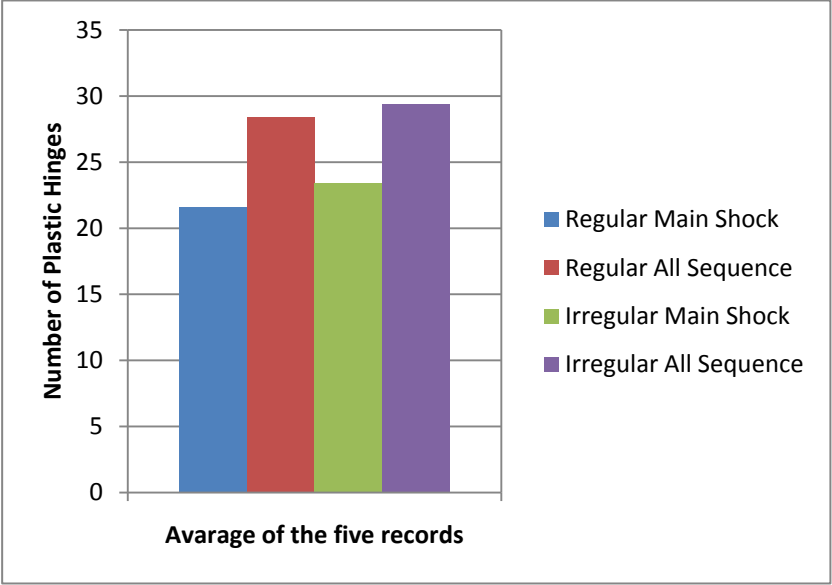


Figure 6.77 : Mean number of the developed plastic hinges in school building

It is also observed that, the plastic hinge distributions differ between the regular and irregular structure especially on shear walls. While the plastic hinges on shear walls are formed on the basement floor in regular structure, they are formed on the first floor in irregular structure due to the locations of the shear walls. The shear walls are located in the middle of the building and connected with beams to basement walls in original case but in remodeled case, the shear walls are at the edge of the building and connected directly to the basement walls. Same situation was seen in nonlinear static analysis. The formation of the plastic hinges can be seen in Figure 6.83, 6.84 6.85 and 6.86.

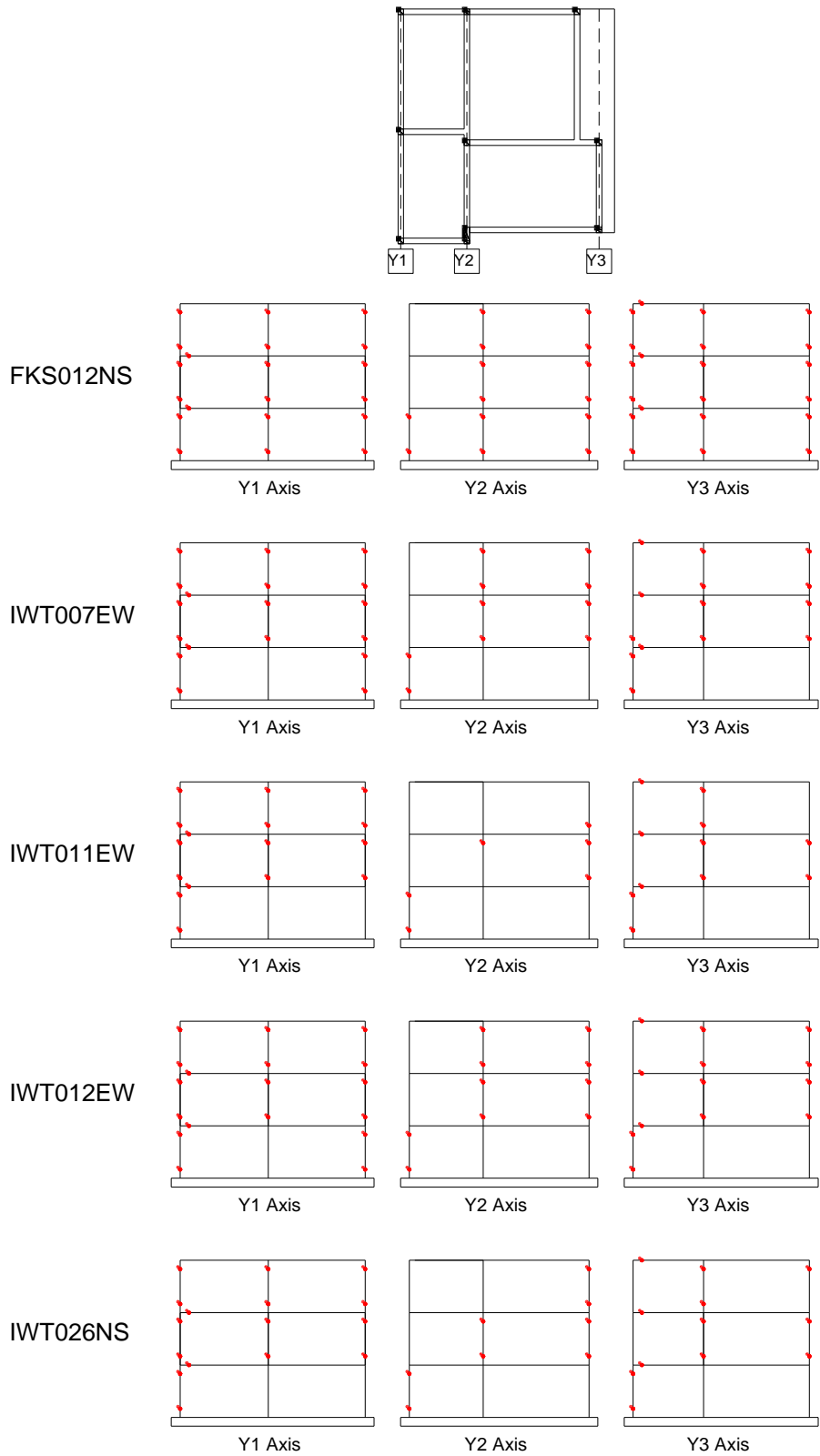


Figure 6.78 : Plastic hinge locations of SPEAR building for regular- main shock case

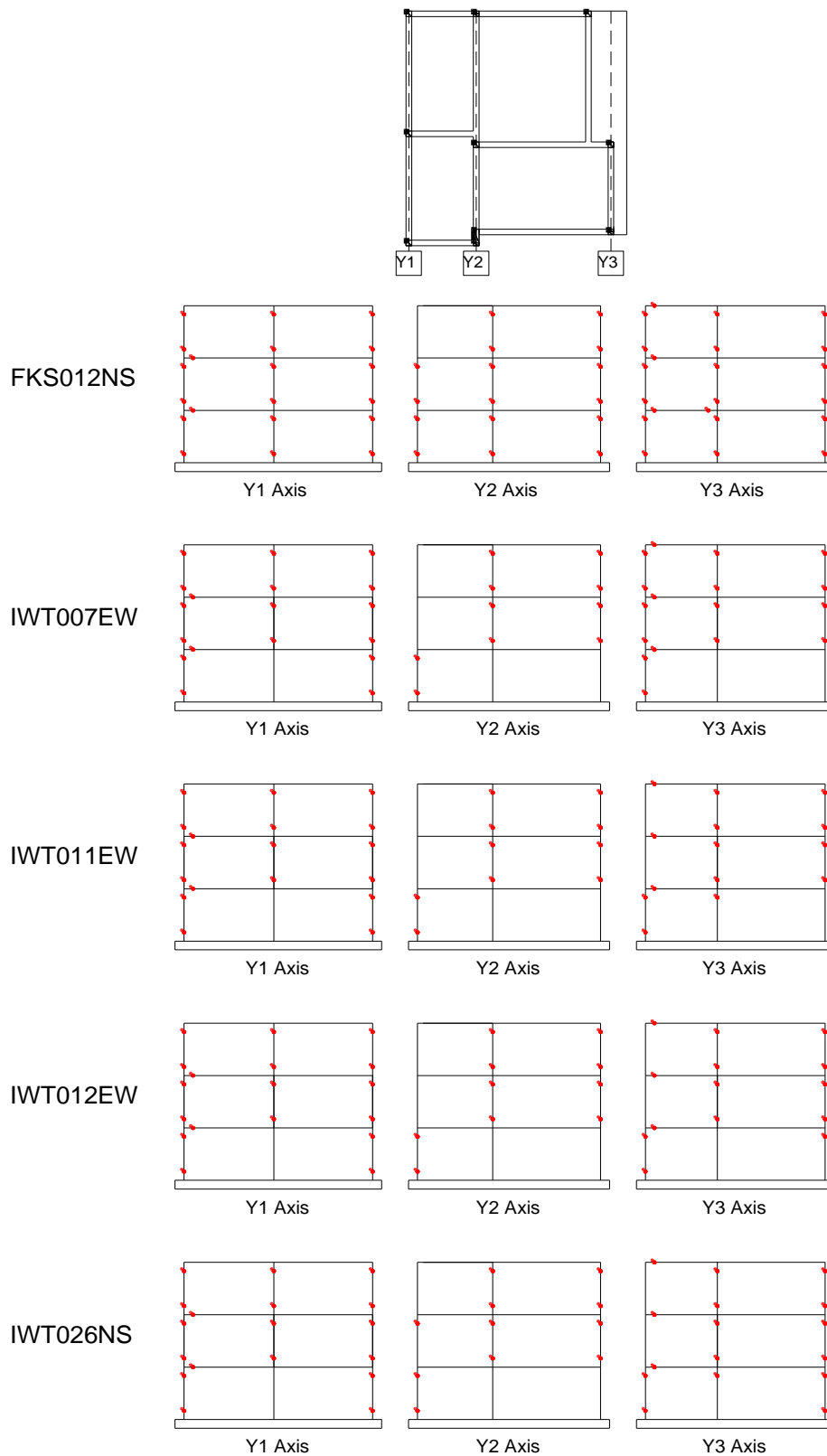


Figure 6.79 : Plastic hinge locations of SPEAR building for regular – all sequence case

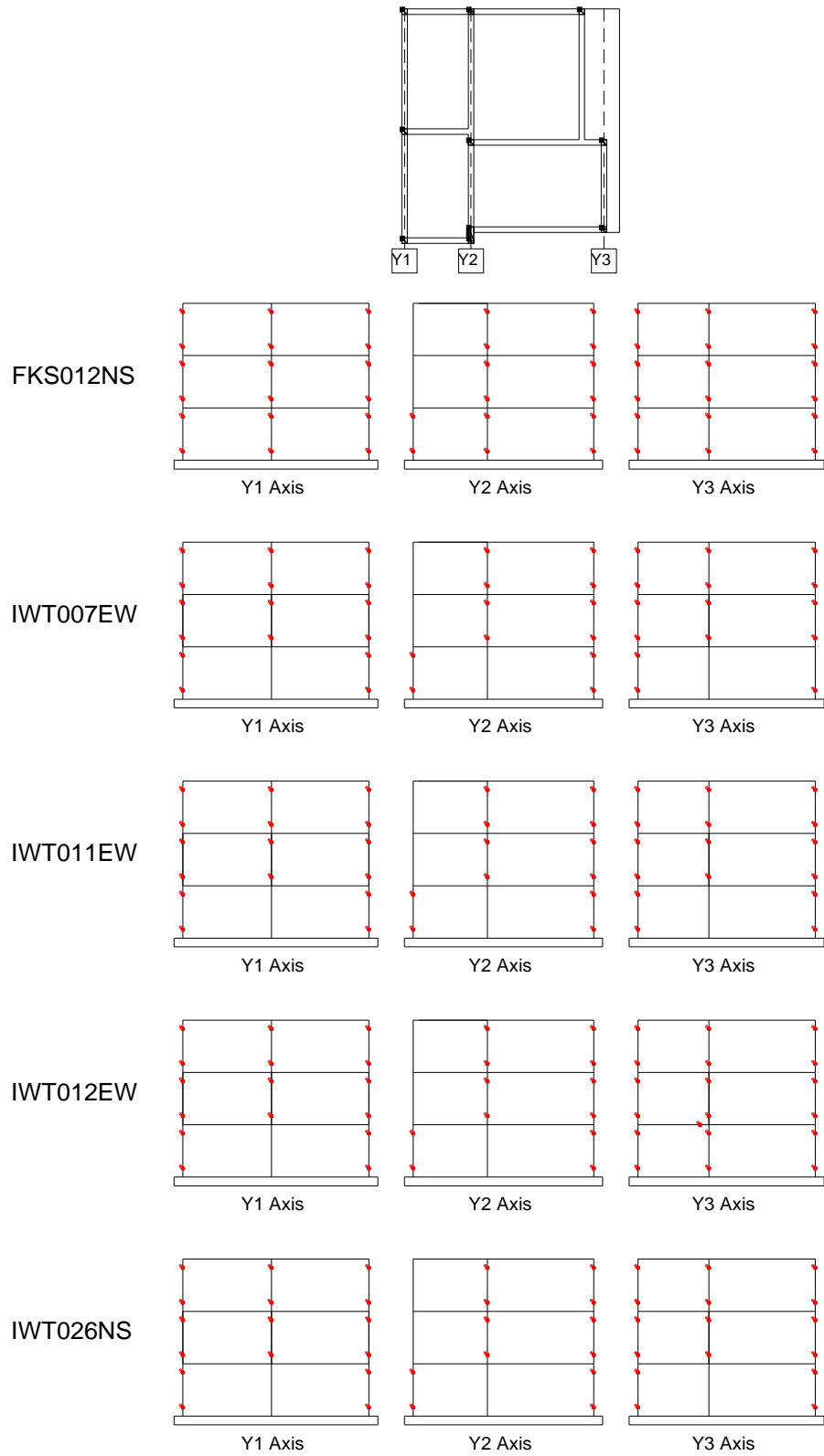


Figure 6.80 : Plastic hinge locations of SPEAR building for irregular – main shock case

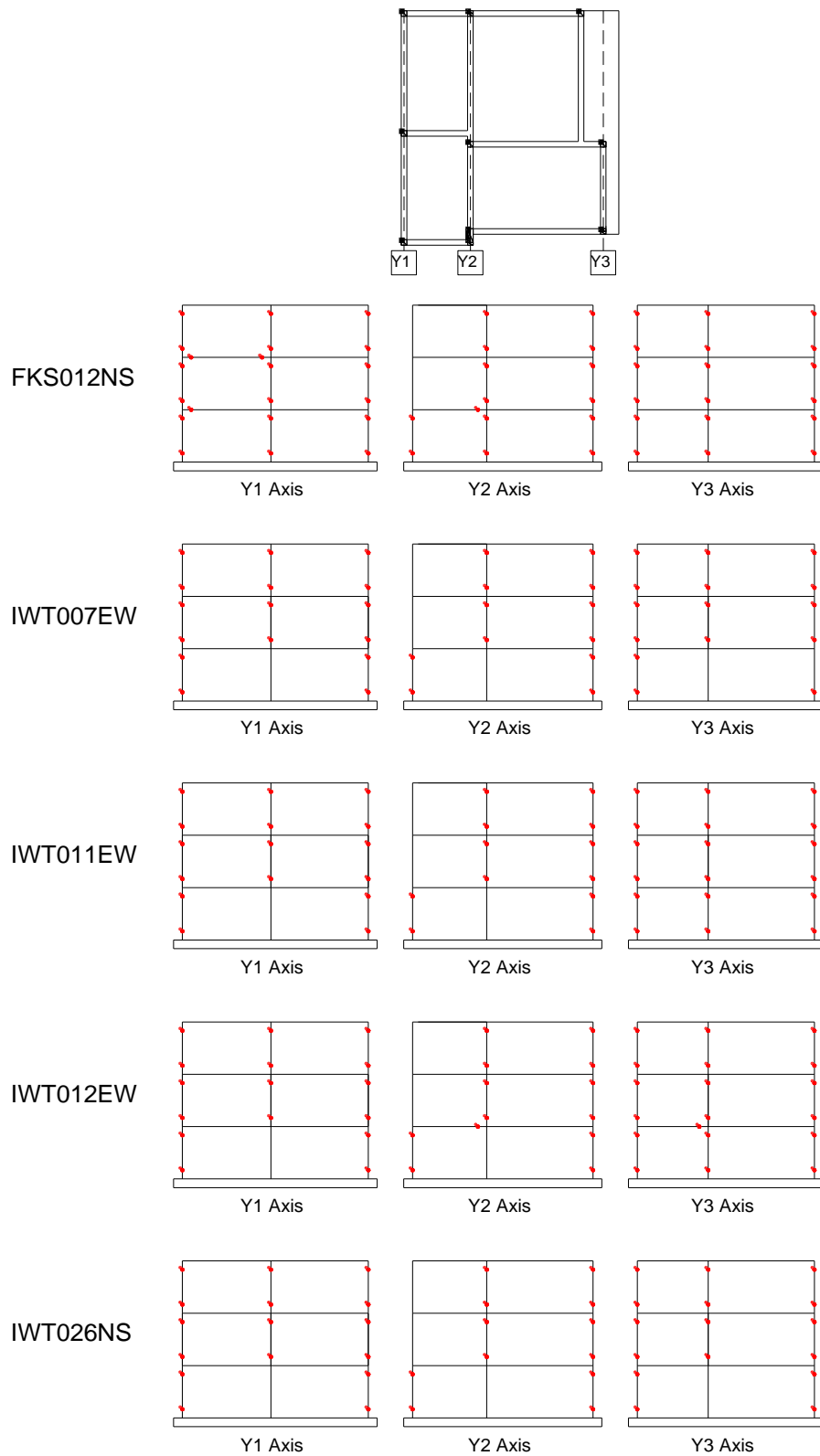


Figure 6.81 : Plastic hinge locations of SPEAR building for irregular – all sequence case

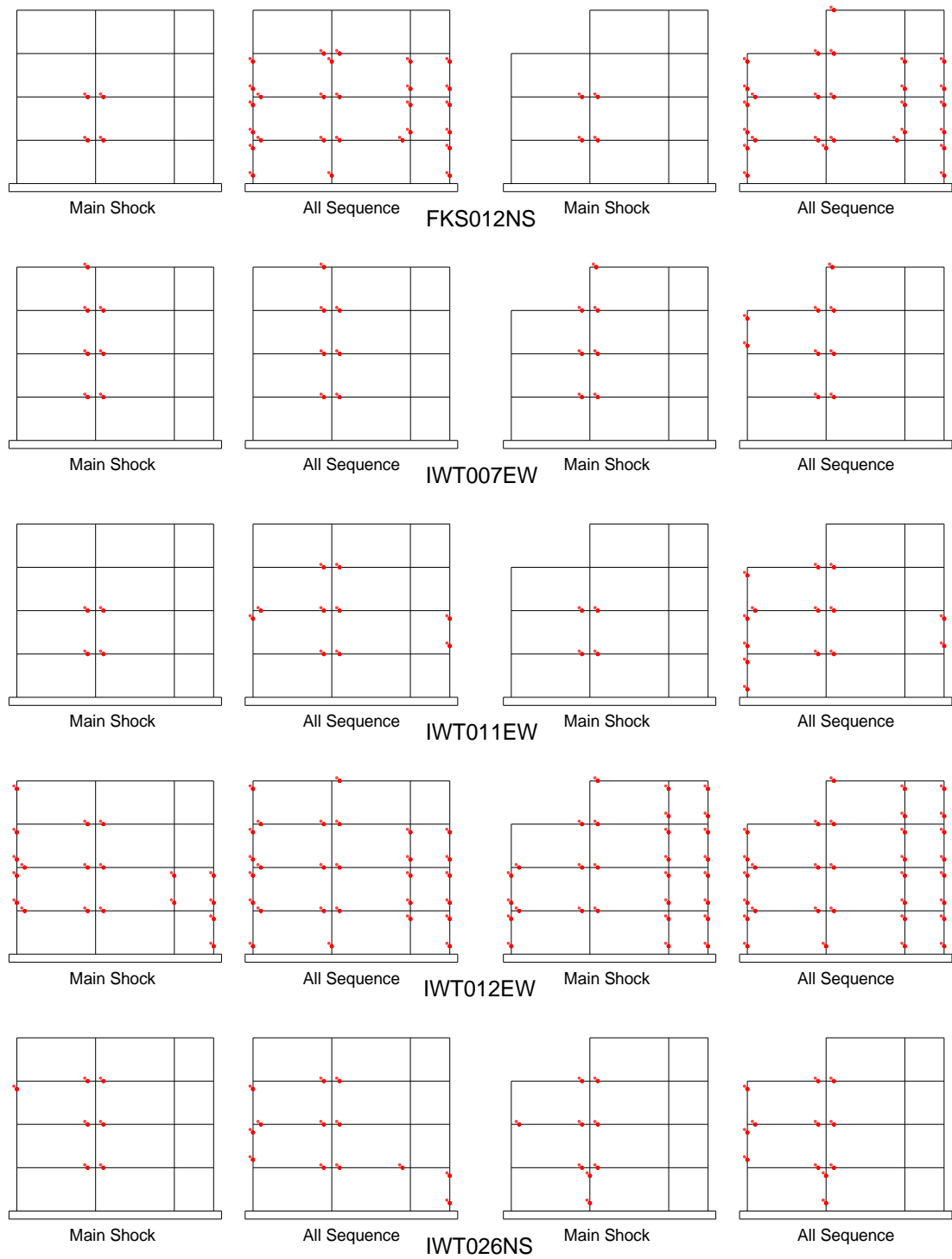


Figure 6.82 : Plastic hinge locations of ICON building for original (left) and remodeled (right) case

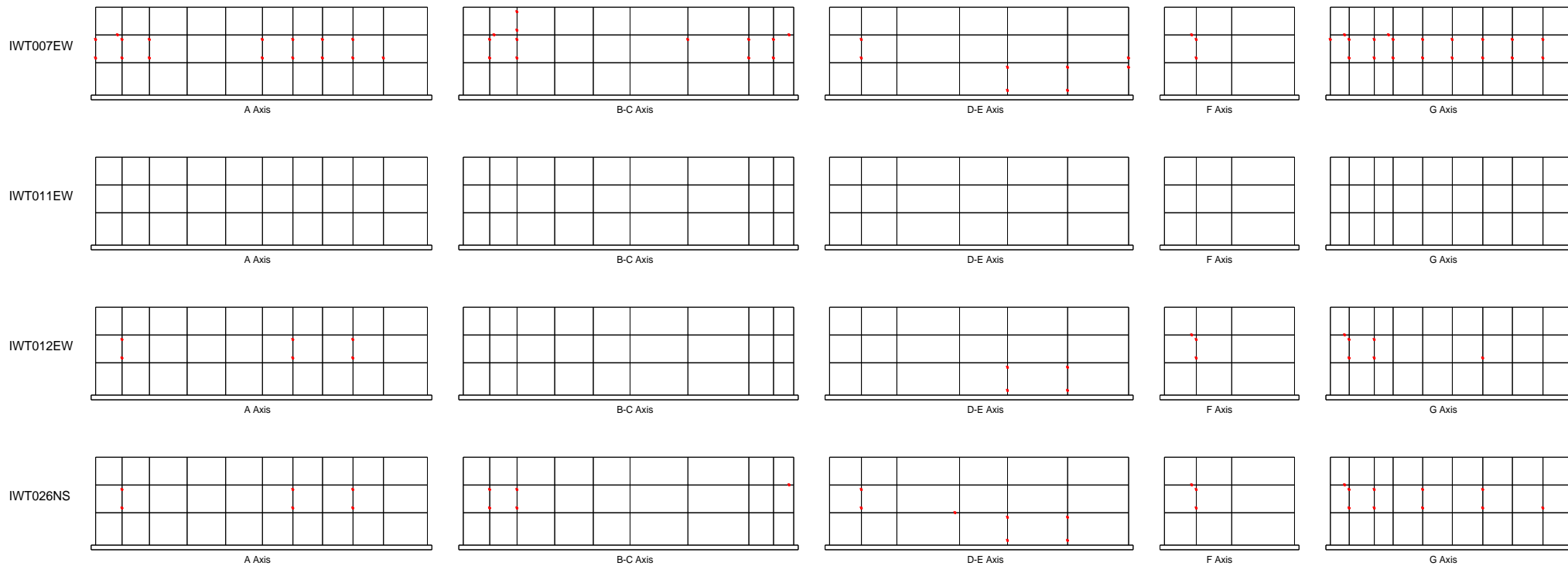


Figure 6.83 : Plastic hinge locations of school building for regular case in main shock

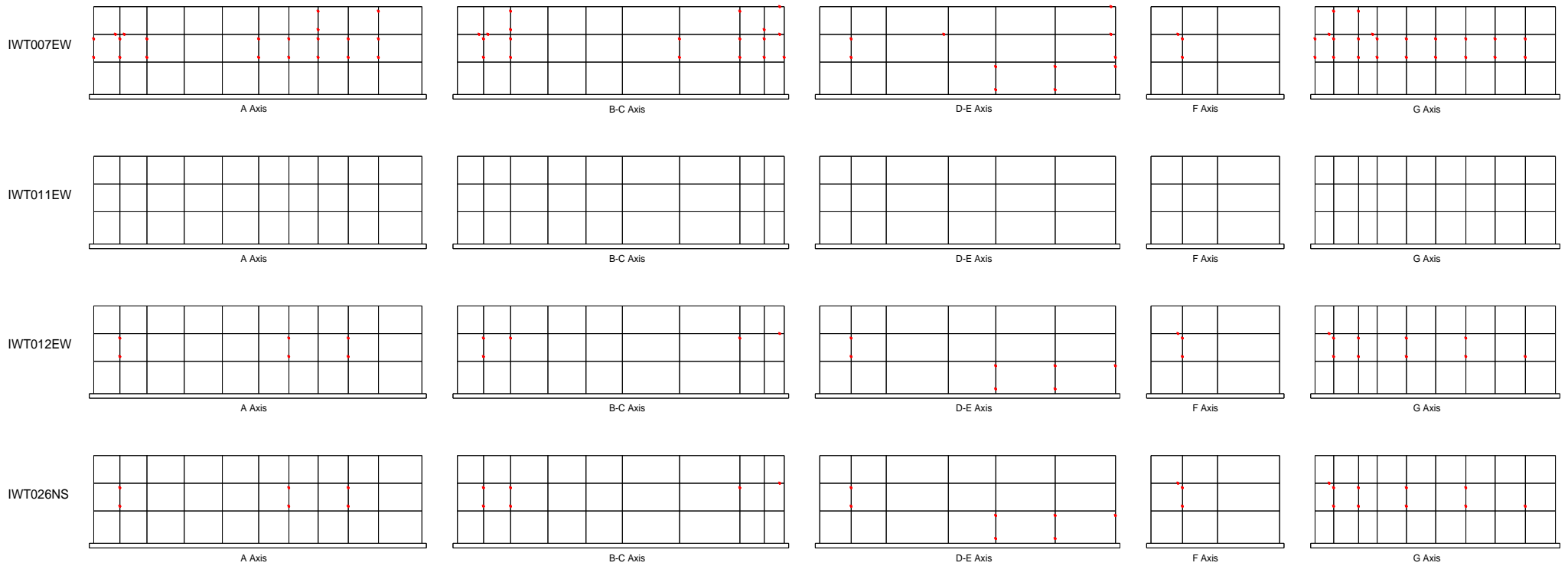


Figure 6.84 : Plastic hinge locations of school building for regular case in all sequence

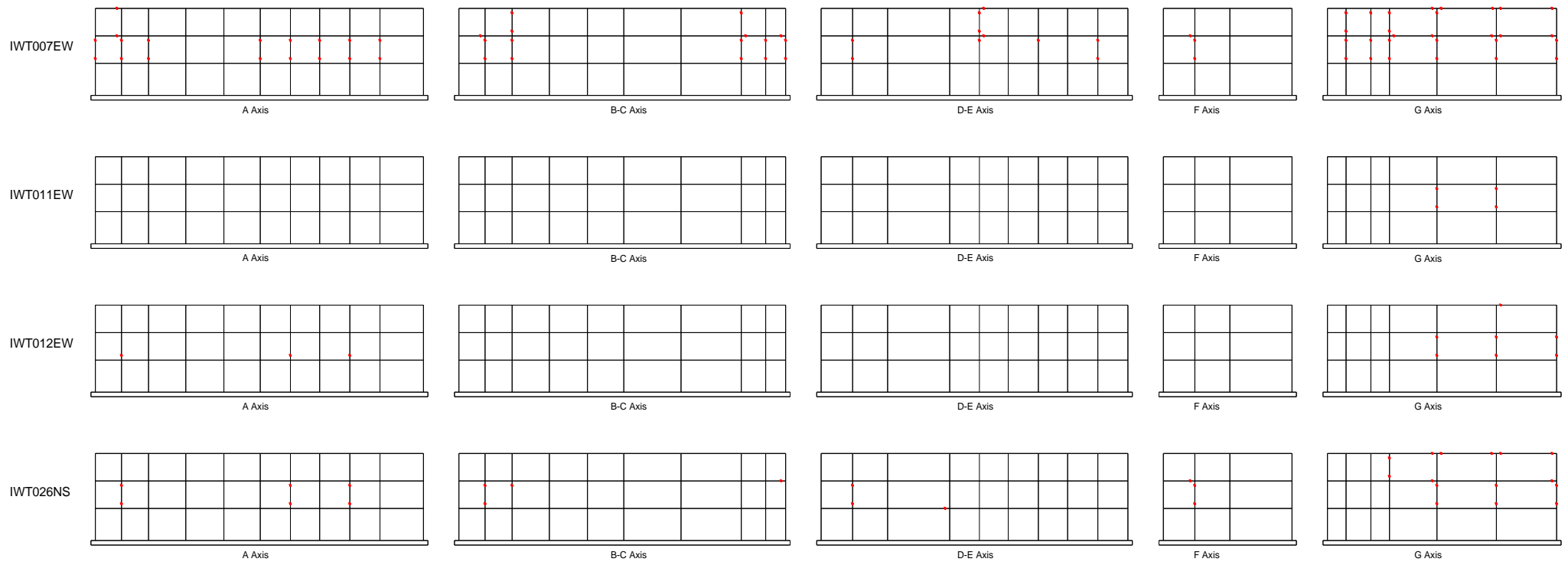


Figure 6.85 : Plastic hinge locations of school building for irregular case in main shock

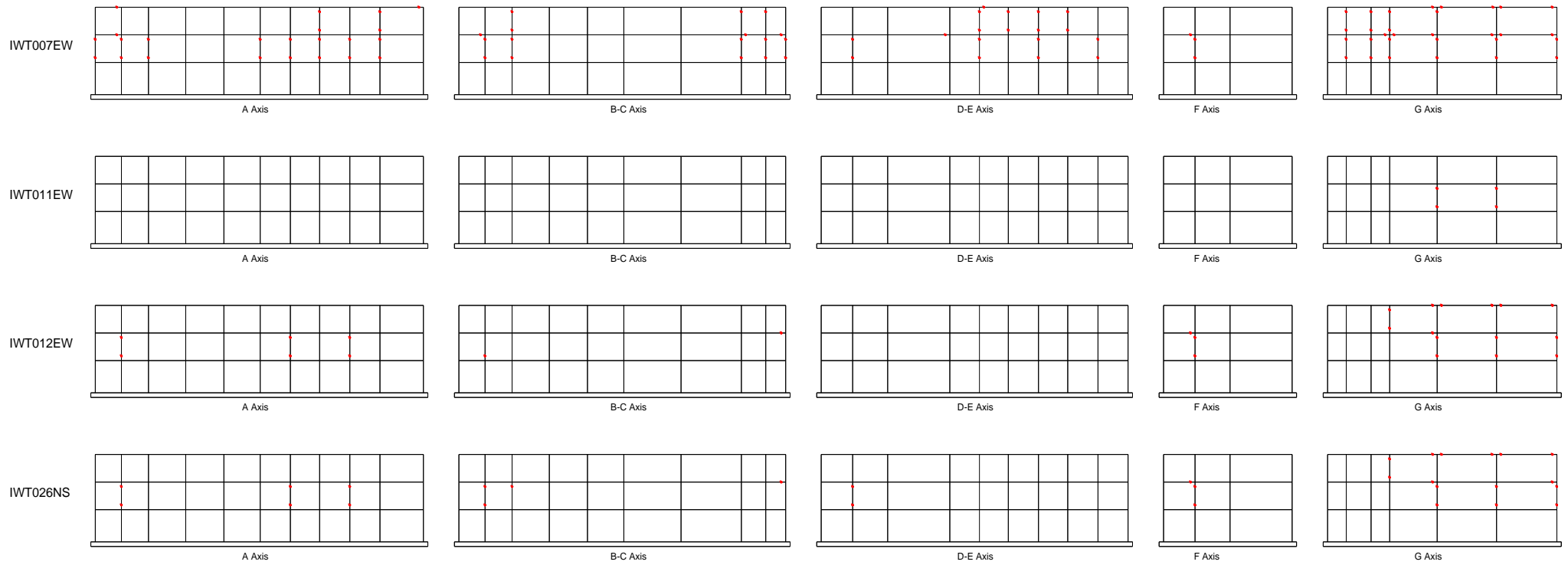


Figure 6.86 : Plastic hinge locations of school building for irregular case in all sequence

7. CONCLUSION

In this study, the effects of irregularities are examined for different types of buildings under substantial sets of Tohoku earthquake sequences with using degrading material models. First, the capacity of the buildings is determined using nonlinear static procedures. Then seismic performance of the buildings are assessed using nonlinear dynamic analysis. The results indicate that irregularity effects increase the dispersed damage on the buildings when structures are subjected to multiple ground motions. Though there are some studies concerning the effects of multiple excitation on the structures, there is not enough literature focusing on the irregularity effects that arise on the RC structures. The results are summarized following substances.

- Degradation effect is seen clearly in residual displacements. The non-degrading models showed limited residual displacements compared to degrading models.
- Irregular structures showed more permanent displacements both for main-shock and all sequence case. However, increase in residual displacement ratios between the main shock and all sequence is almost same for both regular and irregular in plan (SPEAR), irregular in elevation (ICON) buildings. This case is opposite for both plan and elevation irregular buildings (School building).
- Generally, the buildings experienced maximum top displacements during the main shock in degrading models. Even if following aftershocks have greater PGA, maximum top displacement of buildings did not exceed the previous top displacements due to the strength deterioration and stiffness degradation in material.
- During the main shock, more plastic hinges are developed in irregular buildings compared to regular ones, therefore when the irregular structures experienced aftershocks, increase in plastic hinges is less than the regular

case. Hence, when the mean results are compared between regular and irregular buildings, it is observed that, increase in ratio of the plastic hinges while the multiple excitations are larger in regular structures compared to irregular ones. Nevertheless, number of developed hinges are higher in irregular ones when the all sequence is finished.

- Minimum difference in number of plastic hinges between the main shock and all sequence was observed for SPEAR building in both regular and irregular cases. However, lots of plastic hinges was developed in main shock, so number of plastic hinges increased less in all sequence case for SPEAR building. When compared to this aspect, normally school building showed a minimum increasing in number of plastic hinges due to the shear walls.
- Conventional nonlinear static results differ from the nonlinear dynamic results, but when the relevant local quantities are multiplied by calculated factors, which are determined by using extended N2 method, similar results are captured with nonlinear dynamic analysis. Therefore, a good prediction can be made by the extended N2 method in terms of plastic hinge distribution.
- Seismic response of buildings which are built in accordance with a seismic design code are found to be better than non-engineered ones.

Consequently, more attention must be shown for multiple earthquake excitations during the design phase especially important buildings, which include the irregularity effects.

REFERENCES

- [1] **Url-2** <http://cires1.colorado.edu/~bilham/Honshu2011/Aftershocks.pdf>, date reviewed 08.09.2015.
- [2] **Erdik, M., Kamer, Y., Demircioglu, M. B. and Sesetyan, K.** (2012). Report on 2012 Van (Turkey) Earthquakes, Proceedings of the International Symposium on Engineering Lessons Learned from the 2011 Great East Japan Earthquake, March 1-4, 2012, Tokyo, Japan
- [3] **Ozacar, A., Kaymakci, S., Akkar, S., Azari, A., Sandikkaya, M. A., Kale, O., Ay, B. O., Gulerce, Z., Yilmaz, M. T., Huvaj, N., Saglam, S., Unsever, Y., Yakut, A., Binici, B., Canbay, E., Erberik, A., Saritas, A., Aldemir, A., Demirel, I. O. and Erdil, B. and Demirtas, R.** (2011). 23 Ekim 2011 Mw 7.2 Van Depremi Sismik ve Yapısal Hasara İlişkin Saha Gözlemleri, Rapor No:METU:EERC 2011-04, Kasım 2011/ Ankara (in Turkish)
- [4] **Akkar, S., Ozacar, A., Kale, O., Sandikkaya, M. A., Binici, B., Canbay, E., Ozcebe, G., Yakut, A., Aldemir, A., Demirel, I. O. and Erdil, B.** (2012). 9 Kasım 2011 Mw 5.6 Van-Edremit Depremi Sismik ve Yapısal Hasara İlişkin Gözlemler, Rapor No:METU:EERC/İMO 2012-01, Şubat 2012/ Ankara (in Turkish)
- [5] **Abdelnaby, A. E.** (2012). Multiple Earthquake Effects on Degrading Reinforced Concrete Structures, Ph.D Dissertation, University of Illinois at Urbana-Champaign
- [6] **Abdelnaby, A. E. and Elnashai A. S.** (2014). Performance of Degrading Reinforced Concrete Frame Systems Under the Tohoku and Christchurch Earthquake Sequences, Journal of Earthquake Engineering, 18:7, 1009-1036
- [7] **Mahin, A. S.** (1980). Effects of Duration And Aftershocks On Inelastic Design Earthquakes, Proceedings of the 7th World Conference On Earthquake Engineering, Vol 5, pp. 677-80
- [8] **Aschheim, M. and Black, E.** (1999). Effects of Prior Earthquake Damage on Response of Simple Stiffness-Degrading Structures, Engineering Spectra, 15, 1-24
- [9] **Amadio, C., Fragiaco, M. and Macorini, L.** (2003) The Effects of Repeated Earthquake Ground Motions on The Non-linear Response of SDOF Systems, Earthquake Engineering and Structural Dynamics, 32, 291-308
- [10] **Hatzigeorgiou, G. D. and Beskos D. E.** (2009) Inelastic displacement ratios for SDOF structures subjected to repeated earthquakes, Engineering Structures, 31, 2744-2755
- [11] **Frangiaco, M., Amadio, C. and Macorini L.** (2004) Seismic Response of Steel Frames Under Repeated Earthquake Ground Motions, Engineering Structures, 26, 2021-2035

- [12] **Li, Q. and Ellingwood, B. R.** (2007). Performance Evaluation and Damage Assessment of Steel Frame Buildings Under Main Shock-Aftershock Earthquake Sequences, *Earthquake Engineering and Structural Dynamics*, 36, 405-427
- [13] **Chopra, A. K. and Goel, R. K.** (2002). A Modal Pushover Analysis Procedure For Estimating Seismic Demands For Buildings, *Earthquake Engineering and Structural Dynamics*, 31, 561-582
- [14] **Gross, J. L.** (1998). A Connection Model For The Seismic Analysis of Welded Steel Moment Frames, *Engineering Structures*, Vol 20, pp. 390-397
- [15] **Hatzigeorgiou, G. D. and Liolios, A. A.** (2010) Nonlinear Behavior of RC Frames Under Repeated Strong Ground Motions, *Soil Dynamics and Earthquake Engineering*, 30, 1010-1025
- [16] **Sarno, L. D.** (2013) Effects of Multiple Earthquakes on Inelastic Structural Response, *Engineering Structures*, 56, 673-681
- [17] **Lee, J. and Fenves, G.** (1998). Plastic Damage Model for Cyclic Loading of Concrete Structures, *Journal of Engineering Mechanics*, Vol. 124, No. 8, pp. 829-900
- [18] **Menegotto, M. and Pinto, P.** (1973). Method of Analysis for Cyclically Loaded RC Plane Frames Including Changes in Geometry and Non-elastic Behavior of Elements Under Combined Normal Force and Bending, *Symp. Resistance and Ultimate Deformability of Structures Acted on by Well Defined Repeated Loads*, IABSE Reports Vol 13, Lisbon
- [19] **Gomes, A. and Appleton, J.** (1997). Nonlinear Cyclic Stress-Strain Relationship of Reinforcing Bars Including Buckling, *Engineering Structures*, Vol 19, No. 10, pp. 822-826
- [20] **Fardis, M.N.** (2002). Design of an Irregular Building for the SPEAR Project
- [21] **Stratan, A. and Fajfar, P.** (2003). Seismic Assessment Of The Spear Test Structure, IKPIR Report, University of Ljubljana, Czech Republic, January
- [22] **Jeong, S-H. and Elnashai, A. S.** (2004). Analytical Assessment of an Irregular RC Full Scale 3D Test Structure, Mid-America Earthquake Centre, University of Illinois at Urbana-Champaign, U.S.A, March
- [23] **Papanikolaou, V. K., Elnashai A. S. and Pareja, J. F.** (2005). Limits of Applicability of Conventional and Adaptive Pushover Analysis for Seismic Response Assessment, Mid-America Earthquake Centre, University of Illinois at Urbana-Champaign, U.S.A, March
- [24] **Eurocode 8** (2004). Design of Structures for Earthquake Resistance, Part 1: General Rules, Seismic Actions and Rules for Buildings. European Standard EN 1998-1, European Committee for Standardization, Brussels,

- [25] **Carvalho, E. C., Coelho, E. and Compos-Costa, A.** (1999). Preparation of the Full-Scale Test on Reinforced Concrete Frames: Characteristic of the Test Specimens, Materials and Testing Conditions, ICON Report, Innovative Seismic Design Concepts for New and Existing Structures, European TMR Network, LNEC
- [26] **Pinto, A., Varum, H. and Molina, J.** Experimental Assessment and Retrofit of Full-Scale Models of Existing RC Frames, European Laboratory for Structural Assessment, Joint Research Centre, Ispra, Italy, March
- [27] **Pinho, R. and Elnashai, A. S.** (2000). Dynamic Collapse Testing of a Full-Scale Four Storey RC Frame, ISET Journal of Earthquake Technology, Paper No.406, Vol 37, No 4, December, pp.143-163
- [28] **TEC 2007** (2007). Turkish Earthquake Code, Ministry of Public Works and Settlement, Ankara, Turkey (in Turkish)
- [29] **Mander, J. B., Priestley, M. J. N. and Park, R.** (1986). Theoretical Stress-Strain Model for Confined Concrete, Journal of Structural Engineering, Vol. 114, No.8
- [30] **Filippou, F. C., Popov E. P. and Bertero, V. V.** (1983). Effects of bond deterioration on hysteric behavior of reinforced concrete joints, Earthquake Engineering Research Center, Report UCB/EERC-83/19, University of California, Berkeley
- [31] **Elnashai, A. S., Papanikolaou, V. and Lee, D-H.** (2002) “Zeus-NL User Manual”, Mid-America Earthquake Center (MAE) Report
- [32] **Jeong, S-H. and Elnashai, A. S.** (2004). Analytical Assessment of an Irregular RC Full Scale 3D Test Structure, Mid-America Earthquake Centre, University of Illinois at Urbana-Champaign, U.S.A, March
- [33] **Eurocode 2** (2004). Design of Structures for Earthquake Resistance, Part 1: General Rules, Seismic Actions and Rules for Buildings. European Standard EN 1998-1, European Committee for Standardization, Brussels,
- [34] **Takewaki, I., Murakami, S., Fujita, K., Yoshitomi, S. and Tsuji, M.** (2011). The 2011 Off the Pacific Coast of Tohoku Earthquake and Response of High-Rise Buildings Under Long Period Ground Motions, Soil Dynamics and Earthquake Engineering, 31, 1511-1528
- [35] **Japan Meteorological Agency**
http://www.jma.go.jp/jma/en/2011_Earthquake/chart/2011_Earthquake_CMT.pdf, date revised 16.11.2015.
- [36] **Goto, H. and Morikawa, H.** (2012). Ground Motion Characteristics During the 2011 Off the Pacific Coast of Tohoku Earthquake, Soils and Foundations, 52(5), 769-779
- [37] **Zhao, D.** (2015). The 2011 Tohoku Earthquake (Mw 9.0) Sequence and Subduction Dynamics in Western Pacific and East Asia, Journal of Asian Earth Sciences, 98, 26-49
- [38] **Kazama, M. and Noda, T.** (2012). Damage Statistics (Summary of the 2011 off the Pacific Coast of Tohoku Earthquake damage), Soils and Foundations, 52(5), 780-792

- [39] **Huang, Z. and Zhao, D.** (2013). Mechanism of the 2011 Tohoku-oki Earthquake (Mw 9.0) and Tsunami: Insight From Seismic Tomography, *Journal of Asian Earth Sciences*, 70-71, 160-168
- [40] **Adhikari, G. and Pinho, R.** (2010). Development and Application of Nonlinear Static Procedures For Plan-Asymmetric Buildings, Research Report Rose, 2010/01, IUSS Press
- [41] **NIED.** National Research Institute for Earth Science and Disaster Prevention Strong-Motion Seismograph Networks, <http://www.kyoshin.bosai.go.jp/>, date reviewed 16.11.2015.
- [42] **ATC-76-6** (2010). Applicability of Nonlinear Multiple-Degree-of-Freedom Modeling for Design, National Institute of Standards and Technology
- [43] **Fajfar, P. and Gaspersic, P.** (1996). The N2 Method for The Seismic Damage Analysis of RC Buildings, *Earthquake Engineering and Structural Dynamics*, Vol. 25, 31-46
- [44] **Kreslin, M. and Fajfar, P.** (2012). The Extended N2 Method Considering Higher Mode Effects in Both Plan and Elevation, *Bulletin of Earthquake Engineering*, Vol 10, pp.695-715
- [45] **Fajfar, P.** (2000). A Nonlinear Analysis Method for Performance Based Seismic Design, *Earthquake Spectra*, Vol. 16, No. 3, pp. 573-592
- [46] **Tomaz, V., Peter, F. and Matej, F.** (1994). Consistent Inelastic Design Spectra: Strength and Displacement, *Earthquake Engineering and Structural Dynamics*, Vol. 23, 507-521
- [47] **SAP2000**, Computers and Structures Inc., integrated finite element analysis and design of structures, software, Berkeley, CA

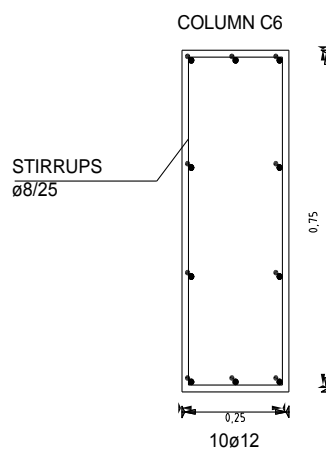
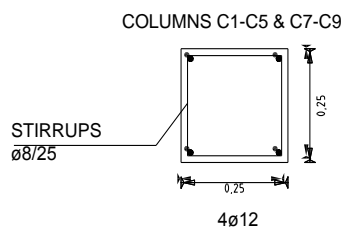
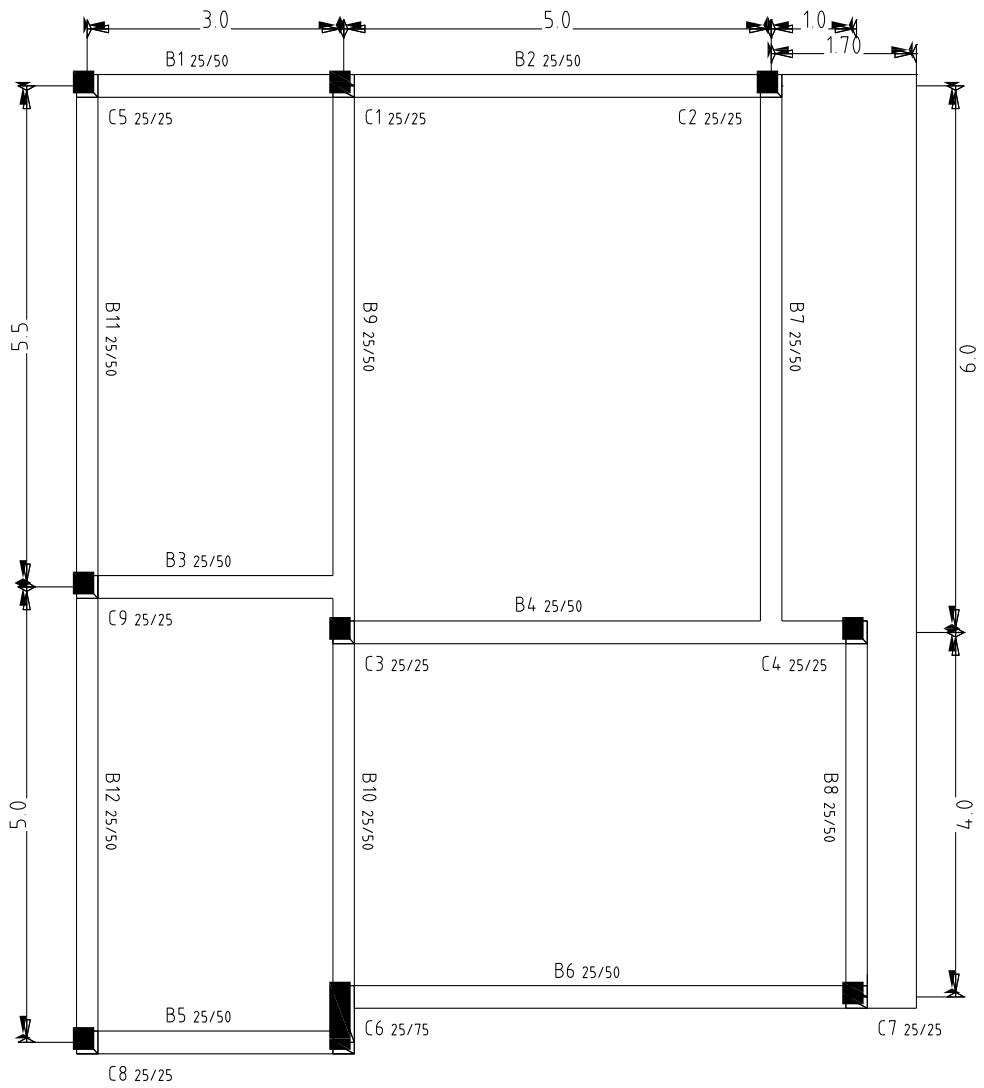
APPENDICES

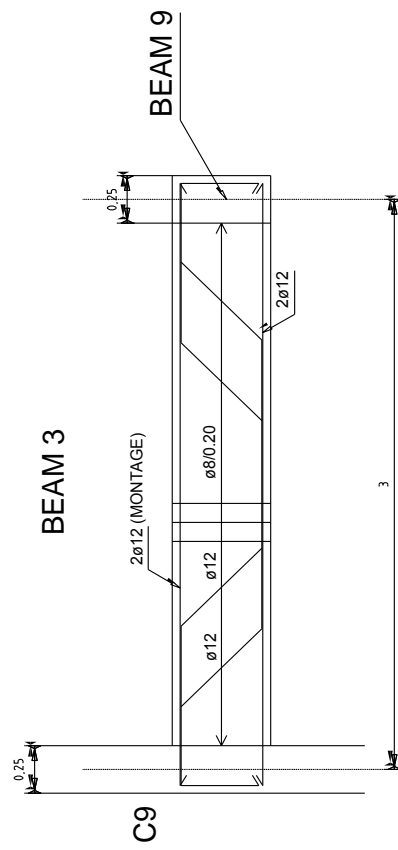
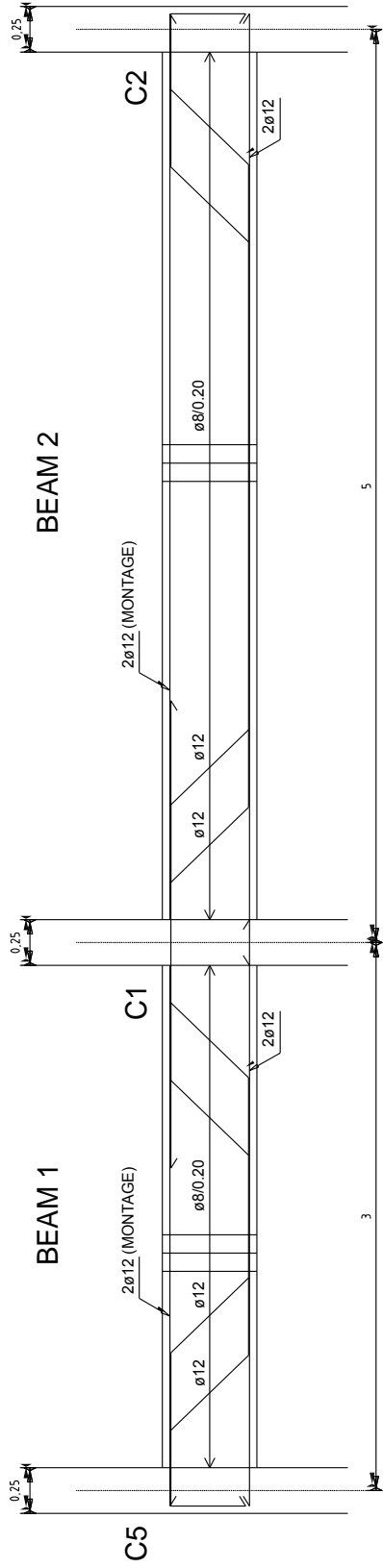
APPENDIX A: SPEAR Building

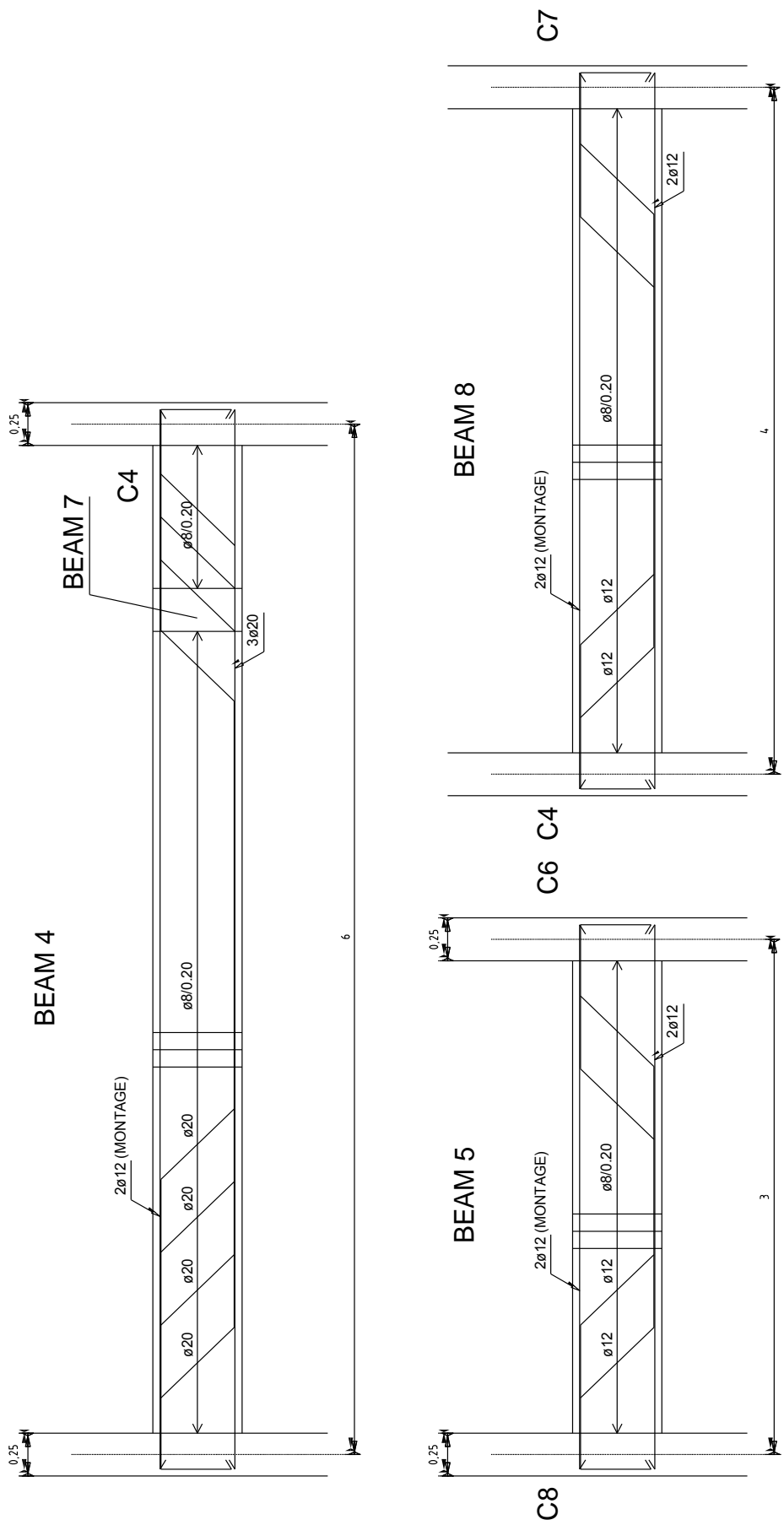
APPENDIX B: ICON Building

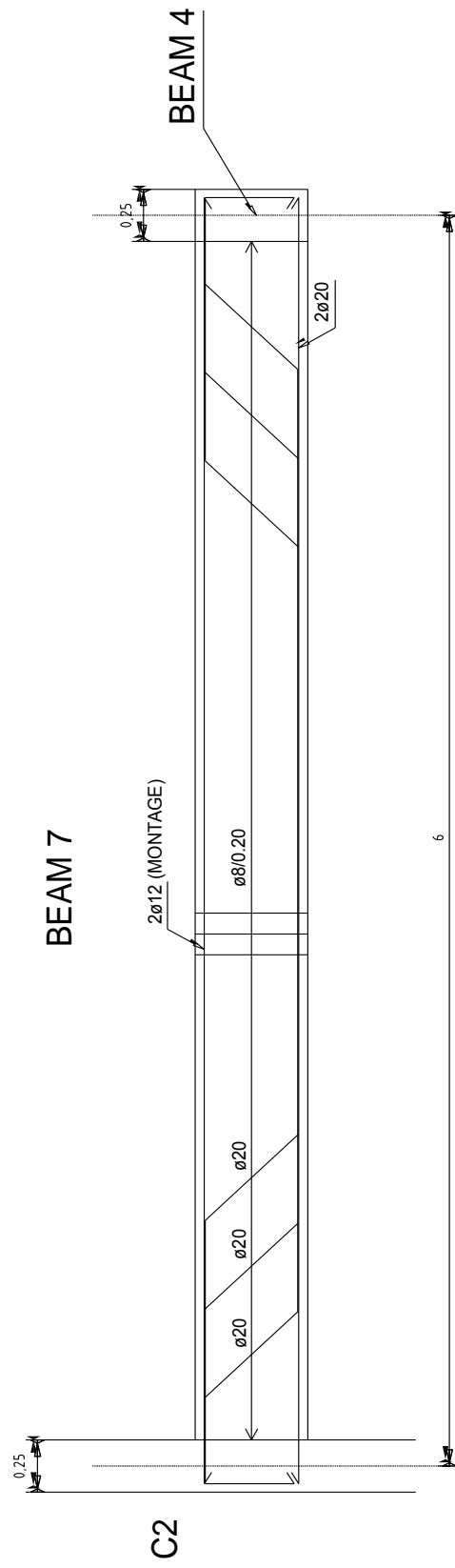
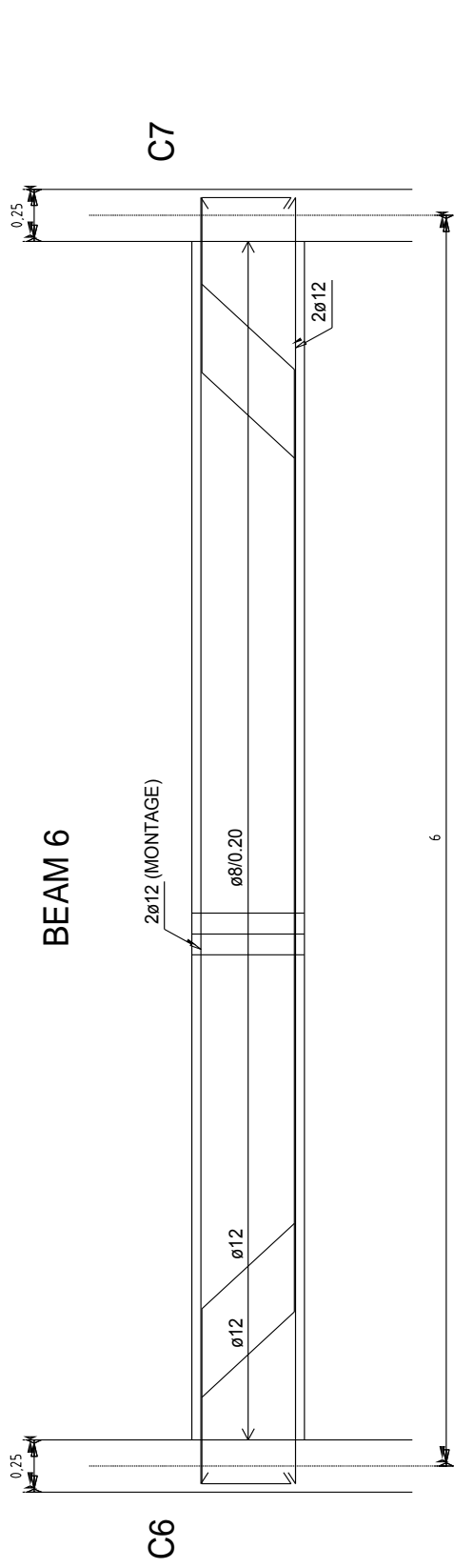
APPENDIX C: Records

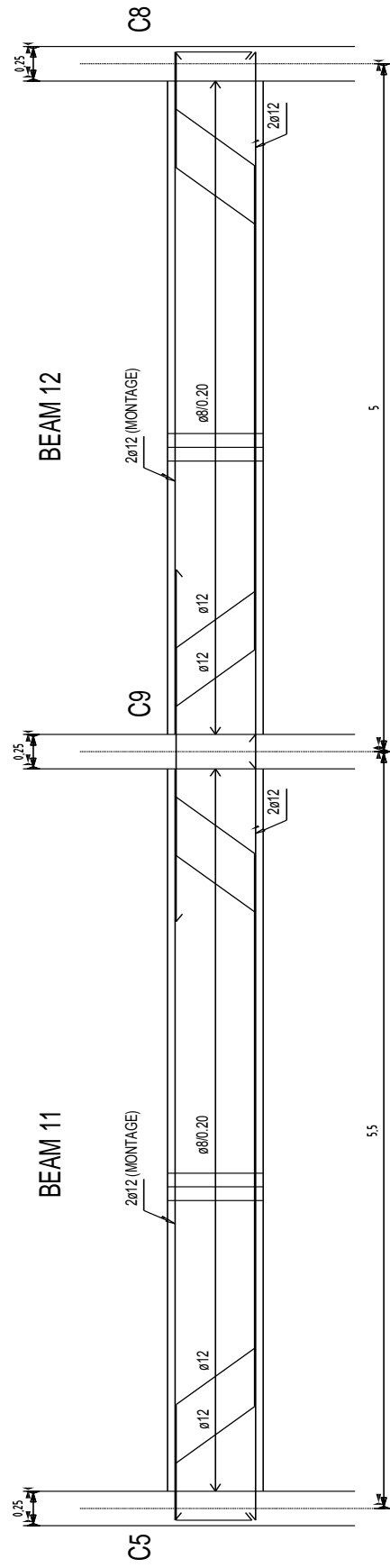
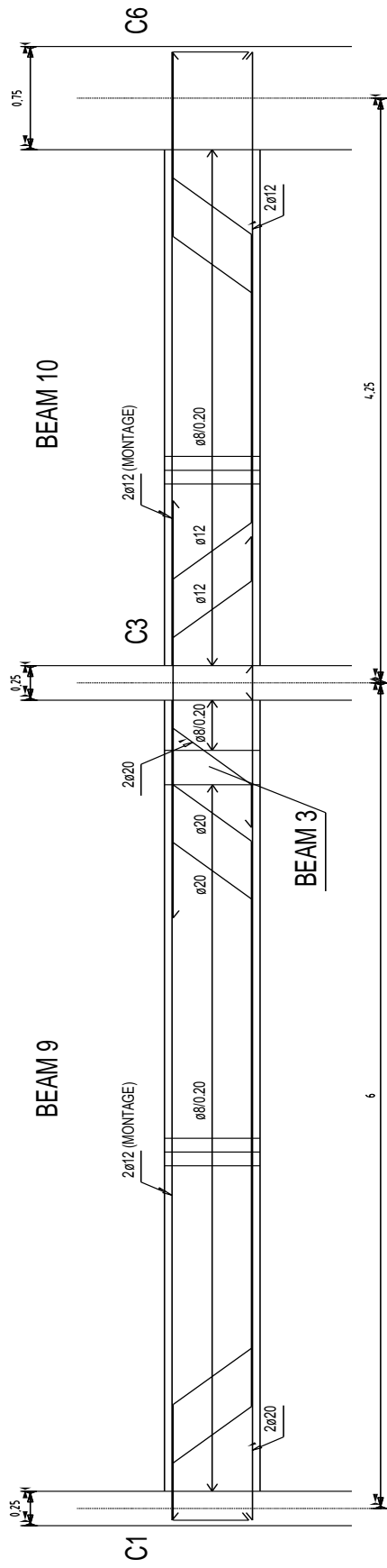
APPENDIX A

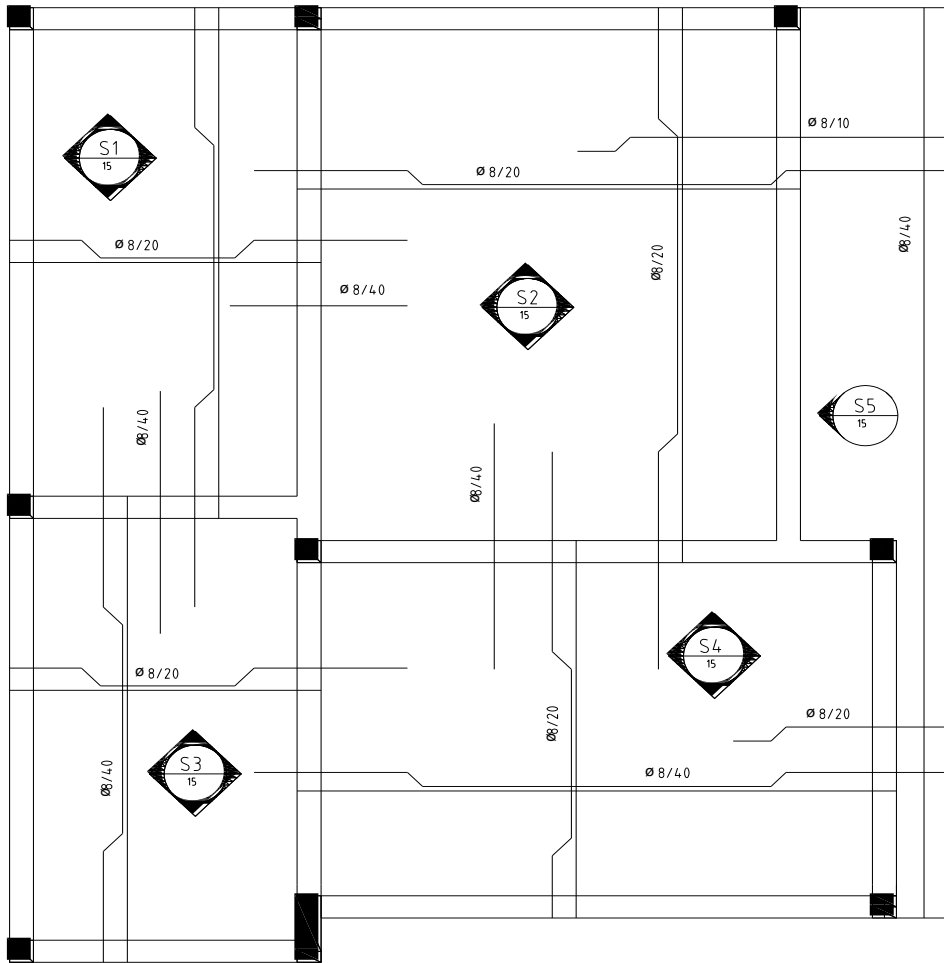




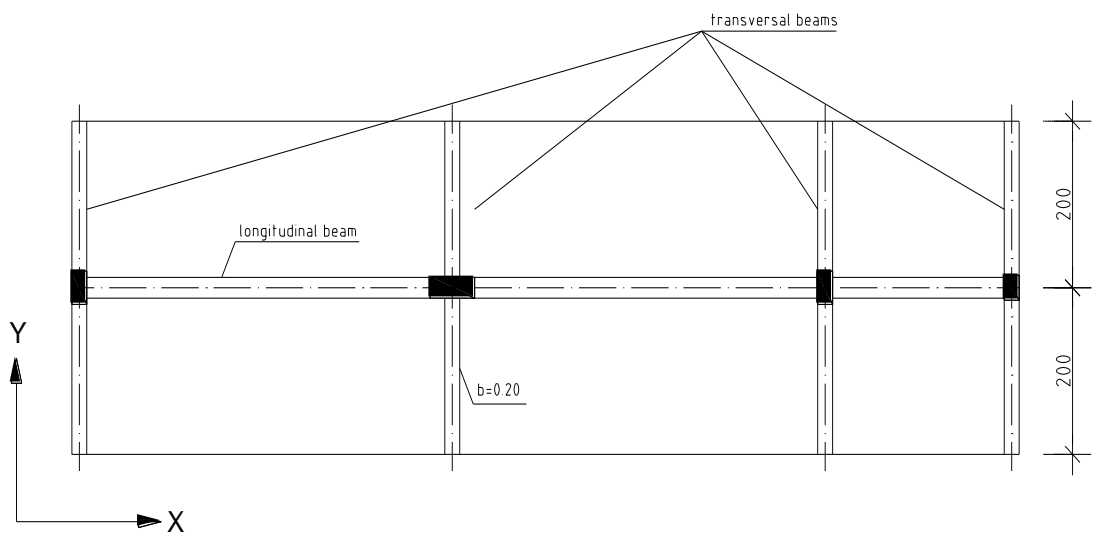
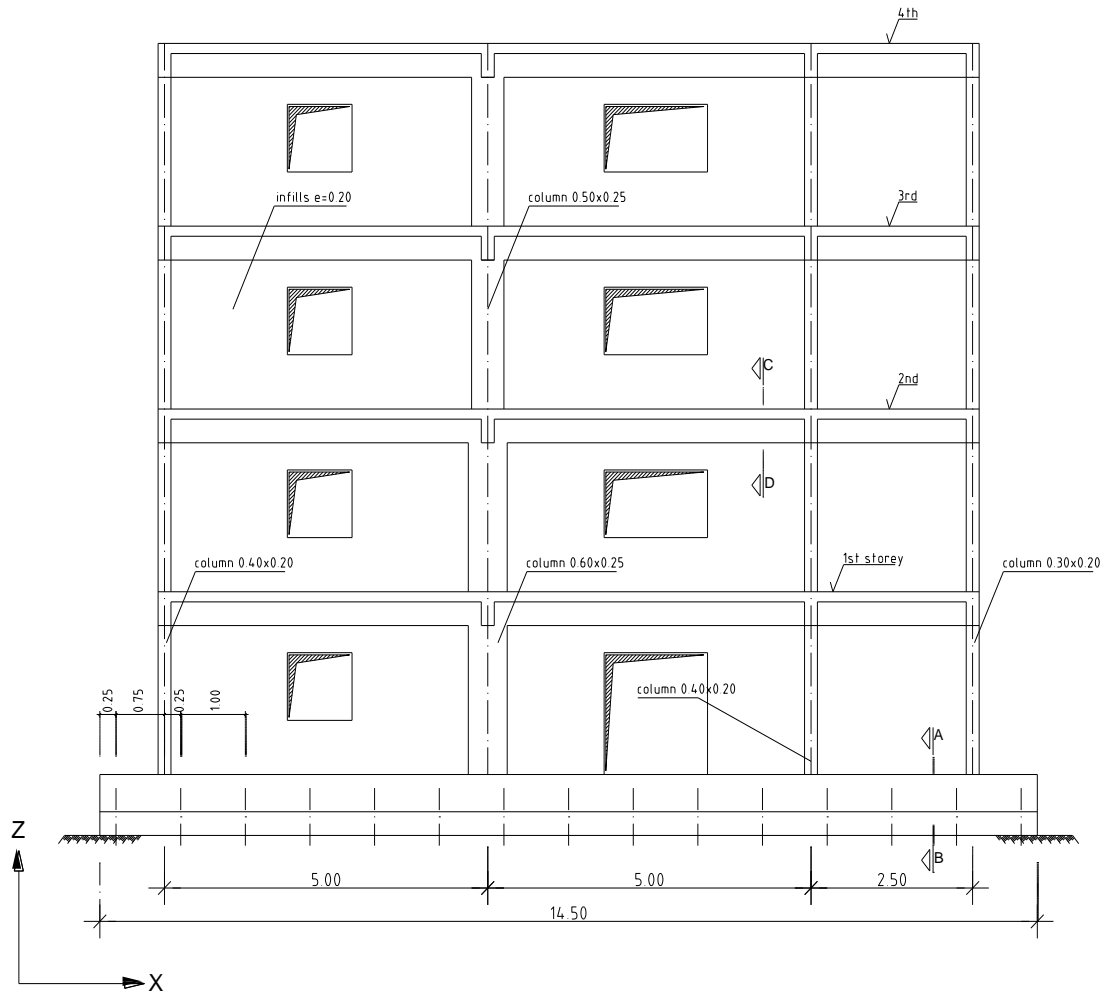


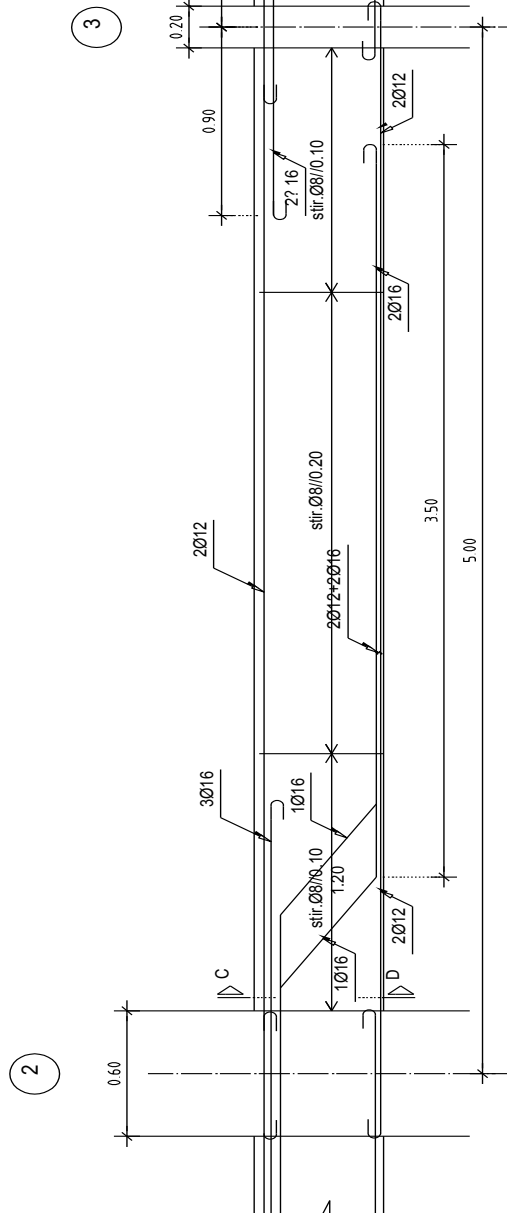
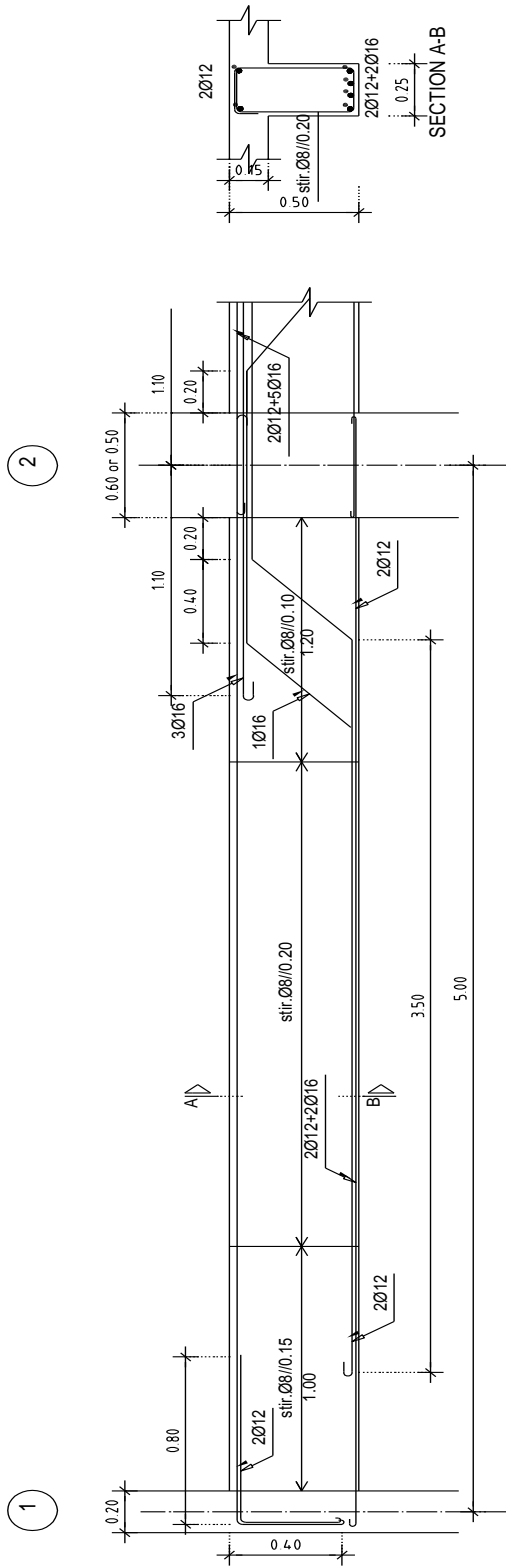


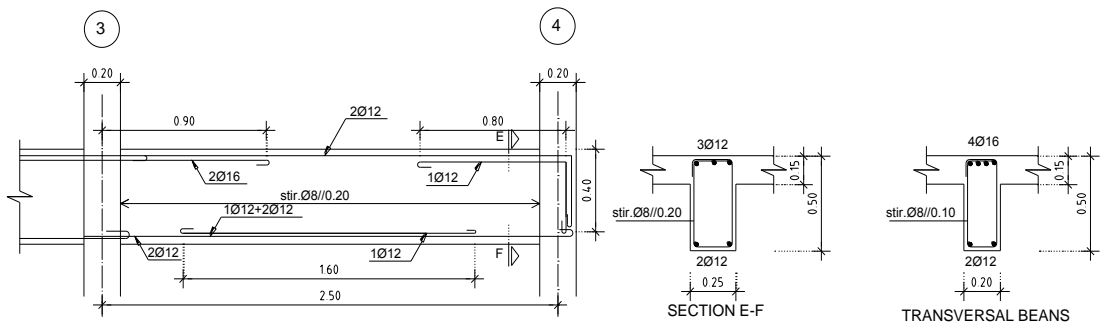




APPENDIX B

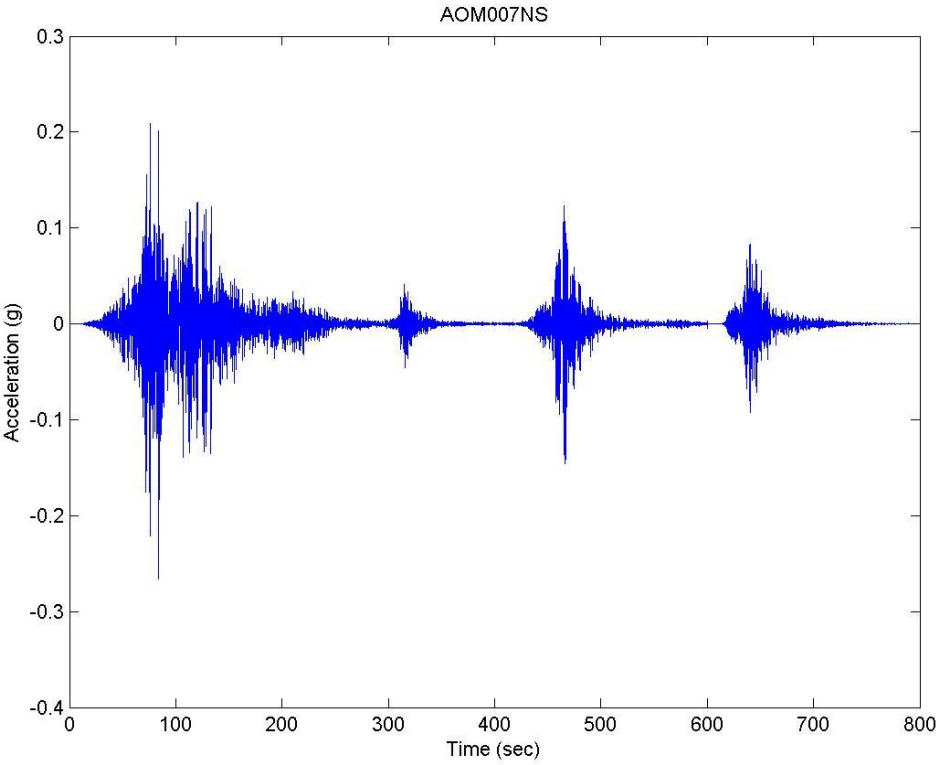


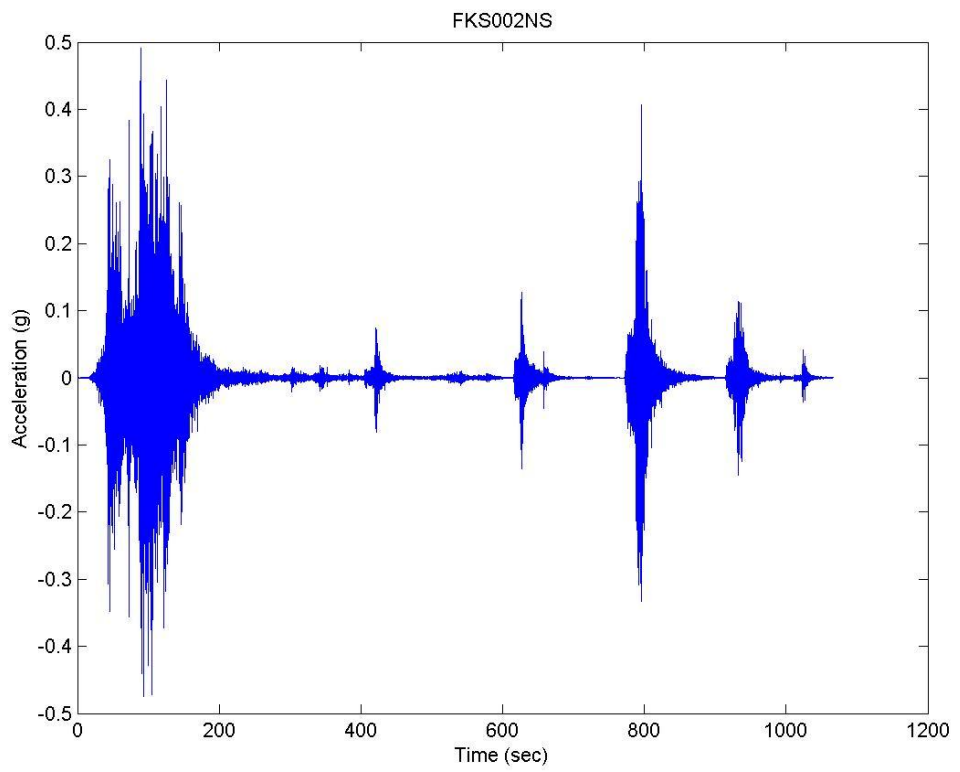
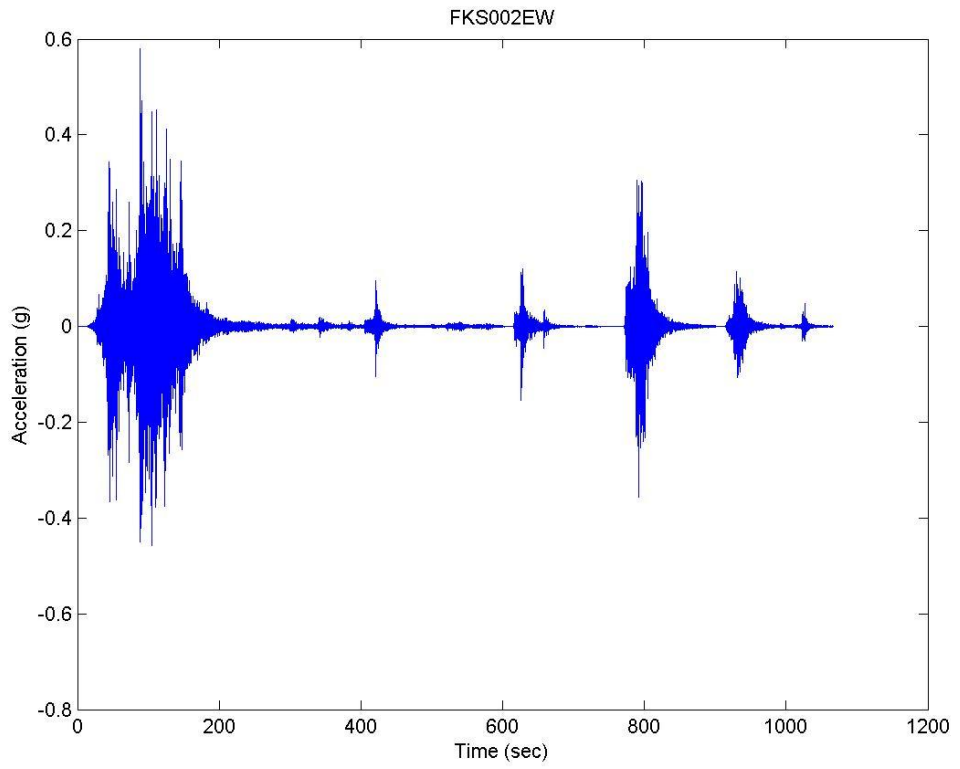


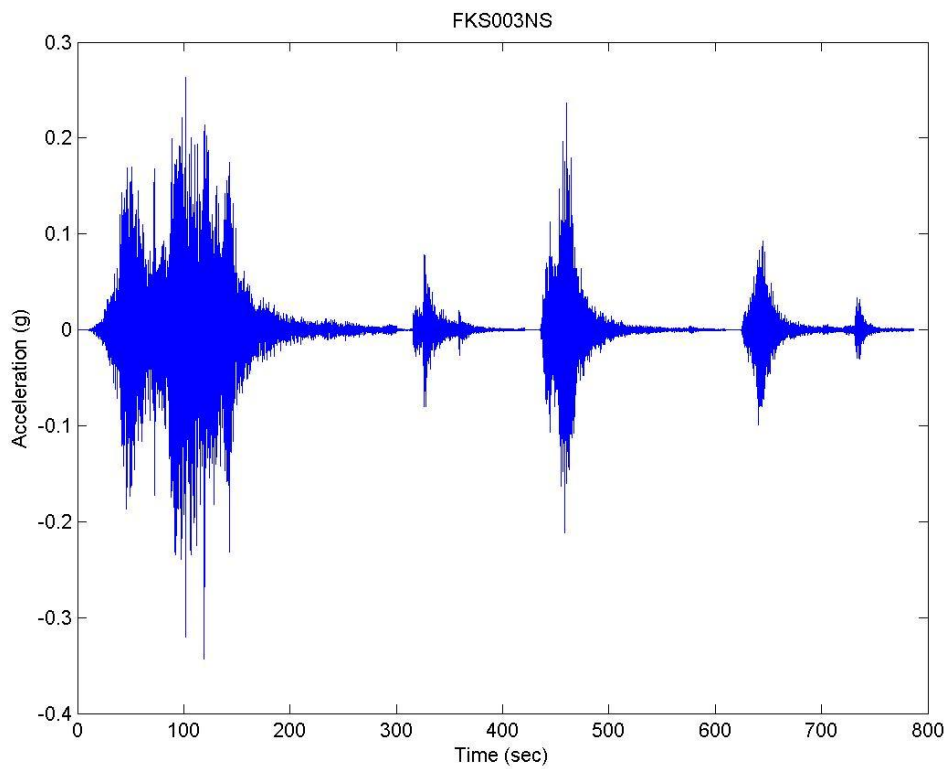
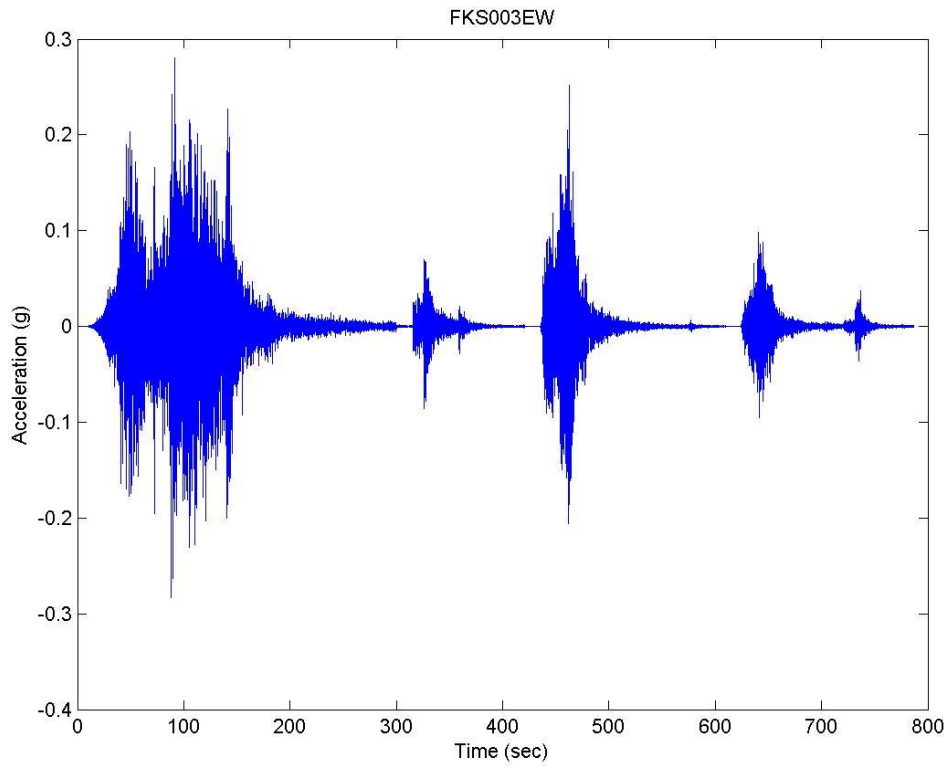


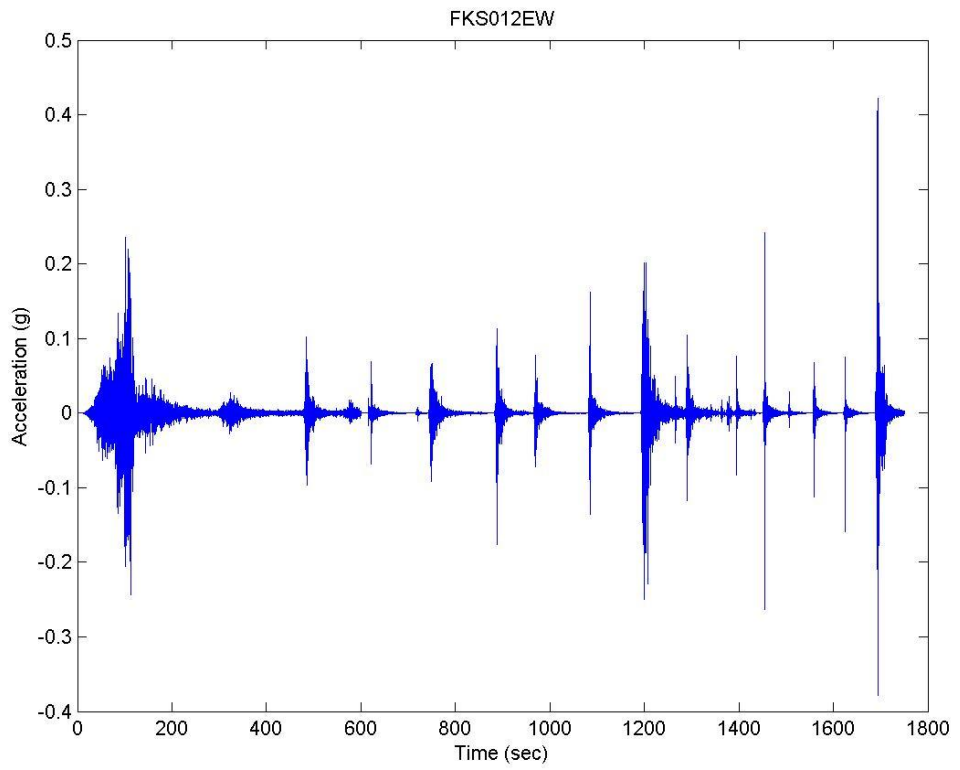
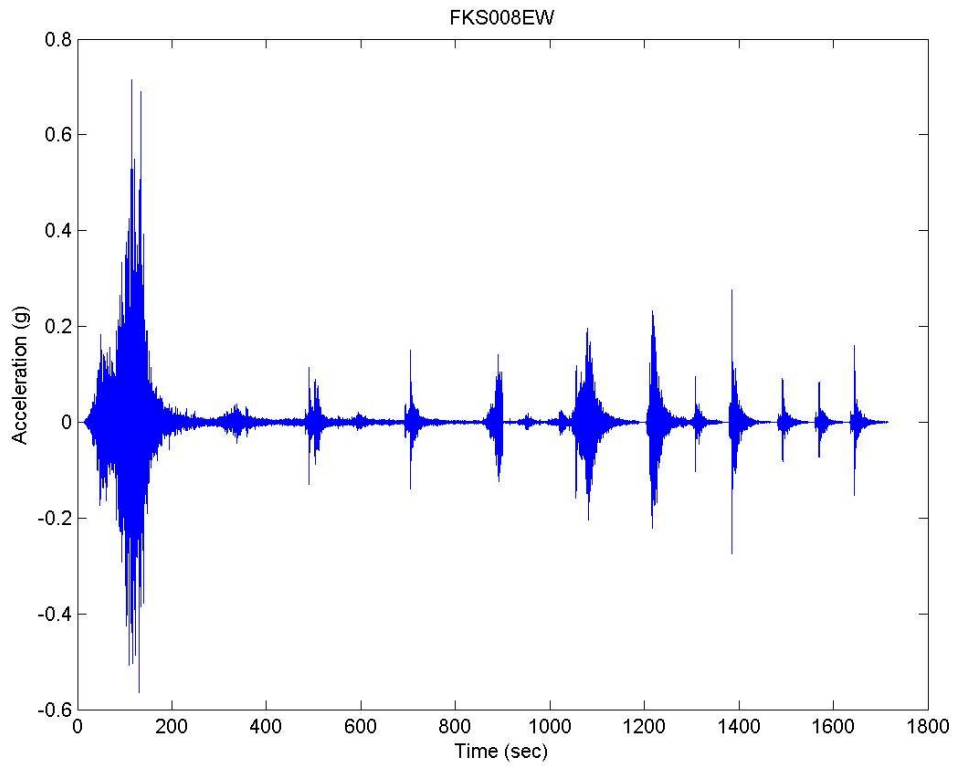
Story	1	2	3	4
4	<p>6Ø12 0.40 0.20 stir.Ø6//0.15</p>	<p>4Ø16+2Ø12 0.25 0.50 stir.Ø6//0.15</p>	<p>6Ø12 0.40 0.20 stir.Ø6//0.15</p>	<p>6Ø12 0.30 0.20 stir.Ø6//0.15</p>
2	<p>6Ø12 0.40 0.20 stir.Ø6//0.15</p>	<p>8Ø16+2Ø12 0.25 0.60 stir.Ø6//0.15</p>	<p>8Ø12 0.40 0.20 stir.Ø6//0.15</p>	<p>6Ø12 0.30 0.20 stir.Ø6//0.15</p>
0				

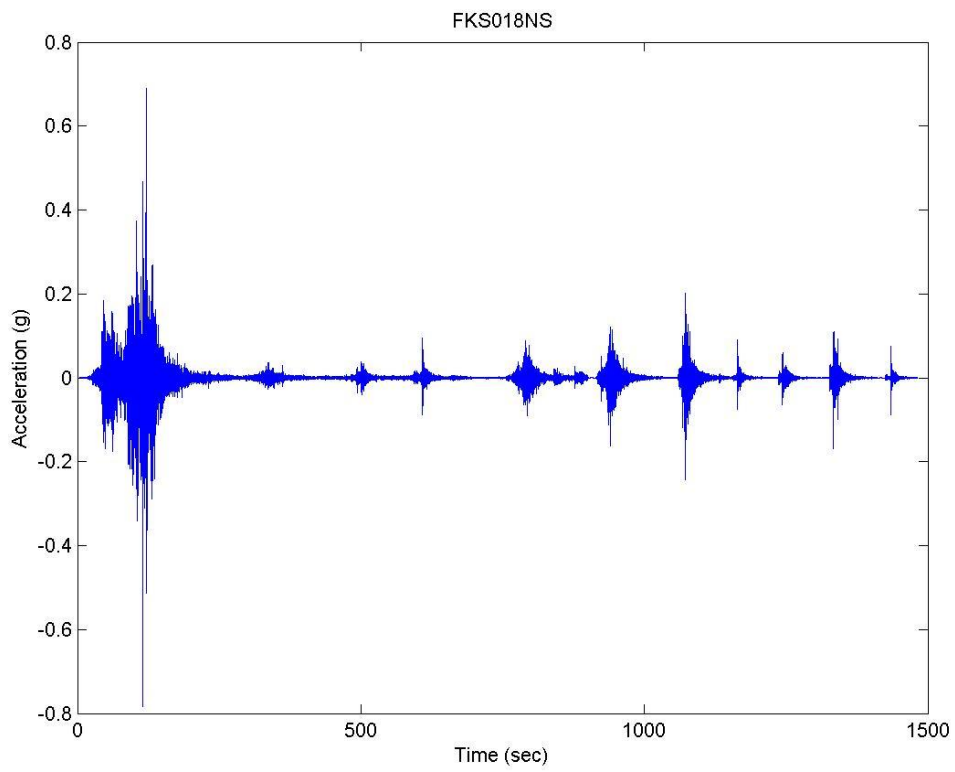
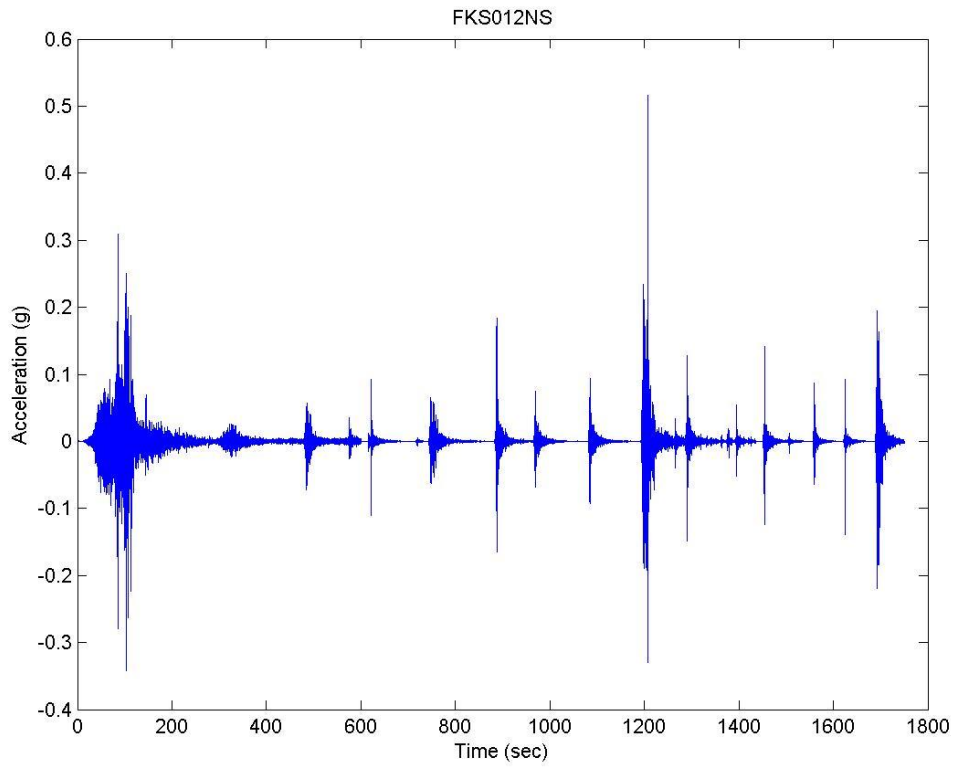
APPENDIX C

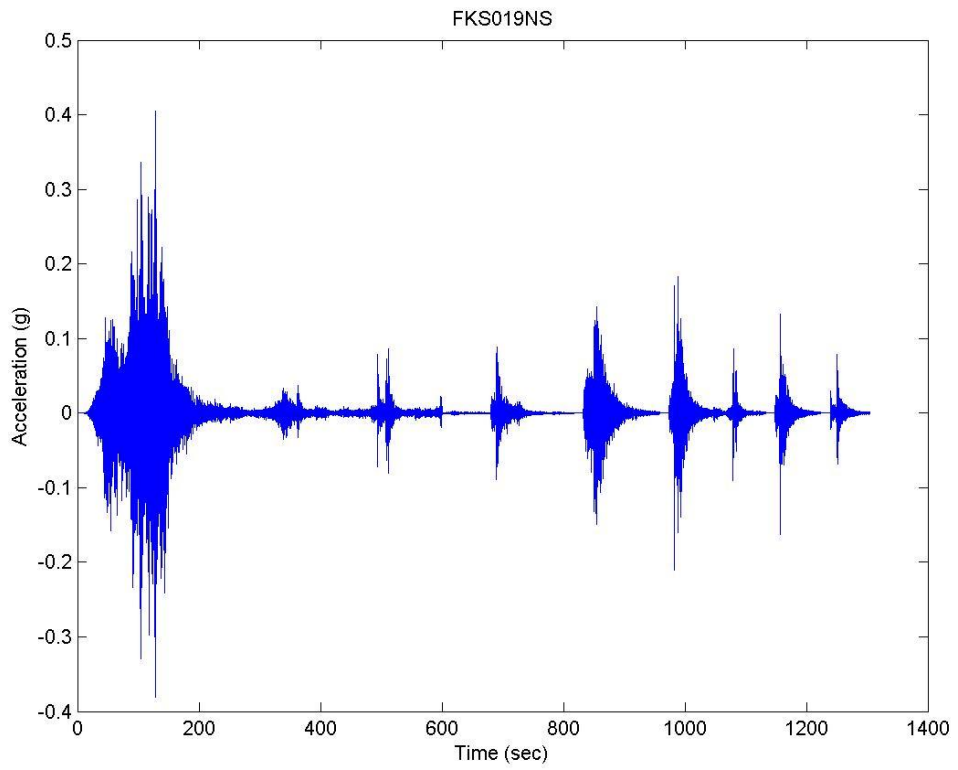
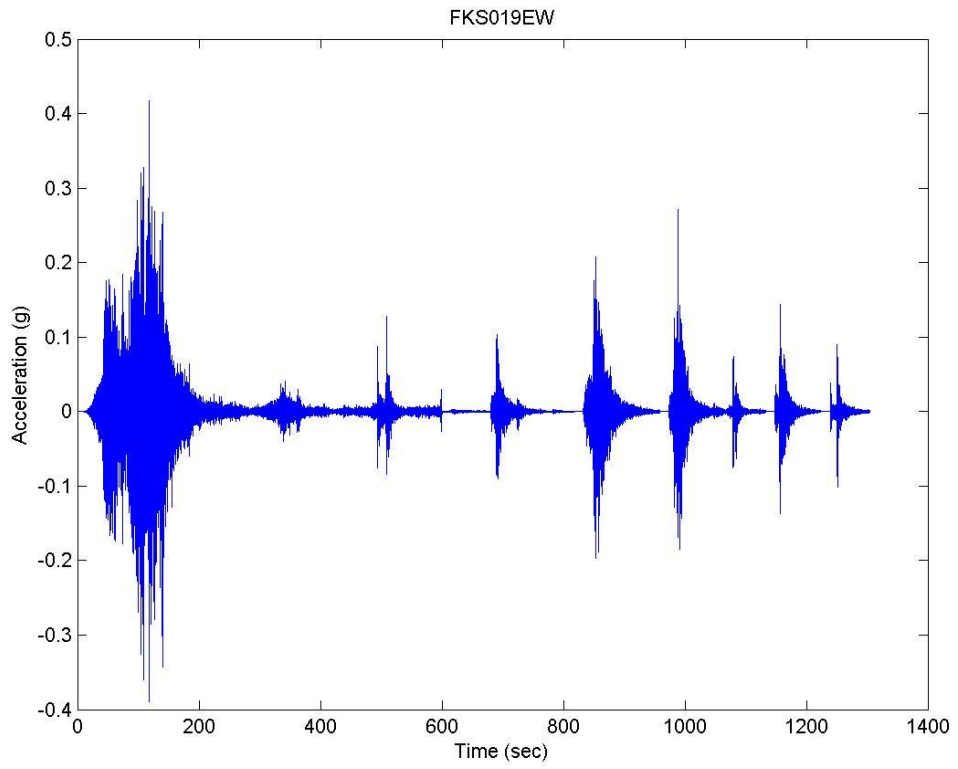


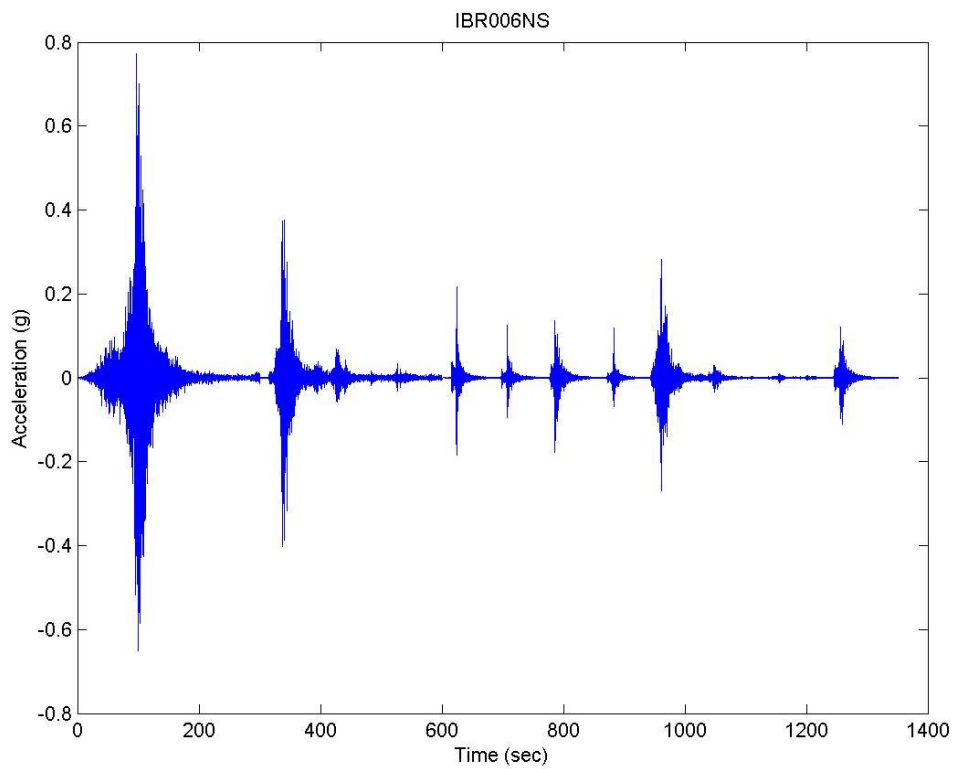
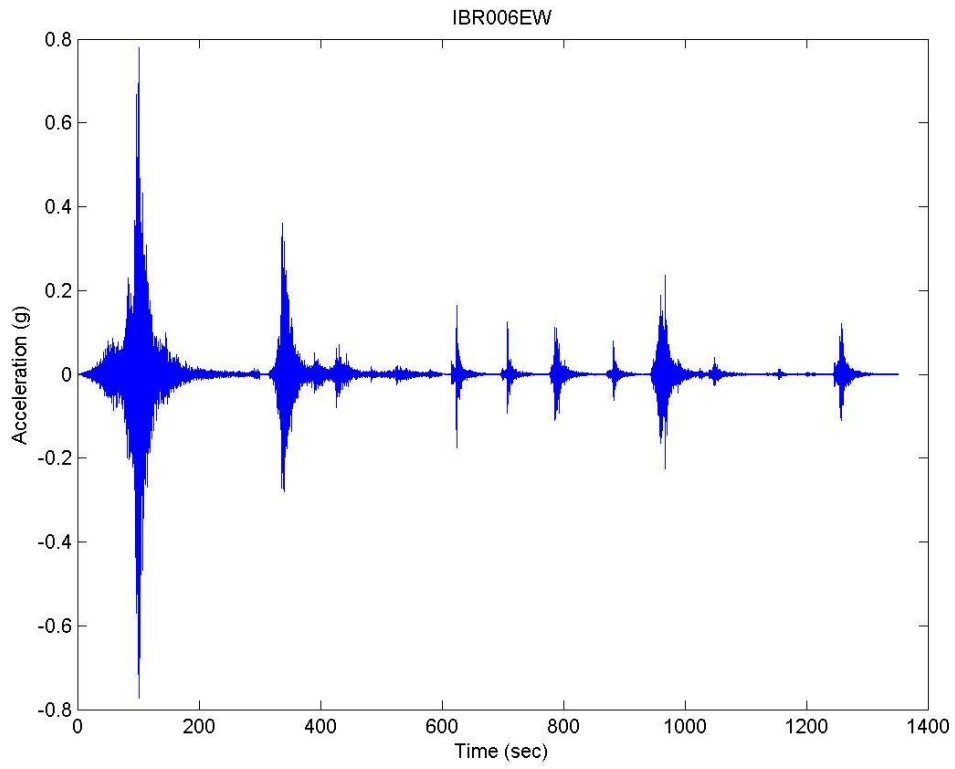


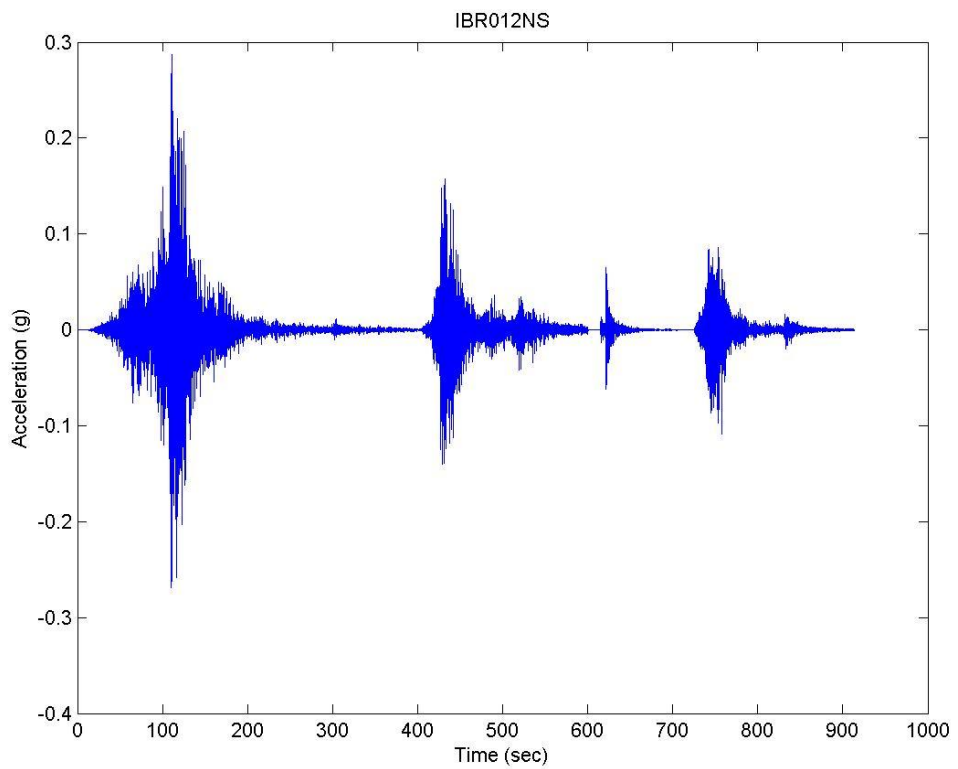
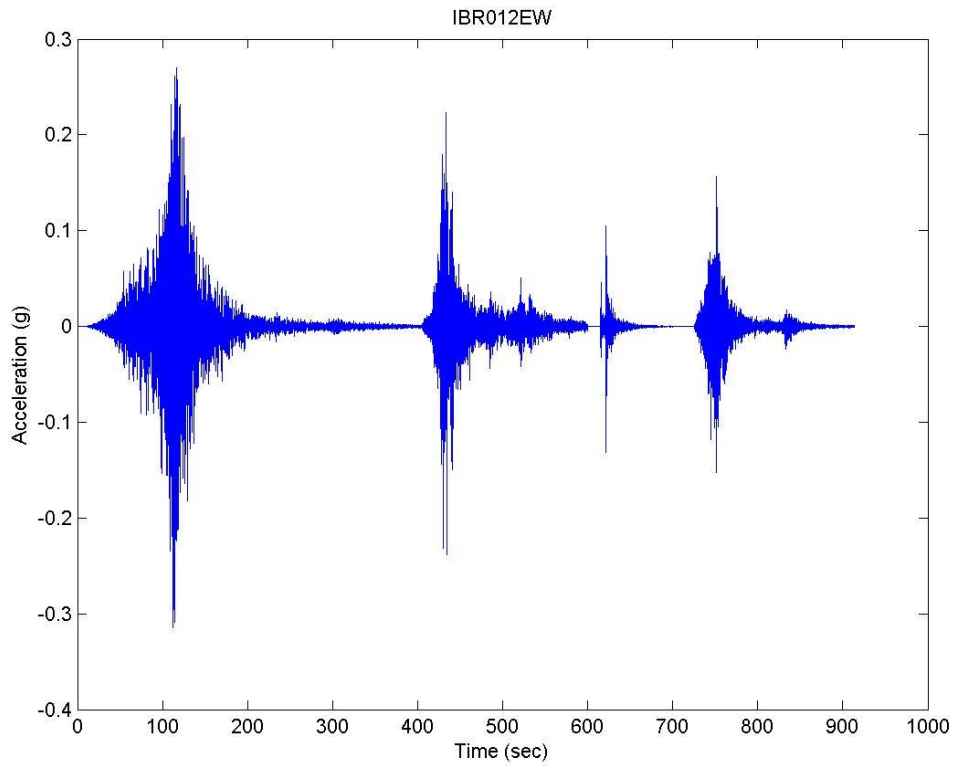


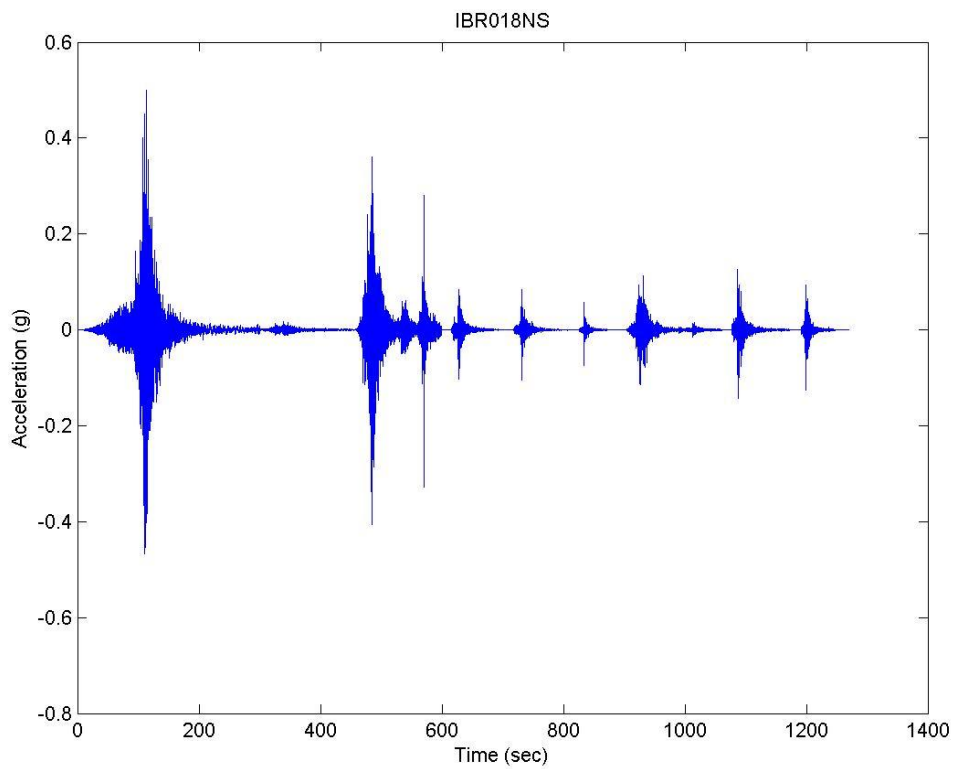
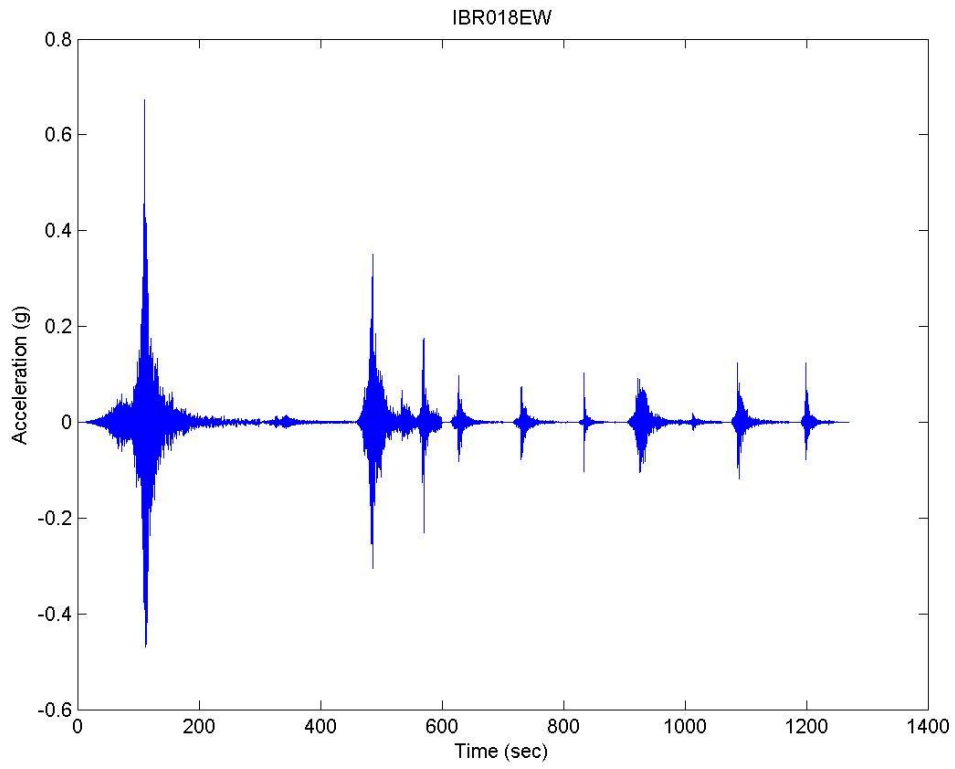


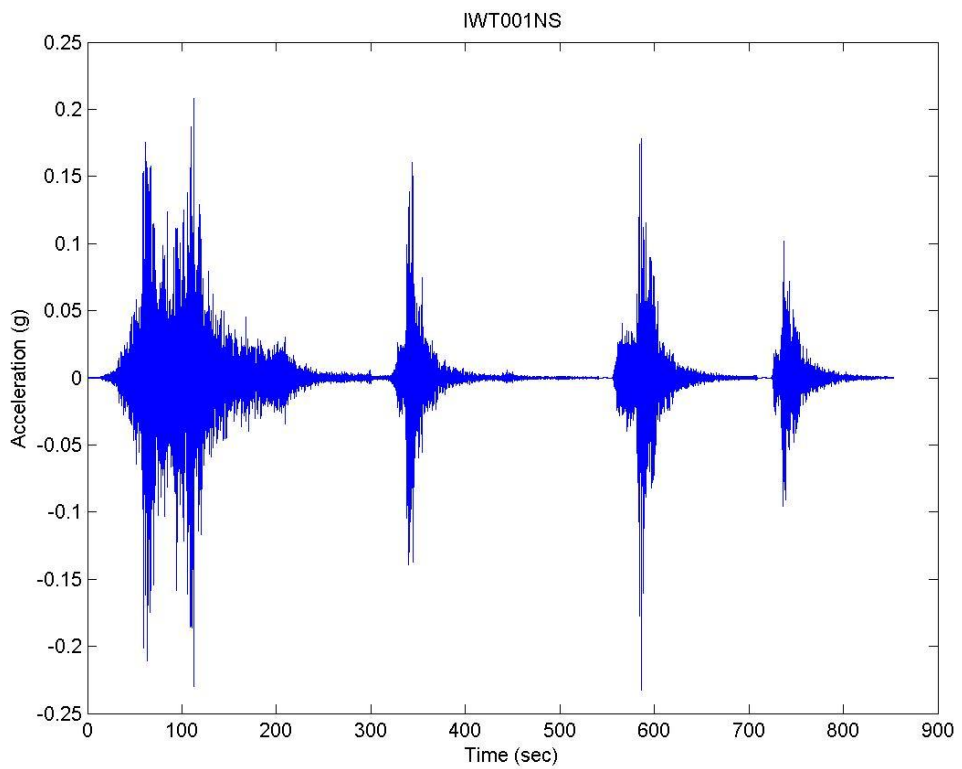
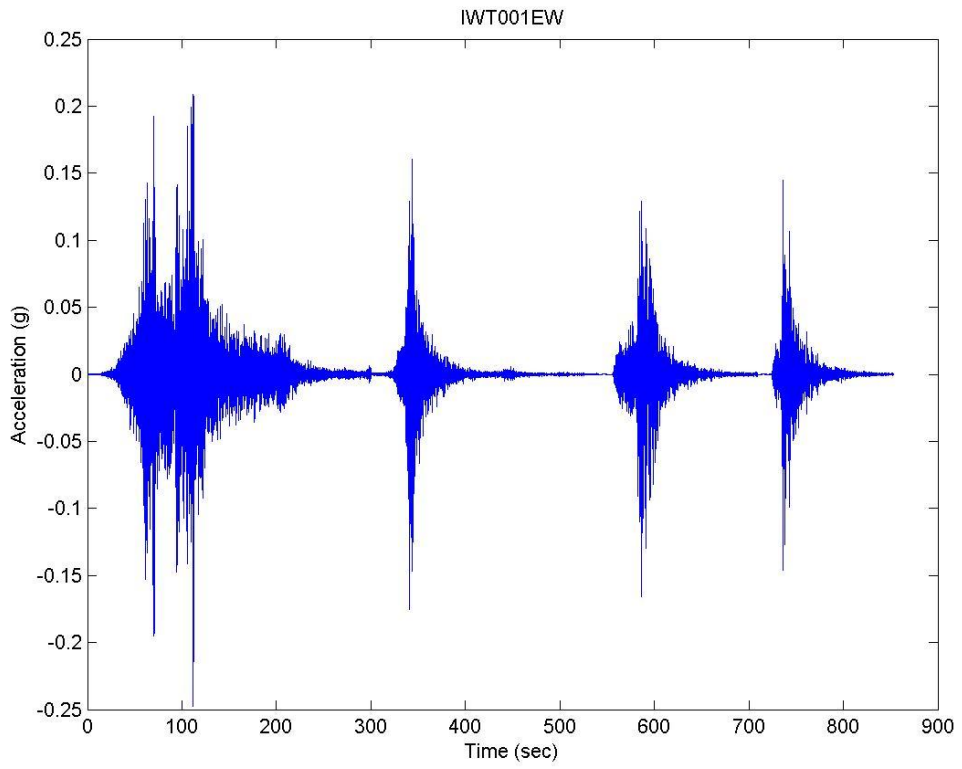


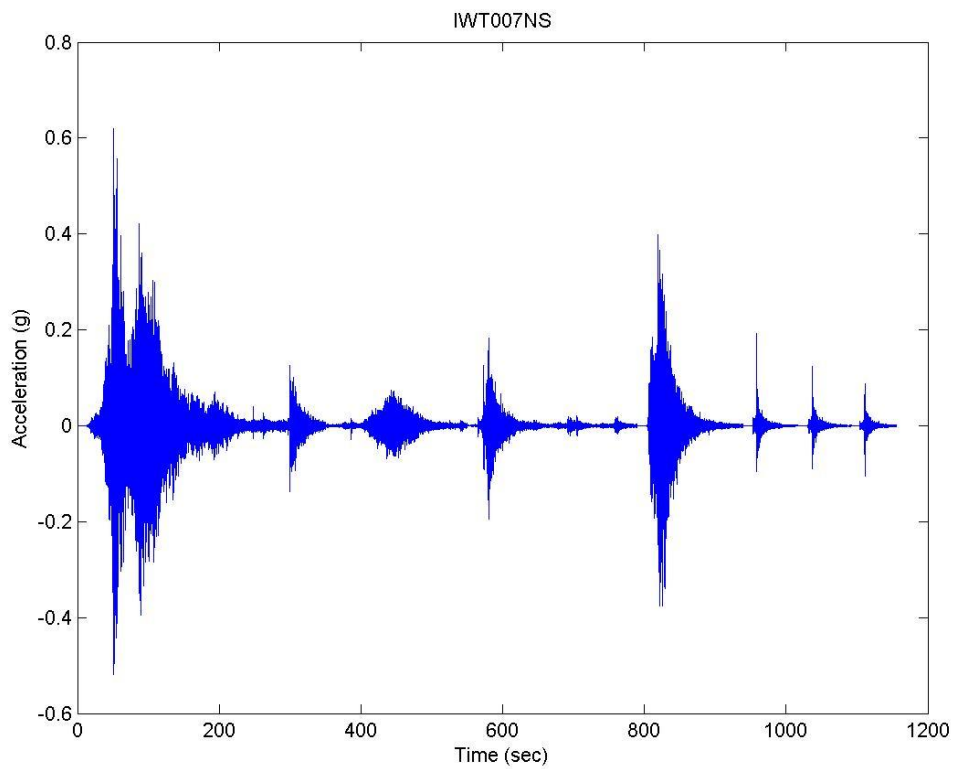
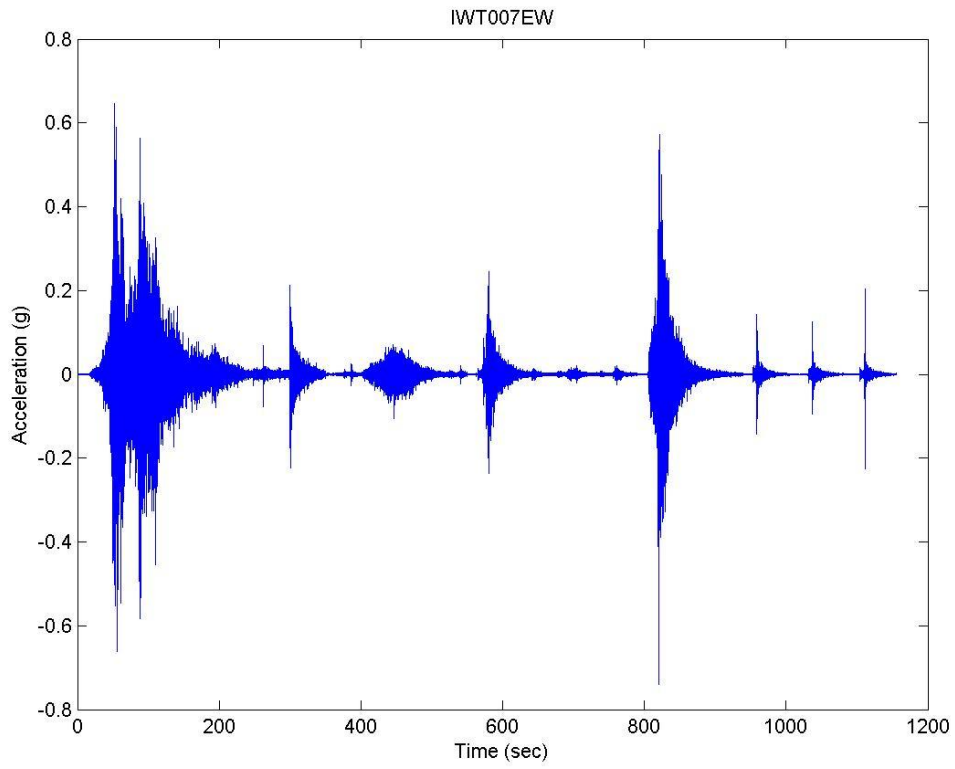


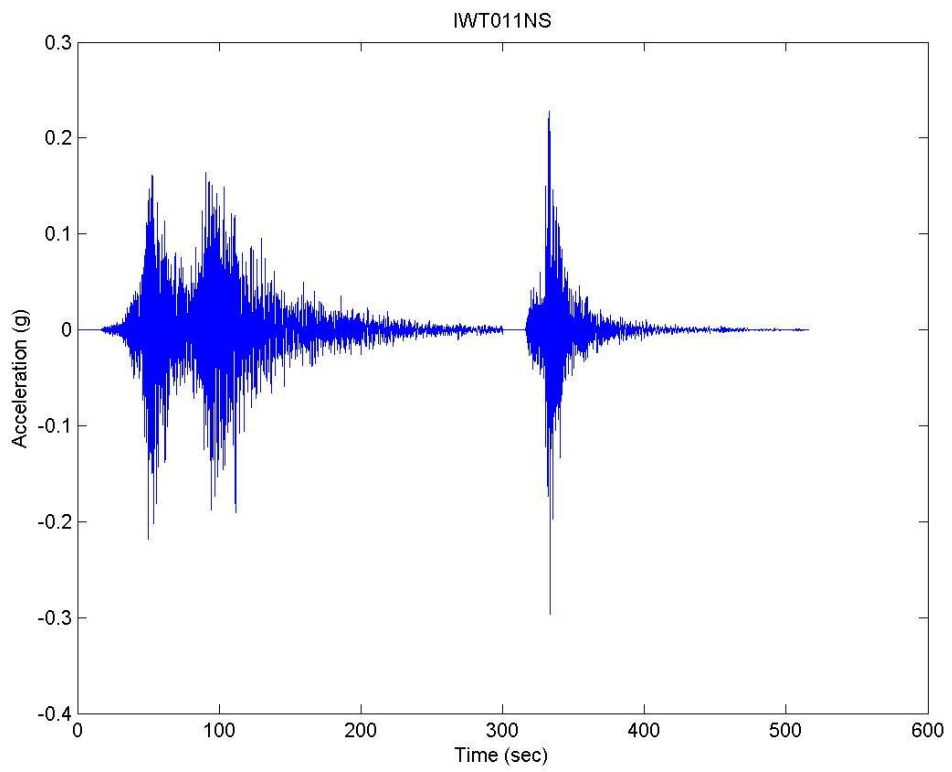
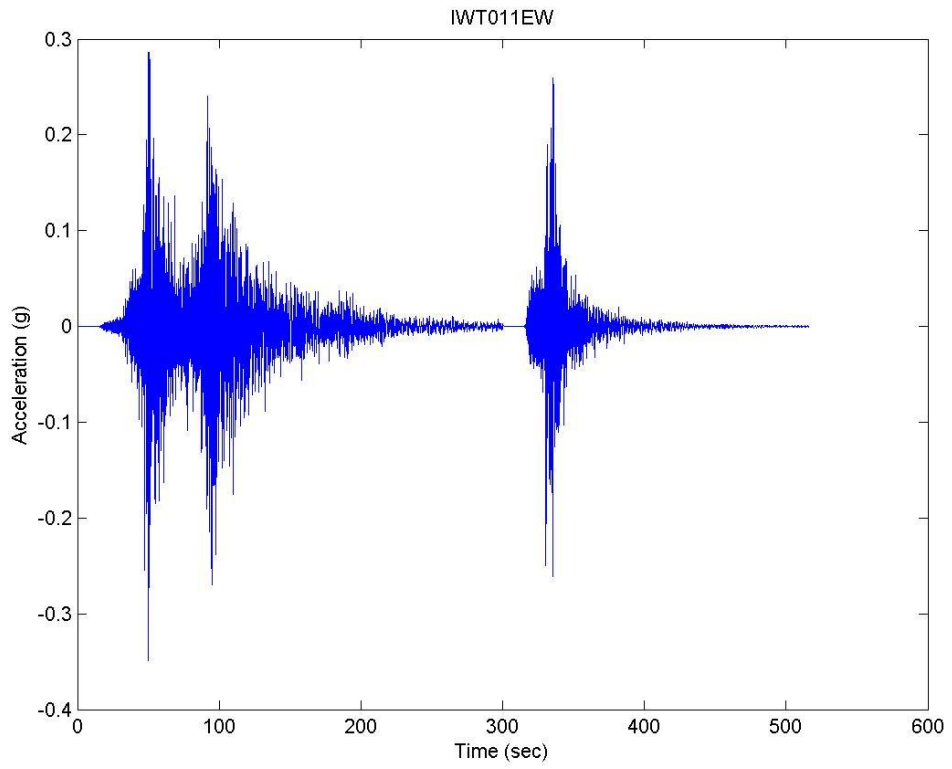


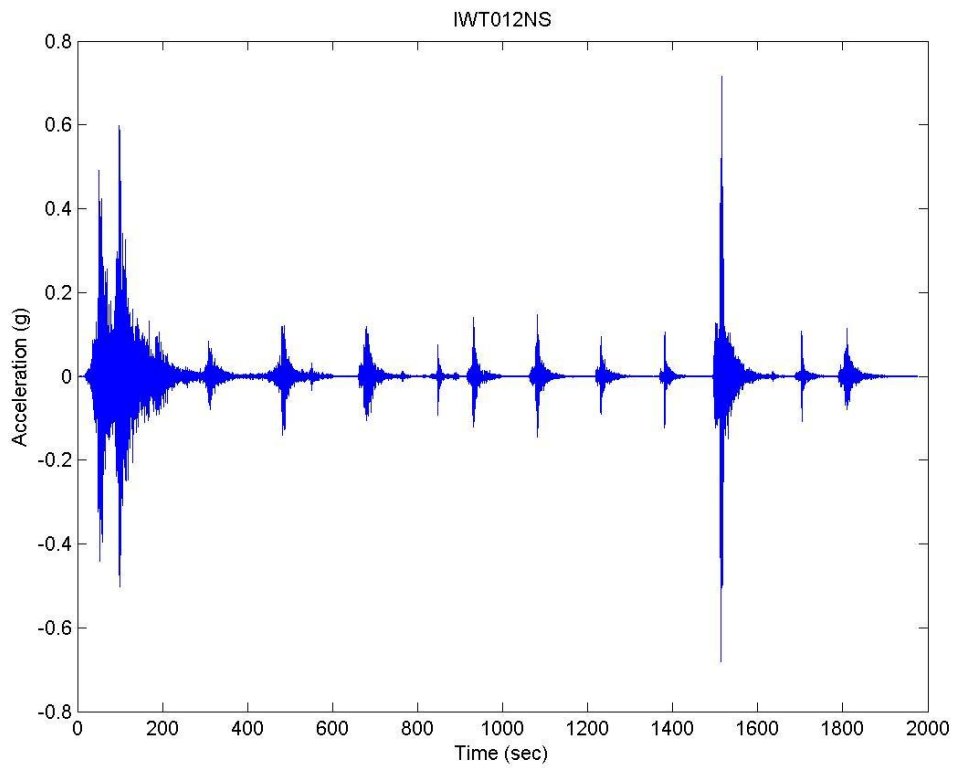
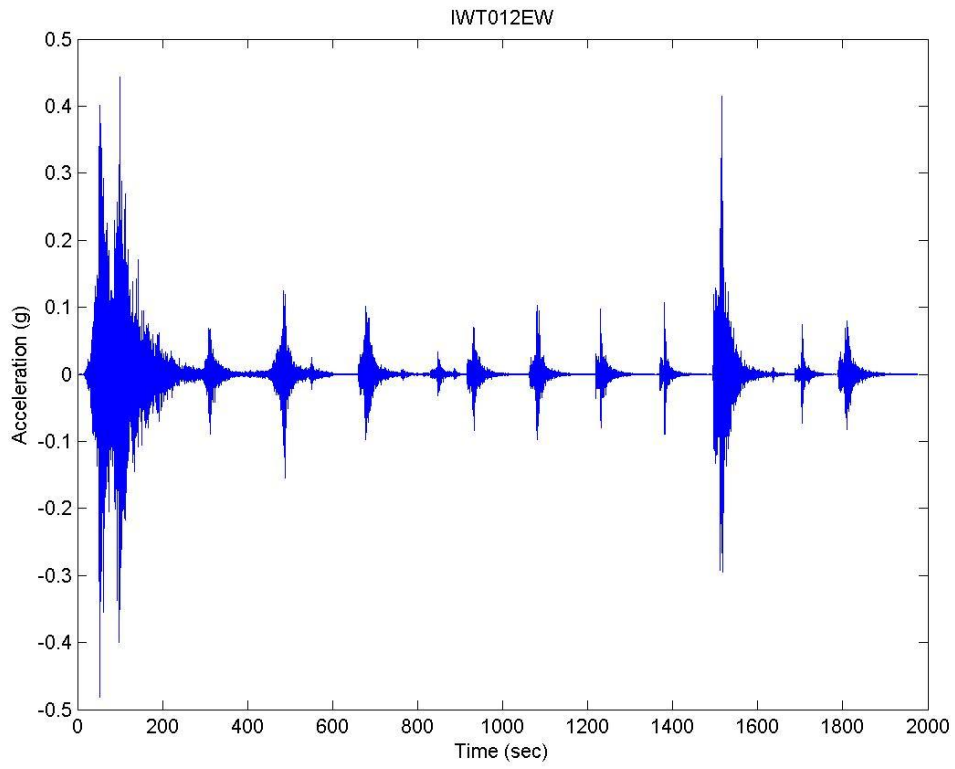


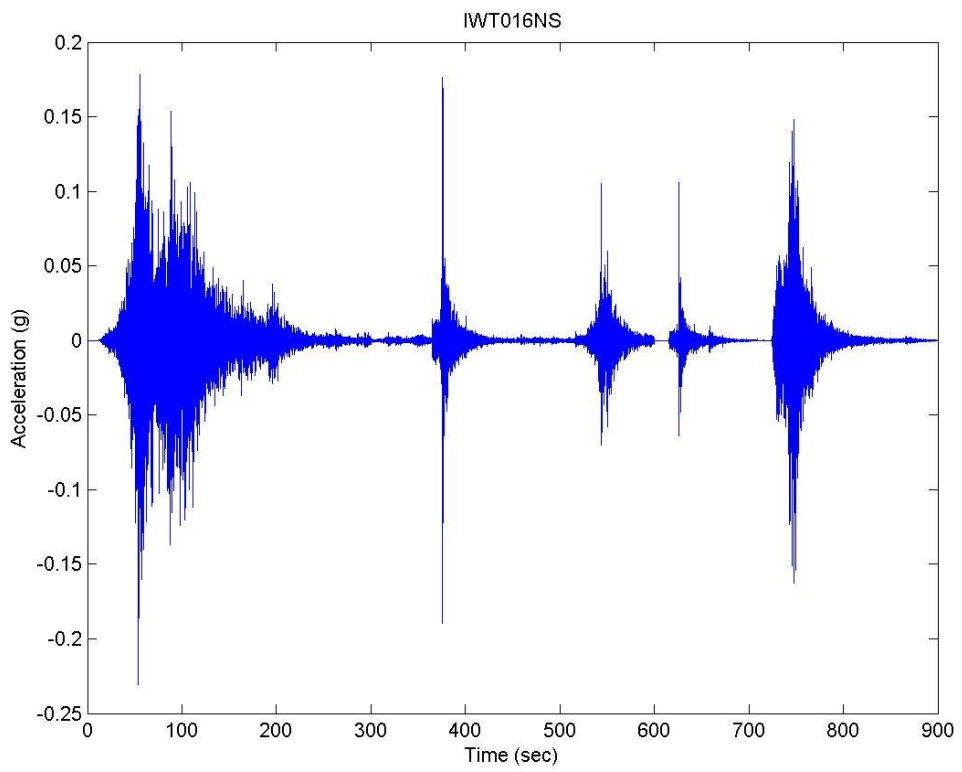
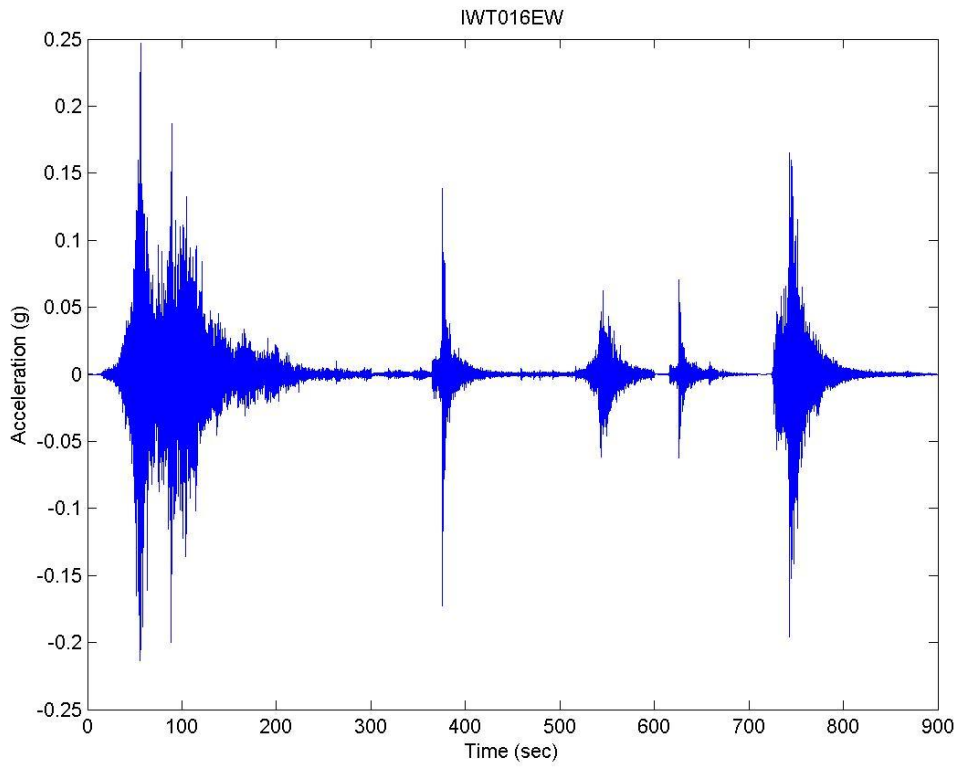


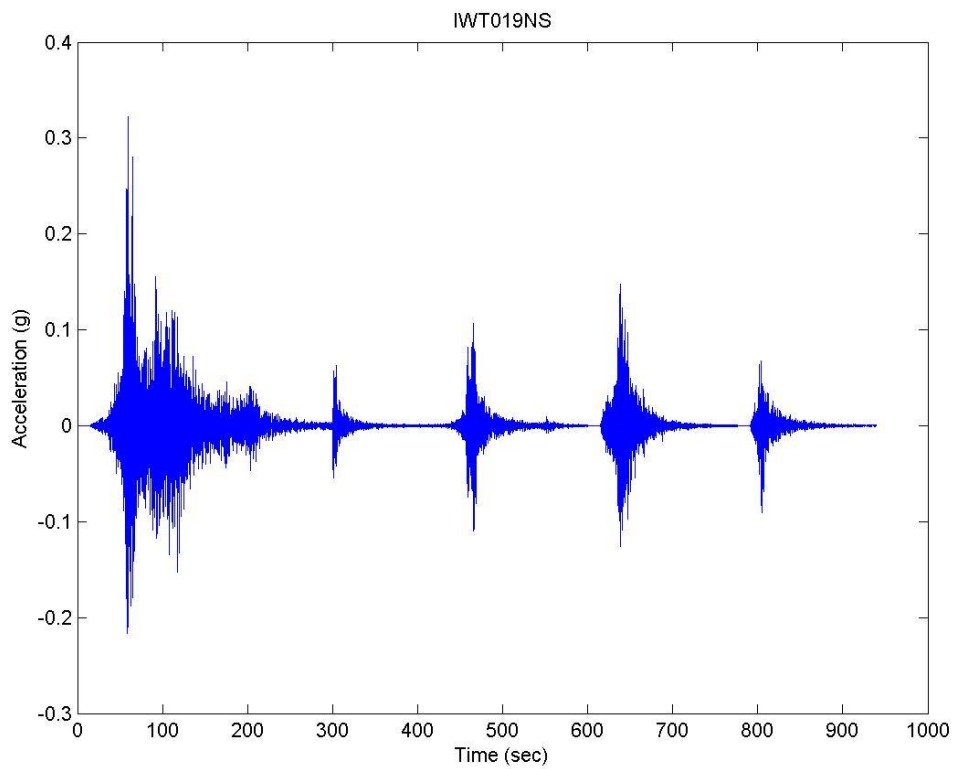
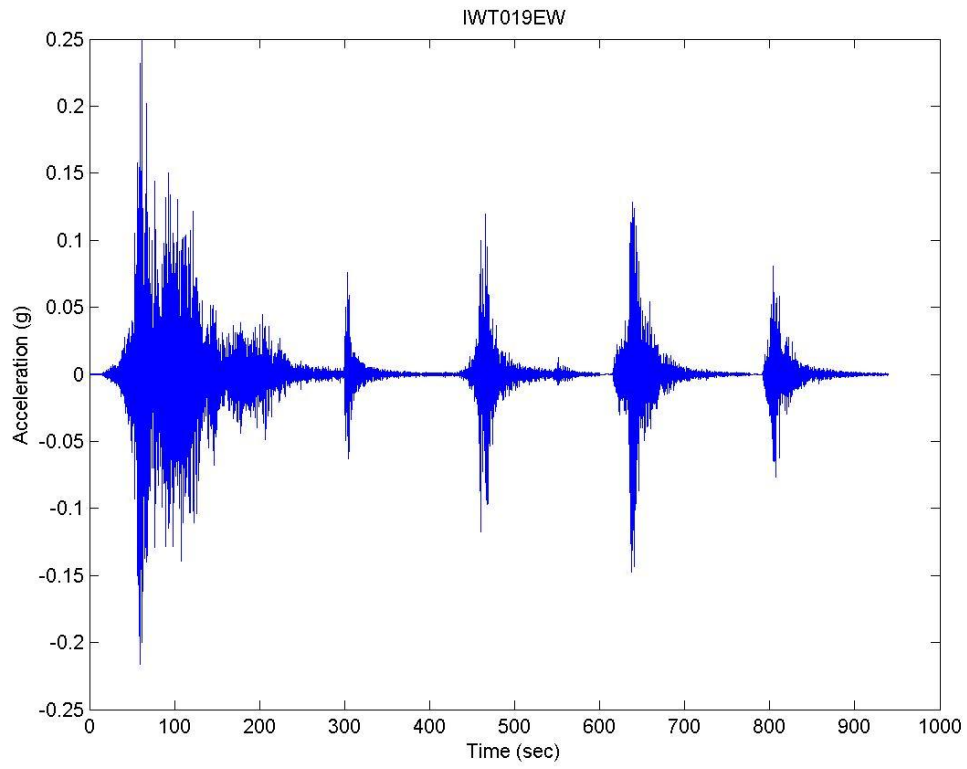


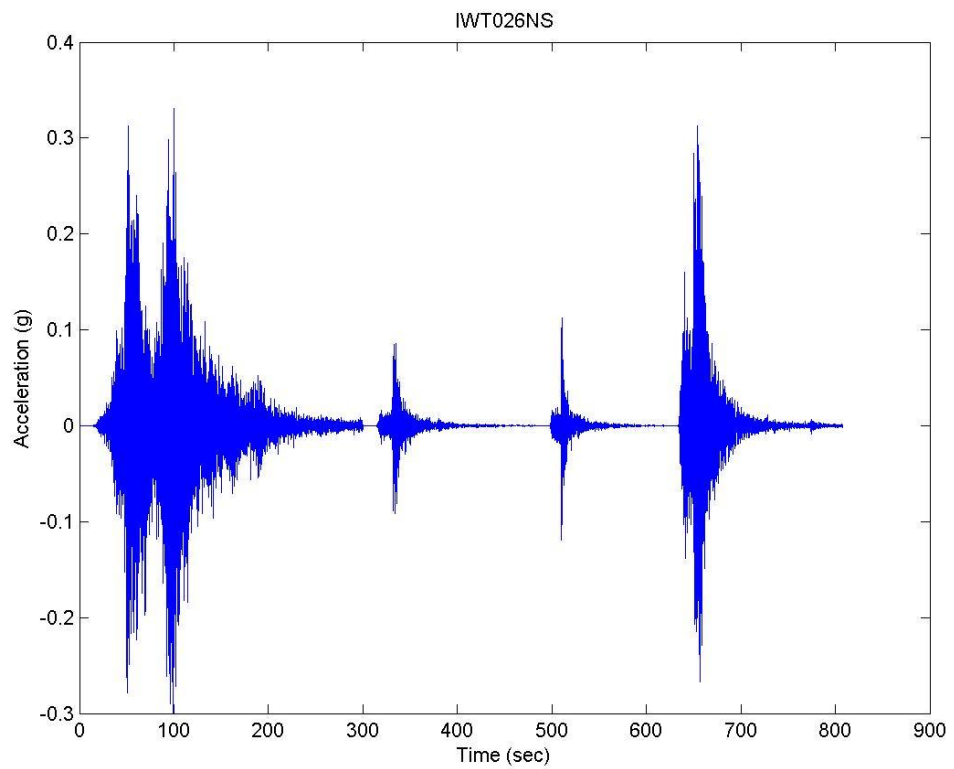
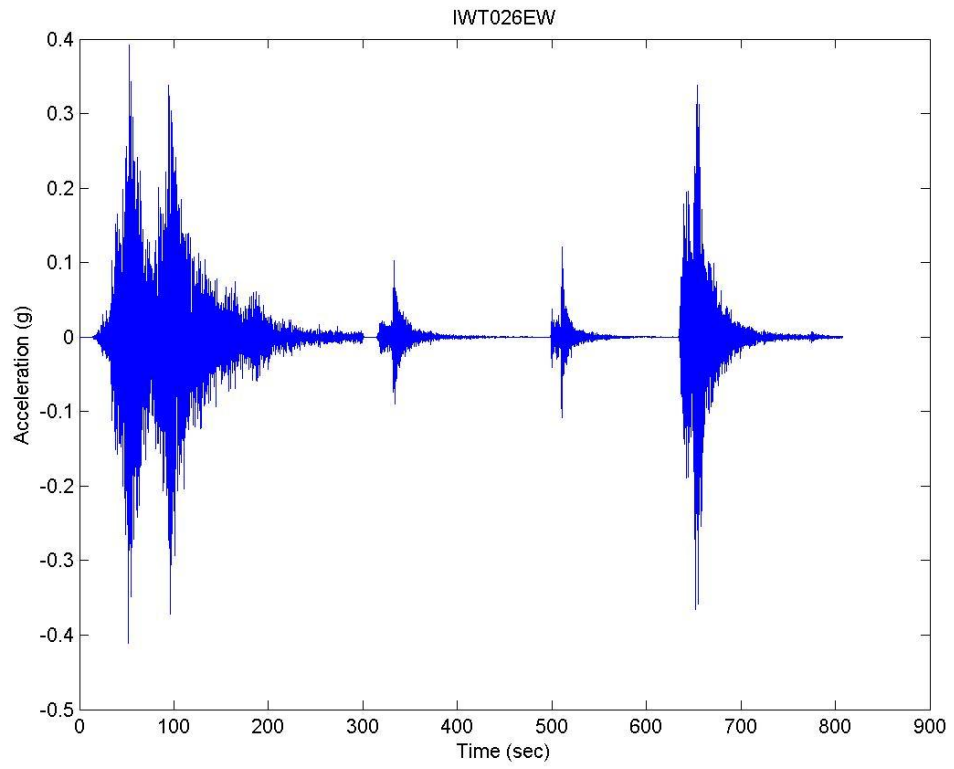


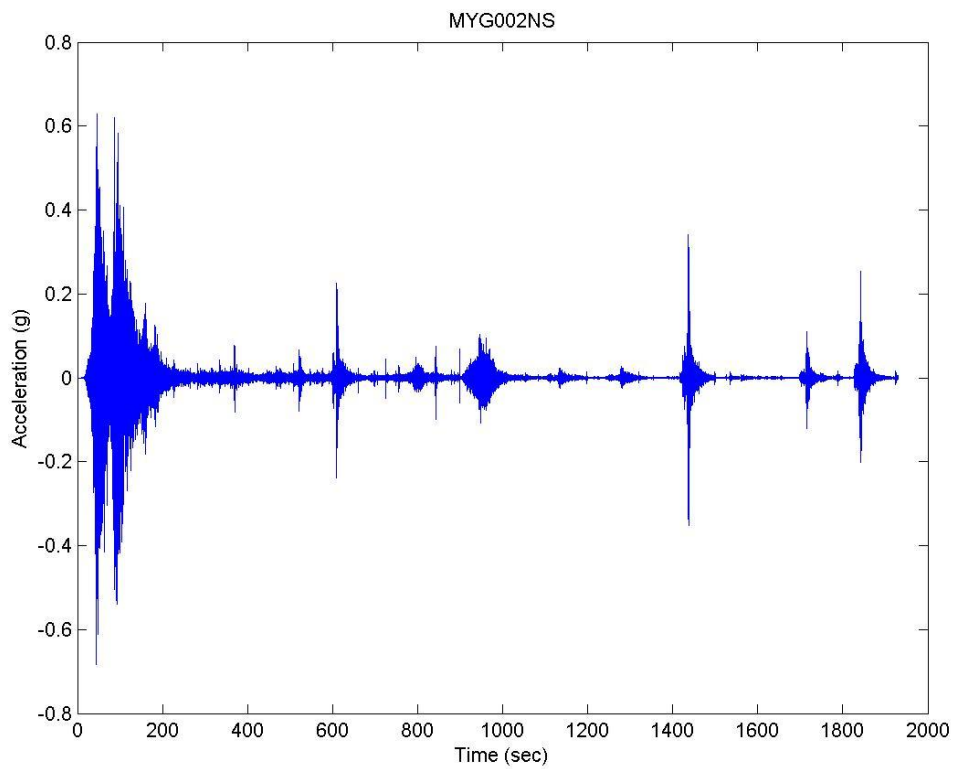
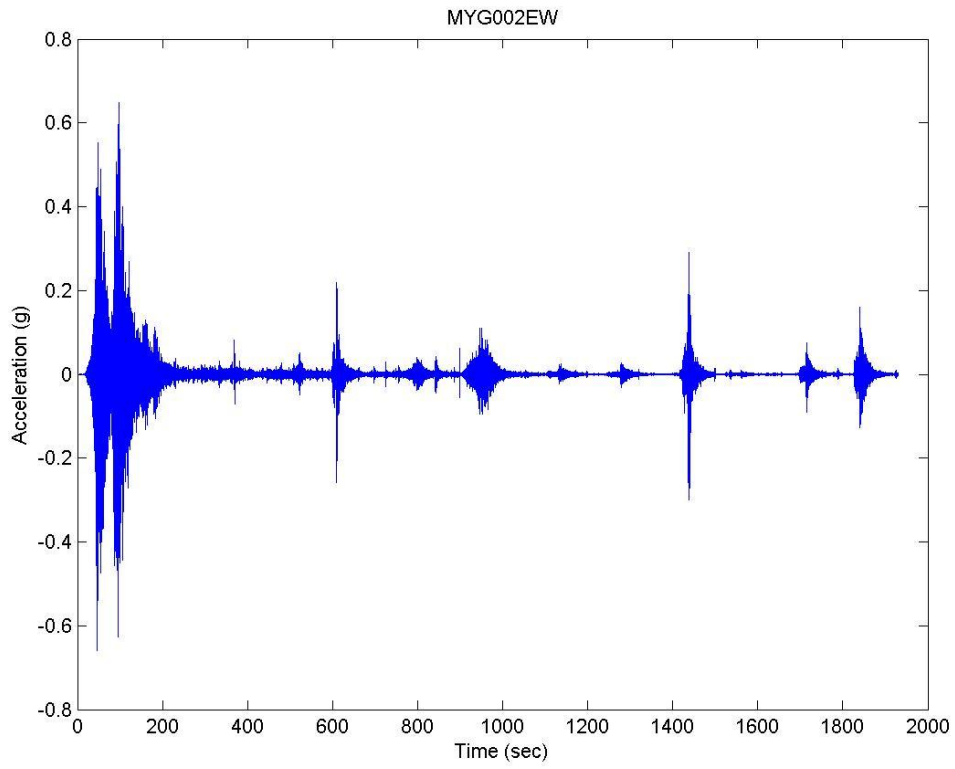


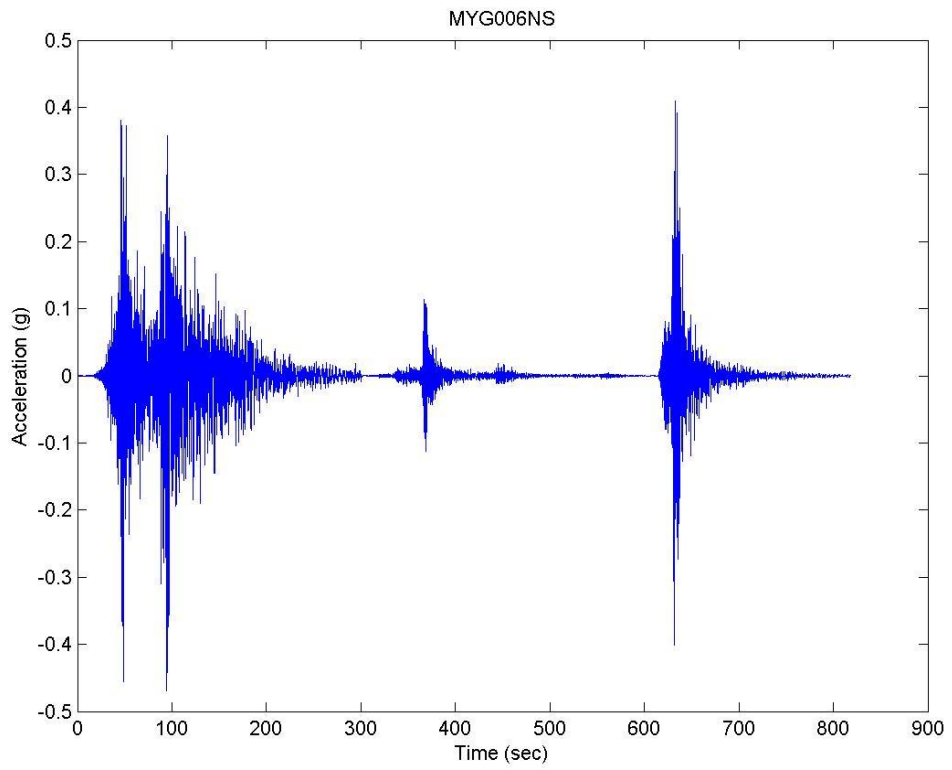
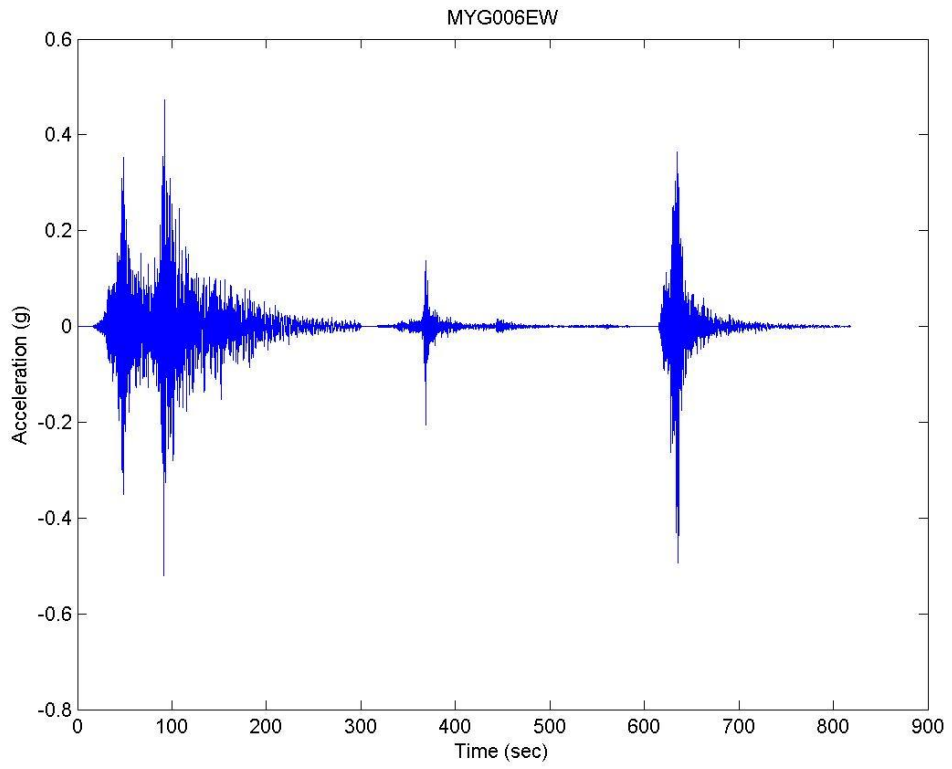


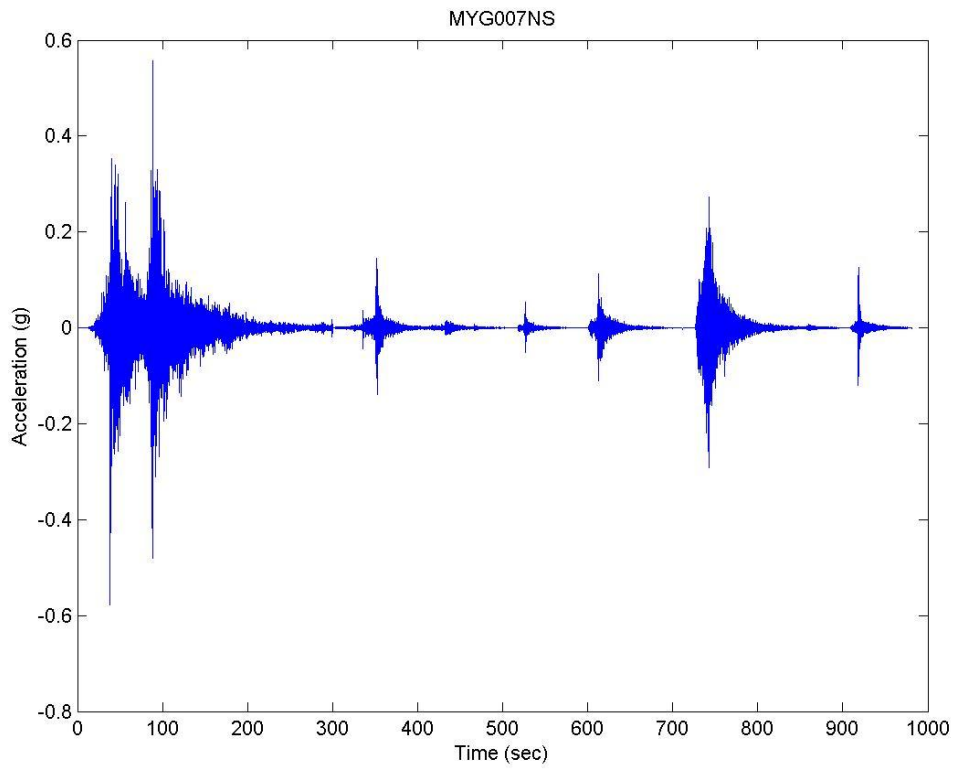
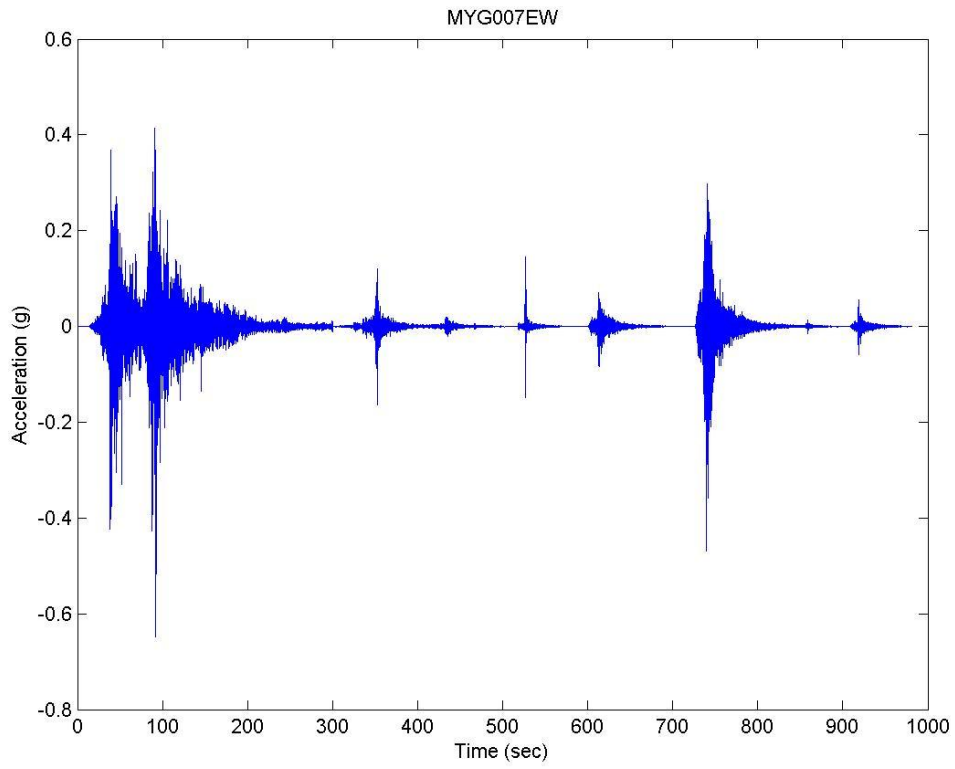


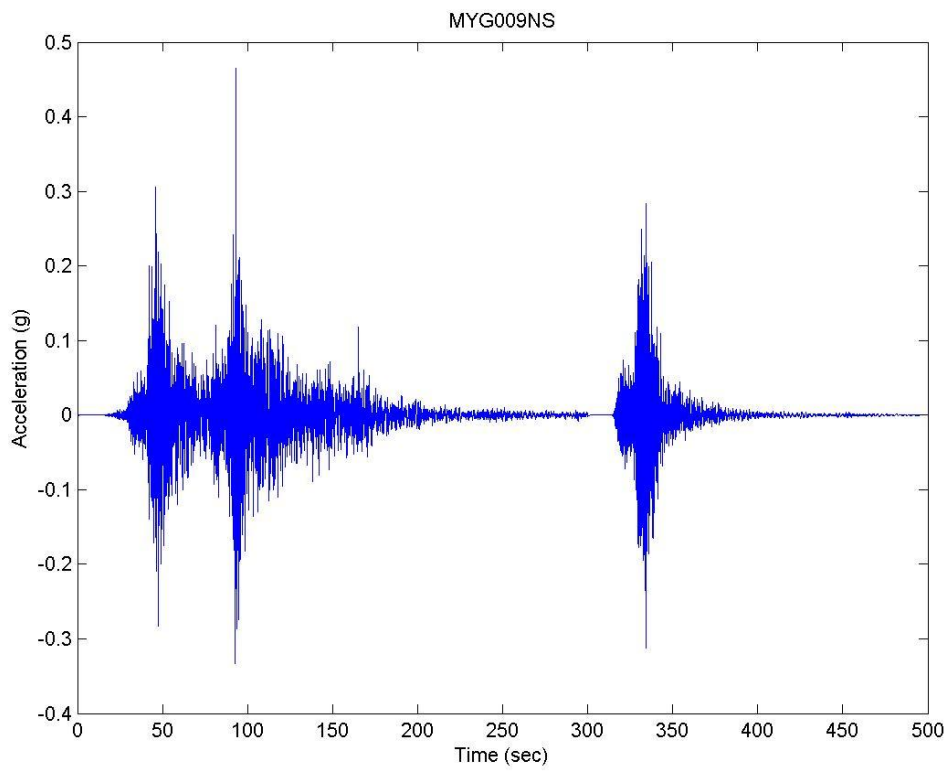
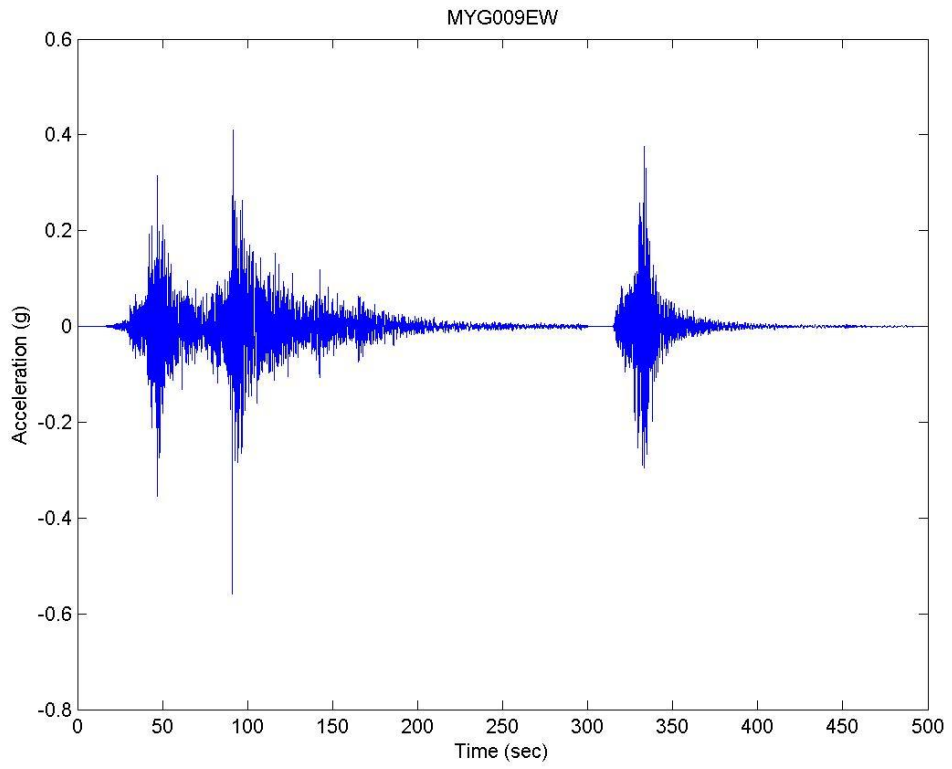


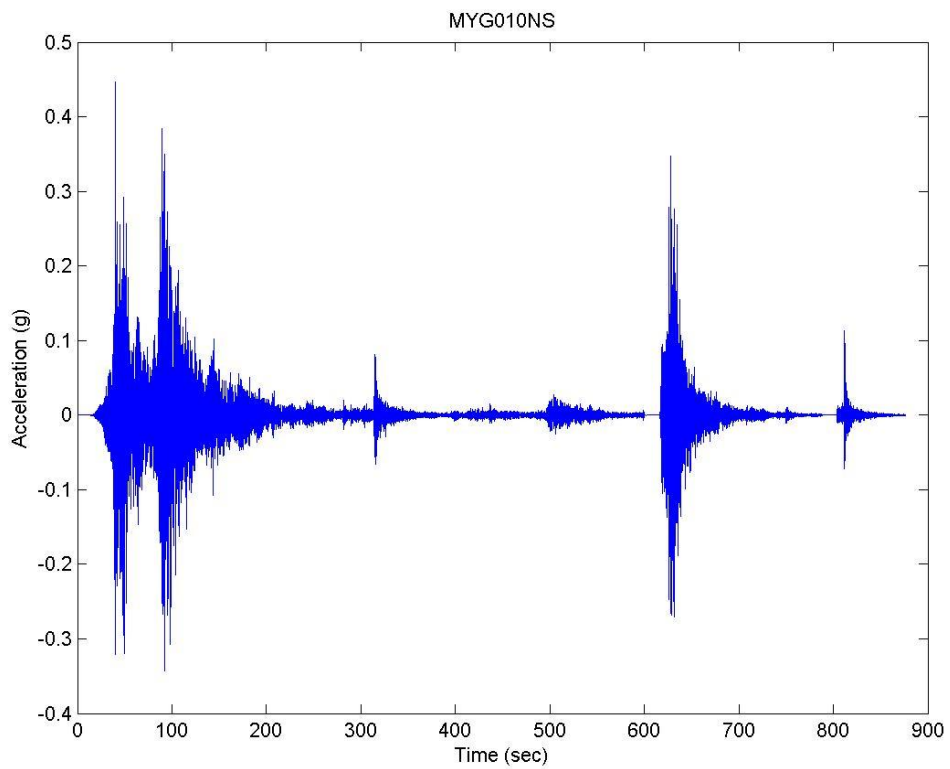
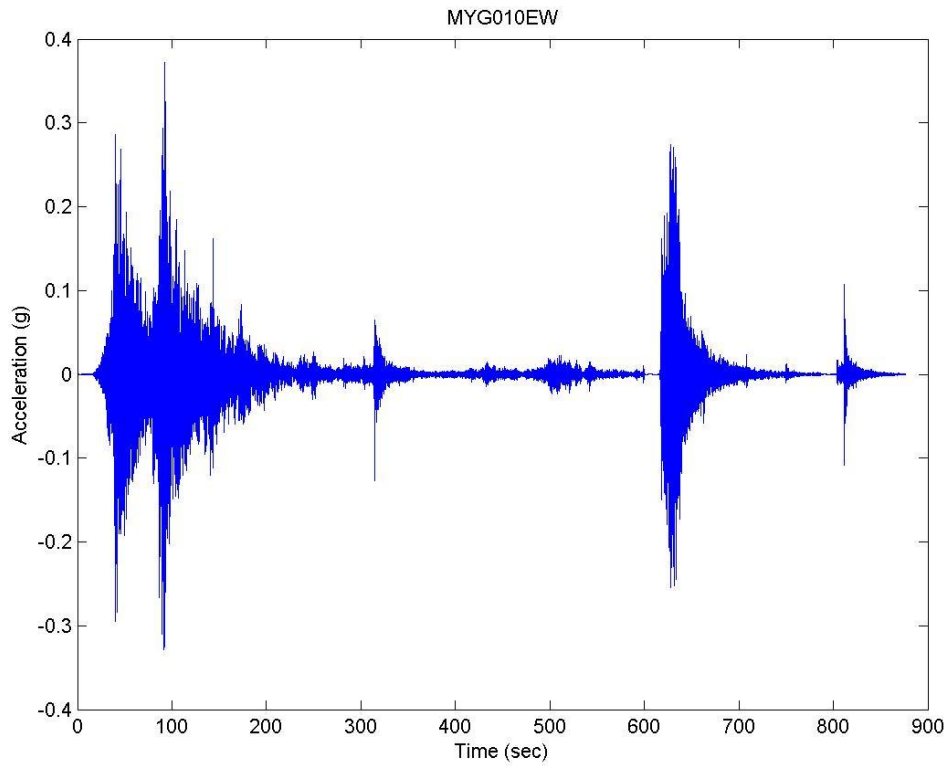


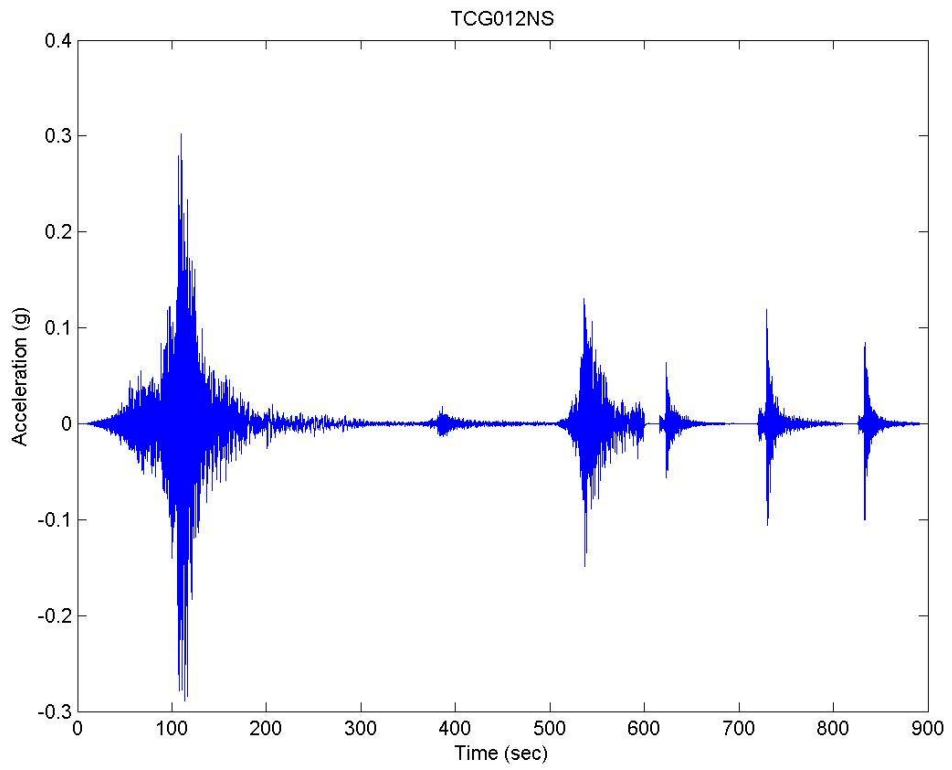
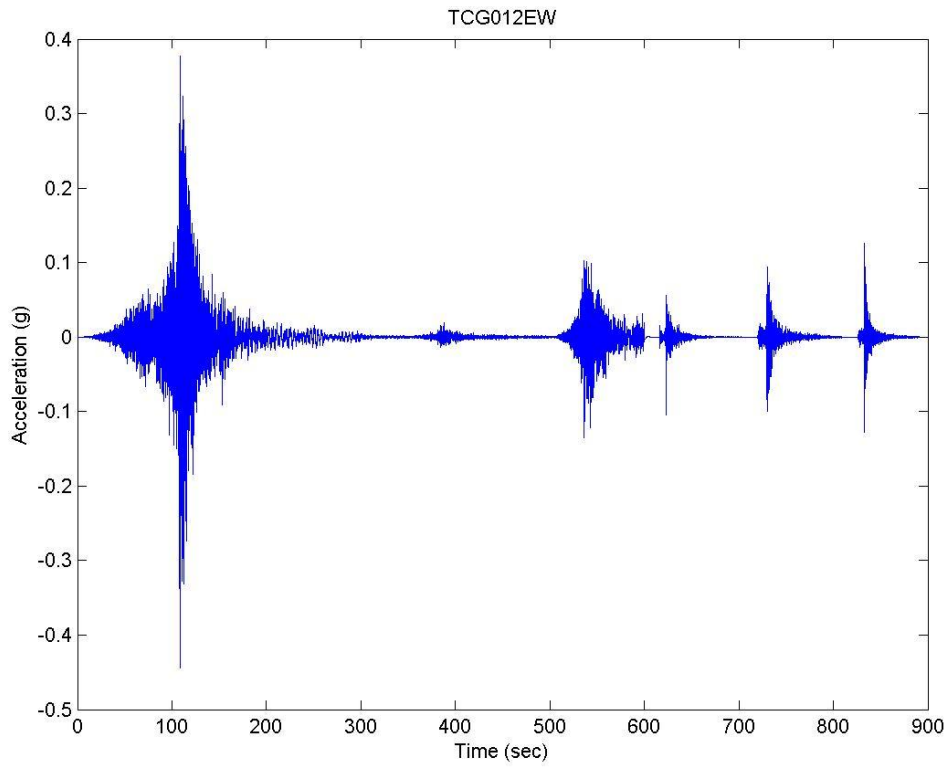




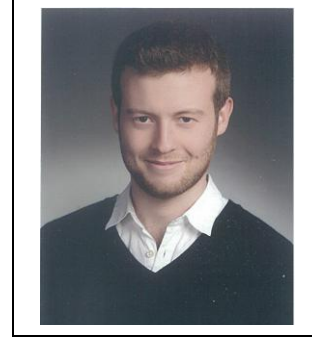








CURRICULUM VITAE



Name Surname: Çağatay TOROS

Place and Date of Birth: Zonguldak/1990

E-Mail: cagataytoros@gmail.com

EDUCATION:

B.Sc.: 2012, Eskişehir Osmangazi Üniversitesi,
Mühendislik ve Mimarlık Fakültesi, İnşaat
Mühendisliği Anabilim Dalı